Upgrading Concepts for the Implementation of Sustainable DTG Fuels

Zur Erlangung des akademischen Grades eines
DOKTORS DER INGENIEURWISSENSCHAFTEN (DR.-ING.)

von der KIT-Fakultät für Chemieingenieurwesen und Verfahrenstechnik des
Karlsruher Instituts für Technologie (KIT)
genehmigte

DISSERTATION

von
David Graf, M.Sc.
aus Oberkirch

Tag der mündlichen Prüfung: 23.10.2026

Erstgutachter: Prof. Dr. Reinhard Rauch

Zweitgutachter: Prof. Dr. Nicolaus Dahmen

Acknowledgments

I would like to express my sincere gratitude to my supervisor, Prof. Dr. techn. Reinhard Rauch, for the confidence he placed in me and his support in sharpening my critical thinking and developing a professional approach to research. I am equally grateful for his continuous guidance throughout this long journey. I would also like to thank Prof. Dr. Nicolaus Dahmen for his kind interest in this thesis and for readily agreeing to serve as its second examiner.

My thanks go to all my colleagues at EBI and IKFT. In particular, I would like to thank Wiebke Asbahr and Dr. Philipp Neuner for their support and the many helpful discussions. My deepest gratitude goes to my students Diego Guajardo Pasillas, Henning Rädel, Jakob Krause, Timur Rafailov, Can Tülek, Cherie Hsu, Franco Vélez, Johannes Waßmuth, Josua Bauer, and Xhesika Koroveshi. Without their dedication and commitment, this thesis would not have been possible.

Finally, I would like to express my deepest gratitude to my parents, Vera and Herbert, for making my doctoral thesis possible and for always supporting me through difficult and exhausting times. With all my love, I thank Teresa for encouraging me countless times and for bringing us our greatest joy, our son Elio.

Thank you!

Abstract

The defossilization of the transportation sector is a central pillar of current climate mitigation strategies. Despite rapid progress in electrification, liquid hydrocarbon fuels will continue to play an important role, particularly in aviation and maritime transport. Additionally a substantial vehicle fleet still relies on internal combustion engines. Greenhouse gas-neutral synthetic hydrocarbons produced via methanol-to-gasoline (MTG) and dimethyl ether-to-gasoline (DTG) represent a promising solution due to their compatibility with existing engines and fuel infrastructures. However, such gasoline by a large share contains aromatic-rich heavy gasoline, characterized by elevated durene contents and unfavorable volatility and emissions-related properties. The upgrading and integration of these fractions constitute a key challenge for the large-scale deployment of synthetic fuels. This dissertation addresses this challenge by developing two hydroprocessing-based concepts for the utilization of heavy gasoline.

For the first approach, the hydroprocessing of bioliq® heavy gasoline is studied using bifunctional Pt/zeolite catalysts (Pt/HZSM-5, Pt/SAPO-11, and Pt/Mordenite) in a laboratory-scale fixed-bed reactor. Catalyst- and process-induced effects on octane numbers and volatility parameters are systematically analyzed. Hydroprocessing experiments reveal a dependence of motor octane number on catalyst choice, with Pt/HZSM-5 > Pt/SAPO-11 > Pt/Mordenite, attributable to shape-selective isomerization. Elevated reaction temperatures enhance cracking, leading to significant increases in crucial low-volatility parameters. To finally meet the European gasoline standard EN 228, an advanced blending strategy is developed to address remaining volatility deficiencies by incorporating oxygenates (methanol, ethanol, MTBE, and ETBE) and a distillate of hydrocracked Fischer–Tropsch waxes. Blending experiments demonstrate that oxygenates exert distinct and partly non-linear effects on the boiling curve. Methanol is particularly effective in increasing low-end volatility, while MTBE and ETBE enable more uniform boiling behavior. A near-standard-compliant gasoline blend is obtained, with methanol/ETBE-based formulations offering the most balanced performance in terms of volatility and octane numbers.

In a second approach, a refinery integration is explored by co-hydroprocessing aromatic-rich bioliq® heavy gasoline with fossil middle distillates under industrial hydrotreating conditions. Long-term experiments are conducted to assess isomerization selectivity and crucial petrochemical parameters. Additionally, fuel yields are investigated, supported by the development of lumping-based kinetic models for yield prediction. Co-hydroprocessing experiments show that aromatic hydrogenation dominates over isomerization at elevated temperatures, enabling an effective removal of heavy aromatics. Diesel fractions produced from co-processing comply with the European diesel standard EN 590 cetane number requirements. Lumping models accurately describe product yield distributions, identifying hydrogenation, cracking from heavy to light fractions, and the dealkylation of ring-attached hydrocarbon chains as the dominant reaction pathways.

This work demonstrates that hydroprocessing is a suitable solution for upgrading heavy gasoline fractions mechanistically formed in MTG and DTG syntheses. While hydroprocessing alone is insufficient to meet gasoline specifications, its combination with carefully selected oxygenates enables the production of gasoline that meets specifications. Moreover, the successful co-hydroprocessing of bio-based heavy gasoline in existing middle distillate hydrotreaters highlights the short-term feasibility of refinery integration without major capital investment.

Zusammenfassung

Die Dekarbonisierung des Verkehrssektors ist ein zentraler Pfeiler des Klimaschutzes. Trotz rascher Fortschritte bei der Elektrifizierung werden Kraftstoffe allerdings, insbesondere in der Luft- und Seeschifffahrt, weiterhin eine wichtige Rolle spielen. Außerdem, da ein Großteil der Fahrzeugflotte nach wie vor auf Verbrennungsmotoren basiert. Treibhausgasneutrale synthetische Kohlenwasserstoffe, die durch methanol-to-gasoline (MTG) und dimethyl ether-to-gasoline (DTG) hergestellt werden, stellen aufgrund ihrer Kompatibilität mit bestehenden Motoren und Kraftstoffinfrastrukturen eine vielversprechende Lösung dar. Allerdings enthält dieses Benzin aromatenreiches Schwerbenzin, das sich durch einen erhöhten Durolgehalt, geringe Flüchtigkeit und erhöhte Emissionen auszeichnet. Die Aufbereitung und Integration dieser Fraktionen stellt eine zentrale Herausforderung für den großtechnischen Einsatz synthetischer Kraftstoffe dar. Diese Dissertation befasst sich mit dieser Fragestellung, indem zwei auf Hydroprocessing basierende Konzepte für die Verwertung von Schwerbenzin entwickelt werden.

Für den ersten Ansatz wird das Hydroprocessing von bioliq®-Schwerbenzin unter Verwendung bifunktioneller Pt/Zeolith-Katalysatoren (Pt/HZSM-5, Pt/SAPO-11 und Pt/Mordenit) in einem Laborfestbettreaktor untersucht. Katalysator- und prozessbedingte Auswirkungen auf Oktanzahlen und Flüchtigkeitsparameter werden systematisch analysiert. Die Experimente zeigen eine ausgeprägte Abhängigkeit der Motoroktanzahl von der Wahl des Katalysators, wobei die Reihenfolge Pt/HZSM-5 > Pt/SAPO-11 > Pt/Mordenit gilt, was auf eine formselektive Isomerisierung zurückzuführen ist. Erhöhte Reaktionstemperaturen verstärken das Cracken, was zu einem deutlichen Anstieg der wichtigsten Flüchtigkeitsparameter führt. Um die europäische Benzinnorm EN 228 erfüllen zu können, wird ein weiterführendes Blending-Konzept entwickelt, um verbleibende Volatilitätsdefizite durch die Einbeziehung von Oxygenaten (Methanol, Ethanol, MTBE und ETBE) und einem Benzindestillat aus hydrogekrackten Fischer-Tropsch-Wachsen zu beheben. Blending-Versuche zeigen, dass Oxygenate deutliche und teilweise nichtlineare Auswirkungen auf die Destillationskurve haben. Methanol ist besonders wirksam bei der Erhöhung der Flüchtigkeit im unteren Siedebereich, während MTBE und ETBE ein gleichmäßigeres Siedeverhalten ermöglichen. Es wird eine nahezu normkonformes Benzin erhalten, wobei Formulierungen auf Methanol-/ETBE-Basis die besten Ergebnisse in Bezug auf Flüchtigkeit und Oktanzahl erzielen.

In einem zweiten Ansatz wird eine Raffinerieintegration untersucht, indem aromatenreiches bioliq®-Schwerbenzin unter industriellen Hydrotreating-Bedingungen gemeinsam mit fossilem Mitteldestillat hydroprocessed wird. Langzeitversuche werden durchgeführt, um die Isomerisierungsselektivität und wichtige petrochemische Parameter zu bewerten. Zusätzlich werden die Ausbeuten wichtiger Kraftstofffraktionen, unterstützt durch die Entwicklung von lumping-basierten kinetischen Modellen zur Ausbeutevorhersage, untersucht. Die Ergebnisse zeigen, dass die Aromatenhydrierung bei erhöhten Temperaturen gegenüber der Isomerisierung dominiert. Hierdurch wird eine effektive Entfernung schwerer Aromaten ermöglicht. Die aus dem co-processing gewonnenen Dieselfraktionen entsprechen den Anforderungen der europäischen Dieselnorm EN 590 an die Cetanzahl. Die aufgestellten Lumping-Modelle beschreiben die Produktausbeuten zuverlässig und identifizieren die Hydrierung, das Cracken von schweren zu leichten Fraktionen und die Dealkylierung von an Naphthenen sowie Aromaten gebundenen Kohlenwasserstoffketten als die dominierenden Reaktionen.

Die vorliegende Arbeit zeigt, dass Hydroprocessing eine geeignete Prozessoption für das Upgrading schwerer aromatenreicher Benzinfraktionen ist, die bei MTG- und DTG-Synthesen mechanistisch gebildet werden. Während Hydroprocessing alleine nicht ausreicht, um die EN 228 zu erfüllen, ermöglicht das Blending mit Oxygenaten die Herstellung von Benzin, das den Spezifikationen entspricht. Darüber hinaus unterstreicht das erfolgreiche co-processing von biobasiertem Schwerbenzin in bestehenden Mitteldestillat-Hydrotreatern die kurzfristige Machbarkeit einer Raffinerieintegration.

Table of Contents

Acknowledgments i

Abstract ii

Zusammenfassung iii

Abbreviations vii

Nomenclature ix

List of Tables xi

List of Figures xii

Preamble xiv

1 Introduction 1
1.1 Background and Motivation 1
1.2 Objectives and Outline 2

2 Upgrading via Hydroprocessing Using Bifunctional Zeolite Catalysts 5
2.1 Introduction 5
2.2 Greenhouse Gas Neutral Gasoline Supply in a Refinery 5
2.2.1 Processes for the Production of Synthetic Gasoline 5
2.2.2 Upgrading Strategy for a Synthetic MTG/DTG Gasoline 7
2.2.3 Hydroprocessing of Streams Rich in Heavy Aromatics 8
2.3 Materials and Methods 10
2.4 Results and Discussion 12
2.4.1 Adjustment of Petrochemical Parameters 12
2.4.2 Blending 17
2.5 Summary and Conclusions 19

3 Advanced Blending Concept 20
3.1 Introduction 20
3.1.1 Requirements for Synthetic Gasoline to Meet EN 228 20
3.1.2 Synthesis Gas-Based Renewable Gasoline Supply and Associated Challenges . . 21
3.1.3 The Potential of Oxygenates in Blending and Associated Challenges 23
3.2 Materials and Methods 24
3.3 Results and Discussion 27
3.3.1 Influence of Hydroprocessing on Boiling Characteristics and Vapor Pressure . . 27
3.3.2 Influence of Oxygenates on Boiling Characteristics and Vapor Pressure 28
3.3.3 Combination of Two Oxygenates and their Effect on Boiling Characteristics and Vapor Pressure 31

3.3.4 Expanded Blending Concept . . . 32
3.4 Summary and Conclusions . . . 34

4 Upgrading Via Co-Hydroprocessing Using a Hydrotreating Catalysts . . . 35
4.1 Introduction . . . 35
4.1.1 Processing of Feedstocks Rich in Heavy Mono-Ring Aromatics . . . 35
4.1.2 Modeling of Hydroprocessing . . . 36
4.2 Materials and Methods . . . 37
4.2.1 Experimental Setup and Procedure . . . 37
4.2.2 Model Structure and Procedure . . . 40
4.3 Results and Discussion . . . 42
4.3.1 Influence of Reaction Parameters on Catalyst Performance . . . 42
4.3.2 Fuel Yields and Qualities . . . 45
4.3.3 Parameter Estimation and Model Validation . . . 47
4.4 Summary and Conclusions . . . 51

5 Summary . . . 53

Bibliography . . . 57

Appendix A. Additional Information on Chapter 2 . . . 68

Appendix B. Additional Information on Chapter 3 . . . 74

Appendix C. Additional Information on Chapter 4 . . . 77

Appendix D. Original Publications . . . 80

Appendix E. Author Contributions . . . 151

Abbreviations

Abbreviation	Full Name
ASTM	American Society for Testing and Materials
BMUV	German Federal Ministry for the Environment, Nature Conservation, Nuclear Safety and Consumer Protection (German: Bundesministerium für Umwelt, Naturschutz, nukleare Sicherheit und Verbraucherschutz)
CFR	Cooperative Fuel Research
DMCP	Dimethylcyclopentane
DMDS	Dimethyl Disulfide
DME	Dimethyl Ether
DTG	Dimethyl Ether-to-Gasoline
EBI	Engler-Bunte-Institute
ECP	Ethylcyclopentane
EN	European Standard (German: Europäische Norm)
ETBE	Ethyl Tert-Butyl Ether
EU	European Union
FAME	Fatty Acid Methyl Esters
FCC	Fluid Catalytic Cracking
FT	Fischer-Tropsch
FTIR	Fourier-Transform Infrared
GC	Gas Chromatograph
GHG	Greenhouse Gas
HDS	Hydrodesulfurization
HG	Heavy Gasoline
HP	Hydroprocessing
HTFT	High-Temperature Fischer-Tropsch
ISO	International Organization for Standardization
KIT	Karlsruhe Institute of Technology
LCO	Light Cycle Oil
LTFT	Low-Temperature Fischer-Tropsch
MCH	Methylcyclohexane
MFC	Mass Flow Controller
MiRO	Mineral Oil Refinery Oberrhein
MTBE	Methyl Tert-Butyl Ether
MTG	Methanol-to-Gasoline
MTO	Methanol-to-Olefins
ODE	Ordinary Differential Equation
ON	Octane Number

Continued on next page ...

PAH	Polycyclic Aromatic Hydrocarbon
PTL	Power-to-Liquid
RC	Ring Contraction
RO	Ring Opening
SAS	Sasol Advanced Synthol
VGO	Vacuum Gas Oil

Nomenclature

Nomenclature	Full Name	Unit
$CFPP$	Cold Filter Plugging Point	°C
CN	Cetane Number	-
$E_{A,j}$	Activation Energy of Reaction j	kJ mol^{-1}
$E70$	Volume Fraction Evaporated at 70 °C	vol.%
$E100$	Volume Fraction Evaporated at 100 °C	vol.%
$E150$	Volume Fraction Evaporated at 150 °C	vol.%
$E180$	Volume Fraction Evaporated at 180 °C	vol.%
FBP	Final Boiling Point	°C
$F_{1-\alpha}$	Critical Value of F-Distribution	-
HoV	Heat of Vaporization	kJ kg^{-1}
IBP	Initial Boiling Point	°C
k_j	Rate Constant of Reaction j	$\mathrm{cm}^3_{\mathrm{Feed}}$ h^{-1} $\mathrm{cm}^{-3}_{\mathrm{Cat}}$
$k_{0,j}$	Pre-Exponential Factor of Reaction j	$\mathrm{cm}^3_{\mathrm{Feed}}$ h^{-1} $\mathrm{cm}^{-3}_{\mathrm{Cat}}$
$LHSV$	Liquid Hourly Space Velocity	h^{-1}
$m_{\mathrm{oxygen-equivalent}}$	Mass Fraction of Blended O_2	%
$\dot{m}_i$	Mass Flow of Component i	g min^{-1}
MON	Motor Octane Number	-
n_l, n_e, n_ex, n_p	Number of Lumps, Equations, Experiments, and Parameters	-
p	Total Pressure	bar
p_i	Partial Pressure of Component i	bar
p_v	Vapor Pressure	kPa
R	Ideal Gas Constant	kJ mol^{-1} K^{-1}
R_i^2	Coefficient of Determination of Model i	-
RON	Research Octane Number	-
$S_{\mathrm{iso-C10}}$	Isomerization Selectivity of Durene	-
SSE_i	Sum of Square Errors of Model i	%^{2}
T	Reaction Temperature	°C
T_b	Boiling Temperature	°C
$T_{\mathrm{FB,max}}$, $T_{\mathrm{FB,min}}$	Measured Max and Min Temperature in the Fixed Bed	°C
TOS	Time on Stream	h
T_{Ref}	Reference Temperature for the Arrhenius Equation	°C
T_{Target}	Target Temperature for the Fixed Bed Reactor	°C
T_{25}	Distillation Temperature to Evaporate 25 vol.%	°C
T_{50}	Distillation Temperature to Evaporate 50 vol.%	°C
T_{75}	Distillation Temperature to Evaporate 75 vol.%	°C
t_R	Reaction Time	min

Continued on next page ...

$\dot{V}_i$	Volume Flow of Component i	mL min^{-1}
w_i	Mass Fraction of Component i	%
$WHSV$	Weight Hourly Space Velocity	h^{-1}
X_i	Conversion of Component i	-
$x_{\mathrm{RC,C7}}$	Mole Fraction of C_7 Ring Contraction Products	-
Y_{Gasoline}	Gasoline Yield	%
α	Probability of Error	%
$\Delta H^0_{\mathrm{R},298}$	Enthalpy of Reaction	kJ mol^{-1}
ν_i	Degrees of Freedom of Model i	-
ρ	Density	kg m^{-3}
τ	Space-Time	$\mathrm{cm}^3_{\mathrm{Cat}}$ h $\mathrm{cm}^{-3}_{\mathrm{Feed}}$
φ_{Dist}	Distilled Volume Fraction	%
φ_i	Volume Fraction of Component i	%

List of Tables

2.1 Petrochemical parameters of bioliq® raw gasoline, light gasoline, and heavy gasoline after rectification compared to EN 228. . . . 7
2.2 Catalysts used for the hydroprocessing experiments. . . . 11
2.3 Parameter ranges investigated with the different catalysts. . . . 13

3.1 Properties of oxygenates in comparison to fossil oxygenate-free gasoline . . . 23
3.2 Petrochemical parameters of hydrocarbon streams used for the blending experiments. . . . 25
3.3 Fractions used for the blends A and B. . . . 32

4.1 Hydrocarbon fractions used for the co-hydroprocessing experiments. . . . 38
4.2 Boiling ranges, compositions, and initial mass fractions of the lumps used for modeling. . . . 40
4.3 Pre-exponential factors $k_{0,j}$ and activation energies $E_{A,j}$ of the different models. . . . 49
4.4 Statistical comparison of the reduced model with the sequential and combined model according to Fisher's exact test for the experimental validation dataset at 370 °C. . . . 51

A.1 Composition of bioliq® heavy gasoline as used for Chapter 2. . . . 68
A.2 Petrochemical data obtained by hydroprocessing bioliq® heavy gasoline in a fixed bed reactor under variation of temperature. . . . 69
A.3 Petrochemical data obtained by hydroprocessing bioliq® heavy gasoline in a fixed bed reactor under variation of space velocity and pressure for Pt/HZSM-5. . . . 69
A.4 Composition of product fractions obtained by hydroprocessing bioliq® heavy gasoline in a fixed bed reactor under variation of temperature. . . . 70
A.5 Composition of product fractions obtained by hydroprocessing bioliq® heavy gasoline in a fixed bed reactor under variation of space velocity. . . . 71
A.6 Composition of the bioliq® blend . . . 72
A.7 Petrochemical parameters of the bioliq® blend. . . . 73
B.1 Composition of bioliq® light gasoline. . . . 74
B.2 Composition of heavy gasoline hydroprocessed at 270 °C. . . . 74
B.3 Composition of heavy gasoline hydroprocessed at 310 °C. . . . 75
B.4 Composition of heavy gasoline hydroprocessed at 330 °C. . . . 75
B.5 Composition of the gasoline cut of hydroprocessed Fischer-Tropsch wax. . . . 75
B.6 Composition of bioliq® heavy gasoline as used for Chapter 3. . . . 76
B.7 Composition of blend A. . . . 76
B.8 Composition of blend B. . . . 76
C.1 Measured lump weight fractions at 340 °C, 350 °C, 370 °C, 380 °C and 390 °C for the co-hydroprocessing of 15 wt.% durene and 85 wt.% middle distillate. . . . 79

List of Figures

1.1 Scope of this doctoral thesis. . . . 3

2.1 Production of synthetic gasoline using the bioliq® process. . . . 6
2.2 Schematic flow diagram for upgrading an MTG/DTG gasoline. . . . 8
2.3 Reaction pathways for hydroprocessing of durene. . . . 9
2.4 Flow diagram of the laboratory setup used for the hydroprocessing experiments. . . . 11
2.5 Photographs of bioliq® heavy gasoline, product after hydroprocessing with Pt/HZSM-5 and bioliq® blend. . . . 13
2.6 RON and MON as a function of gasoline yield adjusted by reaction temperature and space velocity. . . . 14
2.7 Gasoline composition as a function of gasoline yield for the experiments conducted under variation of reaction temperature and space velocity for Pt/HZSM-5. . . . 15
2.8 Ring contraction of methylcyclohexane for Pt/HZSM-5 and Pt/Mordenite. . . . 16
2.9 Boiling characteristics E70, E100, E150, and E180 as a function of gasoline yield. . . . 17
2.10 Density and vapor pressure as a function of gasoline yield. . . . 18
2.11 Petrochemical parameters of bioliq® raw gasoline and bioliq® blend in comparison with EN 228. . . . 18

3.1 Boiling curves of bioliq® light gasoline, hydroprocessed heavy gasoline for different processing temperatures and gasoline cut of hydroprocessed Fischer–Tropsch wax. . . . 26
3.2 Influence of blending heavy gasoline hydroprocessed at 270 °C, at 310 °C and at 330 °C into bioliq® light gasoline on the volatility characteristics E70, E100 and the vapor pressure. . . . 27
3.3 Influence of different oxygenates on the volatility characteristics E70, E100, E150, and vapor pressure of bioliq® base gasoline. . . . 29
3.4 Influence of different oxygenates on the boiling curve of bioliq® base gasoline 30
3.5 Influence on boiling characteristics, vapor pressure, and boiling curve for blends of bioliq® base gasoline and methanol with ethanol, MTBE, and ETBE. . . . 31
3.6 Petrochemical parameters and boiling curves of blend A, blend B, and bioliq® light gasoline. 33

4.1 Lumping model with n lumps and m reactions. . . . 37
4.2 Weekly experimental procedure for the parameter study with a feedstock of 85 wt.% middle distillate and 15 wt.% bioliq® heavy gasoline. . . . 39
4.3 Durene conversion and durene isomerization selectivity for the co-hydroprocessing of durene and middle distillate at constant space velocity, and C_{10} aromatic conversion for the co-hydroprocessing of heavy gasoline and middle distillate. . . . 43
4.4 Yield of diesel, kerosene, and light gasoline, cetane number of diesel, and RON and MON of light gasoline for the co-hydroprocessing of heavy gasoline and middle distillate. . . . 45
4.5 Concentration of aromatics and naphthenes in light gasoline in dependence on space-time at 370 °C. . . . 46
4.6 Structures of the sequential model, combined model, and reduced model. . . . 48
4.7 Parity plots of the sequential model and combined model for the experimental validation dataset at 370 °C. . . . 49

4.8 Parity plot and curve fitting results of the reduced model for the experimental validation dataset at 370 °C. 50

A.1 Parity plot of RON and MON for modeled values and measurements taken with a CFR test engine. 68
A.2 C_5 iso-/n-paraffins and C_4 iso-paraffins as a function of gasoline yield for Pt/Mordenite and Pt/HZSM-5. 70
C.1 Durene and C_{10} aromatics conversion at a reference point for the co-hydroprocessing of 15 wt.% durene and 85 wt.% middle distillate. 77
C.2 Durene conversion under variation of temperature for the co-hydroprocessing of 15 wt.% durene and 85 wt.% middle distillate. 77
C.3 Fitting results for the reduced model at 350 °C, 380 °C, and 390 °C for the co-hydroprocessing of 15 wt.% durene and 85 wt.% middle distillate. 78

Preamble

The research presented in this doctoral thesis was carried out at the Engler-Bunte-Institute (EBI) of the Karlsruhe Institute of Technology (KIT) between March 2019 to March 2023. During this time, a total of five peer reviewed articles [1–5] as well as one patent [6] were elaborated as first author and further two peer reviewed articles as second author [7, 8]. The content of the following three publications, i.e.,

- D. Graf, P. Neuner, and R. Rauch, "Hydroprocessing and Blending of a Biomass-Based DTG-Gasoline", *Energy Engineering*, vol. 119, no. 6, pp. 2169–2192, 2022. Doi: 10.32604/ee.2022.022759. [1],
- D. Graf, P. Neuner, and R. Rauch, "Standard-Compliant Gasoline by Upgrading a DTG-Based Fuel through Hydroprocessing the Heavy-Ends and Blending of Oxygenates", *Fuels*, vol. 4, no. 2, pp. 156–173, 2023. Doi: 10.3390/fuels4020010. [2], and,
- D. Graf, J. Waßmuth, and R. Rauch, "Co-Hydroprocessing of Fossil Middle Distillate and Bio-Derived Durene-Rich Heavy Ends under Hydrotreating Conditions", *Reactions*, vol. 4, no. 3, pp. 531–551, 2023. Doi: 10.3390/reactions4030032. [3],

were incorporated in Chapters 2, 3, and 4, respectively, of this thesis. Changes were made to formatting, layout and structure. Additional information were added for a deeper understanding, if available. Tables, figures and citation style have been adapted to the style of this doctoral thesis. When linguistically required, minor changes were made to the text, without altering the original statement. The introductions of Chapters 2, 3, and 4, were shortened from the original publications due to redundancy and partly incorporated in Chapter 1. The publications and respective declarations on the authors' contributions are attached to the end of this doctoral thesis in Appendix D and E.

1 Introduction

1.1 Background and Motivation

Primary energy consumption has risen steadily over the last few centuries, showing an exponential increase since 1940 [9]. While most of the 20th century's demand was met with fossil energy carriers, global warming and its evermore noticeable repercussions urgently call for a greenhouse gas (GHG)-neutral, cross-sector energy supply. The European Union (EU) committed its willingness toward GHG neutrality with the European Green Deal [10]. In June 2021, the European Parliament and Council enforced a binding regulation to all member states to lower the EU's GHG emissions by 55 % until 2030 compared to 1990 [11]. With the 'Fit for 55' action plan, the European Commission has published proposals for adapting laws to the climate targets mentioned above [12] and to pave the way to full GHG-neutrality by 2050.

Transportation is one of the most intensively debated sectors and was recently involved in an incisive decision: the EU-wide ban of cars relying on internal combustion engines by 2035 [13]. However, a ban does not equate to the immediate disappearance of liquid hydrocarbon-fueled vehicles. Especially, aviation and maritime transport will further rely on energy carriers with high energy densities. The EU has recognized this and supports the implementation of synthetic fuels in these sectors [12]. Germany, for example, aims to produce at least 200,000 t a^{-1} of Power-to-Liquid (PTL) kerosene by 2030 [14]. Synthetic fuels will further play an important role during the transition toward technologies such as electrification. Registration rates of electric vehicles were still modest in 2022, e.g., 21 % and 29 % for Europe and China, respectively, as the fastest-growing markets [15]. Moreover, automobiles on European roads are on average twelve years old [16]. Consequently, vehicles relying on liquid hydrocarbon fuels will only gradually disappear, and it is therefore inevitable to supply GHG-neutral synthetic fuels in order to reach the EU's ambitious targets.

Over the last decades, bioethanol and fatty acid methyl esters (FAME) were blended into gasoline and diesel, respectively, to meet the mandatory renewable shares [17, 18]. The blending rate of bioethanol and FAME is limited by the applicable standards to 10 vol.% and 7 vol.%, respectively [19, 20]. Higher shares are possible but may require the adjustment of engine components, as both bioethanol [21, 22] and FAME [23] can cause problems with plastics and metals. Another approach is the blending of GHG-neutral synthetic hydrocarbons. Owing to their similarity to fossil hydrocarbons, the advantage of such synthetic fuels is their unfettered applicability, even in older vehicles, without the necessity for constructional adjustments.

Methanol-to-gasoline (MTG) and dimethyl ether (DME)-to-gasoline (DTG) are processes based on Mobil's discovery for synthesizing high-octane gasoline using a zeolite catalyst [24]. The high octane number (ON) is due to the composition of the fuels, consisting of paraffins, naphthenes, olefins, and, for the largest share, methylated aromatics [25]. Both process variants were already commercialized by Mobil and Haldor Topsøe, respectively [26, 27], producing similar hydrocarbon product ranges [28]. Research is still underway, for example, with the bioliq® pilot plant at the KIT, which produces synthetic gasoline from straw. A decentralized fast pyrolysis is used for biomass liquefaction [29, 30], followed by a centralized entrained flow gasification process [31] and a DTG synthesis [32, 33].

Synthetic hydrocarbons are a great measure to gradually defossilize the refinery sector in its product variety. For example, mineral oil refinery Oberrhein (MiRO) in Karlsruhe, Germany, recently announced plans to integrate such GHG-neutral hydrocarbon streams into its portfolio [34]. Also, Porsche, Siemens Energy, and Exxon Mobil invested in an MTG plant in Punta Arenas, Chile commissioned in December 2022 [35]. During the pilot phase, the plant is expected to produce 130,000 liters per year, which shall be scaled up to 550 million liters per year within the last years of this decade.

Raw products of an MTG or DTG synthesis are usually separated into light gasoline and heavy gasoline to get rid of 1,2,4,5-tetramethylbenzene (durene). Durene is the largest compound occurring in significant amounts of 3–6 wt.% as a consequence of the underlying methanol-to-hydrocarbon mechanism [36]. While the aromatic-rich light gasoline can be easily incorporated into a refinery due to its similarity to fossil reformate, heavy gasoline consists almost entirely of C_9–C_{11} aromatics and is especially rich in durene. Durene tends to crystallize due to its high melting temperature of 79 °C, which bears the danger of clogging the fuel injection system, causing driveability problems [25]. A further reason for cutting off the heavy aromatics is their strong correlation with increased engine-out hydrocarbon [37] and soot emissions [38], one of the main factors for reduced life expectancy worldwide [39].

Besides its drawbacks, heavy gasoline originating from a sustainably operated MTG or DTG plant has a GHG-reduction potential and thus is of high economic value. Consequently, refineries must search for solutions to process streams rich in heavy aromatics and overcome the negative properties.

Involving various reactions, e.g., hydrogenation and dehydrogenation, C–C bond scission, hydrogen transfer, and disproportionation [40], hydroprocessing is a well suited process for precisely tuning physical and chemical properties, depending on the catalyst involved and the reaction parameters. By deftly choosing the catalyst and the process conditions aromatics can be converted into less sooting naphthenes and paraffins [41]. With hydroprocessing being already available in most petrochemical refineries [42], this additionally opens the chance to incorporate bio-based feedstocks into an existing process environment, resulting in more price competitive bio-fuels by saving capital investment as one can draw on an existing processing and blending infrastructure [43–46].

1.2 Objectives and Outline

The main objective of this work is to demonstrate that hydroprocessing is suitable for upgrading heavy gasoline, formed during MTG and DTG synthesis, to a valuable fuel component, using two different processing strategies. As shown in Figure 1.1, this doctoral thesis is structured in three main chapters, whose' main objectives are presented bellow.

Chapter 2: In this chapter, the upgrading of aromatic-rich DTG fuel from the bioliq® process is investigated. MTG and DTG fuels come with two major downsides, they are low in light-boiling components due to their aromatic nature and contain a critical concentration of durene. Current state industrial solutions apply after-treatments such as hydroisomerization or hydrogenation of excess aromatics. Hydroisomerization preserves the heavy nature of aromatic fuels causing emission issues, while hydrogenation bears the risk of lowering the ON. The major disadvantage of both strategies is that they do not challenge the lack of low-boiling components, making additional low-boiling hydrocarbons necessary.

Another approach is investigated in this chapter, where bioliq® raw gasoline is first separated into light gasoline and heavy gasoline. A single hydroprocessing reaction step is applied afterwards to the heavy gasoline to hydrogenate aromatics and simultaneously isomerize hydrogenation products. Three commercially available Pt/Zeolite catalysts, i.e., 0.3 wt.% Pt/Mordenite, 0.3 wt.% Pt/SAPO-11 and

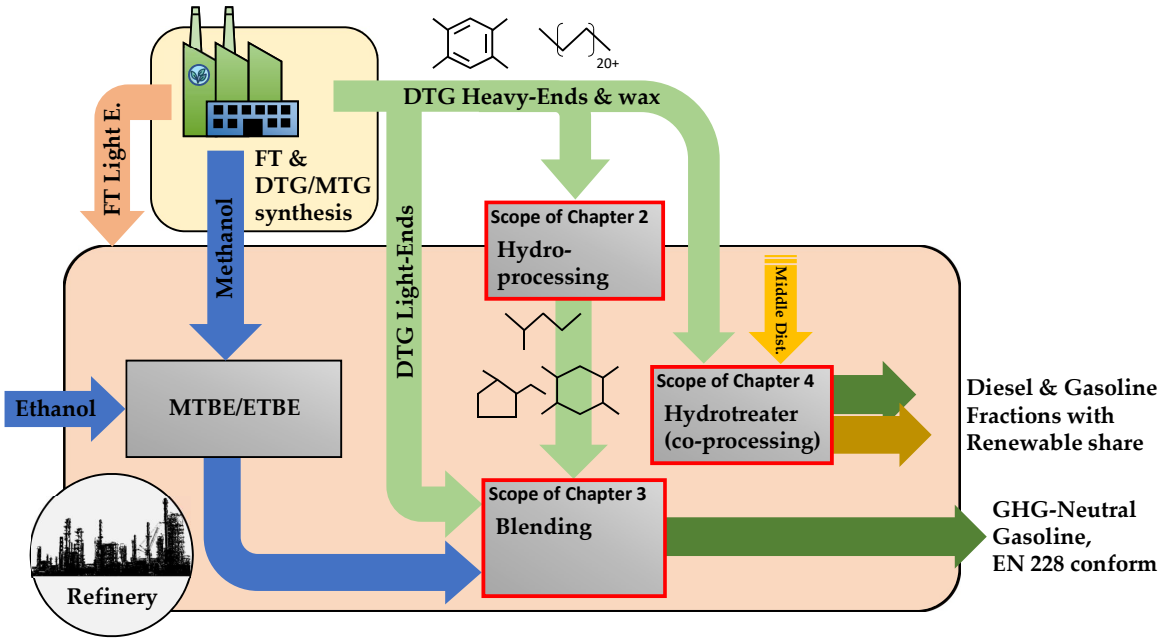


Figure 1.1: Scope of this doctoral thesis.

0.3 wt.% Pt/HZSM-5, were investigated over a wide range of temperature and space velocity. In a final step, hydroprocessed heavy gasoline was back-blended with light gasoline, to provide a DTG-based fuel with improved petrochemical parameters. In this chapter, the following questions are answered:

- *Question 1:* What influence has the catalyst choice on important petrochemical parameters, i.e. volatility parameters as well as research octane number *RON* and motor octane number *MON*?
- *Question 2:* How do process parameters influence petrochemical parameters and which ones are most promising to achieve high ONs?
- *Question 3:* Can an EN 228 compliant gasoline be obtained solely by hydroprocessing bioliq® heavy gasoline followed by back-blending?
- *Question 4:* Which petrochemical parameters are most critical and potentially need to be improved further to meet EN 228?

Based on the results of Chapter 2, the story line is carried on in Chapter 3, taking up the answers to *Question 3* and *Question 4*.

Chapter 3: In this chapter, a blending procedure is developed to supply EN 228 compliant gasoline based on the bioliq® DTG process. Due to high concentrations of aromatics, DTG and MTG fuels are of low volatility and thus scarcely meet EN 228's volatility parameters, i.e. vapor pressure p_v and the boiling characteristics *E*70, *E*100 and *E*150. After-treating procedures to convert parts of the synthetic fuel to lighter components are limited since cracking at severe conditions comes with the downside of increased gaseous losses. A consequent blending is required which has not yet been discussed for the particular case of MTG and DTG fuels in the literature.

For the blending experiments in this chapter, several streams are considered, i.e. bioliq® light gasoline and hydroprocessed heavy gasoline, gasoline of hydroprocessed Fischer-Tropsch (FT) wax as well as the oxygenates methanol, ethanol, methyl tert-butyl ether (MTBE) and ethyl tert-butyl ether (ETBE). Based on the results found in Chapter 2, three gasoline qualities are produced by hydroprocessing

bioliq® heavy gasoline at different reaction temperatures. Subsequent blends were formulated with the mentioned oxygenates, blended as single components and in combination of up to two. Finally, two of the most promising combinations were formulated and its petrochemical parameters fully compared to EN 228. The following questions are approached in this chapter:

- *Question 5:* Which blending components are most contemplable to manipulate the volatility parameters in the desired way?
- *Question 6:* Can a gasoline with high renewable share be blended based on an MTG- or DTG-process?

Chapter 4: A major challenge of renewable fuels is to keep the production costs low for being a real alternative to fossil competitors. A decisive lowering of costs can be achieved by applying existing refinery infrastructure for processing of bio-based feedstocks together with fossil streams.

This chapter discusses the co-hydroprocessing of bio-derived bioliq® heavy gasoline with fossil middle distillate, considering the technical constraints of hydrotreaters in refinery operation. Co-hydroprocessing experiments were conducted with a mixture of bioliq® heavy gasoline (or pure durene) and middle distillate in a laboratory-scale fixed bed reactor using an industrial CoMo/γ-Al_2O_3 catalyst over a wide range of temperature and space-time. Special attention was paid to the reaction parameter dependencies of ONs *RON* and *MON* as well as the cetane number (*CN*) of gasoline and diesel distillates, respectively. Since the composition of a particular product is directly linked to its *RON*, *MON* and *CN*, hydrogenation and isomerization selectivities of durene were investigated. Besides fuel qualities, the quantities of different fuel fractions are of importance to a refinery. Therefore, yields of the high demanded fuels gasoline, diesel and kerosene were also investigated. To make predictions on relevant fuel yields, depending on the processing conditions, a six-lump model with ten parameters was developed, parametrized and validated.

- *Question 7:* Is durene sufficiently hydrogenated or is the isomerization reaction predominant, and which process conditions are favorable?
- *Question 8:* How does co-hydroprocessing of aromatic-rich bioliq® heavy gasoline and middle distillate influence the cetane number *CN* of the diesel fraction?
- *Question 9:* Is a lumping-model sufficiently accurate to predict fuel yields for the co-hydroprocessing of bioliq® heavy gasoline with middle distillate and which model structure is most suitable?

2 Upgrading via Hydroprocessing Using Bifunctional Zeolite Catalysts

2.1 Introduction

In refineries, several upgrading strategies are available or can be integrated, which are: a) transalkylation/disproportionation, b) extraction/crystallization, c) dilution and d) upgrading by hydroprocessing. Processes for transalkylation and disproportionation have already been commercialized, for example with the Mobil TransPlus^{SM} process, which converts heavy aromatics into valuable BTX aromatics [47]. However, transalkylation is not implemented in all refineries. Owing to the increased process demands caused by high reaction temperatures and thermodynamically limited conversion rates, substantial capital investments are required. Crystallization or extraction of durene is promising as it opens synthesis routes with durene as a basic chemical, e.g., the production of polyimides [48]. However, this might only be a long-term solution, as new processes and infrastructure are required. Without major investment, durene could be diluted into other hydrocarbon streams in the refinery by implementing a metering unit. Laboratory tests showed satisfactory engine performances with durene concentrations up to 5 wt.% [25, 36, 49]. A further strategy is the precise adjustment of chemical properties by hydroprocessing. In 2018, Haldor Topsøe announced an isomerization process to upgrade synthetic gasoline [50]. To some extent, isomerization converts durene into other isomers. In this manner, crystallization can be avoided, however, without simultaneously addressing negative emission tendencies. Besides isomerization, hydroprocessing involves various reactions, e.g., hydrogenation and dehydrogenation, C–C bond scission, hydrogen transfer, and disproportionation [40]. By deftly choosing the catalyst and the process conditions aromatics can be converted into less sooting naphthenes and paraffins [41].

The object of this chapter is a process approach in which bioliq®'s heavy aromatics are separated as part of the heavy gasoline, converted by hydroprocessing, and finally blended back with the light gasoline. It is shown how a deft catalyst choice can provide high-quality gasoline free of heavy aromatics like durene. For this purpose, three commercially available Pt/Zeolites, i.e., 0.3 wt% Pt/Mordenite, 0.3 wt.% Pt/SAPO-11 and 0.3 wt.% Pt/HZSM-5, are investigated over a wide range of temperature and space velocity.

2.2 Greenhouse Gas Neutral Gasoline Supply in a Refinery

2.2.1 Processes for the Production of Synthetic Gasoline

For the production of synthetic gasoline, various processes are available, e.g., MTG and DTG, which are indirect catalytic processes using methanol and DME, respectively. Both processes are based on Mobil Oil's discovery in the 1970s that methanol can be catalytically converted to hydrocarbons by a ZSM-5 zeolite [36]. The ZSM-5 zeolite has pores of medium size at relatively high acid strength, which determines its selectivity to products in the boiling range of gasoline [51]. Almost similar product

spectra are observed for the MTG and DTG processes, consisting of paraffins, olefins, and especially methylated aromatics [24]. The bioliq® DTG raw gasoline is characterized by a high concentration of aromatics (approx. 75 wt.%), leading to a low proportion of light ends with boiling temperatures up to 150 °C [52]. Such fuels are suitable for gasoline engines since the high aromatic concentration is accompanied by an increased ON [24, 36]. The aromatic distribution ranges from C_6 to C_{12} and has a maximum at C_8. Depending on the synthesis conditions, the product contains 3 wt.%—6 wt.% of durene, while the concentration in fossil gasoline is only 0.2 wt.%—0.3 wt.% [36].

DTG offers an economic advantage over MTG due to lower investment costs. It is directly based on synthesis gas and does not need methanol as an intermediate product [32]. Furthermore, the increased economic efficiency results from the sequential reactions involved. Methanol formed in the equilibrium Reaction (2.1),

$$CO + 2\,H_2 \rightleftharpoons CH_3OH,\ \Delta H^0_{R,298} = -182\,\mathrm{kJ\,mol^{-1}}, \tag{2.1}$$

reacts directly to DME in Reaction (2.2),

$$CH_3OH \rightleftharpoons CH_3OCH_3 + H_2O,\ \Delta H^0_{R,298} = -23\,\mathrm{kJ\,mol^{-1}}, \tag{2.2}$$

which accelerates the conversion of synthesis gas due to the constant removal of the intermediate product methanol [53]. In addition, the water formed in Reaction (2.2) is converted with carbon monoxide by the water-gas shift Reaction (2.3),

$$H_2O + CO \rightleftharpoons H_2 + CO_2,\ \Delta H^0_{R,298} = -41\,\mathrm{kJ\,mol^{-1}}. \tag{2.3}$$

This further increases the driving force, since the hydrogen formed is involved in the methanol synthesis of Reaction (2.1) [54]. Consequently, the conversion is higher and the resulting recycle flow is lower, further reducing operating costs [55].

The feasibility of direct DME synthesis has already been demonstrated by companies such as JFE Holdings Inc., starting operation in 1999 in Hokkaido, Japan, and Haldor Topsøe A/S in Houston, USA [56]. On a pilot scale, the bioliq® process, developed at the KIT allows the conversion of low-grade lignocellulosic biomass into synthetic fuels [57, 58]. As shown in Figure 2.1, raw materials such as residual waste wood or straw are collected and liquefied in regional fast pyrolysis plants [30]. The fast

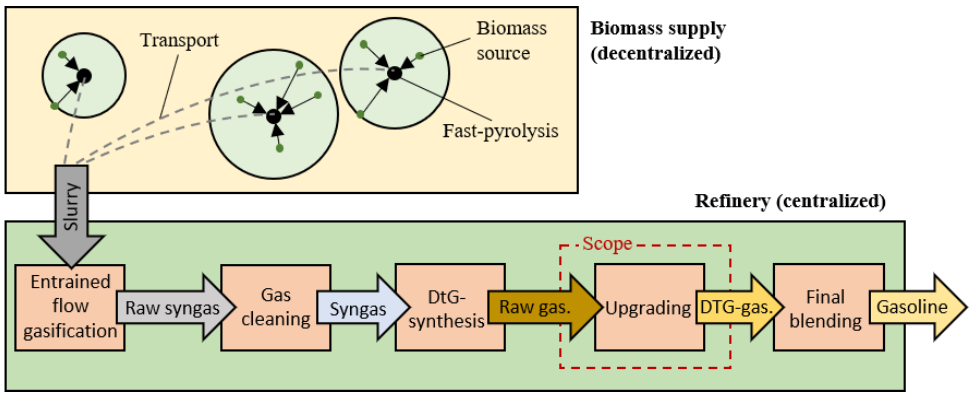


Figure 2.1: Production of synthetic gasoline using the bioliq® process. The biomass supply is decentralized and the DTG synthesis is centralized. Highlighted in red is the scope of this chapter, the upgrading of a DTG gasoline.

pyrolysis produces a slurry with ten times the energy density of the original biomass, resulting in lower transportation costs. In a central refinery, the slurry is converted into raw synthesis gas in an entrained flow gasifier [31]. Particulates and acid gas are subsequently removed in several gas purification stages to supply the refinery with high-quality, sulfur-free synthesis gas [58]. In the bioliq® process,

Table 2.1: Petrochemical parameters of bioliq® raw gasoline, light gasoline, and heavy gasoline after rectification compared to EN 228 [19].

Parameter	EN 228	bioliq® Raw Gasoline	bioliq® Light Gasoline	bioliq® Heavy Gasoline
RON / -	min. 95	N/A	101.7	N/A
MON / -	min. 85	N/A	93.7	N/A
ρ / kg m^{-3}	720.0–775.0	845.76	828.91	891.72
p_v (Class A) / kPa	45–60	45±4	31±5	0.15±0.15
$E70$ / vol.%	22.0–50.0	1.2±0.7	1.1±0.7	0.0
$E100$ / vol.%	46.0–72.0	5.7±0.7	6.4±0.7	0.0
$E150$ / vol.%	min. 75.0	46.4±0.7	85.4±0.7	0.0
FBP / °C	max. 210	245±4	171±4	290±4
φ_{Benzene} / vol.%	max. 1.00	1.2±0.7	1.6±0.7	0.0
$\varphi_{\text{Olefines}}$ / vol.%	max. 18.0	1.3±0.1	1.1±0.1	traces
$\varphi_{\text{Aromatics}}$ / vol.%	max. 35.0	82.3±0.7	76.3±0.7	96.5±0.7
$\varphi_{\text{Oxygenates}}$ / wt.%	max. 3.7	traces	traces	0.0

the synthesis gas is fed to a DTG synthesis to produce raw gasoline [52]. Detailed considerations of efficiency and production cost estimates of the bioliq® process can be found in the work of Haro et al. [56] and Henrich et al. [59]. Regardless of their origin, synthetic DTG fuels do not necessarily meet motor gasoline standards. A further downstream upgrading is inevitably required, after which the upgraded DTG gasoline is piped into a blending unit, where it is mixed with additives such as ethanol or other hydrocarbon streams.

2.2.2 Upgrading Strategy for a Synthetic MTG/DTG Gasoline

In this chapter, DTG gasoline from the bioliq® pilot plant at KIT in Karlsruhe, Germany, was considered. The standard EN 228 must be met for gasoline in Germany [19]. Table 2.1 shows the petrochemical parameters of the raw gasoline as obtained directly from the bioliq® DTG synthesis. Compared with EN 228, it can be seen that the boiling characteristics $E70$, $E100$, and $E150$ are lower than the EN 228 specification limits, indicating a shortage of light ends. These values indicate the volume fraction evaporated at a given temperature during distillation. For example, the measured value $E70$ is the volume fraction evaporated at 70 °C. The aromatic concentration significantly exceeds the permissible upper limit of 35 vol.%. Due to the high aromatic concentration, the density ρ is too high and the vapor pressure p_v is too low. It can be concluded that a stream containing an appropriate high proportion of saturated light ends is required to improve boiling characteristics while lowering the aromatic concentration.

In this chapter it is investigated to upgrade the heavy gasoline in a downstream process by hydroprocessing. As shown in Figure 2.2, the total volume of raw gasoline is split into two-thirds light gasoline and one-third heavy gasoline by an atmospheric rectification. The petrochemical parameters for both fractions obtained by rectification are listed in Table 2.1. Due to its high concentration of aromatics (1.7 vol.% benzene, 17.2 vol.% toluene, 43.2 vol.% xylenes, 15.1 vol.% trimethylbenzens), bioliq® light gasoline is considered a valuable blending component. As shown in Figure 2.2, heavy gasoline is forwarded to a hydroprocessing unit where petrochemical parameters are adjusted accordingly. This fraction is then piped into a blending unit, where it is blended back into the light gasoline. In addition to adjusting the above parameters, RON and MON of the hydroprocessed heavy gasoline should remain

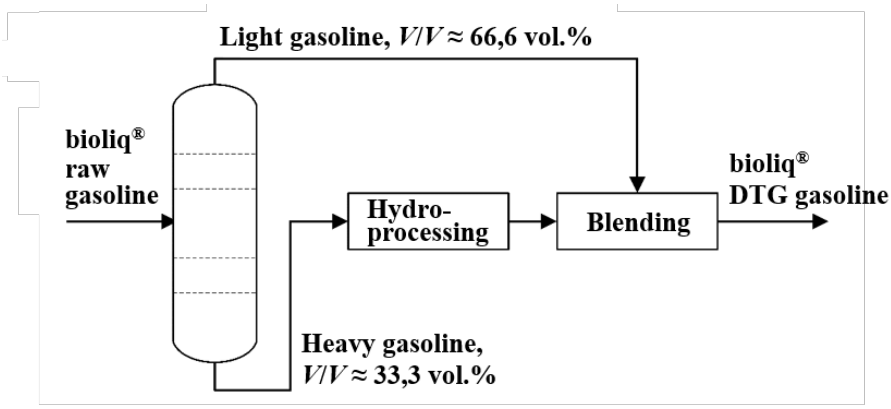


Figure 2.2: Schematic flow diagram for upgrading an MTG/DTG gasoline. The upgrading process consists of a rectification column, a hydroprocessing reactor, and a blending unit that yields the final DTG product by blending the light gasoline and the upgraded heavy gasoline.

as high as possible. Otherwise, there is a risk that the ONs of the blend will fall below the specifications required by EN 228. Maintaining ONs can be challenging because saturated hydrocarbons usually have lower ones than aromatics [60]. If there is no volume loss during hydroprocessing, the ratio of light gasoline to upgraded heavy gasoline must remain 2 : 1 as delivered during rectification. Table 2.1 shows that nearly 97 vol.% (96.95 wt.%) of the heavy gasoline is composed of aromatic hydrocarbons. At approx. 52.6 wt.%, the largest proportion consists of C_{10} (21.4 wt.% durene) and approx. 10.4 wt.% of C_{12} aromatics. Accounting for 33.6 wt.%, the C_9 aromatics have the second largest share. The remaining 3 wt.% are mostly naphthenic. Measured data on the exact feed composition can be found in Table A.1 in the Appendix.

2.2.3 Hydroprocessing of Streams Rich in Heavy Aromatics

Hydroprocessing is a promising process for converting heavy aromatic hydrocarbons into light and saturated molecules. The term hydroprocessing is used for different reactions with hydrogen. Depending on the process conditions and the chosen catalysts, this includes hydrogenation, hydrocracking, and hydroisomerization. Which reaction regime is most promising for a given feedstock depends on how the target petrochemical parameters are to be adjusted.

Depending on the used catalyst, hydrocracking can follow four reaction pathways, i.e., hydrocracking over bifunctional catalysts, hydrogenolysis on metal sites, catalytic hydrocracking on monofunctional catalysts (also referred to as Haag-Dessau mechanism), and thermal hydrocracking [61]. By using a bifunctional metal/zeolite catalyst, hydrocracking allows almost complete hydrogenation of aromatics in one reaction step. Simultaneously, a certain amount of highly branched naphthenes and paraffins are formed [62]. The saturated products have lower boiling temperatures than aromatics with the same number of carbon atoms. A further lowering of the boiling temperatures results from the formation of low-molecular cracking products.

Noble metals are particularly suitable as active sites for deep aromatic saturation. They can achieve high hydrogenation activities even at relatively low temperatures, where the thermodynamic equilibrium is on the side of the saturated products [63]. Therefore, the hydrogen pressure can be kept low. This maintains some flexibility in terms of operating temperature and pressure [64]. The latter is important because biomass-derived fuels are variable and contain a wide range of hydrocarbons that are not easily hydrogenated. With the operating temperature, the yield of light ends can be adjusted. The catalyst

support must be chosen accordingly. Figueras et al. [65] described how the presence of an acidic support induced an electron deficit in palladium and thereby accelerated the benzene hydrogenation. Moreover, Tri et al. [66] explained the influence on the selectivity of co-hydrogenation of a benzene-toluene mixture by the electrophilic character of platinum resulting from the support's acidity. Due to their sufficient acidity, aluminosilicates are beneficial as catalytic supports. More precisely, the subgroup zeolites are in particular suitable for hydroprocessing. An advantage over their forerunners in acid-catalyzed reactions, i.e., amorphous silica-alumina, is the superior acid strength of zeolites [67]. Further beneficial is the possible formation of selectively desired products by steric constraints within their structural environment [68]. Naphthenes, resulting from the hydrogenation of aromatics, can undergo sequential reactions. Mignard et al. [69] studied the reaction of methylcyclohexane (MCH) over a bifunctional Pt/USY catalyst. They observed that naphthenes undergo a ring contraction (RC) reaction, where C_6 rings shrink to C_5 rings while the molar mass remains constant. Figueras et al. [70], studying the RC reaction of MCH over platinum impregnated sulfated zirconias, showed that the distribution of acid strength has the greatest influence on selectivity and activity. Weitkamp et al. [71] also used MCH as probe molecule over Pt/HZSM-5, Pt/CaY, and Pd/LaY, among other naphthenes. Based on the isomer distribution, they demonstrated the shape selective influence of the zeolite structure, as some isomers were not found in the product mixture for HZSM-5. Using a Pt-Ir/ZrO_2-SO_4^{2-} and a pure ZrO_2-SO_4^{2-} catalyst, Belatel et al. [72] suggested that besides an acid site, a metal component also plays an active role in the isomerization process of MCH. The dehydrogenation at the metal site leads to a cycloalkene, which is protonated at a Brønsted acid site, yielding a (cyclic) carbenium ion [61]. RC leads to a variety of isomers that increase with the number of carbon atoms in the naphthene. The isomers differ considerably in their petrochemical parameters such as ON [73] and the boiling temperature, which vary within a certain range.

For a better understanding, Figure 2.3 shows the typical reaction pathways for the hydroprocessing of aromatic hydrocarbons using the example of durene, since it is the substance with the highest concentration in the feed. Reaction (i) shows the hydrogenation of durene, followed by RC in reaction

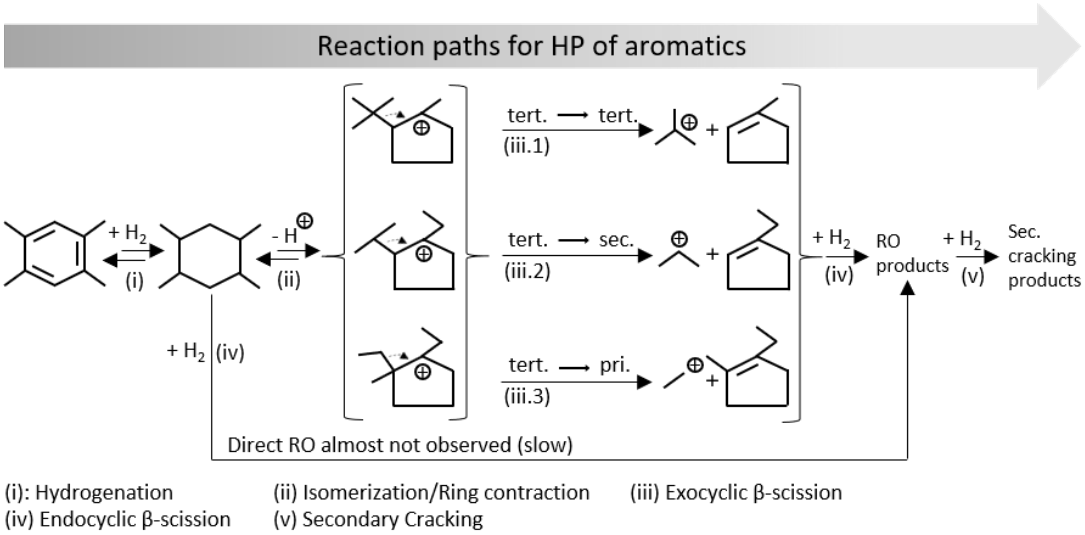


Figure 2.3: Reaction pathways for hydroprocessing of durene, including **(i)** Hydrogenation, **(ii)** Isomerization/RC, **(iii)** Exocyclic β-scission, **(iv)** Endocyclic β-scission, and **(v)** Secondary cracking.

(ii). It should be noted that many other isomers can be formed, e.g., two methyl groups instead of one ethyl group attached to the ring at different positions. As explained above, the distribution is highly dependent on a) the acid strength distribution and b) the shape selective influence of the used

catalyst. Besides hydrogenation and RC, β-scission of endo-and exocyclic carbon-carbon bonds are important reactions in bifunctional hydrocracking. Both reactions proceed via the formation of a carbenium ion. However, it can be stated that endocyclic carbon-carbon bonds are more difficult to break and the reaction is correspondingly slower [74]. Brouwer et al. [75] found the cause in the unfavorable orientation of the p-orbital of a positively charged carbon atom to the C-C bond to be broken. Endocyclic β-scission, also called ring opening (RO), yields paraffins. In general, RC products can subsequently be ring opened. Reaction (ii) shows the rearrangement of carbon atoms, which allows the formation of a stable tertiary cyclic carbenium ion in the ring structure. For naphthenes $\geq C_{10}$, the fast tertiary-tertiary β-scission is the predominant subsequent reaction, yielding an iso-butyl carbenium ion and methylcyclopentene (in case of durene) as products (Reaction (iii.1)). Sullivan et al. [76] referred to this reaction as the paring reaction. Interestingly, the product spectrum of the paring reaction proved to be independent of the isomer configuration of the reactant [77]. It can be concluded that isomerization reactions (endo- and exocyclic alkyl shifts) are faster than exocyclic β-scission. Reactions (iii.2) and (iii.3) describe the tertiary-secondary and the tertiary-primary exocyclic β-scission of a C_{10} naphthene. The resulting secondary and primary carbenium ions lead to the formation of the products propane and ethane after a final hydrogen transfer. In an uninhibited reaction, the rates decrease in the order: tertiary-tertiary > tertiary-secondary > tertiary-primary, according to the stability of the respective carbenium ions. However, this might be influenced by shape selective constraints of the zeolites used on the bulky intermediates. As a result, a slower mechanism incorporating less spacious intermediates may be favored over the fast paring mechanism. Naphthenes $< C_9$ can only follow reaction pathways via the formation of secondary and primary carbenium ions, since tertiary-tertiary exocyclic β-scission is mechanistically hindered.

Bifunctional hydrocracking gained increased interest with the growing demand for fuels. Polynuclear aromatics are the least desirable products in diesel fuels. Besides too high densities, unfavorable cold-flow properties, and low cetane numbers [78], they also exhibit too high emission tendencies. Several approaches exist, one of which is the selective RO to yield products with high *CN*s, while maintaining high fuel yields [78–80]. The same considerations were made for heavy mononuclear aromatics in gasoline. Lower densities, higher ONs, and better combustion characteristics are possible when the rings are opened to form branched paraffins [73, 81–83].

2.3 Materials and Methods

For the experiments in this chapter, a lab-scale hydroprocessing setup with a maximum throughput of approx. 7.2 L d^{-1} was used. As shown in Figure 2.4, a fixed bed reactor with an inner diameter of 14.9 mm, was operated top-down in co-current mode. The reactor was electrically heated using three heat brackets. A central probe tube with an outer diameter of 1/8″ was available to measure the catalyst bed temperature by axially moving a K-type thermocouple.

Clariant Produkte (Deutschland) GmbH loaded the three pelletized commercial catalysts with 0.3 wt.% platinum. The hand-grinded and sieved 100–200 µm fraction was diluted with silicon carbide of the same particle size distribution in a ratio of approx. 1 : 2 (V/V) and filled into the reactor between two further layers of pure silicon carbide. Table 2.2 lists the catalysts used in this work. Catalyst bulk densities, and thus bed heights, varied due to the manual grinding process. Since the activity of Pt/SAPO-11 was the lowest observed, the catalyst mass was increased. This resulted from the need to produce large sample quantities for the analysis of the petrochemical parameters.

The feed was placed in a storage tank tempered to 50 °C to keep the durene dissolved. To build up the reaction pressure on the liquid side and to pipe the heavy gasoline at a flow rate of 0.01–5.00 mL

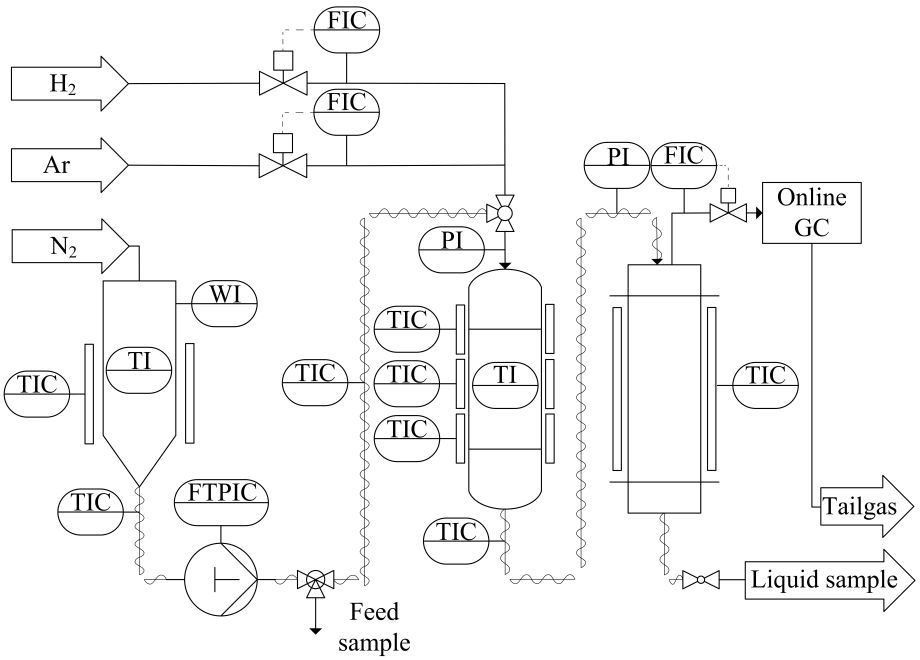


Figure 2.4: Flow diagram of the laboratory setup used for the hydroprocessing experiments.

min^{-1}, a Bischoff (Leonberg, Germany) HPD pump–Multitherm 3351 heated to 50 °C was used. In addition to the liquid feed, the gas was also fed to the top of the reactor. H_2 with a purity of 99.999 % was metered with a Bronkhorst (Ruurlo, NL) EL-Flow® Select mass flow controller (MFC) and premixed with the liquid phase in the first 20 cm of the fixed bed, which consisted of pure silicon carbide and was tempered to reaction temperature. In a downstream separator with a volume of approx. 800 mL, the liquid-gas product mixture was separated at ambient temperature and reaction pressure. The liquid product was drawn off at the bottom of the separator via a cooling coil tempered to 0 °C, in order that no noticeable pressure drop occurred in the reactor.

The extracted liquid product was stored gas-tight at below 0 °C and analyzed offline according to the parameters specified in EN 228. A Reformulyzer M4 from the company PAC (Houston, TX, USA) and an Agilent (Santa Clara, CA, USA) gas chromatograph (GC) 7890A calibrated according to ASTM D6730–01 [84] were used to measure the compositions of the liquid hydrocarbon samples. The Reformulyzer M4 provided a comprehensive insight into the sample by having the instrument distinguish between groups of substances and the number of carbon atoms. To measure individual components, e.g., the concentration of durene, the Agilent 7890A GC was used as a complementary method.

RON and *MON* were determined following ISO 5164 [85] and ISO 5163 [86], respectively, by PetroLab (Speyer, Germany), using a frequently inspected Cooperative Fuel Research (CFR) test engine. In

Table 2.2: Catalysts used for the hydroprocessing experiments.

Metal and Zeolite	**Metal loading m_M / wt.%**	**Catalyst mass m_{Cat} / g**	**Catalyst bed height h_B / mm**
Pt/HZSM-5	0.3	12.694	405
Pt/Mordenite	0.3	12.689	466
Pt/SAPO-11	0.3	20.005	453

addition, ONs were measured using a PAC OptiFuel based on an Fourier-Transform Infrared (FTIR) measurement followed by automatic spectrum analysis. Since the hydrocarbon mixtures studied were either rich in aromatics (feed) or naphthenes (products), the model underlying the OptiFuel was extended as part of the work. ONs measured with a CFR test engine were used to train the new model, and a certain number of samples were retained for validation. An error of ±4 and ±2 could be determined for *RON* and *MON* using the validation samples, respectively, which can be comprehended in the parity plot shown in Figure A.1 in the Appendix.

The calculation of *E*70, *E*100, and *E*150 values according to EN 228 was based on the boiling curve measured with a PAC OptiDist calibrated according to ASTM D86 [87] for sample volumes > 100 mL or a PAC OptiPMD calibrated according to ASTM D7345 [88] for sample volumes < 100 mL. By interpolation between two measuring points recorded with a resolution of 1 vol.%, *E*70, *E*100, and *E*150 were calculated.

The vapor pressure was measured using a PAC Herzog HVP 972 according to ASTM D6378 [89] at 37.8 °C. Finally, the density was measured at 15 °C according to a self-developed method utilizing a Mettler-Toledo (Greifensee, CH) D5. The gas stream leaving the separator was directed to a Bronkhorst EL-Press® MFC, which was used to control the reaction pressure. Subsequently, it was depressurized to atmospheric pressure and fed into an Agilent 7890A GC. To calculate the mass balance, argon with a purity of 99.999 % was fed as internal standard into the top of the reactor, using a Bronkhorst EL-Flow® Select MFC. Based on the change in argon concentration due to the reactions between the feedstock and hydrogen, the total outlet volume flow could be calculated.

Additional experiments were conducted in a self-designed batch reactor. The reactor was equipped with a hydrogen inlet by which the reaction pressure was adjusted. A heating jacket provided the necessary heat, while there was no cooling option. The hydrogen was dispersed into the liquid phase with a self-priming stirrer operated at 800 min^{-1}. Liquid samples were taken after predefined time intervals and analyzed offline using the Agilent 7890A GC as described above. A model mixture of 27.1 wt.% toluene, 31.2 wt.% xylene isomers, 35.3 wt.% 1,2,4-trimethylbenzene and 6.3 wt.% 1,2,4,5-tetramethlybenzene was used as feed. For each experiment, 0.3 g catalyst with a particle size distribution of 20–63 µm was added to 70 g of feed. All measurements were repeated whenever possible and statistically evaluated according to the student's t-distribution, assuming a 95 % confidence interval.

2.4 Results and Discussion

2.4.1 Adjustment of Petrochemical Parameters

As shown in Figure 2.5, several gasoline qualities were produced by hydroprocessing bioliq® heavy gasoline with a fixed bed reactor to investigate how the petrochemical parameters can be adjusted. Figure 2.5a shows the heavy gasoline stored at approx. 20 °C (left) and 0 °C (right). A representative product fraction after hydroprocessing can be seen in Figure 2.5b. Comparing the mentioned photographs qualitatively shows the effect of hydroprocessing the heavy gasoline. While durene forms crystals in the heavy gasoline at 0 °C there is nothing such observed after hydroprocessing.

For each experiment, a target temperature T_{Target} for the catalyst bed was set. Due to the exothermic nature of the hydrogenation reaction, it was not possible to provide fully isothermal conditions. $T_{FB,min}$ and $T_{FB,max}$ are the minimum and maximum temperatures measured in the fixed bed and provided in Table A.2 in the Appendix, if measured. As explained in the theoretical part on hydroprocessing, cracking reactions lead to the formation of gaseous products, which reduces the yield of products in

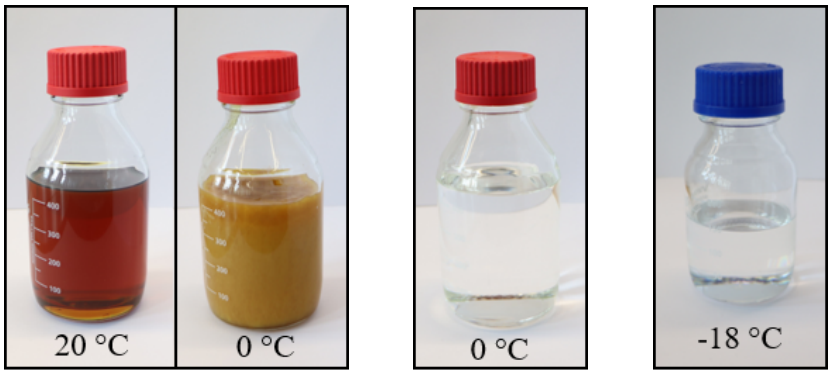


Figure 2.5: **(a)** bioliq® heavy gasoline, **(b)** product after hydroprocessing with Pt/HZSM-5 (p =50 bar, T = 270 °C and weight hourly space velocity $WHSV$ = 1.39 h^{-1}) and **(c)** bioliq® blend as discussed in section 2.4.2, stored at temperatures as indicated in the respective images.

the boiling range of gasoline. The decision for a particular operating point is therefore not based solely on the maximum achievable quality of the product, but requires a comparison to the gasoline yield,

$$Y_{\text{Gasoline}} = \frac{\dot{m}_{\text{Gasoline}}}{\dot{m}_{\text{Feed}}}. \tag{2.4}$$

Therefore, the petrochemical parameters to be optimized are discussed as a function of the gasoline yield. The pressures for the experiments were set to achieve an almost complete conversion of the aromatics. Table 2.3 shows the parameter ranges investigated for each catalyst. The Pt/HZSM-5 catalyst exhibited the highest hydrogenation activity, based on the applied pressures. An almost complete conversion of aromatics was already achieved at a pressure of 50 bar. For the other catalysts Pt/SAPO-11 and

Table 2.3: Parameter ranges investigated with the different catalysts.

	Pt/HZSM-5	**Pt/Mordenite**	**Pt/SAPO-11**
T / °C	230–330	250–270	270–350
p / bar	50–70	90	90
$WHSV$ / h^{-1}	0.84–2.66	1.39	1.39 and 0.88

Pt/Mordenite, a pressure of up to 90 bar was required. Due to equilibrium limitations at temperatures of ≥ 310 °C, the $WHSV$ had to be additionally reduced from 1.39 h^{-1} to 0.88 h^{-1} for Pt/SAPO-11.

Data obtained from CFR motor experiments and FTIR measurements are used for evaluating *MON* and *RON*. The standard deviation of ±4 for *RON*-FTIR measurements is considered too high for a solid discussion. Therefore, these data are not used in this study, and no *RON* values can be reported for experiments with Pt/SAPO-11 since no CFR measurements were performed. The ONs measured in this study, as a function of various parameters, are displayed in Figure 2.6. Figure 2.6a shows the *MON* and *RON* as a function of the gasoline yield. Pressure and space velocity were kept constant during the experiments, while the gasoline yield was adjusted by varying the reaction temperature. The corresponding data can be found in Table A.2 in the Appendix. Throughout the investigated parameter range, *MON* consistently exceeds *RON*, which is probably due to the samples' high C_9 and C_{10} naphthene content [90]. For Pt/HZSM-5, the *MON* increases by 3.5 between gasoline yields of 99 wt.% and 78 wt.%, whereas the *RON* increases by only by 1.1. Compared to a *MON* of 85, as required by EN 228, the measured values of up to 80 are promising. On the other hand, measured *RON* values of

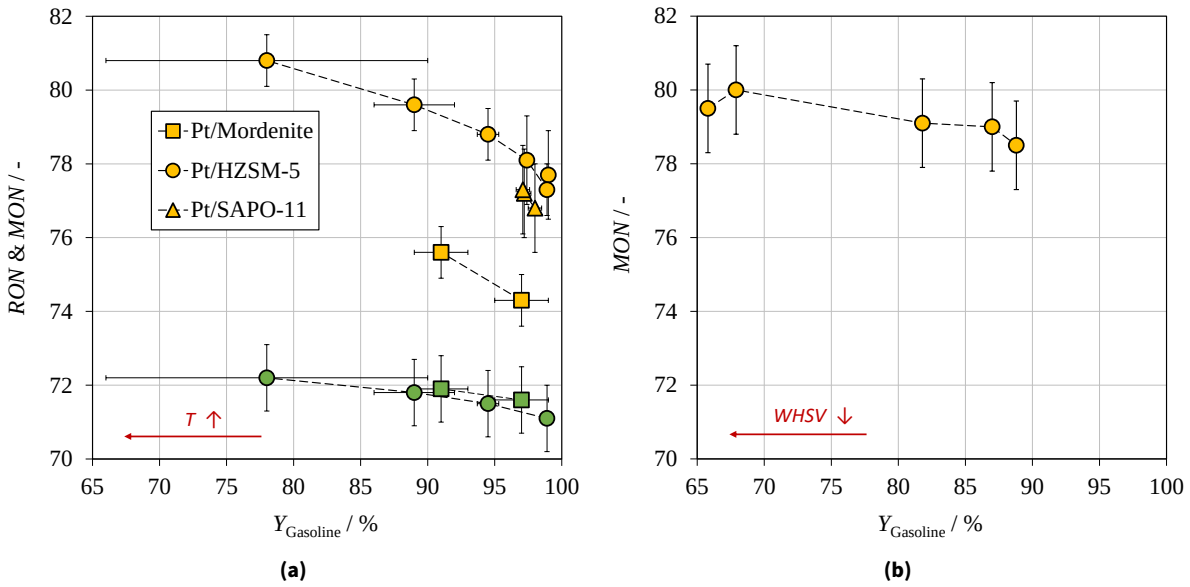


Figure 2.6: *RON* (green symbols) and *MON* (yellow symbols) as a function of gasoline yield, adjusted **(a)** by reaction temperature and **(b)** by space velocity. Experiments with Pt/Mordenite, Pt/HZSM-5, and Pt/SAPO-11 were performed in a fixed bed reactor. Parameters and measurements listed in Table A.2 (*T* variation) and Table A.3 (*WHSV* variation) in the Appendix.

up to 72 do not meet 95 as demanded by the standard. However, it can be stated that the overall *RON* and *MON* values are favorable, as naphthenes larger than C_9 typically exhibit values below 35 and 30, respectively. [91].

MON varies depending on the catalyst used. It can be observed that *MON* increases in the order: Pt/HZSM-5 > Pt/SAPO-11 > Pt/Mordenite. The selective isomerization of naphthenes explains these results since, especially at high gasoline yields of 97 wt.%–100 wt.%, hardly any paraffins are formed besides a negligible concentration of aromatics. McVicker et al. [92] found the same order as reported above for the RC of MCH expressed as the 1, 2-dimethylcyclopentane (DMCP)/1, 3-DMCP ratio. For Pt/HZSM-5, almost no 1, 2-DMCP was formed, whereas the isomer distribution was almost in equilibrium for Pt/Mordenite. In conclusion, the differences in *MON* values can clearly be attributed to the shape selective influence of the catalysts.

In contrast to *MON*, no dependency on the catalyst selectivity is evident for *RON* in the studied parameter range. The values obtained by the CFR engine are nearly congruent for Pt/Mordenite and Pt/HZSM-5. This is probably due to the less harsh test conditions for *RON* measurements, since the degree of isomerization and thus the thermal stability of the molecule does not play such a crucial role. In addition, the produced samples do not correspond to any standard fuel. The sample matrix and thus the high content of naphthenes must be considered. Considering the *MON* values for Pt/SAPO-11 lying between those of the other two investigated catalysts, it can be assumed that the *RON* values for Pt/SAPO-11 are comparable to those of Pt/Mordenite and Pt/HZSM-5.

Figure 2.6b shows the *MON* for a constant reaction temperature of 330 °C at a pressure of 60 bar for Pt/HZSM-5 under variation of *WHSV*. In contrast to Figure 2.6a, *MON* does not increase as distinct. Figure 2.7 shows the gasoline composition for both experiments carried out with Pt/HZSM-5 under variation of temperature (yellow symbols) and space velocity (green symbols). The fractions can be described with sufficient agreement by straight lines. In the experiments under variation of *WHSV* (green symbols), the increasing yield of iso-paraffins does not drive the ONs as expected (Figure 2.6b).

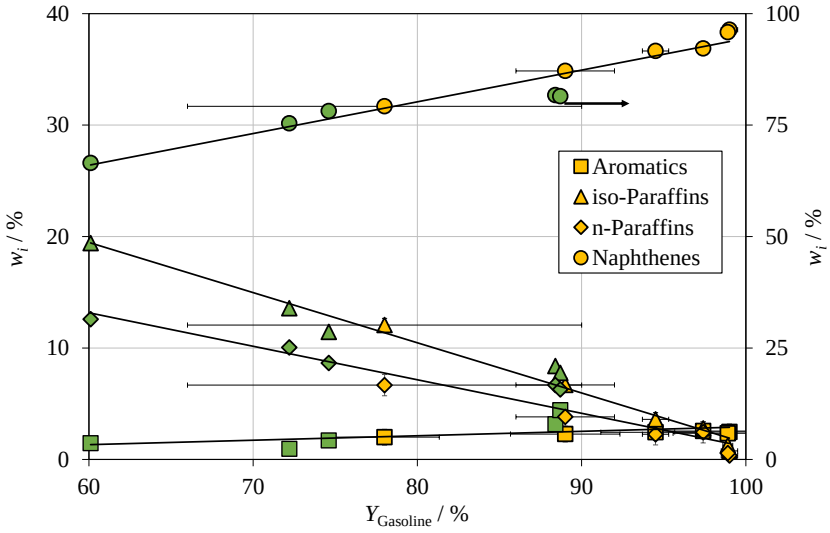


Figure 2.7: Gasoline composition as a function of gasoline yield for the experiments conducted under variation of reaction temperature (yellow symbols) and *WHSV* (green symbols). Experiments were performed with Pt/HZSM-5 in a fixed bed reactor. Parameters and measurements are listed in Table A.4 (*T* variation) and Table A.5 (*WHSV* variation) in the Appendix.

It is believed that the RC of naphthenes due to elevated reaction temperatures is responsible for the observed increase in the ONs, rather than the iso-paraffin yield. As described in Section 2.3, additional hydroprocessing experiments were performed in a batch reactor with a model mixture of aromatics. The RC of C_7 naphthenes,

$$x_{RC,C7} = \frac{\sum x_{DMCP-isomers} + x_{ECP}}{\sum x_{C7-naphthenes}}, \tag{2.5}$$

is calculated to prove this statement. RC of MCH is a well-known model reaction in the literature due to the accessible product spectrum [60, 69, 71, 73, 92]. During RC of MCH (hydrogenation product of toluene), DMCP isomers and ethylcyclopentane (ECP) are formed. Figure 2.8 shows the RC as a function of time (Figure 2.8a) and reaction temperature (Figure 2.8b) for Pt/HZSM-5 and Pt/Mordenite. No RC was observed for Pt/SAPO-11 in the investigated temperature range. It is remarkable how fast the RC products in Figure 2.8a for Pt/HZSM-5 reach a steady state, while the RC reaction for Pt/Mordenite still proceeds after four hours. This can be linked to the observations in Figure 2.6b, where no clear dependence of *MON* on *WHSV* is seen for Pt/HZSM-5. In Figure 2.8b, the temperature influence is shown on RC. The RC products increase over reaction temperature for both catalysts, which is especially pronounced for Pt/Mordenite. A dependence on reaction temperature was also described by Belatel et al. [72]. The degree of secondary isomerization of ECP to DMCP was strongly connected to the reaction temperature in their experiments. Overall, it is concluded that the RC of naphthenes, originating from the primary hydrogenation of aromatics and from exocyclic β-scission, is responsible for increased ONs.

One main objective of this chapter is the production of light ends from heavy gasoline. The description of involved hydroprocessing reactions in Figure 2.3 is recommended to better understand the following discussions of cracking mechanisms. Figure 2.9 illustrates the boiling characteristics *E*70, *E*100, and *E*150 as defined according to EN 228 and the additional value *E*180. *E*150 and *E*100 benefit most clearly from cracking. At a gasoline yield of 90 % using Pt/HZSM-5, the *E*150 increases to almost 40 vol.%. A similarly sharp rise is observed for Pt/Mordenite. However, only two points were measured here. Pt/SAPO-11, on the other hand, shows only a slight cracking activity in the investigated temperature range. Most probably, the sharp increases in *E*150 and *E*100 are due to fast tertiary-tertiary exocyclic β-scission

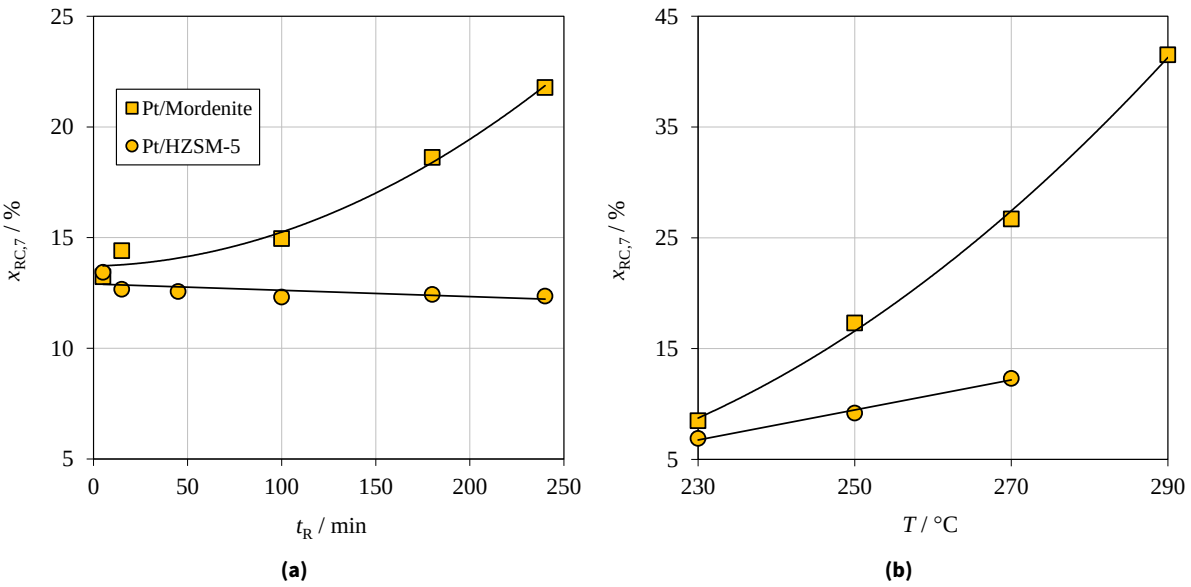


Figure 2.8: RC of MCH at a pressure of 50 bar for Pt/HZSM-5 and Pt/Mordenite measured in a batch reactor **(a)** as a function of reaction time at a temperature of 270 °C and **(b)** as a function of temperature for a reaction time of 100 min.

(paring reaction) of C_{10} naphthenes resulting in the production of C_6 naphthenes and iso-butane. The slightly higher $E100$ for Pt/HZSM-5 than for Pt/Mordenite for all measured data points can be attributed to the shape selective influence of the zeolites. The narrower pores of HZSM-5 sterically hindered the paring reaction. On the one hand, this was verified by a higher yield of C_5 paraffins in the product spectrum, which were significantly lower with Pt/Mordenite. On the other hand, iso-butane yield was clearly higher for Pt/Mordenite underlining the presence of the paring reaction (see Figure A.2 and Tables A.4 and A.5 in the Appendix). C_5 paraffins are formed by the slow direct RO of C_9 and C_{10} naphthenes, followed by secondary cracking of the resulting paraffins. Direct RO results in a higher gasoline yield because less C_4 is formed. The same applies to the $E70$, which also benefits from an increased C_5 yield. The $E150$ also benefits from the slower tertiary-secondary and tertiary-primary exocyclic β-scission. This was verified by a high yield of C_6–C_8 naphthenes and corresponding ethane and propane in the product stream. The difference between the bioliq® raw gasoline and EN 228 is particularly pronounced in the case of $E70$ and is therefore the most crucial parameter. The proportion of light ends with a boiling temperature of up to 70 °C is 1.2 vol.%, while the standard requires at least 22 vol.% (see Table 2.1). This parameter increases slowly for a decreasing gasoline yield and rises sharply at approx. 88 wt.%. The observed is probably due to the slow endocyclic β-scission (RO) of C_6 naphthenes previously formed by exocyclic β-scission, producing hexanes (see Table A.4 in the Appendix). From a process engineering point of view, the range below a mass yield of 90 % is excluded because of the high carbon loss due to cracking.

Table 2.1 shows further optimization potential for density and vapor pressure of bioliq® raw gasoline, which are too high and too low, respectively. Figure 2.10 shows how density and vapor pressure change with gasoline yield. An almost linear correlation with gasoline yield can be observed for both parameters. Density decreases and vapor pressure increases as a result of cracking reactions. Low molecular ring structures and paraffins lead to the observed trends in Figure 2.10, which can also be comprehended in Figure 2.7. There is little influence of the catalysts used on both parameters. For Pt/SAPO-11, a slightly higher density and lower vapor pressure result from lower cracking activity, as it was already concluded in Figure 2.9.

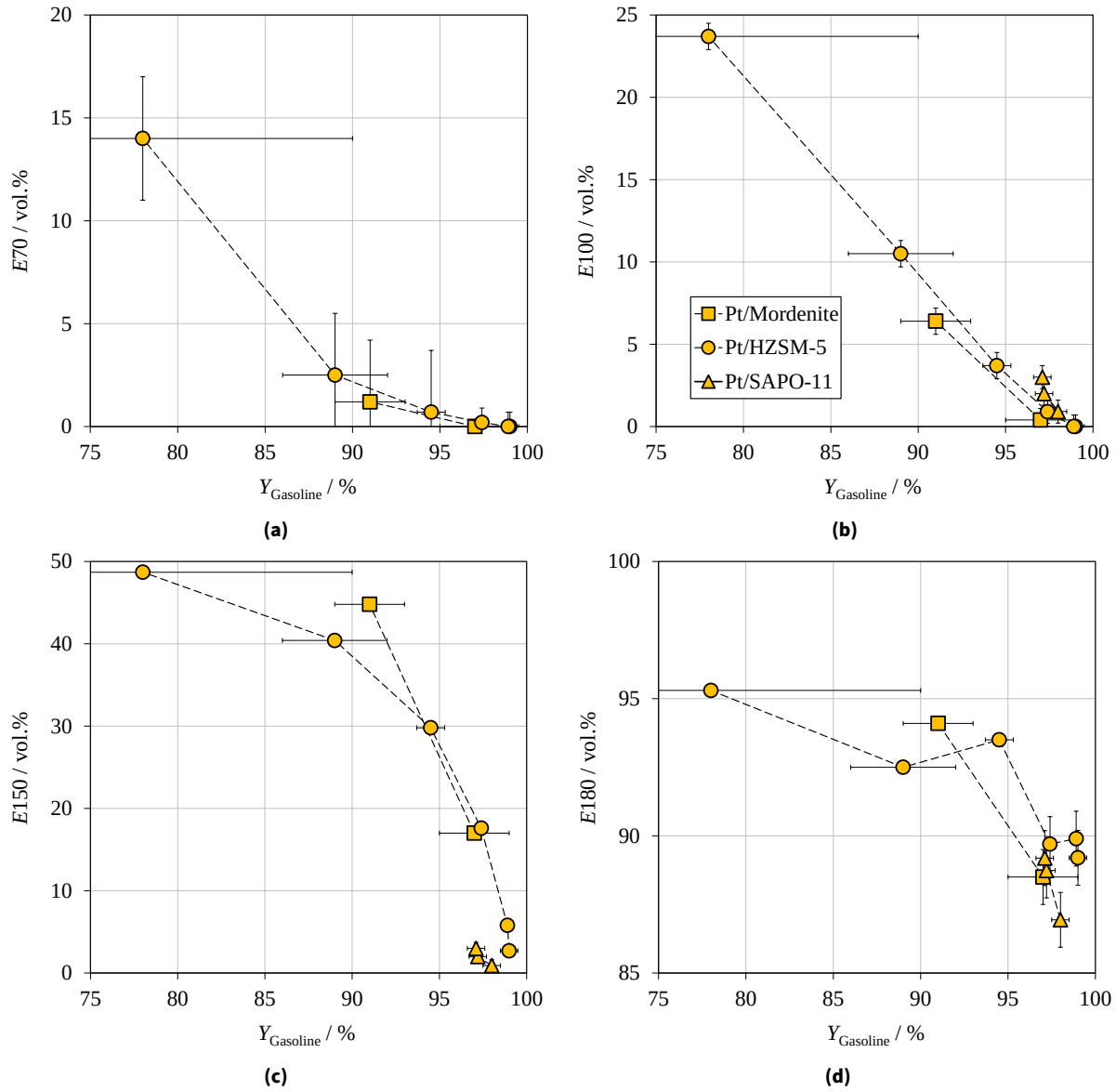


Figure 2.9: Boiling characteristics **(a)** *E*70, **(b)** *E*100, **(c)** *E*150, and **(d)** *E*180 as a function of gasoline yield. Experiments were performed with Pt/Mordenite, Pt/HZSM-5, and Pt/SAPO-11 in a fixed bed reactor under variation of reaction temperature. Parameters and measurements are listed in Table A.2 in the Appendix.

2.4.2 Blending

For a final discussion, blending experiments with bioliq® light gasoline and upgraded heavy gasoline were conducted. Heavy gasoline was upgraded in a fixed bed reactor with a capacity of 1 L h^{-1} filled with 0.3 wt.% Pt/HZSM-5 pellets. The product quality was comparable to that obtained in the lab-scale experiments discussed above, with the exception that it was rectified to an *FBP* of approximately 170 °C. The bioliq® blend consisted of two-thirds light gasoline and one-third upgraded heavy gasoline, as this was the original volume ratio of light gasoline to heavy gasoline after separation following the bioliq® DTG synthesis.

All relevant data, such as composition, can be found in Tables A.6 and A.7 in the Appendix. An image of the final blend at -18 °C is shown in Figure 2.5c. No crystals formed as a result of durene removal,

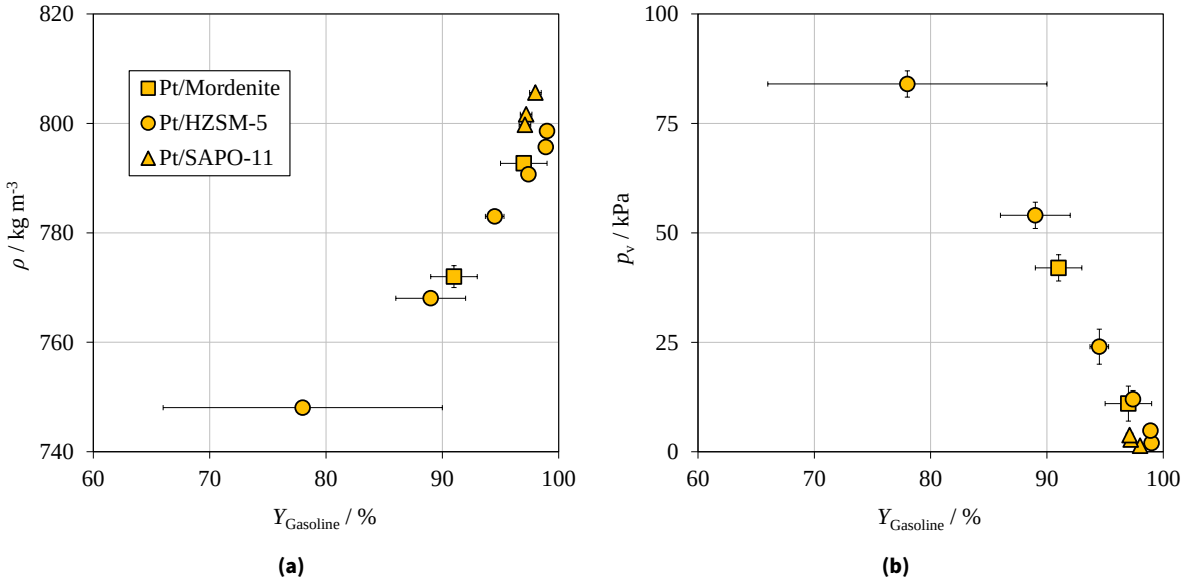


Figure 2.10: **(a)** Density and **(b)** vapor pressure as a function of gasoline yield. Experiments with Pt/Mordenite, Pt/HZSM-5, and Pt/SAPO-11 were performed in a fixed bed reactor under variation of reaction temperature. Parameters and measurements are listed in Table A.2 in the Appendix.

indicating the gasoline's operability under cold conditions. Figure 2.11 shows bioliq® raw gasoline in comparison with the blend. The most obvious change can be seen for the *FBP*, which results from the applied rectification. The aromatic concentration was relatively reduced by 37.5 %, but remained too high compared to EN 228. With the removal of most heavy aromatics and the lower *FBP* in general, a significant decrease in engine-out emissions is expected. The ONs of the blend decreased because the ones of upgraded heavy gasoline were lower than those of bioliq® light gasoline. However, both remained within the minimum values of the standard. A slight improvement is observed in the density, which has decreased but still does not fall within the permissible range specified by EN 228. The boiling characteristics *E*70, *E*100, and *E*150 could also be improved. In particular, *E*150 has increased

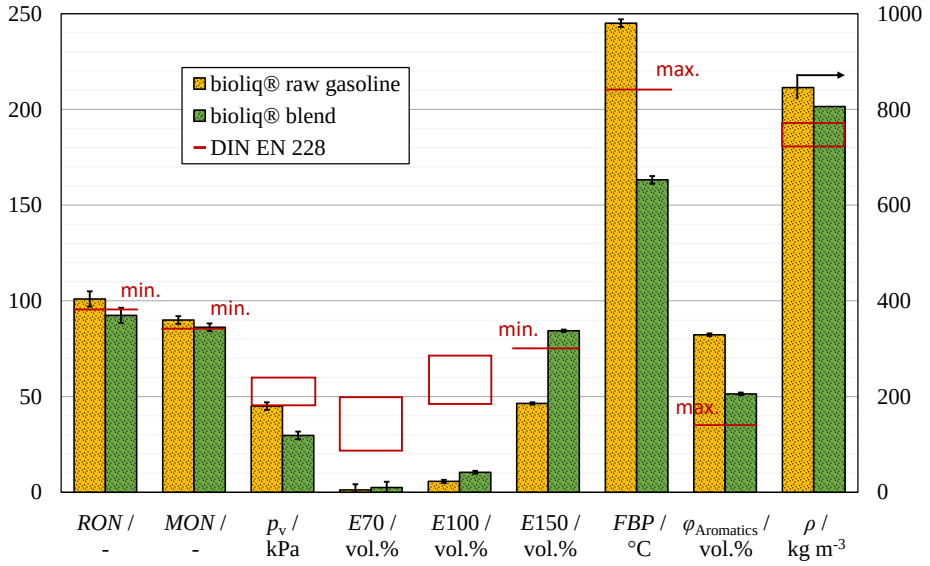


Figure 2.11: Petrochemical parameters of bioliq® raw gasoline and bioliq® blend in comparison with EN 228.

significantly and meets the minimum value specified in the standard. The *E*70 and *E*100 values improved slightly but still remain below the lower limits specified by EN 228. When density and vapor pressure are additionally taken into account, it becomes evident that additional low-boiling components are required to meet the standard.

In EN 228, up to 3.7 wt.% of O_2-equivalent oxygenates are allowed depending on the substance. Ethanol is the most common species and is limited to 10 vol.%. In contrast, MTBE and ETBE can be blended with gasoline at almost 22 vol.%, having boiling temperatures of 55.2 °C and 73 °C, respectively. With these considerations, *E*70 could possibly reach 22 vol.%, as specified by EN 228. For adjusting the *E*100, an additional blending stream is necessary, since it is almost 36 vol.% below the minimum value of 46 vol.% defined in EN 228. Methanol to olefin (MTO) products or light ends from hydrocracked FT waxes are potentially renewable and available in a future refinery. The latter offers the possibility of co-hydroprocessing with bioliq® heavy gasoline.

2.5 Summary and Conclusions

In this chapter, the single-stage upgrading of aromatic-rich heavy gasoline from the bioliq® process is investigated. Heavy gasoline is separated from light gasoline and hydroprocessed using three different Pt/zeolites. Among the investigated catalysts, Pt/HZSM-5 performs the best for the purpose presented. With Pt/HZSM-5 the highest ONs are achieved, which is most likely due to selective RC at elevated temperatures. There is almost no difference in the yield of light ends between Pt/HZSM-5 and Pt/Mordenite. Pt/SAPO-11 shows only little cracking activity. In addition to the complete hydrogenation of aromatic hydrocarbons, light ends with boiling temperatures of up to 150 °C (*E*150) and 100 °C (*E*100) increase by approx. 40 vol.% and 10 vol.%, respectively, at a gasoline yield of 90 wt.%. Light ends are produced by fast tertiary-tertiary exocyclic β-scission, forming C_6 naphthenes and iso-butane. Moreover, the slower tertiary-secondary and tertiary-primary exocyclic β-scission, in which C_6–C_8 naphthenes and corresponding ethane and propane are formed, lead to a sharp increase in *E*150. Further RO results in a slight increase in the fraction of light ends with boiling temperatures of up to 70 °C (*E*70).

The petrochemical parameters of the bioliq® DTG gasoline improve significantly by blending of the upgraded heavy gasoline with light gasoline. The *E*150 and *FBP* of the bioliq® blend meet EN 228. The aromatic content is 37.5 % lower than in the bioliq® raw gasoline, which significantly improves the suitability as a drop-in in fossil fuel. A standard-compliant stand-alone fuel is not achieved since a total aromatic concentration of 51.4 vol.% exceeds the maximum limit of 35 vol.%. The high aromatics content is also responsible that the volatility parameters E70 and E100 in particular, remain well below the minimum limit of EN 228, as they depend on low-boiling components. This leads to the conclusion that a more comprehensive blending concept, which also includes oxygenates, is required.

3 Advanced Blending Concept

3.1 Introduction

To date, the highest renewable share in the fuel market is covered by blending biogenic ethanol [18]. However, the share of bio-ethanol in gasoline can only be increased with limitations. Ethanol can lead to corrosion problems of engine parts [21, 22], for example, the fuel injection delivery system [93]. Furthermore, blending rates of alcohol might result in the swelling or stiffening of polymeric materials, as used for O-rings and hoses [21, 22]. Therefore, vehicles must be suitable for blends with high shares of ethanol or must be modified. The mentioned issues limit the potential impact of alcohol–gasoline blends, as a large share of the fleet is left out due to incompatibility. Besides blending single oxygenates, there is the approach to replace fossil gasoline with a renewable gasoline-like synthetic hydrocarbon mix. The clear advantage is that a vehicle's engine does not need to be modified, as synthetic fuels are chemically similar and meet the required standard. Therefore, such an approach provides a solution for all systems relying on fossil gasoline. Processes for the synthesis of hydrocarbons in the boiling range of gasoline are the FT synthesis, the MTG synthesis, and the further developed DTG synthesis. Porsche, Siemens Energy, and Exxon Mobil, for example, invested in an MTG plant in Punta Arenas, Chile commissioned in December 2022 [35]. During the pilot phase, the plant is expected to produce 130,000 liters per year, which shall be scaled up to 550 mil liters per year within the last years of this decade. These processes, however, do not directly produce standard-compliant gasoline and consequently require an after-treatment and sophisticated blending concept.

This chapter presents an after-treatment and blending route based on a DTG process to provide gasoline with a high renewable share, which can replace fossil gasoline without constraints. Firstly, the requirements on EN 228 are discussed and the challenges to meet the standard are highlighted. In this regard, it is shown that hydroprocessing can help to convert heavy-ends into low-boiling blending components. Further, options are discussed in which a deliberated combination of oxygenates plays a major role in adjusting the boiling characteristics. Finally, a blend and its petrochemical parameters, which can be easily implemented based on an MTG or DTG synthesis and a regular blending infrastructure, is discussed.

3.1.1 Requirements for Synthetic Gasoline to Meet EN 228

The use of fuels in internal combustion engines is linked to compliance with standards such as EN 228 for gasoline in Europe [19]. Fossil and renewable fuels are subject to the same regulations. In recent years, the government released directives to increase the renewable share of gasoline. An increase in renewables is, for example, notable by an increased oxygen content of up to 3.7 wt.% of O_2-equivalent in EN 228. Ethanol is the most widely blended oxygenate in gasoline, as it can be produced via the biological fermentation of sugar-containing feedstocks [94, 95]. Further oxygenates such as ethers possessing five or more carbon atoms and higher alcohols are also permitted. Certain concentration limits apply to the various oxygenates, but these must not exceed the 3.7 wt.% O_2-equivalent already mentioned. Additional discussions on the pros and cons of oxygenates are offered in the following

chapters. Besides an increased renewable share, oxygenates are blended due to their high ONs [91]. The ON is essential because it is directly linked to a gasoline's market price [96] and is crucial for the engine's performance and efficiency. With the ON, the propensity of the fuel to resist auto-ignition when the fuel/air mixture is compressed within a spark ignition engine is expressed [97]. A higher ON allows for an increased compression ratio, hence a higher thermal efficiency [98]. Several definitions for the ON exist, of which the *RON* and *MON* are applied within EN 228. The *RON* represents a drive under mild conditions, whereby the *MON* is measured under severe conditions, as it is to expect, for example, on a climb with a high load and increased engine speed [73, 99]. Besides oxygenates, aromatics are used to adjust the ON [18]. However, aromatics tend to increase engine-out hydrocarbons [37, 100] and to form soot [41], wherefore their concentration is limited to 35 vol.% in EN 228. Besides *RON* and *MON*, the volatility of gasoline is of particular importance. In EN 228, the volatility is provided in terms of the boiling curve and vapor pressure. The boiling curve is defined by the evaporation characteristics $E70$, $E100$, and $E150$, representing the volume fractions evaporated at 70 °C, 100 °C, and 150 °C, respectively, and the final boiling point *FBP*. As high ambient temperatures result in environmental issues due to the evaporation of highly volatile substances, which contribute to atmospheric pollution [101], the $E70$ has to stay within a certain range, which varies slightly depending on the time of the year. The front-end volatility is further important to ensure good cold-starting [96, 102, 103] and to assess the potential vapor lock under hot weather conditions [102]. The mid-range volatility ($E100$) is related to the cold weather performance, a hot engine's operational readiness and acceleration behavior under load [102]. The end-point volatility ($E150$ and *FBP*) is important to ensure a good fuel economy after engine warm-up, minimum engine deposits, fuel dilution of oil, and emissions of volatile organic hydrocarbons [102, 103]. Automotive manufacturers usually demand fuels whose *FBP* is below the maximum value of 210 °C defined in EN 228, as large molecules tend to form soot [38]. The vapor pressure p_v is closely connected to the boiling curve and regulated in EN 228. As roughly proportional to the losses by evaporation, a high vapor pressure contributes to pollution [104], while a low one negatively influences cold start conditions [105]. It is also reasonable that low vapor pressures contribute to increased particle emissions due to diffusion combustion, as it bears an additional risk of condensation in the combustion chamber [106]. Consequently, the vapor pressure has to stay within a certain range depending on the time of the year. Finally, the gasoline density ρ must comply with EN 228, which is usually the case if the other parameters meet EN 228.

3.1.2 Synthesis Gas-Based Renewable Gasoline Supply and Associated Challenges

Well-investigated processes for the supply of synthetic gasoline are the FT, MTG, and DTG synthesis. These processes are based on syngas, which can be produced from biomass via gasification or from renewable electricity.

3.1.2.1 Fischer-Tropsch

FT was developed in the 1920s and is a synthesis route based on Co or Fe catalysts for producing linear paraffins, olefins, and oxygenates from syngas via a polymerization reaction [107]. The high-temperature FT (HTFT) is best suited for producing liquid hydrocarbons in the gasoline boiling range. It was successfully demonstrated in 1989 and commercialized under the Sasol Advanced Synthol (SAS) process [108, 109]. With a carbon selectivity of 48 %, the process produces gasoline and diesel in a ratio of 3 : 1, both rich in olefins [109]. However, further downstream processing is inevitable to increase the ON due to the low degree of olefin branching and low aromatic content [110].

FT in its low-temperature variant (LTFT) is applied to synthesize high-quality diesel [111]. LTFT is furthermore discussed for producing kerosene from syngas [112]. The German Federal Ministry for the Environment, Nature Conservation, Nuclear Safety and Consumer Protection (BMUV) aims with its PTL roadmap for a ramp-up to at least 200,000 t a^{-1} of PTL kerosene by 2030 [14], underlining the perspective of processes like LTFT. Besides diesel and kerosene, LTFT yields a certain amount of waxes due to the underlying chain growth mechanism [113]. Downstream hydrocracking of waxes is usually considered to increase kerosene yields and obtain valuable iso-paraffins that meet the freezing point requirements for Jet A-1 [112]. Hydrocracking of waxes also yields iso-paraffins in the gasoline boiling range, which show similar properties to fossil isomerate (see also Section 3.2).

This chapter discusses approaches for using gasoline from hydrocracking of waxes as a valuable isomerate replacement.

3.1.2.2 Methanol and Dimethyl Ether to Gasoline

In the 1970s, Chang and Silvestri (MobilOil) discovered a synthesis route of high-octane gasoline from methanol using a zeolite catalyst [24]. A complex reaction network of aromatics methylation and subsequent cracking yields paraffins, naphthenes, olefins, and mono-ring aromatics [25]. The product spectrum strongly depends on the zeolite topology and aromatic species trapped therein [114]. MTG and DTG processes are usually catalyzed using an HZSM-5 zeolite as it produces hydrocarbons in the desired boiling range and possesses superior stability against coking [25]. The first commercial MTG plant was commissioned in New Zealand by Mobil in 1985, which supplied approx. 33 % of the country's gasoline needs [26]. Other plants were brought into operation, e.g., in Shanxi, China in 2009 [25].

Haldor Topsøe was the first company to demonstrate the feasibility of direct DME synthesis as part of a 1 t d^{-1} plant for the production of synthetic gasoline [27]. DTG combines the methanol synthesis and the subsequent DME formation in one reactor. The integrated synthesis increases process efficiency and lowers investment costs, as no methanol isolation is required [25]. Since then, much effort has been made in further developing the DTG synthesis. The bioliq® demonstration plant was commissioned in 2014 [31, 58]. A decentralized biomass fast pyrolysis is used to increase the energy density of the feedstock significantly [29, 30]. The so-called biosyncrude® is then transported and fed to a centralized entrained flow gasifier where syngas free of tar is produced [57]. After several gas conditioning steps, the syngas is fed to a direct DME synthesis [32, 115], followed by a DTG reactor [33].

This chapter shows that DTG synthesis such as the bioliq® process can be used to supply high-quality gasoline and highlights remaining challenges with potential solutions. It is important to note that MTG and DTG provide similar gasoline compositions [28]. Therefore, considerations made within this work apply to both process variants.

3.1.2.3 Suitability of MTG and DTG for Providing Drop-In and Stand-Alone Fuels

Recently, the suitability of synthetic DTG fuel as a drop-in was demonstrated. Michler et al. could successfully blend 10 vol.% of bioliq® gasoline into conventional E95 [52]. However, in their experiments, the aromatic concentration reached 33 vol.% with a relatively low drop-in rate. The high aromatic content resulted in limited direct applicability, as the blend must meet a maximum concentration of 35 vol.% according to EN 228 [19]. Additionally, the fuel had to be separated into light gasoline and heavy gasoline to get rid of 1,2,4,5-tetramethylbenzene (durene) as part of the heavy gasoline. Durene is the largest aromatic hydrocarbon emerging in significant quantities due to the underlying mechanism

in the methanol-to-hydrocarbon reaction [36]. Due to its symmetry, it has a high melting temperature of 79 °C and tends to crystallize, which can clog fuel injection systems or cause drivability problems [25]. Michler et al. only used the light gasoline for their blending experiments. As a result, valuable bio-based hydrocarbons are left out, which directly affects the economics of the underlying process. In the conducted engine tests, the blend showed significantly increased particle emissions compared to the pure E95 since high molecular aromatics in general form soot [60, 116]. Therefore, a sophisticated after-treatment is necessary, which allows the use of the entire product but also reduces the aromatic content. Mobil also recognized this problem originating from the heavy aromatics and decided to split the product into light gasoline and heavy gasoline for their fixed bed MTG process in New Zealand and the pilot-scale fluidized bed version [117]. The heavy gasoline was forwarded to a treatment reactor where the durene concentration could be lowered below 2 wt.% and was subsequently blended back into the light gasoline. The heavy gasoline treatment was developed to improve issues resulting from durene but neglected emission issues related to heavy aromatics. In the prior Chapter 2, heavy gasoline from the bioliq® process was converted into highly isomerized paraffins and naphthenes by hydroprocessing using a 0.3 wt.% Pt/HZSM-5 catalyst and subsequent blending experiments with bioliq® light gasoline were conducted. The combination of noble metals with zeolites gained much attention for processing biomass(-derivatives) due to superior shape selectivity coupled with an increased hydrogenation activity [118]. As a result, the aromatic concentration could be significantly lowered while simultaneously improving petrochemical parameters. The suitability as drop-in fuel was greatly improved, but a stand-alone DTG fuel could not be achieved. Especially the $E70$ and $E100$ were significantly too low and needed to be addressed further.

In this chapter, hydroprocessing is highlighted from a blending perspective, as the process was already discussed previously in Chapter 2. The effects of three produced fuel qualities on gasoline volatility were systematically evaluated through blending experiments.

3.1.3 The Potential of Oxygenates in Blending and Associated Challenges

Oxygenates are interesting blending components as they possess superior ONs and high renewable shares. Table 3.1 shows petrochemical parameters and properties of oxygenates permitted within EN 228 [90, 98, 119–121]. Methanol, ethanol, MTBE, and ETBE are considered in this chapter due to their low boiling temperatures of well below 100 °C. Ethanol is mainly produced by fermentation and thus

Table 3.1: Properties of oxygenates in comparison to fossil oxygenate-free gasoline [90, 98, 119–121].

	Methanol	Ethanol	MTBE	ETBE	Gasoline
RON / -	122	111	118	118	≥ 95
MON / -	93	96	101	102	≥ 85
T_b / °C	64.6	78.4	55.2	73.0	≤ 210
HoV / kJ kg^{-1}	1170	921	338	290	$\approx$ 335–350
O_2-content / wt.%	49.9	34.7	18.2	15.7	0
Renewable share / wt.%	100	100	35.21	44.10	0

comes with a renewable share of 100 % [94]. The methanol synthesis is a well-established syngas-based process, which can be sustainably operated by using biomass or renewable electrical energy [122]. MTBE and ETBE are produced based on methanol and ethanol, respectively. To the authors' best knowledge, there is no process commissioned for the renewable synthesis of iso-butene yet, which is also required for the synthesis. Therefore, MTBE and ETBE have a renewable share of 35.21 wt.% and

44.1 wt.%, respectively, the one of ETBE being higher as the molecular contribution of ethanol is higher compared to the one of methanol.

Oxygenates in general reduce emissions of incomplete combustion, i.e., CO and hydrocarbons, by the so-called "leaning effect", which means a replacement of high-sooting hydrocarbons by less-sooting oxygenates [123]. Oxygenates can further help to reduce soot formation, which is one main reason for reduced life expectancy worldwide [39]. However, the physical properties of oxygenates also bear a risk of increased soot formation. Table 3.1 shows the heat of vaporization HoV for the prior discussed oxygenates. Small alcohols such as methanol and ethanol possess high HoVs compared to MTBE and ETBE, which have HoVs in the gasoline range. When the fuel/air mixture is loaded into the combustion chamber and evaporates, a high HoV results in the charge-cooling effect [124]. Charge-cooling improves knocking resistance as the fuel/air mixture's temperature is reduced, which is, in general, positive [125]. However, charge-cooling might lead to disadvantages for existing engines, e.g., increased emissions for aromatic-rich fuels [120, 126]. Oxygenates with high HoVs delay the evaporation of the fuel, which might result in the impingement of the spray with the cylinder walls or the piston top, resulting in fuel-rich combustion [124] and, consequently, the formation of particulate matter [127]. Additionally, alcohols are associated with an increased vapor pressure and depression of the front end of the boiling curve due to the formation of positive azeotropic mixtures with hydrocarbons [121]. A high vapor pressure leads to increased evaporative emissions and a request after more expensive high-boiling blending fractions such as reformate in place of cheaper ones such as butane [96]. Due to their carbon-rich structure, ethers do not form azeotropic mixtures with hydrocarbons and therefore blend similarly to hydrocarbons [128]. MTBE and ETBE have boiling temperatures below 100 °C, hence are known to alter the mid-section of a gasoline's boiling curve [121]. As shown in Table 3.1, MTBE and ETBE can be blended in higher ratios than methanol, and ethanol until EN 228's limit of 3.7 wt.% is reached due to their lower oxygen content. While methanol and ethanol have a molecular oxygen content of 49.9 wt.% and 34.7 wt.%, MTBE and ETBE only come with 18.2 wt.% and 15.7 wt.%, respectively.

In the present chapter, it is examined, to which extend the mentioned oxygenates can improve the volatility of a DTG fuel to meet EN 228. Careful balancing must be observed in the case of alcohols, as a high blending rate carries the risk of emission issues and may limit applicability in older vehicles. However, a certain azeotropic effect might be beneficial as the considered DTG base fuel is of heavy nature and fossil butane as a volatility booster shall not be considered.

3.2 Materials and Methods

Table 3.2 lists the petrochemical parameters of bioliq® light gasoline and hydrocarbon fractions originating from the hydroprocessing of bioliq® heavy gasoline (HG-HP) and FT wax (FT-HP), as used for the blending experiments in this chapter. The compositions of all samples were measured with a Reformulyzer M4 from AC PAC (Houston, TX, USA) and can be found in the Appendix in Tables B.1–B.5. Figure 3.1 shows the boiling curves, measured according to ASTM D7345 [88] using an OptiPMD from PAC. Each boiling curve was measured with a resolution of 1 vol.% and is depicted as a solid line for clearness reasons. The boiling curve is further used to calculate the boiling characteristics $E70$, $E100$, and $E150$.

For the reasons discussed in the Introduction, bioliq® raw gasoline was rectified, yielding light gasoline and heavy gasoline (for composition see Table B.6 in the Appendix) in a ratio of 2 : 1. The light gasoline, with an FBP of 163.0 °C, is free of C_{10} aromatics such as durene. Due to its high C_7 and C_8 aromatic content (16.0 vol.% toluene, 43.1 vol.% C_8 aromatics, 16.3 vol.% C_9 aromatics) resulting in a high ON, the light gasoline is considered a valuable blending component. It has to be mentioned that the gasoline

Table 3.2: Petrochemical parameters of hydrocarbon streams used for the blending experiments.

Parameter	EN 288 [19]	bioliq® light gasoline	bioliq® HG-HP@270 °C	bioliq® HG-HP@310 °C	bioliq® HG-HP@330°C	FT-HP
RON / -	≥ 95	102±2.7	76.9±2.7	75.9±2.7	77.0±2.7	79.9±2.7
MON / -	≥ 85	91.2±1.0	79.6±1.0	77.4±1.0	77.0±1.0	73.9±1.0
ρ^1@15 °C / kg m^{-3}	720-775	835.02±0.05	n.A.	n.A.	n.A.	n.A.
ρ^1@20 °C / kg m^{-3}	-	829.30±0.05	782.78±0.05	753.86±0.05	731.20±0.05	673.03±0.05
$p_v^{1,2}$ / kPa	45-60	23.0±2.0	10.0±2.0	36.0±2.0	41.0±2.0	n.A.
$E70^{1,2}$ / vol.%	22-50	1.1±0.9	0.0	5.5±0.9	14.7±0.9	35.1±0.9
$E100^{1,2}$ / vol.%	46-72	8.0±0.8	1.2±0.8	20.1±0.8	37.6±0.8	67.9±0.8
$E150^{1,2}$ / vol.%	75	90.7±0.6	39.5±0.6	66.0±0.6	81.7±0.6	96.4±0.6
FBP^1 / °C	≤ 210	163.0±2.0	163.0±2.0	163.0±2.0	163.0±2.0	168.0±2.0
$\varphi_{\text{Benzene}}{}^1$ / vol.%	≤ 1	1.4±0.7	0.0	0.2±0.7	0.0	0.0
$\varphi_{\text{Olefines}}{}^1$ / vol.%	≤ 18	2.3±0.1	0.1±0.1	0.0	0.0	0.0
$\varphi_{\text{Naphthenes}}{}^1$ / vol.%	-	5.5±0.1	96.2±0.1	79.6±0.1	67.0±0.1	4.5±0.1
$\varphi_{\text{Paraffines}}{}^1$ / vol.%	-	15.3±0.6	3.2±0.6	18.8±0.6	32.5±0.6	95.5±0.6
$\varphi_{\text{Aromatics}}{}^1$ / vol.%	≤ 35	76.9±0.7	0.5±0.7	1.6±0.7	0.4±0.7	0.1±0.7

[1]Measurement errors estimated using a representative sample. [2]Volatility class A.

slightly differs from the one used for Chapter 2 due to variations in the bioliq® synthesis and rectification. However, the challenges remain the same. Significant derivations of 20.9 vol.% and 38.0 vol.% compared to EN 228 can be seen for *E*70 and *E*100, respectively. Thus, bioliq® light gasoline lacks a significant amount of light boiling components with temperatures of up to 100 °C. The heavy nature of bioliq® light gasoline is also reflected in the relatively flat boiling curve shown in Figure 3.1. Following the procedure from prior Chapter 2, bioliq® heavy gasoline was hydroprocessed at 270 °C, 310 °C and 330 °C using a 0.3 wt.% Pt/HZSM-5 catalyst in a fixed bed reactor. The final blending components were obtained by rectification to an *FBP* slightly above 160 °C. Depending on the reaction temperature, the hydroprocessing experiments were either conducted under hydrogenation or hydrocracking conditions yielding streams rich in naphthenes and paraffins. In Table 3.2, it can be seen that *E*70, *E*100, and *E*150 increase significantly from 0 vol.% to 14.7 vol.%, 1.2 vol.% to 37.6 vol.% and 39.5 vol.% to 81.7 vol.%, respectively, for the process temperature increased from 270 °C to 330 °C. In Figure 3.1, the improvement of the boiling characteristics also can be seen as the front end of the boiling curve is further depressed as the reaction temperature increases. For an hydroprocessing temperature of 270 °C, the boiling curve lies above the one of bioliq® light gasoline because the reaction was carried out in the hydrogenation regime where cracking reactions were strongly suppressed. Therefore, the product is rich in heavy C_9 and C_{10} naphthenes, having boiling temperatures of approx. 140–155 °C.

RON and *MON* were determined using an OptiFuel from PAC. The device's method was extended by training the underlying model with a data set obtained from a frequently inspected CFR test engine at PetroLab in Speyer, Germany. *RON* and *MON* could be predicted using a held-back validation data set with an accuracy of ±2.7 and ±1.0, respectively. Interestingly, the MONs are higher than the RONs for heavy gasoline hydroprocessed at 270 °C and 310 °C, and both are equal for an hydroprocessing temperature of 330 °C. Comparably high MONs are detected due to the high content of naphthenes, which was already reported in Chapter 2. The difference between *MON* and *RON* decreases for higher reaction temperatures as the paraffin content increases due to intensified cracking reactions. The comparably high *MON*s are of interest as blending could result in gasoline having a lower octane

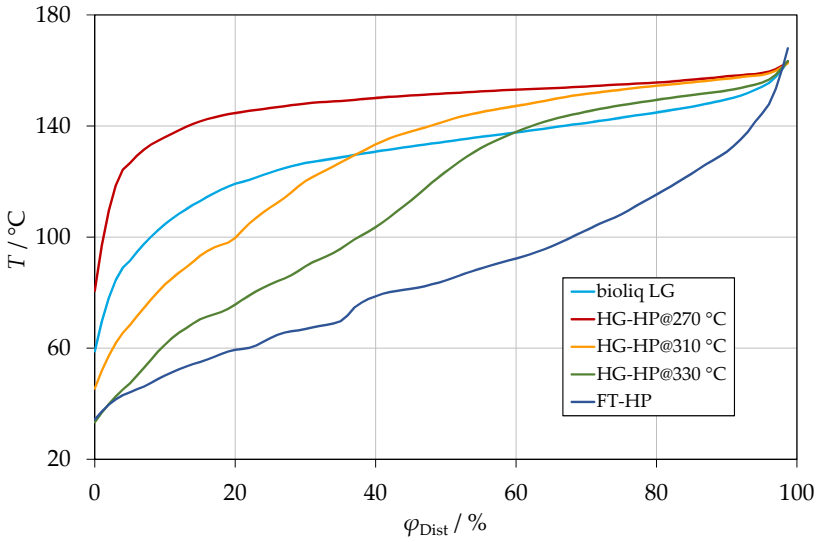


Figure 3.1: Boiling curves of bioliq® light gasoline (LG), hydroprocessed heavy gasoline (HG-HP) for different processing temperatures and hydroprocessed Fischer–Tropsch wax (FT-HP).

sensitivity (difference of *RON* and *MON*), which provides higher reliability under different driving conditions [128].

The FT gasoline was produced by hydroprocessing of wax, as described elsewhere [7]. Neuner et al. studied the production of high-quality pharmaceutical oils from low-valuable FT wax using a 0.3 wt.% Pt/SAPO-11 catalyst. Besides the desired oil, 10–20 wt.% of highly isomerized paraffinic gasoline was produced. As no laboratory FT synthesis in the required scale was available, wax from SASOL (Sandton, South Africa) was used for simulating a potentially GHG-neutral FT wax. The FT gasoline was rectified to an *FBP* of approx. 168 °C. Due to its high paraffinic content and high content of light-ends, it can be most likely compared to fossil isomerate [121, 128]. The main difference is a comparably lower ON and a higher *FBP* of the FT gasoline.

In addition to the mentioned hydrocarbon streams, methanol (≥ 99.5 %, VWR chemicals, Radnor, PA, USA), ethanol (99.95 %, VWR chemicals), MTBE (≥ 99.0 %, Merck, Darmstadt, Germany), and ETBE (77.7 vol.%, Mineralölraffinerie Oberrhein, Karlsruhe, Germany) were used for the blending experiments. ETBE was provided by Mineralölraffinerie Oberrhein, Germany from an industrial scale plant in operation, therefore having approx. 22 vol.% by-products, mainly iso-butene (10.5 vol.%) and pentane (6.5 vol.%).

An HVP 972 from Herzog PAC was used for measuring the vapor pressure at 37.8 °C according to ASTM D6378 [87]. The density was measured with a density meter Excellent D5 from Mettler-Toledo (Greifensee, CH) using a self-developed method.

For the blending experiments, the share of each compound or fraction was calculated on a volume basis, as most of the petrochemical parameters listed in EN 228 are given as volume fractions. However, due to the higher precision of weighting, the density of each fraction or substance was measured at 20 °C and the mass required for a given volume calculated.

All measurements were repeated whenever possible and were statistically evaluated according to the student's t-distribution, assuming a 95 % confidential interval.

3.3 Results and Discussion

As mentioned, the bioliq® raw gasoline was distilled and the heavy gasoline hydroprocessed at different reaction temperatures according to the procedure described in Chapter 2. In the following, it is discussed how hydroprocessing can help to improve the blending volatility characteristics, especially *E*70 and *E*100. It is also investigated how oxygenates might help to further improve the boiling characteristics. Finally, it is examined if a blend with a high renewable share, which also meets the petrochemical parameters of EN 228, can be provided.

3.3.1 Influence of Hydroprocessing on Boiling Characteristics and Vapor Pressure

The hydroprocessed heavy gasoline's petrochemical parameters are greatly dependent on the reaction temperature; thus, three qualities were produced. Figure 3.2 shows the obtained results for *E*70, *E*100, and vapor pressure for the blending experiments by continuously increasing the blending rate of HG-HP into bioliq® light gasoline. Figure 3.2a shows a directly proportional dependency of the *E*70 and *E*100 on

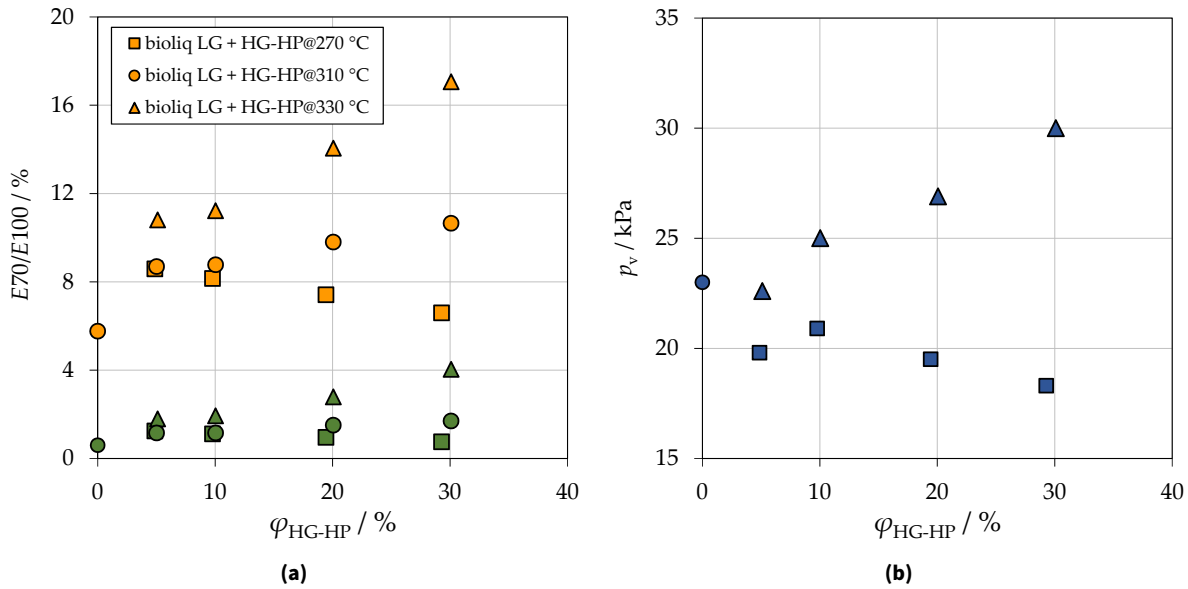


Figure 3.2: Influence of blending HG-HP@270 °C (squares), HG-HP@310 °C (circles) and HG-HP@330 °C (triangles) into bioliq® light gasoline on **(a)** the volatility characteristics *E*70 (green), *E*100 (orange) and **(b)** the vapor pressure.

the blending rate of the respective HG-HP fractions. This dependency can be attributed to the similar nature of bioliq® light gasoline and HG-HP, consisting exclusively of hydrocarbons. A more substantial increase in *E*70 and *E*100 can be seen for HG-HP@330 °C than for HG-HP@310 °C as that fraction contains more light-ends in the respective boiling ranges. The same applies to HG-HP@270 °C, for which *E*70 and *E*100 decrease with the blending rate. For an hydroprocessing temperature of 330 °C and a blending rate of 30 vol.%, *E*70 and *E*100 reach 4.0 vol.% and 17.1 vol.%, respectively. However, *E*70 and *E*100 have to meet 22 vol.% and 46 vol.%, respectively, according to EN 228. Therefore, hydroprocessing can help to increase the light-ends, but further measures must be taken. A higher blending ratio of HG-HP with light gasoline as the original 1 : 2 cannot be realized in this specific case, as this was roughly the split right after rectification, as explained in Materials and Methods. A higher hydroprocessing temperature has not been investigated, as it was expected that cracking losses would no longer be justified.

Similar tendencies as for the boiling characteristics can be observed for the vapor pressure, as shown in Figure 3.2b. A higher overall vapor pressure is observed for blends with HG-HP@330 °C than those with HG-HP@270 °C. While the vapor pressure increases for a higher blending ratio of HG-HP@330 °C, it decreases for HG-HP@270 °C. The direct proportional dependency can again be attributed to the similar nature of the hydrocarbon fractions. As outlined in the Introduction, the vapor pressure is crucial for a correct engine functioning but is also connected to evaporative emissions. For 330 °C, the highest reaction temperature investigated, and a blending rate of 30 vol.%, the vapor pressure is far from violating the upper boundary of 60 kPa of EN 228 for summertime gasoline (Class A). Hydroprocessing seems to be an effective tool for adjusting the vapor pressure in a particular range.

As outlined above, comparing *E*70, *E*100, and vapor pressure to EN 228, the necessity of further blending components becomes apparent, even for an hydroprocessing temperature of 330 °C. In the Introduction, it was discussed that oxygenates can help to lower the boiling curve due to low boiling temperatures and by forming an azeotropic mixture with gasoline hydrocarbons. Therefore, the influence of the common oxygenates methanol, ethanol, MTBE, and ETBE on the boiling curve of bioliq® gasoline is discussed in the following.

3.3.2 Influence of Oxygenates on Boiling Characteristics and Vapor Pressure

Figure 3.3 shows the boiling characteristics *E*70, *E*100, and *E*150 together with the vapor pressure in dependence on the oxygen mass fraction. The oxygen mass fraction is limited in EN 228 to 3.7 wt.% and thus chosen over the blended volume fraction. The maximum share of each oxygenate is chosen accordingly to the maximum permitted in EN 228, such that Figure 3.3 represents the potential effect of each oxygenate. As base gasoline, a blend of two-thirds bioliq® light gasoline and one-third HG-HP@270 °C was chosen, with an *E*70, *E*100, and *E*150 of 0.6 vol.%, 5.8 vol.%, and 85.0 vol.%, respectively, and a vapor pressure of 13.7 kPa. Therefore, it represents the heavy nature of a typical DTG or MTG fuel.

As shown in Figure 3.3a, all blended oxygenates increase the *E*70 as their boiling points are below or in the region of 70 °C (see Table 3.1 for boiling temperatures). While MTBE and ETBE increase the *E*70 up to approx. 4 vol.%, blending of methanol and ethanol results in a maximum *E*70 of 7.8 vol.% and 8.0 vol.%, respectively. It has to be noted that ETBE contains approx. 22 vol.% by-products. Such a strong increase for methanol and ethanol can be attributed to the formation of azeotropic mixtures, as explained in the Introduction. Methanol shows the strongest effect with the blended oxygen equivalent, while a maximum of 3 vol.% could be blended to meet the restriction of EN 228. The overall greatest increase can be seen for ethanol at about 2 wt.% oxygen (5.9 vol.% ethanol) blended. A further addition leads to no further increase of the *E*70. The strong azeotropic effect of methanol and ethanol can also be seen in Figure 3.4, where the boiling curves for their respective highest blending rates are shown. Both alcohols strongly depress the front end of the boiling curve, which is in accordance with other studies [121, 128]. Especially for the blend with ethanol, a distinct step shape can be observed, which indicates the formation of an azeotropic mixture [129]. The boiling curve again reaches the base gasoline's one after the alcohol is distilled completely [129]. No azeotrope seems to be formed for methanol due to the lower volume blended and as smaller alcohols in general tend to form an azeotropic mixture at higher blending rates [119]. An azeotropic mixture is unfavorable as it results in an unsteady evaporating behavior of the fuel, as explained in the Introduction. Thus, methanol seems more promising than ethanol for adjusting the front-end volatility of the considered bioliq® fuel. As indicated above, MTBE and ETBE only slightly increase *E*70. However, considering Figure 3.4, both ethers show a significant flattening, especially of the mid-part of the curve, which is also confirmed by other researchers [121, 128, 130]. The influence on the mid-section can also be seen for the *E*100 in Figure 3.3b, which increases

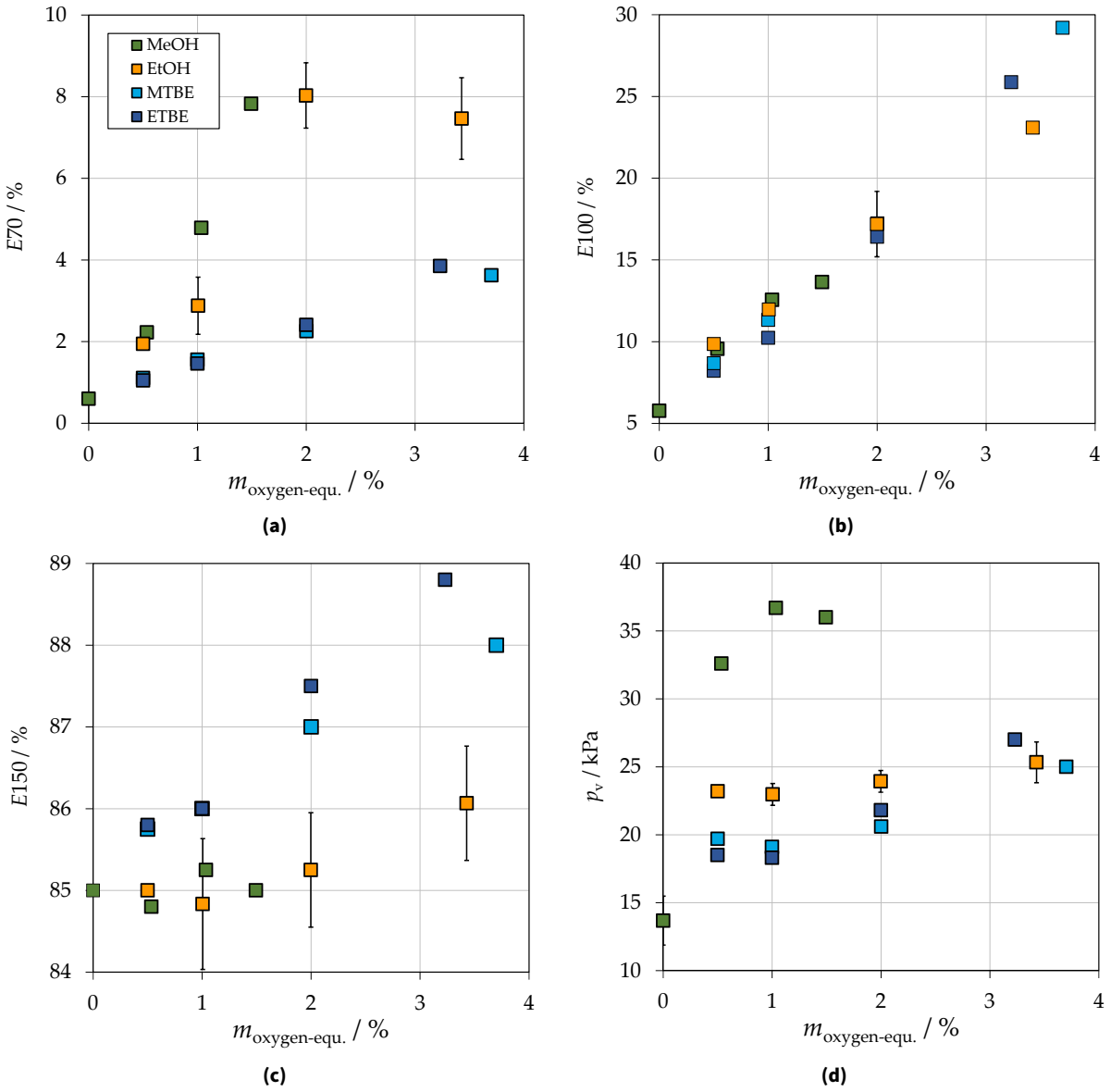


Figure 3.3: Influence of different oxygenates on the volatility characteristics **(a)** *E*70, **(b)** *E*100, **(c)** *E*150, and **(d)** vapor pressure of bioliq® base gasoline (33.3 vol.% HG-HP@270 °C and 66.7 vol.% bioliq® light gasoline).

the most for ETBE and MTBE. Blending MTBE leads to the most substantial increase in the *E*100, as also determined by Petre et al. [130]. In general, however, no significant differences between the investigated oxygenates regarding their influence on the *E*100 with oxygen equivalent blended can be emphasized. Karonis et al. also detected no apparent difference in the *E*100 whether they blended ethanol or ETBE [128]. The overall substantial increase in the *E*100 for MTBE and ETBE can be attributed to the high volume blended, resulting from a low molecular oxygen content and a high permitted blending rate by EN 228. As shown in Figure 3.3c, the *E*150 increases most by blending ETBE, followed by MTBE, and less significantly by ethanol and methanol. The considered alcohols show a less distinct effect on the back end of the boiling curve, as the (near-)azeotropic mixtures do not influence this part of the boiling curve.

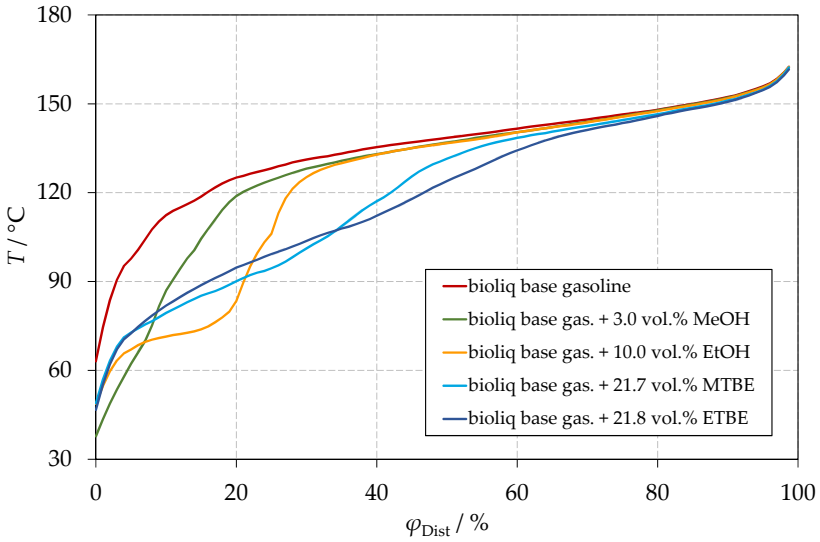


Figure 3.4: Influence of different oxygenates on the boiling curve of bioliq® base gasoline (33.3 vol.% HG-HP@270 °C and 66.7 vol.% bioliq® light gasoline).

Besides a smooth boiling curve, the vapor pressure is important for a well-working engine, emitting fewer emissions, as explained in the Introduction. The influence of the different oxygenates on the vapor pressure can be seen in Figure 3.3d. Remarkable is the substantial increase in the base fuel's vapor pressure if methanol is blended, while the ones of the ethanol blends are in the region of the MTBE and ETBE blends. In other studies, ethanol increased the vapor pressure more significantly [99, 128]. The weak influence of ethanol on the vapor pressure in this work might be due to the heavy nature of the bioliq® gasoline, as the effect of an oxygenate on the volatility is always connected to the base fuel [99, 128]. bioliq® gasoline considered in this chapter is rich in aromatics, which exhibit a lower increase in the vapor pressure when blended with alcohols [99]. As shown in Figure 3.4, the ethanol/gasoline azeotrope does not significantly influence the initial part of the boiling curve compared to MTBE and ETBE. In contrast, a significant lowering can be observed for methanol, probably because it can form a near-azeotropic mixture with light-ends, available in low concentrations. This becomes more obvious by comparing the different blends' initial boiling points *IBP*s. For the blends reported in Figure 3.4 with methanol, ethanol, MTBE, and ETBE, the *IBP*s are 37.8 °C, 48.7 °C, 48.9 °C, and 46.7 °C, respectively. For each oxygenate considered, the vapor pressure increases with a growing blending rate of oxygen equivalent, except for a blending rate of 1 wt.% oxygen equivalent of methanol, after which the vapor pressure seems to drop. This observation is not significant, as not enough data were collected. However, sources report behavior in which the vapor pressure increased for low blending rates and decreased for higher ones or stayed almost the same [128, 131]. For blending rates of up to 2 wt.% oxygen equivalent, the vapor pressure is slightly higher for ethanol than both ethers. The differences disappear for blending rates higher than 3 wt.% oxygen equivalent.

It can be concluded that methanol is promising to improve the boiling characteristics and vapor pressure. Interestingly, the results were obtained with a maximum blending rate of 3 vol.%, which makes it likely that such a fuel would be compatible with older engines, since standard gasoline in Europe contains up to 5 vol.% ethanol. It further seems ETBE is promising as it has a remarkable flattening effect on the boiling curve. MTBE increased the *E*100 the most, which makes it the favorite oxygenate for adjusting the mid-section of the bioliq® fuel.

3.3.3 Combination of Two Oxygenates and their Effect on Boiling Characteristics and Vapor Pressure

In the following, 3 vol.% methanol was blended into bioliq® base gasoline (two-thirds light gasoline and one-third HG-HP@270 °C) and the effect of a second oxygenate blended, i.e., ethanol, MTBE, and ETBE, was investigated, until an oxygen content of 3.7 wt.% was reached. Methanol was chosen as it increases the *E*70 most considerably with the blended oxygen equivalent, as shown in Figure 3.3. There is also no drawback regarding the *E*100 compared to the other oxygenates. Both parameters are critical if the bioliq® DTG gasoline is considered [1]. Methanol also seems a good choice as it is available as a process intermediate in the case of MTG. Figure 3.5 shows the dual-oxygenate blends' boiling characteristics, vapor pressures, and boiling curves. As shown in Figure 3.5a, *E*70, *E*100, and vapor pressure are greatly

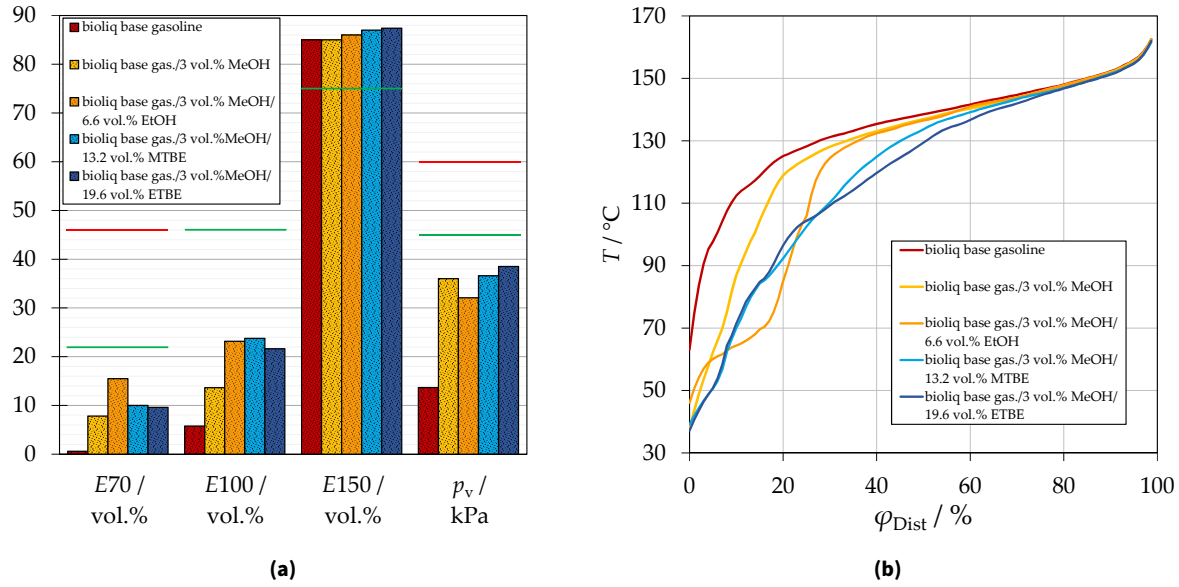


Figure 3.5: Influence on **(a)** the boiling characteristics and vapor pressure and **(b)** the boiling curve for blends of bioliq® base gasoline and methanol with ethanol, MTBE, and ETBE. A green line marks the minimum and a red line the maximum permitted value of the respective petrochemical parameter according to EN 228. No red line is shown for the maximum value of *E*100, which is 72.0 vol.%.

improved for all oxygenates blended into the methanol-containing base gasoline. A significant increase in the *E*70 can be observed for ethanol and a lower one for MTBE and ETBE, which are at similar levels. The differences also become visible in Figure 3.3a, where the same tendencies are observable for the single oxygenate blends. *E*150 increases for the added oxygenates in the order ETBE > MTBE > ethanol, which is once more what was detected for the single oxygenate blends in Figure 3.3c. *E*100 also improves significantly for the dual-oxygenate blends, whereby all values are of the same magnitude. The same was discovered in Figure 3.3b, where all oxygenates improved *E*100 similarly.

Figure 3.5a shows the vapor pressure for the dual-oxygenate blends. The vapor pressure decreases in the order ETBE > MTBE > ethanol, which is turned around when Figure 3.3d is considered. For the blend containing methanol/ethanol, the vapor pressure lies between the vapor pressures measured for the blends with the single oxygenates (Figure 3.3d). The vapor pressure of the blends containing methanol/MTBE and methanol/ETBE are clearly above the values obtained for the blends containing only MTBE and ETBE (Figure 3.3d) and slightly above the one just containing methanol. The observed can be explained in two ways. First, methanol/ethanol may not increase the vapor pressure as significantly as methanol/MTBE and methanol/ETBE since an increased blending rate of alcohol

leads to a decrease in vapor pressure after a certain point. Second, alcohols can form azeotropic mixtures with ethers, as reported, for example, by Domańska et al. [132], which could also explain the disproportionate increase in vapor pressures for these mixtures. A higher vapor pressure for blending methanol/ETBE than methanol/MTBE can be explained by the formation of an (near-)azeotropic mixture of the low-boiling by-products contained in ETBE with methanol. The aforementioned can also be seen in Figure 3.5b, where the *IBP*s are significantly lower for the blends with methanol/MTBE and methanol/ETBE than for those with methanol/ethanol. For all blends, the vapor pressures are within EN 228. Regarding the boiling curve, the observations from Figure 3.4 can be approved for the dual-oxygenate blends. The blend with methanol/ethanol shows a strong step shape, indicating an azeotropic mixture. Both methanol/MTBE and methanol/ETBE help to flatten the boiling curve, whereby the effect is the strongest for methanol/ETBE, as can be seen around a distilled volume of 40 %, where the methanol/MTBE curve shows a slight bump.

The boiling characteristics could be improved by simultaneously blending two different oxygenates into the bioliq® base gasoline. A combination of methanol and ethanol achieved the highest *E*70 of 15.5 vol.%, while for methanol/MTBE and methanol/ETBE, *E*70 reached 10.0 vol.% and 9.6 vol.%, respectively. Regarding *E*100 and *E*150, the values were within a range of 21.6—23.8 vol.% and 86.0—87.4 vol.%, respectively, for all investigated dual-oxygenate blends. *E*70 and *E*100 thus do not meet EN 228, for which at least 22 vol.% and 46 vol.% are required, respectively. Therefore, further light boiling components free of oxygen must be considered. As discussed, the hydroprocessing of heavy gasoline at higher temperatures can increase the *E*70 and *E*100 to some extent. In the Introduction, the possibility of using an FT gasoline fraction as an isomerate replacement was also discussed. In the following, all these measures are combined. A combination of methanol/ethanol and methanol/ETBE was used in the experiments, as they were superior in terms of the boiling characteristics and the shape of the boiling curve, respectively. To prove its suitability as a possible fossil gasoline replacement, the remaining petrochemical parameters covered by EN 228 were measured.

3.3.4 Expanded Blending Concept

Table 3.3 shows the fractions used to prepare the final blends A and B. For blends A and B, a blend

Table 3.3: Fractions used for the blends A and B.

Volume Fraction / %	bioliq® light gasoline	bioliq® HG-HP@330 °C	FT-HP	Methanol	Ethanol	ETBE
Blend A	42.8	14.6	33.7	3.0	5.9	0.0
Blend B	42.7	14.5	21.2	3.1	0.0	18.5

of bioliq® light gasoline and HG-HP@330 °C were chosen as base gasoline, as outlined before. The ratio of light gasoline : HG-HP was lowered due to two reasons. First, a higher hydroprocessing temperature means increased cracking losses. Second, the ON of the HG-HP is comparably low; thus, it was decided to blend more of the high-octane bioliq® light gasoline. Figure 3.6 shows the petrochemical parameters of the blends compared to bioliq® light gasoline and the respective boiling curves. The exact composition of the blends A and B can be found in Tables B.7 and B.8 in the Appendix. As can be seen in Figure 3.6a, the boiling characteristics of blend A and B are significantly improved compared to bioliq® light gasoline. The *E*70 counts 32.1 vol.% and 20.4 vol.% for the blends A and B, respectively. As already shown in Figure 3.5a, the combination of methanol and ethanol highly improves the *E*70 due to the formation of an azeotropic mixture. This can also be seen in Figure 3.6b,

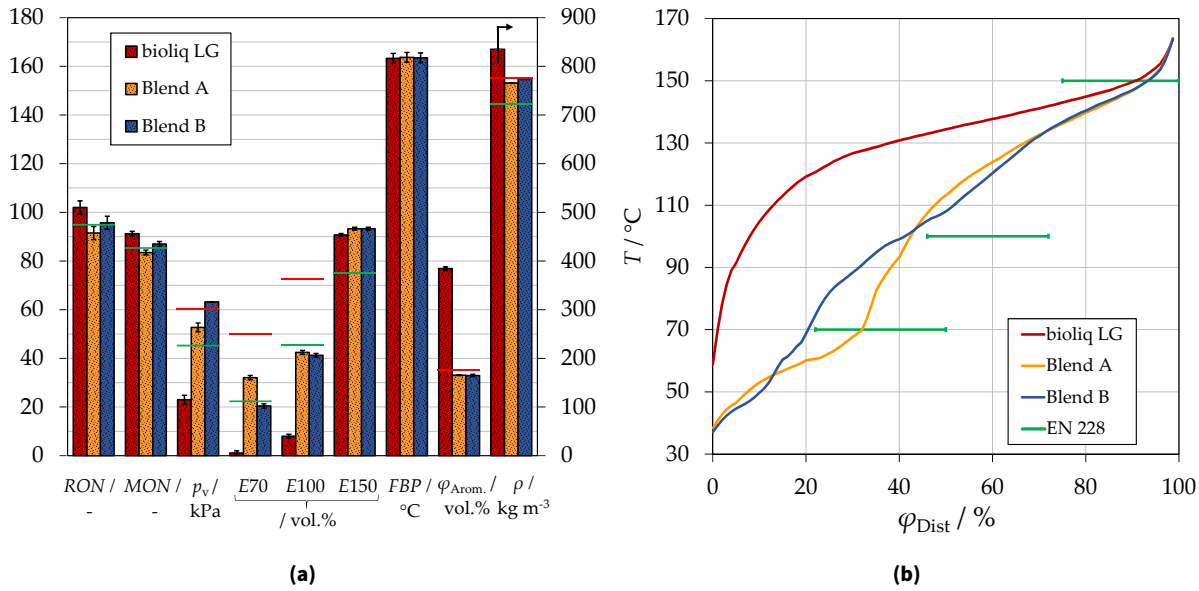


Figure 3.6: **(a)** Petrochemical parameters and **(b)** boiling curves of blend A, blend B, and bioliq® light gasoline. A green line marks the minimum and a red line the maximum value of the respective petrochemical parameter according to EN 228. No line is shown for the *FBP* as its maximum value of 210 °C is out of the diagrams scope.

where the boiling curve of blend A shows a strong depression up to a distilled volume of 30 %. Blend B narrowly misses to meet the 22 vol.% of EN 228 for *E*70. Regarding *E*100, blend A counts 42.4 vol.% and blend B 41.2 vol.%; thus, both do not meet EN 228's minimum value of 46 vol.%. For *E*150, both blends meet EN 228. In general, the boiling characteristics show similar results to the dual-oxygenate blends shown in Figure 3.5a. Regarding the vapor pressure, only blend A was measured, as the quantity of blend B was too low; however, an estimate based on the similarity to the dual-oxygenate blends was made. The vapor pressure of blend A and blend B is 52.7 kPa and 63.2 kPa, respectively. Blend A is within 45–60 kPa for Class A gasoline according to EN 228, while blend B is slightly too high. One might already conclude that MTBE is probably the better choice over ETBE. In Figure 3.5a, *E*70 and *E*100 are slightly higher for the dual-oxygenate blend with MTBE, while the vapor pressure is lower.

For blend A, the *RON* and *MON* are 91.5 and 83.5, respectively, which is too low to satisfy EN 228. The low ONs are explainable by the comparably low ON of HG-HP@330 °C and FT-HP (see Table 3.2), which cannot be compensated by ethanol as its blending rate is relatively low due to its high molecular oxygen content. Counting 95.7 and 87.0 for the *RON* and *MON*, respectively, significantly higher ONs, meeting EN 228, are measured for blend B. ETBE compensates better for the ON loss because its lower molecular oxygen content allows it to be blended at a higher ratio until 3.7 wt.% oxygen equivalent is reached. Additionally, ETBE was determined to increase *RON* and *MON* more distinct than ethanol [128]. The higher ON of blend B offers the possibility to increase the quantity of light-ends, for example, by increasing the share of HG-HP@330 °C or FT-HP. Additionally, with MTBE instead of ETBE, this could help to finally meet EN 228. MTBE and ETBE have similar *RON*s and *MON*s (see Table 3.1); therefore, the ON should not be a limiting factor.

The remaining parameters, density and aromatics content lie within EN 228 for both blends. Regarding the boiling curves, a significant improvement can be seen for both blends compared to bioliq® light gasoline. The stepped shape for blend A with methanol and ethanol is still observable. However, compared to Figure 3.5b, it is shifted towards higher volume fractions. The shift is not surprising, as a higher share of light boiling components was contained in the blends considered in Figure 3.6, as

FT-HP and HG-HP@330 °C were blended here. A smoother boiling curve can be seen for blend B with methanol and ETBE, where no distinct disturbances are visible besides a flat bump between 20 vol.% and 40 vol.%. Therefore, a similar smooth boiling curve can be expected for MTBE, as only a slight difference was detected in Figure 3.5b. Further blending experiments are thus encouraged.

Based on the experiments of Chapter 2 and 3, a standard-compliant blend was developed in cooperation with Porsche [133]. As a result of the combined efforts, 200 L were successfully motor-tested, underlining the applicability of the presented after-treatment and blending strategy.

3.4 Summary and Conclusions

bioliq® light gasoline's critical volatility parameters $E70$ and $E100$ are improved from 0.6 vol.% to 4.0 vol.% and 5.8 vol.% to 17.1 vol.%, respectively, through hydroprocessing the heavy gasoline, using a Pt/HZSM-5 catalyst.

A more significant improvement of the $E70$ from 0.6 vol.% to 7.8 vol.% and 0.6 vol.% to 8.0 vol.% is achieved by blending methanol and ethanol, respectively, within their permitted blending volumes by EN 228. ETBE and MTBE significantly improve the $E100$ from 5.8 vol.% to 25.9 vol.% and from 5.8 vol.% to 29.2 vol.%, respectively. The blending of ETBE additionally leads to a considerable flattening of the boiling curve, while ethanol causes deformations resulting from the formation of an azeotropic mixture. All vapor pressures are within EN 228, while blending of methanol leads to the most substantial increase in bioliq® gasoline's low vapor pressure from 13.7 kPa to 36.7 kPa.

A simultaneous blending of methanol and ethanol with bioliq® gasoline further improves the $E70$ to 15.5 vol.%, while it reaches approx. 10 vol.% when methanol is blended with MTBE or ETBE. The $E100$ increases for all dual-oxygen blends to a similar level of 21.6 vol.% to 23.8 vol.%. Due to the high alcohol content, the boiling curve showes strong deformations for the blend with methanol and ethanol, while it is smooth for the one with methanol and ETBE.

Two final blends are prepared using bioliq® light gasoline, HG-HP@330 °C, FT-HP, and a combination of methanol and ethanol or methanol and ETBE. With 91.5 and 83.5 for RON and MON, respectively, the blend with methanol and ethanol does not meet EN 228 in this regard. The blend with methanol and ETBE meets the standard, with a RON and MON of 95.7 and 87, respectively. With the exceptions of $E70$ and $E100$ having slightly too low values of 20.4 vol.% and 41.2 vol.%, respectively, all petrochemical parameters are met for the latter blend. The blend comes additionally with a low alcohol content of 3 vol.% and should thus be compatible even with older vehicles. A clear advantage over established upgrading processes such as Mobil's [117] is the complete conversion of heavy aromatics to saturated compounds, resulting in lower emission tendencies as reported for such fuels [52].

Further increases in $E70$ and $E100$ may be achieved by applying more severe cracking conditions to either FT wax or heavy gasoline. Since blending methanol and MTBE into bioliq® gasoline results in slightly higher $E70$ and $E100$ values compared to a blend with methanol and ETBE, further investigation should examine whether replacing ETBE with MTBE could help meet the EN 228 requirements. A blend with methanol and MTBE would be additionally beneficial, as these oxygenates would be based entirely on methanol (and iso-butene). It should also be examined to lower the separation temperature of light gasoline and heavy gasoline in the rectification right after the gasoline synthesis. This would lower the boiling curve and is additionally promising as the gasoline supply might be based solely on MTG/DTG with additional oxygenates, allowing the omission of FT wax cracking. Finally, further research should include engine tests, especially under high loads, to investigate whether any evaporation issues exist.

4 Upgrading Via Co-Hydroprocessing Using a Hydrotreating Catalysts

4.1 Introduction

As outlined in the prior Chapters, DTG or MTG fuels are usually separated into light gasoline and heavy gasoline to remove durene, occurring in amounts of 3–6 wt.% [36]. While light gasoline is well suited as fossil reformate-replacement, heavy gasoline consists almost entirely of C_9–C_{12} aromatics, particularly durene. Due to its high melting temperature of 79 °C, heavy gasoline is not suitable as a fuel fraction, as it might cause driveability problems [25] and high engine-out hydrocarbon [37] as well as soot emissions [38]. Nevertheless, heavy gasoline is of bio-derived origin with a GHG reduction potential and, therefore, of high economic value. Refineries must search for solutions to process streams rich in heavy aromatics and overcome negative properties.

In this chapter, the co-hydroprocessing of bioliq® heavy gasoline with fossil middle distillate is investigated. Section 4.1.1 discusses the most promising processing options and outlines the experimental scope of this chapter. A brief overview of modeling approaches on co-processing is presented in Section 4.1.2, including the questions that this chapter aims to answer.

4.1.1 Processing of Feedstocks Rich in Heavy Mono-Ring Aromatics

Refineries have several options to incorporate an aromatic-rich stream. With little effort, the durene-containing heavy gasoline could be blended into reformate or middle distillate to dilute durene below a particular concentration at which it no longer crystallizes. Chang [49] found a concentration below 3 % sufficient, whereas Olsbye et al. [25] emphasized that there might be climate conditions at which crystallization could still occur. Therefore, such a measure would only be feasible for small volumes of heavy gasoline. Additionally, even if crystallization issues are solved, emission tendencies and petrochemical parameters such as the *CN* remain negatively affected by aromatics [134]. Therefore, an after-treatment is usually applied, e.g., isomerization [50, 117] or hydroprocessing [1, 117]. As such processes are capital intensive [135] but are also available in most refineries, the co-processing of bio-derived feedstocks with fossil intermediates is frequently discussed. Besides defossilizing the refinery sector, co-processing bio-derived feedstocks comes with self-evident advantages. It makes biofuels more competitive by saving capital investment, as a highly integrated processing infrastructure [43–45] and a reliable blending and fuel distribution system can be drawn on [46]. Therefore, co-processing is an attractive way to lower production costs while decreasing the GHG impact of fossil fuels.

Processes regularly found in refineries are (a) transalkylation / disproportionation, (b) fluid catalytic cracking (FCC), and (c) hydrotreating or generally hydroprocessing. Even if transalkylation and disproportionation are already commercialized, for example, with the Mobil TransPlus^{SM} process [47], these options are not available in every refinery. Additionally, low molecular aromatic streams such as toluene are required for the transalkylation of C_9-C_{12} aromatics, present in heavy gasoline, toward lighter aromatics. FCC is frequently discussed for the co-processing of various bio-derived and

fossil feedstocks as it is readily found in the refinery environment [136]. Typical FCC feedstocks are vacuum gas oil (VGO) and heavy atmospheric gas oil with boiling temperatures between 280 °C and 580 °C [42]. Therefore, high boiling feedstocks, such as vegetable oils, animal fats [137], and bio-oils obtained, for example, by flash pyrolysis of biomass [44, 138, 139], are usually co-processed in FCC units. Heavy gasoline from MTG and DTG processes comes with a boiling range of approx. 177–290 °C (see Section 4.2.1 for detailed petrochemical parameters) and, therefore, lies below the boiling temperature of typical FCC feedstocks. As heavy gasoline consists almost entirely of aromatics, it is to expect that almost no reaction takes place besides some dealkylation of ring-attached side chains [140]. Like FCC, hydroprocessing is virtually found in any refinery [42]. Typically, hydroprocessing is used to remove heteroatoms such as sulfur, nitrogen, and oxygen from middle distillate [42, 141, 142]. One of the most commonly applied catalysts is a cobalt-molybdenum (CoMo)-based catalyst for hydrodesulfurization (HDS) [43, 143]. Hydroprocessing also became increasingly important for the partial hydrogenation of aromatics [42, 144]. For example, the data of Bisht et al. show that hydrogenation of aromatic compounds to naphthenes helps to improve the *CN* [134]. Simultaneously, the expected emissions are reduced because naphthenes have lower sooting tendencies [41]. Hydroprocessing is reportedly suitable for co-processing aromatic-rich feedstocks such as light cycle oil (LCO), which is comparable to the heavy gasoline considered in this chapter in terms of high aromatic content [144, 145]. Ancheyta-Juárez proved a product quality improvement for the co-hydroprocessing of middle distillate and LCO, using a CoMo/γ-Al_2O_3 catalyst [144]. Sági et al. investigated the co-hydroprocessing of LCO with animal fats and straight run gas oil using a nickel-molybdenum (NiMo)/Al_2O_3 catalyst [145]. Depending on the process conditions, the aromatics were significantly reduced, which resulted in a primarily standard-compliant diesel.

The aim of the experimental part of this chapter was to investigate the suitability of a common hydrotreater for the co-hydroprocessing of fossil middle distillate and durene-rich bioliq® heavy gasoline. Experiments with a feedstock of 15 wt.% durene and 85 wt.% middle distillate were conducted according to a local refinery's reaction parameters using a commercially available CoMo/γ-Al_2O_3 catalyst. An important aim was to find stable operating conditions, as high deactivation rates would affect the product quality and the lifespan of the catalyst before regeneration [135]. The results were further used to calculate the hydrogenation and isomerization selectivity of the durene conversion in order to evaluate the catalyst's suitability to improve important fuel parameters linked to the aromatic content. Additional experiments were conducted with the aim of evaluating the resulting fuel yields and qualities using a feedstock of 15 wt.% bioliq® heavy gasoline and 85 wt.% middle distillate. The fuel yields of gasoline, kerosene, and diesel and the economically important parameters ON, i.e., *RON* and *MON*, and *CN* [96] were of particular interest.

4.1.2 Modeling of Hydroprocessing

Hydroprocessing involves various reactions, e.g., hydrogenation and dehydrogenation, isomerization, C–C bond scission, hydrogen transfer, and disproportionation [40]. C–C bond scission represents all types of cracking reactions, including exo- and endo-cyclic β-scission of cyclic compounds. Exo-cyclic β-scission means the dealkylation of side chains attached to naphthenes and aromatics, while endo-cyclic β-scission is the RO that forms olefins and paraffins [61]. An especially fast mechanism is the so-called paring reaction, becoming relevant for cyclic molecules ≥ C_{10}, yielding iso-butane and the respective remaining cyclic carbenium ion by fast tertiary–tertiary β-scission [76]. Which reaction predominates strongly depends on the catalyst and the reaction conditions used [146]. While mostly hydrogenation, i.e., hydrotreating reactions, are favored at medium temperatures, isomerization and cracking reactions become more predominant as the temperature increases [61, 147].

Due to the numerous reactions involved and the complex compositions of fossil and biomass-derived feedstocks, hydroprocessing is regularly modeled with simplified approaches such as discrete lumping models, e.g., [146–156], and substance group lumping models, e.g., [147, 148]. In discrete and substance group lumping models, the sample is subdivided into lumps of specific boiling ranges or substance groups [148]. Lumps can be typical refinery products, for example, gasoline, kerosene, and diesel, if boiling ranges are considered, or paraffins, naphthenes, and aromatics in the case of substance groups [40, 153]. Lumping by boiling ranges has the advantage of practical accessibility, as boiling curves are convenient to measure [153], while detailed hydrocarbon analysis requires sophisticated techniques such as GC*GC to gain integral information on a sample's composition. Such are available but not as regularly found as boiling range analyzers. As shown in Figure 4.1, lumps are treated as chemical compounds, and a reaction network is constructed in between [155], where all the individual reactions are lumped together [40, 157]. In general, a model's predictive power improves as the number of lumps

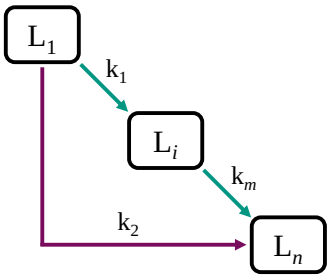


Figure 4.1: Lumping model with n lumps and m reactions.

increases, which, however, is also accompanied by an over-proportional increase in kinetic parameters to be determined [40, 74]. Further modeling techniques, relying on more detailed knowledge, are continuous lumping models, where a feedstock's reactivity is described as a continuous function, e.g., [40, 157], and single event models, where a more in-detail mechanistic knowledge is required, e.g., [74]. Depending on the task, lumping models are as precise as the more complex ones while, however, being restricted to the prediction of prior defined lumps, which must therefore be chosen deftly [146]. Nevertheless, complex reaction systems are relatively straightforward to implement with lumping models, for example, into process simulation software [147, 150].

The aim of this chapter's theoretical part was to develop an application-oriented lumping model for predictions during daily refinery operations about the co-hydroprocessing of bioliq® heavy gasoline and fossil middle distillate. Efforts were made to precisely predict the fuel yields of gasoline, kerosene, and diesel by using this modeling approach. The results of the parameter estimation were further evaluated to gain information on the main reactions involved.

4.2 Materials and Methods

4.2.1 Experimental Setup and Procedure

Besides the relevant information presented here, a more detailed description of the experimental setup can be found in Section 2.3. The co-hydroprocessing experiments were conducted in an electrically heated fixed bed reactor with an inner diameter of 14.9 mm, operated top-down in co-current mode. A total of 67.689 g of a commercially available CoMo/γ-Al_2O_3 catalyst with a particle size distribution of 100–200 µm was filled into the reactor. The first 15 cm of the reactive zone consisted of catalyst diluted

with SiC (weight-ratio 70 : 30) of the same particle size distribution. Further, 30 cm of pure catalyst completed the reactive zone. By this measure, the axial reactor temperature profile could be maintained within ±0.9 °C of the set reaction temperature for all experiments performed. The inlet and outlet of the reactor were additionally filled with SiC (210 µm) over a length of 15 cm and 20 cm, respectively, to keep the catalyst in position and ensure an ideal mixing of the feed components. A central probe tube with an outer diameter of 1/8″ was available for measuring the reactor's temperature profile by axially moving a K-Typ thermocouple.

Table 4.1 lists the petrochemical parameters of the hydrocarbon fractions used for the experiments in this chapter. Middle distillate was provided by ASG Analytik-Service, Neusaess, Germany. It consisted

Table 4.1: Hydrocarbon fractions used for the co-hydroprocessing experiments.

	Middle Distillate	**bioliq® Heavy Gasoline**	**Feedstock**
CN /-	60.3	N/A	N/A
ρ_{20} / kg m^{-3}	823.0	890.0	827.6
w_{Sulfur} / mg kg^{-1}	< 5	0	0
CFPP / °C	-14	N/A	N/A
$w_{\text{Aromatics}}$ / wt.%	5.7	97.0	approx. 19.4
IBP / °C	179.7	176.7	175.0
*T*25 / °C	247.7	185.7	230.6
*T*50 / °C	263.2	190.0	257.5
*T*75 / °C	277.6	198.2	275.1
FBP / °C	365.2	289.8	365.2

mainly of paraffins, about 5.7 wt.% polycyclic aromatic hydrocarbons (PAHs), and had a sulfur content of below 5 wppm. Heavy gasoline was obtained by rectification of bioliq® raw gasoline to a top temperature of approx. 176 °C and consisted of 33.6 wt.% C_9 and 52.6 wt.% C_{10} aromatics, of which 21.4 wt.% was durene. Another large proportion were C_{12} aromatics at 10.4 wt.%, with the remainder consisting mainly of paraffins and naphthenes. Additionally, dimethyl disulfide (DMDS) (≥ 99%, Alfa Aesar, Heysham, United Kingdom) and durene (97 %, Fisher Scientific GmbH, Schwerte, Germany) were used. The feedstock for the experiments consisted of 15 wt.% heavy gasoline and 85 wt.% middle distillate (see right column of Table 4.1), which had a boiling range of 175.0–365.2 °C and an aromatics content of approx. 19.4 wt.%. Additionally, a mixture of 15 wt.% pure durene and 85 wt.% middle distillate with a total aromatic content of approx. 19.8 wt.% was used as feed for several experiments. The boiling range could not be provided as the condenser of the boiling range analyzer got clogged by the crystallization of durene due to its high concentration. Which feed was used for the respective experiments will be indicated in the discussion.

Before the experiments, the CoMo/γ-Al_2O_3 catalyst was activated using a sulfur-enriched stream of middle distillate. Sulfur was added as DMDS, which comes with a sulfur content of 68 wt.% and is frequently used to activate traditional hydrotreating catalysts [152, 158]. The amount of DMDS added to the middle distillate was calculated based on the catalyst mass and expected sulfur uptake according to the manufacturer. To ensure complete catalyst activation, the theoretical mass of sulfur was multiplied with a security factor of 1.25. In total, 15.305 g DMDS dissolved in 716 g middle distillate was used as feed to carry out the activation procedure of 67.689 g catalyst. For the sulfiding process, the following procedure, related to the findings of Texier et al. [158], was applied. Before the sulfidation, the catalyst was dried at 150 °C for 60 h in a pure argon atmosphere. The pump was then set to a feed

flow rate of 0.29 mL min^{-1}. Simultaneously, the gas supply was adjusted to a hydrogen and argon flow of 300 mL min^{-1} and 20 mL min^{-1}, respectively. All flow rates were kept constant over the whole sulfidation process. Right after the flows were adjusted, the temperature was increased from 150 °C to 225 °C with a rate of approx. 18.8 °C h^{-1} and held constant at 225 °C for 8 h. After this period, a second temperature ramp of approx. 14.7 °C h^{-1} was applied for 8.5 h, increasing the temperature from 225 °C to 350 °C. The temperature was again kept constant for 8 h at 350 °C, after which the activation procedure was completed. For all following experiments, the feed was enriched with 1000 wppm of sulfur equivalent in the form of DMDS to preserve the active state of the catalyst.

The first set of experiments focused on the conversion, the selectivity, i.e., differentiation between hydrogenation and isomerization of durene, and the catalyst deactivation. For these experiments, middle distillate was enriched with 15 wt.% of durene. For approx. 860 h on stream, experiments were conducted at 320 °C, 350 °C, and 380 °C for a constant *LHSV* of 0.4 h^{-1}, a constant total pressure of 62.9 bar (59 bar H_2, 3.9 bar Ar), and a ratio $\dot{V}_{H_2}/\dot{V}_{Feed}$ of 1042 $Nm^3\ m^{-3}$. Argon was added as an internal standard for calculating the volume flow rates of the gaseous products. Related product concentrations were measured with an Agilent (Santa Clara, CA, USA) 7890A online GC. All liquid samples' compositions were measured using an Agilent 7890B according to ASTM 6730-01 [84].

As shown in Figure 4.2, a reference point at T = 380 °C and *LHSV* = 0.25 h^{-1} was set every weekend to keep track of possible catalyst deactivation. After approx. 1000 h on stream, the catalyst deactivation was negligibly low and further experiments were conducted under nearly steady-state conditions (see Figure C.1 in the Appendix). For these experiments, 85 wt.% middle distillate was enriched with

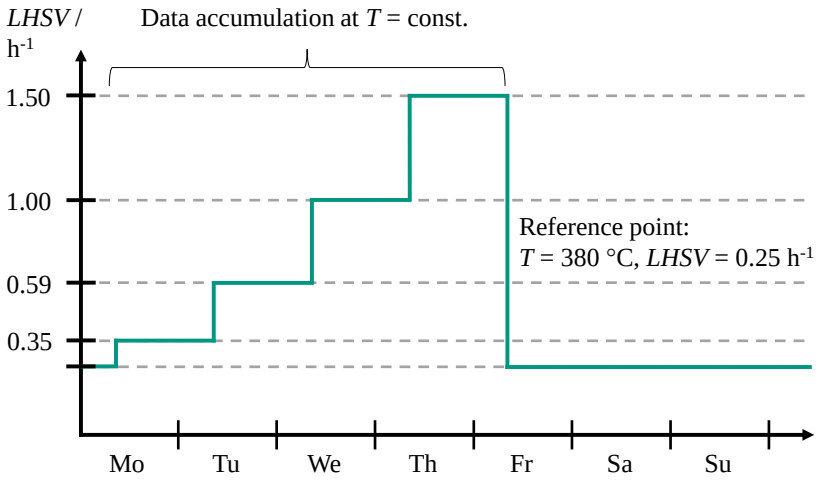


Figure 4.2: Weekly experimental procedure for the parameter study with a feedstock of 85 wt.% middle distillate and 15 wt.% bioliq® heavy gasoline.

15 wt.% bioliq® heavy gasoline (see Table 4.1 for petrochemical parameters). A parameter study was conducted to investigate durene and C_{10} aromatics conversions in dependence on temperature and *LHSV*. Additionally, the fuel yields, i.e., gasoline, kerosene, and diesel, were measured for the conducted experiments. Typical hydroprocessing temperatures of 340–390 °C were set at weekly intervals. As can be seen in Figure 4.2, for 350 °C, 370 °C, 380 °C, and 390 °C, the *LHSV* was set to 0.35 h^{-1}, 0.59 h^{-1}, 1.00 h^{-1}, and 1.50 h^{-1} on a daily basis. At 340 °C, *LHSV*s of 0.25 h^{-1}, 0.50 h^{-1}, 0.75 h^{-1}, and 1.20 h^{-1} were investigated. The ratio $\dot{V}_{H_2}/\dot{V}_{Feed}$ was kept constant at 1042 $Nm^3\ m^{-3}$ for all conducted experiments. All samples obtained from the feedstock consisting of 15 wt.% bioliq® heavy gasoline and 85 wt.% middle distillate were additionally separated into light gasoline (30–170 °C) and diesel (170–365 °C) using a water-cooled laboratory-scale rectification column with a capacity of 250 mL. *RON*, *MON*, and

CN of the obtained gasoline and diesel fractions were measured using an OptiFuel from PAC (Houston, TX, USA). Additionally, the compositions of the gasoline samples were measured using a Reformulyzer M4 from AC PAC. The data obtained from the parameter study were subsequently used to develop three lumping models, the methodology of which is explained in the following.

4.2.2 Model Structure and Procedure

Three lumping models are presented in this chapter, two of which are based on different assumptions regarding the reaction network. Based on the findings, a third optimized model is developed. As mentioned in Section 4.2.1, all models are based on the data obtained from the experiments with a feedstock of 15 wt.% bioliq® heavy gasoline and 85 wt.% middle distillate (see Table 4.1 for petrochemical parameters). Four datasets at reaction temperatures of 340 °C, 350 °C, 380 °C, and 390 °C were used for the parameter estimation, with one dataset at 370 °C left out for independent validation of each model. The experimental data for the parameter estimation can be found in Table C.1 in the Appendix.

Boiling curves of feed and products were measured according to ASTM D7345 [88] and subdivided into lumps. The number of lumps was chosen based on the results of other researchers. Alhumaidan et al. [150] investigated three models for the same dataset having four, five, and ten lumps, respectively. They found no significant increase in the models' performances if the number of lumps was increased from five to ten and highlighted the tendency of over-fitting. Similar results were reported by Ayasse et al. [155], who compared three models with five, six, and seven lumps for modeling the hydrocracking of bitumen. They achieved similar accuracies for all three models and stated an over-determination for the seven-lump model. It can be concluded that the number of lumps should be chosen only as high as necessary to describe the product composition at hand with the required accuracy. In this work, five liquid lumps were found sufficient to describe the fuels of interest, i.e., gasoline, kerosene, and diesel. A sixth lump represents the gaseous losses, calculated based on a mass balance. Table 4.2 lists the six lumps considered in this work. Besides their boiling ranges, information on their rough compositions and initial mass fractions (feedstock) is also given. Gaseous losses (0–30 °C) are represented by lump

Table 4.2: Boiling ranges, compositions, and initial mass fractions of the lumps used for modeling (Naph. ≙ Naphtenes, Par. ≙ Paraffins, Aro. ≙ Aromatics).

Lump	Boiling Range / °C	Approx. Composition	w_i @ τ = 0 / wt.%
1	300–365	Mainly Par.	11.25
2	270–300	Aro., Par.	21.51
3	210–270	Aro., Par.	61.64
4	170–210	Aro., Par. and Naph.	5.61
5	30–170	Aro., Par. and Naph.	0
6	0–30	Par.	0

6, light gasoline (30–170 °C) by lump 5, heavy gasoline by lump 4, kerosene (170–270 °C) by the summation of lumps 3 and 4, and diesel (170–365 °C) by the summation of lumps 1–4. Lumps 1–4 consist primarily of paraffins as they strongly overlap with the middle distillate-rich feedstock. Lumps 2–5 are additionally enriched with aromatics originating from bioliq® heavy gasoline, of which lump 4 has the highest share of aromatics according to the heavy gasoline boiling range. Gas lump 6 is, with good approximation, entirely paraffinic, resulting from cracking and dealkylation reactions. Cracking and hydrogenation reactions will further result in an enrichment of the lighter lumps with paraffins and naphthenes. Discussions on the mass distribution due to hydroprocessing reactions will be presented in Sections 4.3.2 and 4.3.3.

The modeling of the experimental data was based on assumptions, which are highlighted in the following. After approx. 1000 h on stream, the catalyst activity could be considered constant, so the experiments for data acquisition were conducted under near steady-state conditions. For constant monitoring, a reference point was adjusted every 6$^{\text{th}}$ and 7$^{\text{th}}$ day on stream (see Figure 4.2). Deactivation was quantified as a relative conversion loss of 1.1–2.2 % between 1450 h and 2150 h on stream, which is within measurement uncertainty (see Figure C.1 in the Appendix). Furthermore, the experiments were considered to be conducted under isothermal conditions, which was ensured by catalyst dilution, as explained in Section 4.2.1. As proven experimentally [159], hydroprocessing reactions, e.g., HDS, HDN, and hydrocracking, are frequently considered independent of the hydrogen concentration and thus of first order with respect to the feed [147, 150, 154, 155]. Due to a high excess of hydrogen in the experiments of this work, the rate expressions are considered first order. For all three models, the reactions are further considered irreversible. This seems difficult since up to 19.4 wt.% aromatics are present in the feed, whose hydrogenation is a thermodynamically limited equilibrium reaction [63]. However, with such simplification, good results were obtained in the literature [148, 154]. To review the validity of this assumption, an additional temperature variation from 350 °C to 400 °C in 10 °C steps at a relatively low *LHSV* of 0.4 h^{-1} was conducted (see Figure C.2 in the Appendix). It was found that the durene conversion increases rapidly from 350 °C to 380 °C and slower between 380 °C and 390 °C, which indicates the equilibrium getting noticeable. Therefore, it can be assumed that the reverse reactions can be neglected for the parameter range and the catalyst investigated in this work. Considering the above-stated and by assuming ideal plug flow reactor conditions, the component mass balances of each lump,

$$\frac{\mathrm{d}w_i}{\mathrm{d}\tau} = -w_i \sum_{z=1}^{N} k_{i,z} + \sum_{z=1}^{N} w_z \cdot k_{z,i}, \tag{4.1}$$

are developed, where w_i and w_z are the mass fractions of lump i and z , respectively, and $k_{i,z}$ and $k_{z,i}$ are the rate constants for reactions from lump i to z and lump z to i, respectively. The space-time τ,

$$\tau = \frac{1}{LHSV}, \tag{4.2}$$

is directly linked to the *LHSV*, which was calculated based on the actual catalyst volume. For the CoMo/γ-Al_2O_3 catalyst used in this chapter, a particle density of 2.69 ±0.14 g cm^{-3} was measured using an Ultrapyc 1200e from Quantachrome (Boynton Beach, FL, USA). The temperature dependencies of the reaction rates in Equation (4.1) were modeled using the reparameterized Arrhenius equation,

$$k_j = k_{0,j} \cdot \mathrm{e}^{-\frac{E_{\mathrm{A},j}}{R}\left(\frac{1}{T}-\frac{1}{T_{\mathrm{Ref}}}\right)}, \tag{4.3}$$

where k_j is the rate constant of reaction j, $k_{0,j}$ is the pre-exponential factor for a given reference temperature T_{Ref}, $E_{\mathrm{A},j}$ is the activation energy and T the reaction temperature. T_{Ref} was set to 365 °C, which lies in the middle of the investigated temperature range in this work. The reparameterized equation avoids strong correlations between activation energies and rate constants during fitting [147].

The model equations are constructed from Equations (4.1)–(4.3) and solved considering each lump's initial conditions (τ = 0) listed in Table 4.2. Depending on the number of lumps and reactions, the pre-exponential factors and activation energies in the resulting model equations must be determined. The best set of kinetic parameters was obtained by minimization of the objective function,

$$SSE = \sum_{j=1}^{n_{\mathrm{e}}} \sum_{i=1}^{n_{\mathrm{l}}} (w_{\mathrm{exp},i} - w_{\mathrm{calc},i})^2, \tag{4.4}$$

based on the sum of square errors between the measured product weight fractions $w_{\mathrm{exp},i}$ and the calculated product weight fractions $w_{\mathrm{calc},i}$, for all lumps n_{l} and conducted experiments n_{ex} [160]. For the least-squares minimization, the lmfit package in Python was used [161]. A first estimation of the parameter set was either performed by the Levenberg–Marquardt or the Nelder–Mead algorithm. In most cases, the slower but more robust Nelder–Mead algorithm provided a more promising first guess. In contrast, the final parameter estimation was mainly performed with the Levenberg–Marquardt algorithm, as it is strong in finding an optimum if the set of parameters is already close to the global solution [161]. The system of ordinary differential equations (ODEs) was solved using scipy.integrate, a sub-package of scipy [162] based on the Runga–Kutta algorithm. However, in some cases, Runga–Kutta was found to fail. If so, the algorithm was switched automatically using the LSODA algorithm. LSODA is a method with automatic stiffness detection and subsequent switching of the solver, e.g., Adams (non-stiff) to BDF (stiff) [162].

As mentioned, three models are developed and compared based on the same data in this work. If the data are described more precisely by model B than by model A, and model B does so with different degrees of freedom, it is helpful to evaluate whether this improvement is statistically valid, for example, using Fisher's exact test. A lower error with model B than model A is significant if the condition,

$$F_{\mathrm{A-B}} = \frac{\frac{SSE_{\mathrm{A}} - SSE_{\mathrm{B}}}{SSE_{\mathrm{B}}}}{\frac{\nu_{\mathrm{A}} - \nu_{\mathrm{B}}}{\nu_{\mathrm{B}}}} > F_{1-\alpha}(\nu_{\mathrm{A}} - \nu_{\mathrm{B}}, \nu_{\mathrm{B}}), \tag{4.5}$$

is fulfilled, where $F_{1-\alpha}(\nu_{\mathrm{A}} - \nu_{\mathrm{B}}, \nu_{\mathrm{B}})$ is the critical value of the F-distribution, $SSE_{\mathrm{A/B}}$ are the sums of square errors SSE and $\nu_{\mathrm{A/B}}$ the degrees of freedom [147]. The degrees of freedom of model i,

$$\nu_i = n_{\mathrm{l},i} \cdot n_{\mathrm{e},i} - n_{\mathrm{p},i}, \tag{4.6}$$

are calculated based on the number of lumps n_{l}, number of parameters n_{p}, and number of experiments n_{e}. $F_{1-\alpha}(\nu_{\mathrm{A}} - \nu_{\mathrm{B}}, \nu_{\mathrm{B}})$ depends on the level of significance, which was chosen with 95 % (α = 0.05) [147]. If the condition of Equation (4.5) is not fulfilled, the improvement of model B over model A is insignificant, meaning the model with fewer parameters is preferred. The critical values of the F-distribution $F_{1-\alpha}(\nu_{\mathrm{A}} - \nu_{\mathrm{B}}, \nu_{\mathrm{B}})$ were calculated with Excel®'s finv function. Input parameters are the degrees of freedom, ν_{A} and ν_{B}, and the probability α.

4.3 Results and Discussion

4.3.1 Influence of Reaction Parameters on Catalyst Performance

Data discussed in the following were collected over 860 h on stream at three reaction temperatures of 320 °C, 350 °C, and 380 °C for a constant $LHSV$ of 0.4 $\mathrm{h^{-1}}$, a constant total pressure of 62.9 bar (59 bar H_2, 3.9 bar Ar), and a ratio $\dot{V}_{\mathrm{H_2}}/\dot{V}_{\mathrm{Feed}}$ of 1042 $\mathrm{Nm^3\ m^{-3}}$ using a feedstock consisting of 15 wt.% pure durene and 85 wt.% middle distillate. Additionally, data originating from a temperature variation between 350 °C and 400 °C under pseudo-steady state conditions is discussed in this section.

Figure 4.3a shows the durene conversion,

$$X_{\mathrm{durene}} = \frac{w_{\mathrm{durene,in}} - w_{\mathrm{durene,out}}}{w_{\mathrm{durene,in}}}, \tag{4.7}$$

where $w_{\mathrm{durene,in}}$ and $w_{\mathrm{durene,out}}$ are the respective mass fractions of durene in the feedstock and product, respectively, over a time on stream TOS of approx. 860 h, in dependence on temperature. Dashed

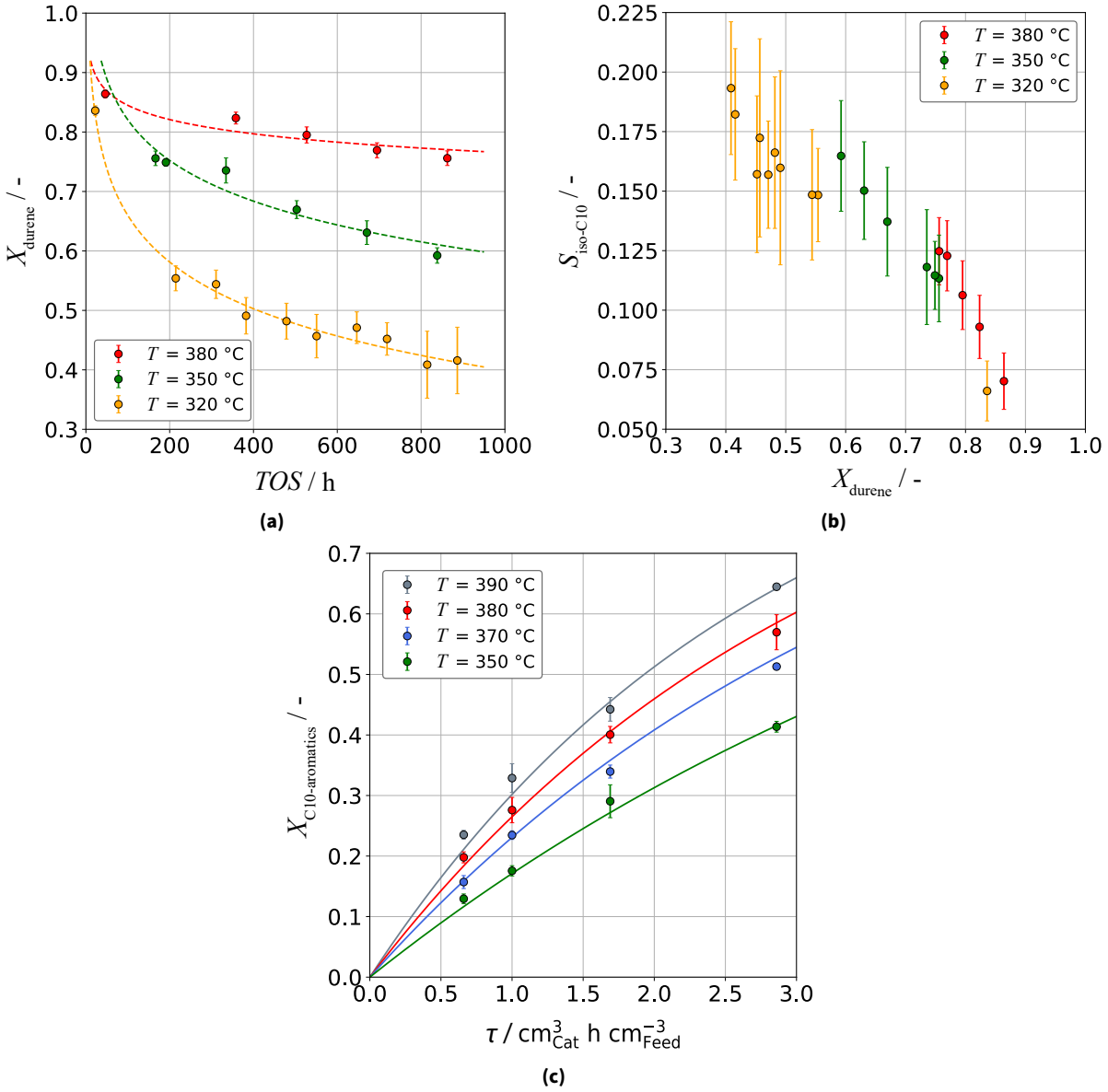


Figure 4.3: (**a**) Durene conversion, (**b**) durene isomerization selectivity for the co-hydroprocessing of durene (15 wt. %) and middle distillate (85 wt. %) at constant $LHSV$ = 0.40 h^{-1}, and (**c**) C_{10} aromatic conversion for the co-hydroprocessing of heavy gasoline (15 wt. %) and middle distillate (85 wt. %); $\dot{V}_{H_2}/\dot{V}_{Feed}$ = 1042 $Nm^3\ m^{-3}$, $\bar{p}_{H_2}$ = 59 bar, and $\bar{p}_{Ar}$ = 3.9 bar.

curves are drawn to clarify the trend and are not based on any mathematical model. At all temperatures studied, especially 320 °C and 350 °C, the durene conversion decreases rapidly in the first hours on stream. The substantial decrease can be explained by catalyst coking, occurring disproportionately in the first hours on stream [152, 163]. After a certain decline, the deactivation seems to continue to decrease linearly at all three temperatures, with a pseudo-steady-state presumed at 380 °C. Similar findings were reported by Vivas-Báez et al. [163], who investigated the hydroprocessing of VGO using a sulfided NiMo/USY catalyst. In their experiments, the catalyst activity decreased significantly in the first 170 h on stream. After this period, deactivation decelerated, and the conversion developed toward a steady-state after approx. 1700 h on stream. In the experiments of the present chapter, it is also noticeable that the hydrogenation conversion increases strongly with increasing reaction temperature, which was also found by other authors [144, 147, 154]. More precisely, in the present work, durene

conversion increased up to the highest reaction temperature investigated, 400 °C (see Figure C.2 in the Appendix), while no conversion maximum was observed as a consequence of equilibrium influence, as found by other authors [145]. This is due to the additional influence of other process parameters on the hydrogenation equilibrium, e.g., an increased hydrogen pressure, which shifts the hydrogenation maximum toward higher reaction temperatures [63, 144]. As explained in Section 4.1.1, aromatics negatively influence a fuel's petrochemical parameters and emission tendencies. Therefore, the durene isomerization selectivity,

$$S_{\mathrm{iso-C10}} = \frac{w_{\mathrm{iso-C10,out}} - w_{\mathrm{iso-C10,in}}}{w_{\mathrm{durene,in}} - w_{\mathrm{durene,out}}}, \tag{4.8}$$

was additionally considered, where $w_{\mathrm{iso-C10,in}}$ and $w_{\mathrm{iso-C10,out}}$ are the mass fractions of all C_{10} aromatics besides durene in the feedstock and product, respectively. From the prior mentioned, the selectivity must be low to favor hydrogenation. In Figure 4.3b, the durene isomerization selectivity is plotted over durene conversion for the temperatures 320 °C, 350 °C, and 380 °C. In general, the isomerization selectivity decreases with conversion, on the first view independent of the reaction temperature. However, slight differences can be observed, although these are not highly significant due to measurement error. The selectivity curve slightly shifts upward at higher reaction temperatures, favoring isomerization. This change in selectivity is most likely due to the influence of the chemical equilibrium on the hydrogenation of aromatics at increased reaction temperatures [63]. An influence of the deactivation is unlikely since the data points were measured over 860 h on stream and no trend could be perceived between points measured early compared to points measured later in the campaign.

Finally, the co-hydroprocessing at nearly steady-state catalyst conditions (1.1–2.2 % of relative activity loss), using a blend of 15 wt.% bioliq® heavy gasoline and 85 wt.% middle distillate as feedstock, was investigated. Additionally, the data obtained from these experiments were used for modeling purposes, as discussed in Section 4.3.3. The experiments' scope can be comprehended in Table C.1 in the Appendix.

Figure 4.3c shows the C_{10} aromatics conversion over space-time in dependence on temperature. The C_{10} aromatics conversion increases with higher temperature, similar to Figure 4.3a for a feedstock containing pure durene. As expected, a higher space-time also increases the conversion of C_{10} aromatics, which is also confirmed by other studies [144, 147, 150, 151]. Figure 4.3c also shows the modeled conversions, applying the reparameterized Arrhenius equation at T_{Ref} = 365 °C. For the hydrogenation of C_{10} aromatics, a pre-exponential factor k_0 of 0.26 $\mathrm{cm^3_{Feed}\ h^{-1}\ cm^{-3}_{Cat}}$ and an activation energy E_{A} of 55.8 kJ $\mathrm{mol^{-1}}$ were found, which lies in the range of activation energies found by other authors for various catalysts and aromatics [63].

It can be concluded that a high reaction temperature is beneficial for the co-hydroprocessing of heavy aromatics such as durene and middle distillate. The overall aromatic conversion is higher, reducing the isomerization selectivity in favor of hydrogenation. An increased reaction temperature of ≥ 380 °C is further beneficial as the catalyst reaches pseudo-steady-state conditions faster. A higher C_{10} aromatics conversion was additionally reached by increasing the space-time (lower *LHSV*). Controlling the aromatic hydrogenation over temperature is preferred due to the mentioned benefits but also for process reasons, as the throughput remains unchanged. At the same time, the reaction temperature cannot be increased without constraints. This is partly for constructional reasons, and partly because the reaction temperature is regularly increased to counteract ongoing deactivation. Therefore, the options need to be weighed individually.

4.3.2 Fuel Yields and Qualities

In addition to removing aromatics, fuel yields, i.e., gasoline, kerosene, and diesel, and the corresponding petrochemical parameters are also of interest to a refinery. The economically most important parameters for gasoline and diesel are the ON, i.e., *RON* and *MON*, and the *CN*, respectively. In the case of kerosene, no further parameters were investigated besides the yield. As the feed mainly consists of linear paraffins and no strong isomerization activity of the catalyst was found in the durene experiments, further downstream processing, such as hydroisomerization, is likely required to meet the low temperature requirements of Jet-A1 [112]. The discussions in this section are based on the samples collected from the experiments presented in Section 4.3.1 with a feedstock of 15 wt.% bioliq® heavy gasoline and 85 wt.% middle distillate.

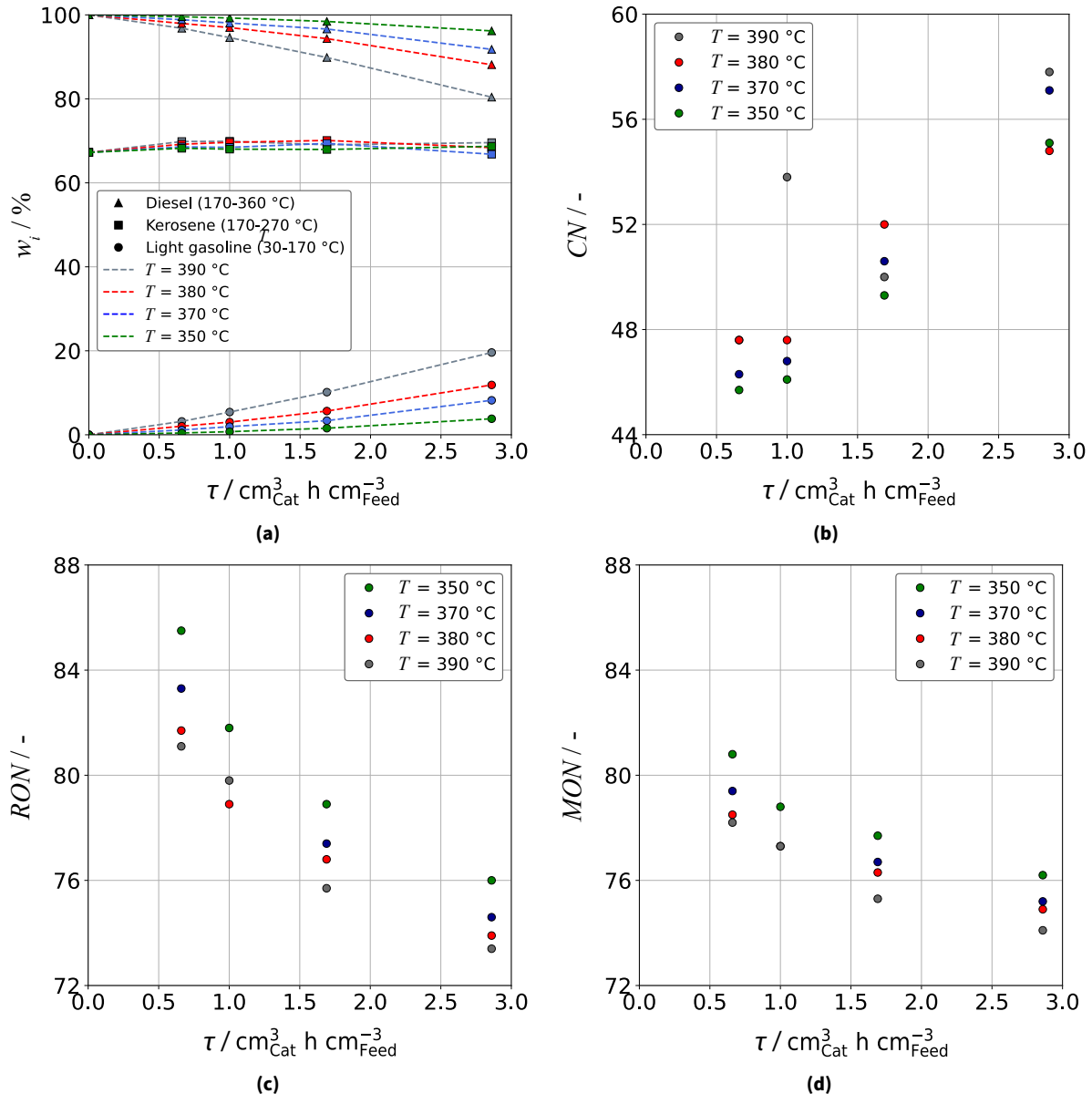


Figure 4.4: (**a**) Yield of diesel (triangles), kerosene (squares), and light gasoline (circles), (**b**) *CN* of diesel, (**c**) *RON* of light gasoline, and (**d**) *MON* of light gasoline for the co-hydroprocessing of heavy gasoline (15 wt.%) and middle distillate (85 wt.%) at $LHSV$ = 0.40 h^{-1}, $\dot{V}_{H_2}/\dot{V}_{Feed}$ = 1042 $Nm^3\ m^{-3}$, $\bar{p}_{H_2}$ = 59 bar and $\bar{p}_{Ar}$ = 3.9 bar.

Figure 4.4a shows the mass fractions of light gasoline, kerosene, and diesel as a function of space-time in dependence on reaction temperature. The gas fraction is not shown, as it does not represent a valuable product fraction. However, further information can be found in Section 4.3.3 and in the Appendix in Figure C.3. It has to be noted that the boiling ranges of kerosene and diesel overlap each other. Consequently, adding up all three fractions would result in a mass fraction above 100 %. The mass fraction of diesel decreases while light gasoline increases with rising space-time. This is further enhanced by a higher reaction temperature, which is especially visible for a temperature increase from 380 °C to 390 °C. The observed is due to temperature-sensitive reactions involved in hydrocracking [156]. Similar dependencies on the process conditions are reported in the literature [149, 150, 154]. For example, Alhumaidan et al. found the same strong influence of the temperature on the hydrocracking of atmospheric residues [150]. In the present work, the hydrogenation of C_9 and C_{10} aromatics in the heavy gasoline forms naphthenes with the same carbon number; however, at a lower boiling range of approx. 140–155 °C. Additionally, the dealkylation of cyclic molecules leads to the formation of smaller aromatics and naphthenes in the gasoline boiling range. This can be comprehended in Figure 4.5, which shows the weight fractions of aromatic and naphthene lumps in light gasoline for a reaction temperature of 370 °C in dependence on space-time. The C_9 and C_{10} aromatics decrease with space-time due to

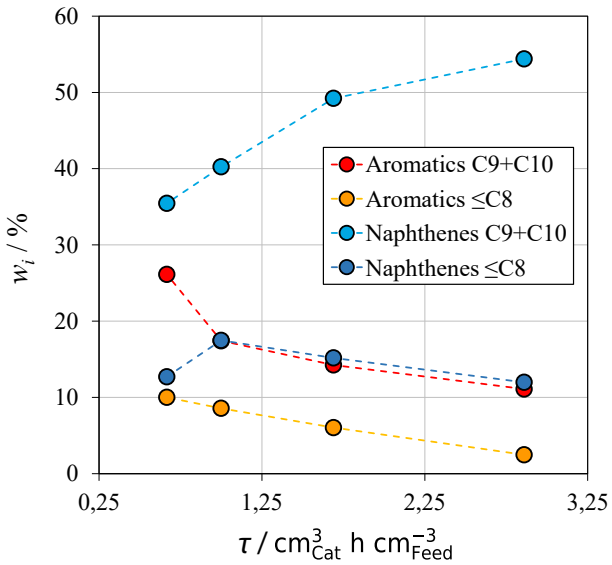


Figure 4.5: Concentration of aromatics and naphthenes in light gasoline in dependence on space-time at T = 370 °C, $\dot{V}_{H_2}/\dot{V}_{Feed}$ = 1042 $Nm^3\ m^{-3}$, $\bar{p}_{H_2}$ = 59 bar and $\bar{p}_{Ar}$ = 3.9 bar.

enhanced hydrogenation, as previously shown in Figure 4.3c, while C_9 and C_{10} naphthenes, the direct hydrogenation products, increase. The weight fraction of ≤ C_8 aromatics follows that of the lumped C_9 and C_{10} aromatics, indicating that the dealkylation of aromatics is responsible for their occurrence. Naphthenes ≤ C_8 are formed by hydrogenation of the respective aromatics and by dealkylation of large naphthenes. Simultaneously, this fraction reacts to paraffins (not shown), thus being an intermediate that shows a maximum at a space-time of 1 cm^3_{Cat} h cm^{-3}_{Feed} in the investigated parameter range.

Following this argumentation, one would also expect a decreasing yield for kerosene, as the boiling range of heavy gasoline strongly overlaps with the one of kerosene (see Table 4.1). However, the kerosene yield stays almost constant over the parameter range investigated. This is probably explained by a pseudo-equilibrium of kerosene-producing and -reducing reactions. In fact, there are reactions that exclusively increase kerosene yield, such as the partial hydrogenation of PAHs already contained in middle distillate. Decalin, the hydrogenation product of the smallest existing PAH naphthalene, has

a boiling temperature of approx. 189 °C. Thus, it can be assumed that hydrogenation products of PAHs increase the kerosene yield (170–270 °C) while being of minor influence on the light gasoline yield (30–170 °C). Additionally, it is reported by several authors that catalysts, as used in the present chapter, are highly cracking selective toward middle distillate fractions [150, 152, 154] while of a comparably low selectivity toward light boiling hydrocarbons such as gasoline and gases. Consistent with the mentioned, gases were reported to be produced mainly from heavy hydrocarbons [149, 151, 152, 155] and, in fact, stayed within 5.4 wt.% in the present work. Authors stated that increasing cracking activation energies [152] and lower overall reaction rates [150] from heavy to light feedstocks are responsible for the observed. Interestingly, such selectivity is typical for catalysts such as CoMo/γ-Al_2O_3, as used in this chapter, whereby hydroprocessing catalysts based on zeolites are reported to produce significantly more gasoline [154].

As outlined in Section 4.2.1, each sample was separated into gasoline and diesel, and the ONs (*RON* and *MON*) and *CN* measured, respectively. Figure 4.4b shows the *CN* in dependence on space-time and temperature. It can be observed that the *CN* increases with space-time and reaction temperature. This is due to a decrease in the concentration of aromatics, as shown in Figure 4.3c, which generally have poor *CN*s [134]. The required space-time to provide a respective *CN* is thus higher if a lower reaction temperature is considered. An increasing diesel quality with higher reaction temperature and space-time was also reported by Ancheyta et al. for the co-processing of middle distillate and LCO [144]. Figure 4.4b shows some outliers, which are due to measurement uncertainties and, in particular, uncertainties in sample distillation. The *CN* reaches over a wide range of approx. 46–58 for the investigated process conditions. Therefore, diesel that meets the minimum *CN* of 51 of EN 590 can be provided for every reaction temperature investigated, even if a loss is observable for all samples taken compared to the pure middle distillate (*CN* = 60.3).

Figure 4.4c and 4.4d shows the *RON* and *MON*, respectively, in dependence on space-time and reaction temperature. It can be seen that *RON* and *MON* decrease with space-time and temperature due to increased hydrogenation of aromatics (see Figure 4.3c), having high ONs [90]. In general, *CN* and ONs are oppositely dependent on the reaction conditions. The more significant decrease in *RON* compared to *MON* can be explained by the change in the chemistry of the samples with increasing degrees of hydrogenation and cracking. While aromatics have high *RON*s, naphthenes and paraffins have comparably high *MON*s [90].

It can be concluded that high reaction temperatures and space-times reduce the diesel yield and increase the gasoline yield, while the kerosene yield remains constant over the range of parameters studied. Additionally, high reaction temperatures and space-times are favorable for the *CN* but negatively influence the *RON* and *MON* due to an enhanced hydrogenation of aromatics. Even if beneficial for ONs, a high aromatic content is not to strive for in the case of this work. As outlined in Section 4.1, heavy aromatics, especially durene, have clear downsides. Therefore, at this point it is emphasized that a further evaluation of the fuels' petrochemical parameters should be carried out. In particular, the *CFPP* should be considered, as durene could have negative effects due to crystallization issues.

4.3.3 Parameter Estimation and Model Validation

To make process decisions in daily operations, refineries must have models that can predict important product yields. Due to the high complexity of the reactions involved in hydroprocessing, lumping models are frequently applied. Discrete lumping models can differ in the number of lumps and reaction paths, making it interesting to investigate how different model frameworks fit the same set of experimental data. Figure 4.6 shows the three lumping models investigated in this chapter, all based on six lumps

but on different assumptions regarding the reaction network. Five liquid lumps and one gaseous one were chosen as it was identified as the sweet spot between predictive power and number of parameters to be estimated (see Section 4.2.2). Figure 4.6a shows the sequential model, consisting of a cascade

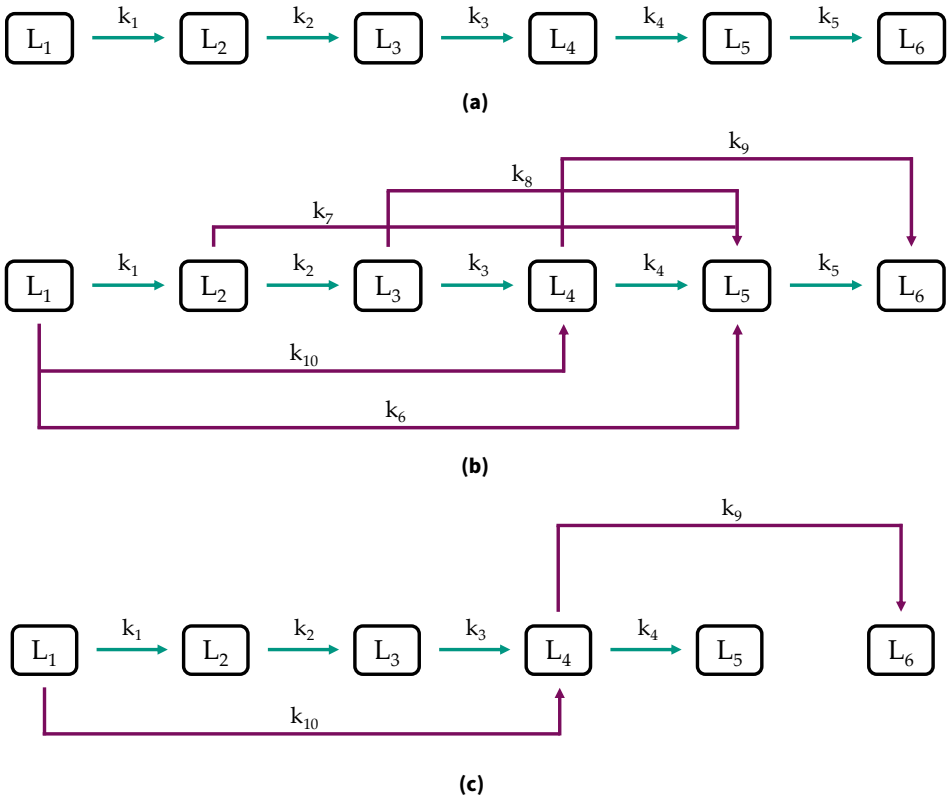


Figure 4.6: Structures of the (**a**) sequential model, (**b**) combined model, and (**c**) reduced model.

of reactions toward lower boiling lumps. It was considered because such simplified models obtained good results in the literature [147, 150, 152]. As shown in Figure 4.6b, the combined model is a detailed discrete lumping model based on the sequential model with additional assumptions, which are also frequently found in the literature [146, 147, 149, 151–155]. As the feedstock used in this chapter consists almost exclusively of paraffins and mono-ring aromatics (see Section 4.2.1), important reactions are the hydrogenation of aromatics and cracking reactions, i.e., dealkylation of naphthenes and aromatics, and cracking of paraffins. An ideal hydrocracking of paraffins was assumed, which was, for example, reported by Becker et al. for the hydroprocessing of VGO using a common hydrotreating catalyst [157]. Ideal hydrocracking predominantly cleaves the hydrocarbon chain near its center, resulting in a bell-shaped molar distribution curve [61]. For example, lump 1, rich in C_{19} paraffins, would react mainly to C_{10} and C_9 paraffins, which end up as a large share in lump 5 (reaction k_{10}) due to their boiling range. The reactions k_6, k_7, k_8, and k_{10} are constructed following the same assumptions. Additionally, as the feed is rich in C_9 and C_{10} aromatics, which are primarily concentrated in lump 4, due to their boiling temperatures, dealkylation was considered with reaction k_9. Dealkylation forms lighter naphthenes and aromatics besides gaseous compounds $\leq C_4$, as outlined in Section 4.1.2. Finally, a reduced model was developed based on the findings obtained from the sequential and combined model to minimize the number of parameters and thus the risk of over-fitting [164]. The experimental datasets used to develop the models can be found in Table C.1 in the Appendix.

Figure 4.7a and 4.7b show the parity plots of the sequential and the combined model, respectively, for the validation dataset at 370 °C. It can be seen that both models provide similar qualitative agreements

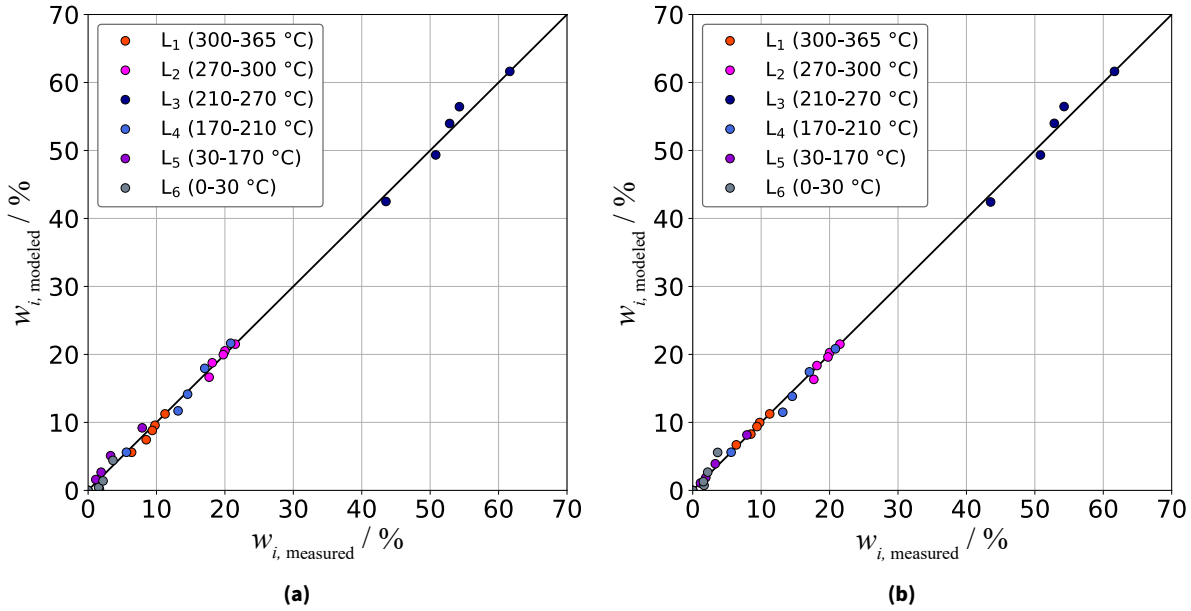


Figure 4.7: Parity plots of the (**a**) sequential model and (**b**) combined model for the experimental validation dataset at T = 370 °C, $\dot{V}_{H_2}/\dot{V}_{Feed}$ = 1042 $Nm^3\ m^{-3}$, $\bar{p}_{H_2}$ = 59 bar and $\bar{p}_{Ar}$ = 3.9 bar.

between the measurements and respective model predictions, whereby the combined model returns a slightly better coefficient of determination (0.9978 > 0.9971). Therefore, it can already be concluded that the additional cracking reactions do not offer significant benefits. The insignificance of ideal hydrocracking may be due to the comparatively low acidity of the CoMo/γ-Al_2O_3 catalyst used. As a result, a non-carbenium ion-based reaction pathway, such as thermal cracking, could become more important [61]. This gets additional meaning since ideal hydrocracking is usually observed at lower reaction temperatures of about 250 °C [61]. Similar good performances of sequential lumping models for the hydrocracking of heavy hydrocarbons were also reported by other authors [147, 150, 152]. The same can be comprehended in Table 4.3, where the reactions k_6, k_7, and k_8 have pre-exponential factors clearly below those of the remaining ones.

Table 4.3: Pre-exponential factors $k_{0,j}$ and activation energies $E_{A,j}$ of the different models.

	$k_{0,j}$ / $cm^3_{Feed}\ h^{-1}\ cm^{-3}_{Cat}$				$E_{A,j}$ / kJ mol^{-1}		
	Sequential	**Combined**	**Reduced**		**Sequential**	**Combined**	**Reduced**
$k_{0,1}$	0.206	0.119	0.123	$E_{A,1}$	116.3	0	0
$k_{0,2}$	0.156	0.135	0.142	$E_{A,2}$	142.4	79.9	89.8
$k_{0,3}$	0.186	0.181	0.185	$E_{A,3}$	54.1	19.1	22.9
$k_{0,4}$	0.264	0.160	0.161	$E_{A,4}$	97.0	109.9	122.4
$k_{0,5}$	0.360	6.09×10^{-7}	-	$E_{A,5}$	0	24.9	-
$k_{0,6}$	-	3.20×10^{-7}	-	$E_{A,6}$	-	0	-
$k_{0,7}$	-	9.25×10^{-8}	-	$E_{A,7}$	-	1845.5	-
$k_{0,8}$	-	9.65×10^{-7}	-	$E_{A,8}$	-	15.8	-
$k_{0,9}$	-	0.126	0.126	$E_{A,9}$	-	12.1	11.0
$k_{0,10}$	-	0.036	0.025	$E_{A,10}$	-	382.6	435.4

The low but still significant pre-exponential factor of reaction k_{10} and the insignificance of reaction k_5 can be interpreted as high cracking selectivity of heavy lumps toward gases, as observed for similar sulfided catalysts [149, 151, 152, 155]. Reaction k_9, with its high pre-exponential factor, in the first view, is not in line with the prior statement as gas is formed from the low boiling light gasoline. The observed can be explained with dealkylation reactions (see Figure 4.5), producing low boiling aromatics, naphthenes, and gases.

For most of the reactions, the calculated activation energies lie in the magnitude found by other authors [146, 151, 152], even though it must be stated that kinetic parameters of lumping models are highly dependent on the system, e.g., feed and model structure, and should therefore be compared with care [155]. The $E_{A,7}$ of the combined model is comparatively high, which, together with the small pre-exponential factor, emphasizes the overall insignificance of reaction k_7. $E_{A,10}$ also appears comparably high, which might be due to two reasons. The investigated temperature range could be too low for a pronounced cracking, and the high activation energy indicates its importance for increased temperatures. More likely is that the reaction is misplaced or another is missing, better representing the actual reaction mechanism. As discussed above, other studies have identified heavy fractions as major sources for the production of low molecular hydrocarbons, which correspond to a reaction of heavy lump 1 (maybe also lump 2) to lump 6.

The results from the sequential and combined models were further used to develop the reduced model shown in Figure 4.6c in which insignificant reactions were omitted. In general, the obtained kinetic parameters (see Table 4.3) agree with those found for the combined model, and the prior interpretation can be drawn on. Figure 4.8 shows the results obtained for the reduced model. The parity plot shown in

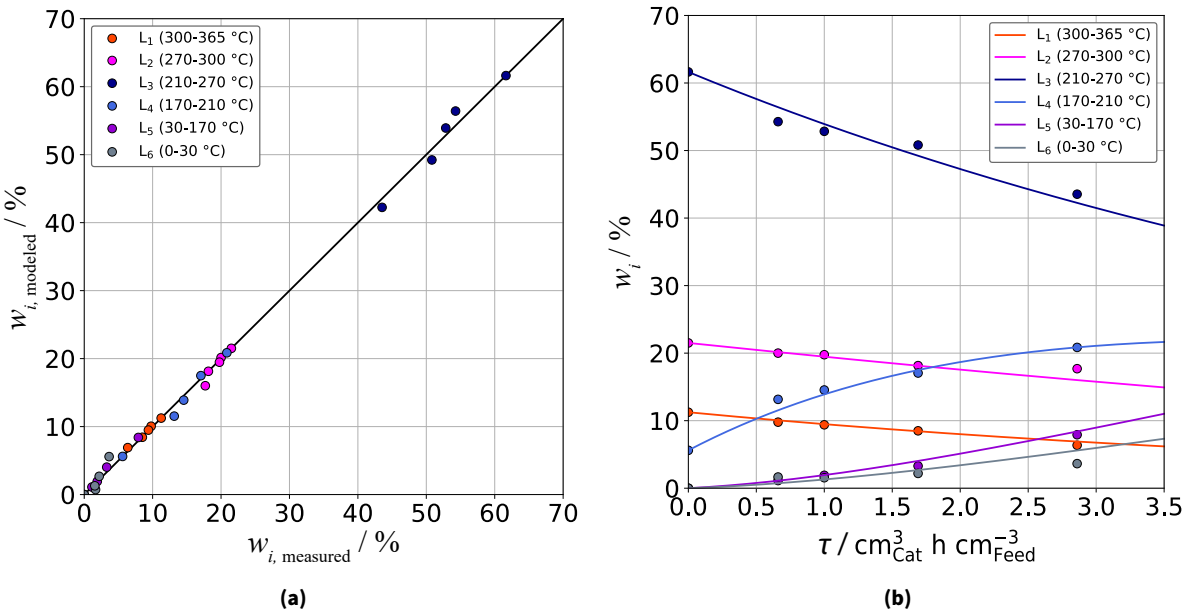


Figure 4.8: (**a**) Parity plot and (**b**) curve fitting results of the reduced model for the experimental validation dataset at T = 370 °C, $\dot{V}_{H_2}/\dot{V}_{Feed}$ = 1042 Nm^3 m^{-3}, $\bar{p}_{H_2}$ = 59 bar and $\bar{p}_{Ar}$ = 3.9 bar.

Figure 4.8a confirms a qualitatively good fit. As expected, with 0.9976, the coefficient of determination lies between the ones for the sequential and combined model ($R^2_C > R^2_R > R^2_S$).

Fisher's exact test was applied to the model predictions for the validation dataset at 370 °C to verify that a parameter reduction justifies a loss of accuracy. Calculations were made according to Equations (4.5) and (4.6) as described in Section 4.2.2. The parameters and results are shown in Table 4.4. By comparing

the sequential and reduced model, it was obtained that $F_{S-R} > F_{1-\alpha}$, which means that the condition is fulfilled. Therefore, the improvement from the sequential to the reduced model is statistically significant, and one should prefer the reduced model. If the reduced and the combined model are compared by Fisher's exact test, it is obtained that $F_{R-C} < F_{1-\alpha}$. The statistical difference between the reduced and combined model is insignificant, so the reduced model should be preferred. Consequently, the combined model is more accurate but insignificant in terms of the higher number of parameters involved.

Figure 4.8b additionally shows measured and computed mass fractions of the different lumps for the experimental validation dataset at 370 °C. As can be seen, all measurements of the different lumps are described very well, and no significant over or under-determination can be recognized.

It can be concluded that the reduced model is very well suited for modeling the co-hydroprocessing of bioliq® heavy gasoline and fossil middle distillate in the investigated parameter range.

Table 4.4: Statistical comparison of the reduced model with the sequential and combined model according to Fisher's exact test for the experimental validation dataset at T = 370 °C.

Parameters	Sequential Model	Reduced Model	Combined Model
n_p	10	12	20
n_l	6	6	6
n_e	16	16	16
ν_i	86	84	76
R_i^2 / -	0.9971	0.9976	0.9978
SSE / kg kg^{-1}	27.16	22.24	20.51
F	-	9.29 ($F_{S\text{-}R}$)	0.8 ($F_{R\text{-}C}$)
$F_{1-\alpha}$	-	3.11	2.06

4.4 Summary and Conclusions

In this chapter, the co-hydroprocessing of heavy gasoline originating from the bioliq® process and fossil middle distillate is investigated over a broad parameter range using a commercial CoMo/γ-Al_2O_3 catalyst under realistic hydrotreating process conditions. Attention is especially paid to 1,2,4,5-tetramethylbenzene (durene), the most critical component originating from MTG and DTG processes because of its crystallization and high emission tendencies.

High reaction temperatures and space-times significantly improve the durene conversion and simultaneously decrease the isomerization selectivity in favor of hydrogenation. Additionally, cracking of aromatics and naphthenes is greatly enhanced, which decreases the diesel yield in favor of the gasoline yield. In contrast, the kerosene yield stays almost constant over the investigated parameter range. At high reaction temperatures, the catalyst reaches pseudo-steady-state conditions faster, for example, after approx. 1000 h on stream at 380 °C.

The hydrogenation of aromatics leads to a considerable improvement of the *CN* in the diesel fraction, while *MON* and, more significantly, *RON* of the gasoline samples decrease. Depending on the parameters applied, a loss of *CN* between approx. 2.3 and 14.3 is found compared to the original middle distillate (*CN* = 60.3). Hence, diesel meeting a *CN* of 51 (EN 590) is provided for the co-hydroprocessing of 15 wt.% bioliq® heavy gasoline and 85 wt.% middle distillate.

In this chapter, three models are developed that can accurately predict the data in the experimentally investigated parameter range. As found by other authors, sequential reactions from heavy to light lumps are the most important for modeling the hydroprocessing reactions [147, 150, 152]. In contrast, adding ideal hydrocracking reactions results in only a little more predictive accuracy. Highly significant are incorporated dealkylation reactions, producing gaseous compounds, as well as aromatics and naphthenes in the gasoline boiling range.

Further experiments should be conducted under variation of the feed compositions, i.e., bioliq® heavy gasoline and heteroatoms, as aromatics are reported to compete in hydrotreating reactions [144]. Co-hydroprocessing of feedstocks rich in aromatics is highly exothermic and thus challenging [135]. Therefore, the experiments performed at a laboratory scale should be repeated at a larger scale where exothermic reactions become a critical factor. In addition, it may be interesting to investigate other catalysts, such as those based on nickel-molybdenum, which are reported to have high aromatics hydrogenation activity [63]. Finally, it should be clarified under which legal regulations and process conditions co-hydroprocessing can be operated economically, as petrochemical parameters such as the *CN* decrease to some extent.

5 Summary

In this dissertation, two upgrading strategies for aromatic-rich fuels are developed, presented, and evaluated. A key finding of this work is a comprehensive concept for the provision of a GHG-neutral synthetic gasoline based on the bioliq® process and suitable blending components.

The heavy gasoline upgrading process in Chapter 2 uses bifunctional Pt/Zeolite catalysts for the upgrading of heavy gasoline, prior separated from raw gasoline. Chapter 3 covers a novel blending procedure for a synthetic gasoline, potentially applicable in high-compression state of the art engines and also compatible with materials used in older engines. In Chapter 4, a short-term realizable process solution for the integration of MTG- and DTG-fuels into existing refinery infrastructures is presented. In this process, heavy gasoline is co-processed in a fossil middle distillate hydrotreater.

Each process offers different advantages and has unsolved challenges. These are briefly discussed below, along with the methodologies used in each chapter and the main results.

Chapter 2: Upgrading Via Hydroprocessing Using Bifunctional Zeolite Catalysts. In this chapter, bioliq® raw gasoline is upgraded: heavy gasoline is separated, upgraded via hydroprocessing and, finally back-blended with light gasoline.

To answer the first both questions of this thesis stated in Section 1.2 „What influence has the catalyst choice on important petrochemical parameters, i.e. volatility parameters as well as *RON* and *MON*?“ and „How do process parameters influence petrochemical parameters and which ones are most promising to achieve high ONs?“ three Pt/Zeolites, i.e., 0.3 wt.% Pt/Mordenite, 0.3 wt.% Pt/HZSM-5 and 0.3 wt.% Pt/SAPO-11, are tested over a wide range of temperature (250–350 °C) and weight hourly space velocity (0.84–2.66 h^{-1}) at industrially relevant pressures (50–90 bar) in a laboratory-scale fixed bed reactor. Most considerably, *MON* shows a clear dependency on the catalyst choice, i.e. in the order Pt/HZSM-5 > Pt/SAPO-11 > Pt/Mordenite, which can be attributed to each catalyst's individual shape selective RC (isomerization). No significant dependency is observed for *RON* (for Pt/HZSM-5, *MON* increases by 3.5 between a gasoline yield of 99 wt.% and 78 wt.%, while only by 1.1 for *RON*), which is due to the fact that *RON* doesn't equally benefit from a high degree of isomerization due to less severe measuring conditions. The reaction temperature can be identified as a significant influencing factor, as an increase in temperature causes greater naphthene isomerization. On the other hand, the space velocity has no influence in the parameter range investigate. This underlines the necessity of increased reaction temperatures to overcome equilibrium limitations.

Furthermore, high reaction temperatures and low space velocities accelerate cracking reactions, leading to changes in the volatility parameters. Most distinctly, $E100$ and $E150$ increase due to fast tertiary-tertiary β-scission (paring reaction). While Pt/SAPO-11 shows almost no cracking activity, differences are observable between Pt/Mordenite and Pt/HZSM-5, where $E100$ increases slightly more for Pt/HZSM-5. This once more is due to shape selective influences. Narrow pores of Pt/HZSM-5 slow down the spacious paring reaction, benefiting slower cracking mechanisms, which yield more hydrocarbons in the gasoline boiling range. For the same reason $E70$ rises slightly steeper for Pt/HZSM-5 as for Pt/Mordenite.

To answer the third question „Can an EN 228 compliant gasoline be obtained solely by hydroprocessing bioliq® heavy gasoline followed by back-blending?“ and fourth question „Which petrochemical parameters are most critical and potentially need to be improved further to meet EN 228?“ of this thesis, blending experiments are conducted, using bioliq® light gasoline and heavy gasoline, hydroprocessed with the most promising catalyst Pt/HZSM-5. The results show that the aromatic concentration is relatively lowered by 37.5 %, but still exceeds EN 228's limit. As a consequence of the removal of aromatics, *RON* and *MON* drop, however, stay just within EN 228. Good results are also achieved for the volatility characteristics, where *E*150 strongly increases to 84.4 vol.% and meets EN 228. *E*70 and *E*100 also increase to 2.5 vol.% and 10.4 vol.%, respectively, however do not comply with the standard. Therefore, standard-compliant gasoline is not achieved solely by upgrading the heavy gasoline fraction of bioliq® raw gasoline. Also considering that the blending process results in too low vapor pressure and too high density, the volatility parameters must be further improved by incorporating low-volatility components.

Chapter 3: Advanced Blending Concept. In this chapter, a blending concept is developed, based on the results of Chapter 2, to supply a potentially GHG-neutral gasoline equivalent to fossil alternatives.

To answer the fifth question of this thesis „Which blending components are most contemplable to manipulate the volatility parameters in the desired way?“ blending experiments are conducted with a bioliq® base gasoline and oxygenates available in large scale and producible with high renewable share, i.e., methanol, ethanol, MTBE, and ETBE. While *E*70 linearly increases by blending MTBE and ETBE up to 4 vol.%, the alcohols methanol and ethanol have an disproportional effect due to the formation of (near) azeotropic mixtures, increasing *E*70 up to 8.0 vol.% and 7.8 vol.%, respectively. However, although ethanol has the strongest effect, it markedly influences the shape of the boiling curve due to the pronounced formation of an azeotrope. This can negatively influence the evaporating behavior, which might lead to increased emissions. For *E*100, no such differences between the oxygenates are observable. All oxygenates lead to a linear increase and their effect only depends on the blending share, making MTBE and ETBE the ones with the most pronounced effect due to their low molecular oxygen content. All together, methanol is highly attractive since it distinctly increases bioliq® gasoline's low *E*70, while it can also be provided fully GHG neutral.

Since methanol's maximum blending rate is limited to 3 vol.% by EN 228, further blending experiments are conducted, adding a second oxygenate, i.e., ethanol, MTBE or ETBE, to the methanol/base gasoline-blend until the upper limit of 3.7 wt.% oxygen-equivalent according to EN 228 is reached. The blend with methanol/ethanol shows the highest *E*70 value of 15.5 vol.%, in comparison to methanol/MTBE (10.0 vol.%) and methanol/ETBE (9.6 vol.%). *E*100 and *E*150 increase by similar magnitudes to 21.6–23.8 vol.% and 86.0–87.4 vol.%, respectively, for all blends. The strong influence on *E*70 for methanol/ethanol is once more due to a strong non-linear influence on the blend's boiling curve, risking an non-uniform evaporation behavior. The remaining blends with methanol/MTBE and methanol/ETBE show relatively uniform boiling curves. It is concluded, that all three combinations of oxygenates are interesting for their own reasons. Methanol/ethanol shows the strongest increase in *E*70, while methanol/MTBE and methanol/ETBE result in a uniform boiling curve.

To answer the sixth question „Can a gasoline with high renewable share be blended based on an MTG- or DTG-process?“ a gasoline fraction of hydrocracked Fischer-Tropsch waxes is considered as potentially GHG-neutral isomerate-replacement for additional blending experiments. For comparison purposes, two blends are produced, the first based on methanol/ethanol and the second on methanol/ETBE. As expected, the blend with methanol/ethanol shows the best results for the volatility parameters (*E*70 = 32.1 vol.% and *E*100 = 42.4 vol.%), however, does not meet *RON* (91.5) and *MON* (83.5) as required by EN 228. The second blend with methanol/ETBE is able to satisfy *RON* (95.7) and *MON* (87.0), however, is slightly below the minimal values for *E*70 (20.4 vol.%) and *E*100 (41.2 vol.%), while

also exceeding the maximum value for vapor pressure (63.2 kPa). A provision of a potentially GHG-neutral fuel was narrowly missed, but can be achieved through further iteration cycles. The blend with methanol/ETBE is clearly to favor over the one with methanol/ethanol. Its low alcohol content of just 3 vol.% makes it potentially suitable for older vehicles and also applicable in nowadays engines with high compression rates, without the risk of increased emissions due to unequal evaporation behavior. A promising measure towards full standard compliance might be the usage of methanol/MTBE instead of methanol/ETBE as this combination shows slightly higher *E*70 and *E*100, while having a lower vapor pressure.

The suitability of the presented is demonstrated in cooperation with Porsche. Based on the results, several hundred liters are blended and successfully motor-tested under real conditions.

Chapter 4: Upgrading Via Co-Hydroprocessing Using a Hydrotreating Catalyst. In this chapter, the co-hydroprocessing of bioliq® heavy gasoline with middle distillate is investigated, drawing on operating conditions found in industry-scale hydrotreaters. A lumping-model is structured, fitted on experimental data and validated for the prediction of important fuel yields.

To answer the seventh question of this thesis „Is durene sufficiently hydrogenated or is the isomerization reaction predominant, and which process conditions are favorable?“ measurements are taken during approx. 900 h on stream with a mixture of 15 wt.% durene and 85 wt.% middle distillate over a wide range of temperature (320–380 °C), in a fixed bed laboratory-scale reactor. In the experiments, it is found that durene hydrogenation generally increases with durene conversion. While higher temperatures (at fixed space velocity) benefit conversion and consequently hydrogenation selectivity, it also slightly increase durene isomerization towards C_{10} aromatics. At a reaction temperature of 380 °C a durene conversion over 85 % is achieved, while the isomerization stays below 7.5 %. Also, considering the observation that almost-steady-state catalyst conditions are only reached at a temperature of 380 °C, it is concluded that higher temperatures are beneficial for the co-hydroprocessing of durene with middle distillate to achieve high durene conversion rates at low isomerization selecitvities.

To answer the eights question „How does co-hydroprocessing of aromatic-rich bioliq® heavy gasoline and middle distillate influence the *CN* of the diesel fraction?“ further experiments with a mixture of 15 wt.% bioliq® heavy gasoline and 85 wt.% middle distillate are conducted over a wide range of temperature (340–390 °C) and *LHSV* (0.25–1.50 h^{-1}) at constant pressure (62.9 bar). For the separated diesel fraction, the *CN* increases if a higher reaction temperature or a lower space velocity is chosen, and therefore, strongly correlates with the hydrogenation of aromatics. *CN*s of all samples are in the range 46–58, thus lower compared to the original middle distillate's *CN* of 60.3, however, sufficient to comply with EN 590's minimum value of 51, even for the high bioliq® heavy gasoline blending rate of 15 wt.% investigated in this chapter.

To answer the last question „Is a lumping-model sufficiently accurate to predict fuel yields for the co-hydroprocessing of bioliq® heavy gasoline with middle distillate and which model structure is most suitable?“ three lumping models, based on six lumps but on different assumptions regarding the reaction network, are constructed, parametrized, and validated. Using a parameter-reduced model the statistically most significant results with a sufficient coefficient of determination of 0.9976 are obtained. Cascade reactions (hydrogenation and cracking) from heavy to light boiling lumps and the cracking of heavy ends to gases are found to be the most pronounced reactions, in accordance with the literature. In contrast, ideal hydrocracking reactions are negligible in the investigated parameter range, most probably due to the high temperatures selected for the experiments. For the investigated blend of middle distillate and bioliq® heavy gasoline an additional dealkylation mechanism of aromatics and naphthenes is proven to be important to describe the yield distribution.

Summarized, this thesis shows that hydroprocessing is promising to utilize undesirable heavy gasoline mechanistically formed in MTG- and DTG-processes. Noble metal-loaded zeolite catalysts are shown to be interesting catalyst options due to their high hydrogenation activity combined with a zeolite-related selectivity directly influencing the petrochemical parameters of the resulting product. It is demonstrated that an EN 228-compliant fuel is achievable by deftly blending different oxygenates with their unique properties and influence on a fuel's boiling behavior. Finally, the results demonstrate that existing middle distillate hydrotreaters are well suited for incorporating bio-based, aromatic-rich fractions into refineries in the short term under typical operating conditions with common industry catalysts.

Bibliography

[1] D. Graf, P. Neuner, and R. Rauch, "Hydroprocessing and Blending of a Biomass-Based DTG-Gasoline", *Energy Engineering*, vol. 119, no. 6, pp. 2169–2192, 2022. DOI: 10.32604/ee.2022.022759.

[2] D. Graf, P. Neuner, and R. Rauch, "Standard-Compliant Gasoline by Upgrading a DTG-Based Fuel through Hydroprocessing the Heavy-Ends and Blending of Oxygenates", *Fuels*, vol. 4, no. 2, pp. 156–173, 2023. DOI: 10.3390/fuels4020010.

[3] D. Graf, J. Waßmuth, and R. Rauch, "Co-Hydroprocessing of Fossil Middle Distillate and Bio-Derived Durene-Rich Heavy Ends under Hydrotreating Conditions", *Reactions*, vol. 4, no. 3, pp. 531–551, 2023. DOI: 10.3390/reactions4030032.

[4] D. Graf, X. Koroveshi, T. Kolb, and R. Rauch, "Konzepte zur Integration erneuerbarer synthetischer Kraftstoffe in einen bestehenden Raffinerieverbund", *Chemie Ingenieur Technik*, vol. 94, no. 3, pp. 267–280, 2022. DOI: 10.1002/cite.202100154.

[5] D. Graf, P. Neuner, and R. Rauch, "Production of Low-Aromatic Light Blending Components by Hydroprocessing of Heavy Biomass-Based Gasoline", in *AIP Conference Proceedings 2681*, ser. AIP Conference Proceedings, AIP Publishing, 2022, pp. 1–8. DOI: 10.1063/5.0115566.

[6] D. Graf, W. Asbahr, and R. Rauch, "Method and Device for Determining the Soot Tendency of a Substance, Use of the Device and Computer Program Product", EP4296651, 2024.

[7] P. Neuner, D. Graf, H. Mild, and R. Rauch, "Catalytic Hydroisomerisation of Fischer–Tropsch Waxes to Lubricating Oil and Investigation of the Correlation between its Physical Properties and the Chemical Composition of the Corresponding Fuel Fractions", *Energies*, vol. 14, no. 14, pp. 1–14, 2021. DOI: 10.3390/en14144202.

[8] P. Neuner et al., "Chemical Conversion of Fischer–Tropsch Waxes and Plastic Waste Pyrolysis Condensate to Lubricating Oil and Potential Steam Cracker Feedstocks", *Reactions*, vol. 3, no. 3, pp. 352–373, 2022. DOI: 10.3390/reactions3030026.

[9] Our World in Data, *Global Direct Primary Energy Consumption*, available online: https://ourworldindata.org/grapher/global-primary-energy (accessed on 6 Februrary 2023).

[10] European Commission, *Communication from the Commission to the European Parliament, the European Council, the Council, the European Economic and Social Committee and the Committee of the Regions: The European Green Deal*, Brussels, Belgium, 2019.

[11] The European Parliament and the Council of the European Union, *Regulation (EU) 2021/1119 of the European Parliament and of the Council of 30 June 2021 establishing the Framework for achieving Climate Neutrality and amending Regulations (EC) No 401/2009 and (EU) 2018/1999 ('European Climate Law'): Regulation 2021/1119*, Strasbourg, France, 2021.

[12] European Commission, *Communication from the Commission to the European Parliament, the Council, the European Economic and Social Committee and the Committee of the Regions: 'Fit for 55': Delivering the EU's 2030 Climat Target on the Way to Climate Neutrality*, Brussels, Belgium, 2021.

[13] Kate Abnett, *EU Approves Effective Ban on New Fossil Fuel Cars from 2035*, Reuters, Ed., available online: https://www.reuters.com/markets/europe/eu-approves-effective-ban-new-fossil-fuel-cars-2035-2022-10-27/ (accessed on 19 September 2023).

[14] Federal Ministry for the Environment, Nature Conservation and Nuclear Safety, *PtL Roadmap: Sustainable Aviation Fuel from Renewable Energy Sources for Aviation in Germany*, Berlin, Germany, 2021.

[15] International Energy Agency (IEA), *Global EV Outlook 2023: Catching up with Climate Ambitions*, Paris, France, 2023.

[16] European Automobile Manufacturers' Association, *Vehicles in Use Europe*, Brussels, Belgium, 2023.

[17] A. Alvarez-Majmutov, S. Badoga, J. Chen, J. Monnier, and Y. Zhang, "Co-Processing of Deoxygenated Pyrolysis Bio-Oil with Vacuum Gas Oil through Hydrocracking", *Energy & Fuels*, vol. 35, no. 12, pp. 9983–9993, 2021. DOI: 10.1021/acs.energyfuels.1c00822.

[18] V. R. Surisetty, A. K. Dalai, and J. Kozinski, "Alcohols as Alternative Fuels: An Overview", *Applied Catalysis A: General*, vol. 404, no. 1-2, pp. 1–11, 2011. DOI: 10.1016/j.apcata.2011.07.021.

[19] Deutsches Institut für Normung e. V. (DIN), *Automotive Fuels – Unleaded Petrol – Requirements and Test Methods; German Version EN 228:2012+A1:2017*, Berlin, Germany, 2017.

[20] Deutsches Institut für Normung e. V. (DIN), *Automotive fuels – Diesel – Requirements and Test Methods; German Version EN 590:2022*, Berlin, Germany, 2022.

[21] N. Jeuland, X. Montagne, and X. Gautrot, "Potentiality of Ethanol as a Fuel for Dedicated Engine", *Oil & Gas Science and Technology - Revue d'IFP Energies nouvelles*, vol. 59, no. 6, pp. 559–570, 2004. DOI: 10.2516/ogst:2004040.

[22] R. Munsin, Y. Laoonual, S. Jugjai, and Y. Imai, "An Experimental Study on Performance and Emissions of a Small SI Engine Generator Set Fuelled by Hydrous Ethanol with High Water Contents up to 40%", *Fuel*, vol. 106, pp. 586–592, 2013. DOI: 10.1016/j.fuel.2012.12.079.

[23] A. Haseeb, M. A. Fazal, M. I. Jahirul, and H. H. Masjuki, "Compatibility of Automotive Materials in Biodiesel: A Review", *Fuel*, vol. 90, no. 3, pp. 922–931, 2011. DOI: 10.1016/j.fuel.2010.10.042.

[24] C. D. Chang and A. J. Silvestri, "The Conversion of Methanol and Other O-Compounds to Hydrocarbons Over Zeolite Catalysts", *Journal of Catalysis*, vol. 47, no. 2, pp. 249–259, 1977. DOI: 10.1016/0021-9517(77)90172-5.

[25] U. Olsbye et al., "Conversion of Methanol to Hydrocarbons: How Zeolite Cavity and Pore Size Controls Product Selectivity", *Angewandte Chemie International Edition*, vol. 51, no. 24, pp. 5810–5831, 2012. DOI: 10.1002/anie.201103657.

[26] C. D. Chang, "The New Zealand Gas-to-Gasoline Plant: An Engineering Tour De Force", *Catalysis Today*, vol. 13, no. 1, pp. 103–111, 1992. DOI: 10.1016/0920-5861(92)80190-X.

[27] J. Topp-Jørgensen, "Topsøe Integrated Gasoline Synthesis – The Tigas Process", *Studies in Surface Science and Catalysis*, vol. 36, pp. 293–305, 1988. DOI: 10.1016/s0167-2991(09)60523-1.

[28] K. Fujimoto, K. Asami, H. Saima, T. Shikada, and H.-o. Tominaga, "Two-Stage Reaction System for Synthesis Gas Conversion to Gasoline", *Industrial & Engineering Chemistry Product Research and Development*, vol. 25, no. 2, pp. 262–267, 1986. DOI: 10.1021/i300022a023.

[29] F. Trippe, M. Fröhling, F. Schultmann, R. Stahl, and E. Henrich, "Techno-Economic Analysis of Fast Pyrolysis as a Process Step Within Biomass-to-Liquid Fuel Production", *Waste and Biomass Valorization*, vol. 1, pp. 415–430, 2010. DOI: 10.1007/s12649-010-9039-1.

[30] C. Pfitzer et al., "Fast Pyrolysis of Wheat Straw in the Bioliq® Pilot Plant", *Energy & Fuels*, vol. 30, no. 10, pp. 8047–8054, 2016. DOI: 10.1021/acs.energyfuels.6b01412.

[31] N. Dahmen, E. Dinjus, T. Kolb, U. Arnold, H. Leibold, and R. Stahl, "State of the Art of the Bioliq® Process for Synthetic Biofuels Production", *Environmental Progress & Sustainable Energy*, vol. 31, no. 2, pp. 176–181, 2012. DOI: 10.1002/ep.10624.

[32] M. Stiefel, R. Ahmad, U. Arnold, and M. Döring, "Direct Synthesis of Dimethyl Ether from Carbon-Monoxide-Rich Synthesis Gas: Influence of Dehydration Catalysts and Operating Conditions", *Fuel Processing Technology*, vol. 92, no. 8, pp. 1466–1474, 2011. DOI: 10.1016/j.fuproc.2011.03.007.

[33] M. C. Zimmermann, T. N. Otto, S. Wodarz, T. A. Zevaco, and S. Pitter, "Mesoporous H–ZSM–5 for the Conversion of Dimethyl Ether to Hydrocarbons", *Chemie Ingenieur Technik*, vol. 91, no. 9, pp. 1302–1313, 2019. DOI: 10.1002/cite.201800217.

[34] S. Amelang, *Pilot Project in Germany's Largest Refinery to Produce Synthetic Fuels*, Clean Energy Wire, Ed., aivailable online: https://www.cleanenergywire.org/news/pilot-project-germanys-largest-refinery-produce-synthetic-fuels (accessed on 8 March 2023).

[35] H.-J. Stappen and P. Gräve, *eFuels Pilot Plant in Chile Officially Opened*, Porsche newsroom, Ed., available online: https://newsroom.porsche.com/en/2022/company/porsche-highly-innovative-fuels-hif-opening-efuels-pilot-plant-haru-oni-chile-synthetic-fuels-30732.html (accessed on 27 January 2023).

[36] D. Liederman, S. Yurchak, J. C. W. Kuo, and W. Lee, "Mobil Methanol-to-Gasoline Process", *Journal of Energy*, vol. 6, no. 5, pp. 340–341, 1982. DOI: 10.2514/3.62614.

[37] A. Petit and X. Montagne, "Effects of the Gasoline Composition on Exhaust Emissions of Regulated and Speciated Pollutants", *SAE Technical Papers*, no. 932681, pp. 1–11, 1993. DOI: 10.4271/932681.

[38] H. F. Calcote and D. M. Manos, "Effect of Molecular Structure on Incipient Soot Formation", *Combustion and Flame*, vol. 49, no. 1-3, pp. 289–304, 1983. DOI: 10.1016/0010-2180(83)90172-4.

[39] S. S. Lim et al., "A Comparative Risk Assessment of Burden of Disease and Injury Attributable to 67 Risk Factors and Risk Factor Clusters in 21 Regions, 1990–2010: A Systematic Analysis for the Global Burden of Disease Study 2010", *The Lancet*, vol. 380, no. 9859, pp. 2224–2260, 2012. DOI: 10.1016/S0140-6736(12)61766-8.

[40] C. S. Laxminarasimhan, R. P. Verma, and P. A. Ramachandran, "Continuous Lumping Model for Simulation of Hydrocracking", *AIChE Journal*, vol. 42, no. 9, pp. 2645–2653, 1996. DOI: 10.1002/aic.690420925.

[41] K. Nakakita et al., "Effect of Hydrocarbon Molecular Structure in Diesel Fuel on In-Cylinder Soot Formation and Exhaust Emissions", *SAE International Journal of Fuels and Lubricants*, vol. 112, pp. 1763–1775, 2003. DOI: 10.4271/2003-01-1914.

[42] S. Bezergianni, A. Dimitriadis, O. Kikhtyanin, and D. Kubička, "Refinery Co-Processing of Renewable Feeds", *Progress in Energy and Combustion Science*, vol. 68, pp. 29–64, 2018. DOI: 10.1016/j.pecs.2018.04.002.

[43] S. van Dyk, J. Su, J. D. McMillan, and J. Saddler, "Potential Synergies of Drop–In Biofuel Production with Further Co–Processing at Oil Refineries", *Biofuels, Bioproducts and Biorefining*, vol. 13, no. 3, pp. 760–775, 2019. DOI: 10.1002/bbb.1974.

[44] A. A. Lappas, S. Bezergianni, and I. A. Vasalos, "Production of Biofuels via Co-Processing in Conventional Refining Processes", *Catalysis Today*, vol. 145, no. 1-2, pp. 55–62, 2009. DOI: 10.1016/j.cattod.2008.07.001.

[45] T. L. Marker, *Opportunities for Biorenewables in Oil Refineries*, United States Department of Energy, Washington, WA, USA, 2005. DOI: 10.2172/861458.

[46] L. Wu, Y. Wang, L. Zheng, M. Shi, and J. Li, "Design and Optimization of Bio-Oil Co-Processing with Vacuum Gas Oil in a Refinery", *Energy Conversion and Management*, vol. 195, pp. 620–629, 2019. DOI: 10.1016/j.enconman.2019.05.041.

[47] T.-C. Tsai, S.-B. Liu, and I. Wang, "Disproportionation and Transalkylation of Alkylbenzenes Over Zeolite Catalysts", *Applied Catalysis A: General*, vol. 181, no. 2, pp. 355–398, 1999. DOI: 10.1016/S0926-860X(98)00396-2.

[48] A. S. Yegorov, V. S. Ivanov, and A. I. Wozniak, "International and Russian Methods of Synthesis and Use of Pyromellitic Acid Dianhydride and Tendencies of their Development (Review)", *Biosciences Biotechnology Research Asia*, vol. 11, no. 3, pp. 1765–1779, 2014. DOI: 10.13005/bbra/1583.

[49] C. D. Chang, "Hydrocarbons from Methanol", *Catalysis Reviews - Science and Engineering*, vol. 25, no. 1, pp. 1–118, 1983. DOI: 10.1080/01614948308078874.

[50] A. H. Vivas and F. Joensen, "Process and Catalyst for Upgrading Gasoline", US10150714B2, 2018.

[51] F. Schmidt, L. Reichelt, and C. Pätzold, "Catalysis of Methanol Conversion to Hydrocarbons", in *Methanol: The Basic Chemical and Energy Feedstock of the Future*, M. Bertau, H. Offermanns, L. Plass, F. Schmidt, and H.-J. Wernicke, Eds., Springer Berlin Heidelberg, 2014, pp. 423–489.

[52] T. Michler et al., "Gasoline from the Bioliq® Process: Production, Characterization and Performance", *Fuel Processing Technology*, vol. 206, no. 106476, pp. 1–13, 2020. DOI: 10.1016/j.fuproc.2020.106476.

[53] T. Ogawa, N. Inoue, T. Shikada, and Y. Ohno, "Direct Dimethyl Ether Synthesis", *Journal of Natural Gas Chemistry*, vol. 12, pp. 219–227, 2003.

[54] D. Mao, J. Xia, Q. Chen, and G. Lu, "Highly Effective Conversion of Syngas to Dimethyl Ether Over the Hybrid Catalysts Containing High-Silica HMCM-22 Zeolites", *Catalysis Communications*, vol. 10, no. 5, pp. 620–624, 2009. DOI: 10.1016/j.catcom.2008.11.003.

[55] T. Rostrup-Nielsen, P. E. Højlund Nielsen, F. Joensen, and J. Madsen, "Polygeneration – Integration of Gasoline Synthesis and IGCC Power Production Using Topsøe's TIGAS Process", in *Risoe international energy conference, Roskilde (Denmark), 22-24 May 2007*, pp. 56–68.

[56] P. Haro, F. Trippe, R. Stahl, and E. Henrich, "Bio-Syngas to Gasoline and Olefins via DME – A Comprehensive Techno-Economic Assessment", *Applied Energy*, vol. 108, pp. 54–65, 2013. DOI: 10.1016/j.apenergy.2013.03.015.

[57] N. Dahmen, E. Henrich, E. Dinjus, and F. Weirich, "The Bioliq® Bioslurry Gasification Process for the Production of Biosynfuels, Organic Chemicals, and Energy", *Energy, Sustainability and Society*, vol. 2, no. 3, pp. 1–44, 2012. DOI: 10.1186/2192-0567-2-3.

[58] N. Dahmen et al., "The Bioliq Process for Producing Synthetic Transportation Fuels", *Wiley Interdisciplinary Reviews: Energy and Environment*, vol. 6, no. 3, pp. 1–10, 2017. DOI: 10.1002/wene.236.

[59] E. Henrich, N. Dahmen, and E. Dinjus, "Cost Estimate for Biosynfuel Production via Biosyncrude Gasification", *Biofuels, Bioproducts & Biorefining*, vol. 3, no. 1, pp. 28–41, 2009. DOI: 10.1002/bbb.126.

[60] P. T. M. Do, S. Crossley, M. Santikunaporn, and D. E. Resasco, "Catalytic Strategies for Improving Specific Fuel Properties", *Catalysis*, vol. 20, pp. 33–64, 2007. DOI: 10.1039/b602366p.

[61] J. Weitkamp, "Catalytic Hydrocracking—Mechanisms and Versatility of the Process", *ChemCatChem*, vol. 4, no. 3, pp. 292–306, 2012. DOI: 10.1002/cctc.201100315.

[62] G. Valavarasu, M. Bhaskar, and K. S. Balaraman, "Mild Hydrocracking—A Review of the Process, Catalysts, Reactions, Kinetics, and Advantages", *Petroleum Science and Technology*, vol. 21, no. 7-8, pp. 1185–1205, 2003. DOI: 10.1081/LFT-120017883.

[63] B. H. Cooper and B. B. Donnis, "Aromatic Saturation of Distillates: An Overview", *Applied Catalysis A: General*, vol. 137, no. 2, pp. 203–223, 1996. DOI: 10.1016/0926-860X(95)00258-8.

[64] J. P. van den Berg, J. P. Lucien, G. Germaine, and G. Thielemans, "Deep Desulphurisation and Aromatics Saturation for Automotive Gasoil Manufacturing", *Fuel Processing Technology*, vol. 35, no. 1-2, pp. 119–136, 1993. DOI: 10.1016/0378-3820(93)90088-L.

[65] F. Figueras, R. Gomez, and M. Primet, "Adsorption and Catalytic Properties of Palladium Supported by Silica, Alumina, Magnesia, and Amorphous and Crystalline Silica-Aluminas", in *Molecular Sieves*, W. M. Meier and J. B. Uytterhoeven, Eds., Washington, WA: American Chemical Society, 1973, pp. 480–489. DOI: 10.1021/ba-1973-0121.ch043.

[66] T. M. Tri, J. Massardier, P. Gallezot, and B. Imelik, "Additives and Support Effects on Pt Catalysts Studied by the Competitive Hydrogenation of Benzene and Toluene", *Studies in Surface Science and Catalysis*, vol. 11, pp. 141–148, 1982. DOI: 10.1016/s0167-2991(09)61385-9.

[67] J. Weitkamp, "Zeolites and Catalysis", *Solid State Ionics*, vol. 131, no. 1-2, pp. 175–188, 2000. DOI: 10.1016/S0167-2738(00)00632-9.

[68] P. B. Weisz, "Molecular Shape Selective Catalysis", *Pure and Applied Chemistry*, vol. 52, no. 9, pp. 2091–2103, 1980. DOI: 10.1351/pac198052092091.

[69] S. Mignard, P. Caillette, and N. Marchal, "Hydroconversion of Methyl-Cyclohexane on a Bifunctional Catalyst", in *Catalytic Hydroprocessing of Petroleum and Disillates*, M. C. Oballa and S. S. Shih, Eds., New York, NY, USA: CRC Press, 1993, pp. 447–458. DOI: 10.1201/9781003067306-24.

[70] F. Figueras, B. Coq, C. Walter, and J.-Y. Carriat, "Hydroconversion of Methylcyclohexane on Bifunctional Sulfated Zirconia-Supported Platinum Catalysts", *Journal of Catalysis*, vol. 169, no. 1, pp. 103–113, 1997. DOI: 10.1006/jcat.1997.1682.

[71] J. Weitkamp, P. A. Jacobs, and S. Ernst, "Shape Selective Isomerization and Hydrocracking of Naphthenes over Pt/HZSM-5 Zeolite", *Studies in Surface Science and Catalysis*, vol. 18, pp. 279–290, 1984. DOI: 10.1016/s0167-2991(09)61164-2.

[72] H. Belatel, H. Al-Kandari, F. Al-Khorafi, A. Katrib, and F. Garin, "Catalytic Reactions of Methylcyclohexane (MCH) on Partially Reduced MoO3", *Applied Catalysis A: General*, vol. 275, no. 1-2, pp. 141–147, 2004. DOI: 10.1016/j.apcata.2004.07.029.

[73] M. Santikunaporn, W. E. Alvarez, and D. E. Resasco, "Ring Contraction and Selective Ring Opening of Naphthenic Molecules for Octane Number Improvement", *Applied Catalysis A: General*, vol. 325, no. 1, pp. 175–187, 2007. DOI: 10.1016/j.apcata.2007.03.029.

[74] G. G. Martens, J. W. Thybaut, and G. B. Marin, "Single-Event Rate Parameters for the Hydrocracking of Cycloalkanes on Pt/US-Y Zeolites", *Industrial & Engineering Chemistry Research*, vol. 40, no. 8, pp. 1832–1844, 2001. DOI: 10.1021/ie000799n.

[75] D. M. Brouwer and H. Hogeveen, "The Importance of Orbital Orientation as a Rate-Controlling Factor in Intramolecular Reactions of Carbonium Ions", *Recueil des Travaux Chimiques des Pays-Bas*, vol. 89, no. 2, pp. 211–224, 1970. DOI: 10.1002/recl.19700890213.

[76] R. F. Sullivan, C. J. Egan, G. E. Langlois, and R. P. Sieg, "A New Reaction that Occurs in the Hydrocracking of Certain Aromatic Hydrocarbons", *Journal of the American Chemical Society*, vol. 83, no. 5, pp. 1156–1160, 1961. DOI: 10.1021/ja01466a036.

[77] C. J. Egan, G. E. Langlois, and R. J. White, "Selective Hydrocracking of C9- to C12-Alkylcyclohexanes on Acidic Catalysts. Evidence for the Paring Reaction", *Journal of the American Chemical Society*, vol. 84, pp. 1204–1212, 1962. DOI: 10.1021/ja00866a028.

[78] R. C. Santana et al., "Evaluation of Different Reaction Strategies for the Improvement of Cetane Number in Diesel Fuels", *Fuel*, vol. 85, no. 5-6, pp. 643–656, 2006. DOI: 10.1016/j.fuel.2005.08.028.

[79] S. Rabl et al., "Catalytic Ring Opening of Decalin on Ir- and Pt-Containing Zeolite Y – Influence of the Nature of the Charge-Compensating Alkali Cations", *Microporous and Mesoporous Materials*, vol. 146, no. 1-3, pp. 190–200, 2011. DOI: 10.1016/j.micromeso.2011.03.045.

[80] V. Calemma, R. Giardino, and M. Ferrari, "Upgrading of LCO by Partial Hydrogenation of Aromatics and Ring Opening of Naphthenes Over Bi-Functional Catalysts", *Fuel Processing Technology*, vol. 91, no. 7, pp. 770–776, 2010. DOI: 10.1016/j.fuproc.2010.02.012.

[81] G. McVicker et al., "Selective Ring Opening of Naphthenic Molecules", *Journal of Catalysis*, vol. 210, no. 1, pp. 137–148, 2002. DOI: 10.1006/jcat.2002.3685.

[82] P. Samoila, M. Boutzeloit, C. Especel, F. Epron, and P. Marécot, "Selective Ring-Opening of Methylcyclopentane on Platinum-Based Bimetallic Catalysts", *Applied Catalysis A: General*, vol. 369, no. 1-2, pp. 104–112, 2009. DOI: 10.1016/j.apcata.2009.09.006.

[83] M. A. Vicerich, V. M. Benitez, C. Especel, F. Epron, and C. L. Pieck, "Influence of Iridium Content on the Behavior of Pt-Ir/Al2O3 and Pt-Ir/TiO2 Catalysts for Selective Ring Opening of Naphthenes", *Applied Catalysis A: General*, vol. 453, pp. 167–174, 2013. DOI: 10.1016/j.apcata.2012.12.015.

[84] *ASTM D6730 – 01, Standard Test Method for Determination of Individual Components in Spark Ignition Engine Fuels by 100-Metre Capillary (with Precolumn) High-Resolution Gas Chromatography*, West Conshohocken, PA, USA, 2001. DOI: 10.1520/D6730-01.

[85] *ISO 5164, Petroleum Products - Determination of Knock Characteristics of Motor Fuels - Research Method*, Geneva, Switzerland, 2014.

[86] *ISO 5163, Petroleum Products - Determination of Knock Characteristics of Motor and Aviation Fuels - Motor Method*, Geneva, Switzerland, 2014.

[87] *ASTM D6378, Standard Test Method for Determination of Vapor Pressure (VPX) of Petroleum Products, Hydrocarbons, and Hydrocarbon-Oxygenate Mixtures (Triple Expansion Method)*, West Conshohocken, PA, USA, 2020. DOI: 10.1520/D6378-20.

[88] *ASTM D7345, Standard Test Method for Distillation of Petroleum Products and Liquid Fuels at Atmospheric Pressure (Micro Distillation Method)*, West Conshohocken, PA, USA, 2017. DOI: 10.1520/D7345-17.

[89] *ASTM D86, Standard Test Method for Distillation of Petroleum Products and Liquid Fuels at Atmospheric Pressure*, West Conshohocken, PA, USA, 2020. DOI: 10.1520/D0086-20B.

[90] W. L. Kubic, "A Group Contribution Method for Estimating Cetane and Octane Numbers", no. LA-UR-16-25529, Los Alamos National Laboratory (LANL), 2016. DOI: 10.2172/1291241.

[91] P. Ghosh, K. J. Hickey, and S. B. Jaffe, "Development of a Detailed Gasoline Composition-Based Octane Model", *Industrial & Engineering Chemistry Research*, vol. 45, no. 1, pp. 337–345, 2006. DOI: 10.1021/ie050811h.

[92] G. B. McVicker et al., "Methylcyclohexane Ring-Contraction: A Sensitive Solid Acidity and Shape Selectivity Probe Reaction", *The Journal of Physical Chemistry B*, vol. 109, no. 6, pp. 2222–2226, 2005. DOI: 10.1021/jp040205k.

[93] H. Jafari, M. H. Idris, A. Ourdjini, H. Rahimi, and B. Ghobadian, "EIS Study of Corrosion Behavior of Metallic Materials in Ethanol Blended Gasoline Containing Water as a Contaminant", *Fuel*, vol. 90, no. 3, pp. 1181–1187, 2011. DOI: 10.1016/j.fuel.2010.12.010.

[94] Federal Office for Agriculture and Food, *Evaluation and Progress Report 2020*, Bonn, Germany, 2021.

[95] M. V. Turdera, "Energy Balance, Forecasting of Bioelectricity Generation and Greenhouse Gas Emission Balance in the Ethanol Production at Sugarcane Mills in the State of Mato Grosso do Sul", *Renewable and Sustainable Energy Reviews*, vol. 19, pp. 582–588, 2013. DOI: 10.1016/j.rser.2012.11.055.

[96] Y. Jiang, S. D. Phillips, A. Singh, S. B. Jones, and D. J. Gaspar, "Potential Economic Values of Low-Vapor-Pressure Gasoline-Range Bio-Blendstocks: Property Estimation and Blending Optimization", *Fuel*, vol. 297, no. 120759, 2021. DOI: 10.1016/j.fuel.2021.120759.

[97] J. B. Heywood, *Internal combustion engine fundamentals*, 2. ed. New York, NY, USA: McGraw-Hill, 1988.

[98] J. Milpied et al., "Impact of Fuel Properties on the Performances and Knock Behaviour of a Downsized Turbocharged DI SI Engine: Focus on Octane Numbers and Latent Heat of Vaporization", *SAE International Journal of Fuels and Lubricants*, vol. 2, no. 1, pp. 118–126, 2009. DOI: 10.4271/2009-01-0324.

[99] R. da Silva, R. Cataluña, E. W. de Menezes, D. Samios, and C. M. S. Piatnicki, "Effect of Additives on the Antiknock Properties and Reid Vapor Pressure of Gasoline", *Fuel*, vol. 84, no. 7-8, pp. 951–959, 2005. DOI: 10.1016/j.fuel.2005.01.008.

[100] T. D. B. Morgan, G. J. den Otter, W. W. Lange, J. Doyon, J. R. Barnes, and T. Yamashita, "An Integrated Study of the Effects of Gasoline Composition on Exhaust Emissions Part I: Programme Outline and Results on Regulated Emissions", *SAE Technical Papers*, no. 932678, 1993. DOI: 10.4271/932678.

[101] R. A. Meyers, *Handbook of Petroleum Refining Processes*, 3. ed. New York, NY, USA: McGraw-Hill, 2003.

[102] T. J. Bruno, A. Wolk, and A. Naydich, "Composition-Explicit Distillation Curves for Mixtures of Gasoline with Four-Carbon Alcohols (Butanols)", *Energy & Fuels*, vol. 23, no. 4, pp. 2295–2306, 2009. DOI: 10.1021/ef801117c.

[103] E. C. D. Tan et al., "Conceptual Process Design and Economics for the Production of High–Octane Gasoline Blendstock via Indirect Liquefaction of Biomass through Methanol/Dimethyl Ether Intermediates", *Biofuels, Bioproducts and Biorefining*, vol. 10, no. 1, pp. 17–35, 2016. DOI: 10.1002/bbb.1611.

[104] R. L. Furey and J. B. King, "Emissions, Fuel Economy, and Driveability Effects of Methanol/Butanol/Gasoline Fuel Blends", *SAE Technical Papers*, no. 821188, pp. 47–59, 1982. DOI: 10.4271/821188.

[105] J. Yanowitz, E. Christensen, and R. L. McCormick, "Utilization of Renewable Oxygenates as Gasoline Blending Components", Technical Report, no. NREL/TP-5400-50791, 2011. DOI: 10.2172/1024518.

[106] K. Aikawa, T. Sakurai, and J. J. Jetter, "Development of a Predictive Model for Gasoline Vehicle Particulate Matter Emissions", *SAE International Journal of Fuels and Lubricants*, vol. 3, no. 2, pp. 610–622, 2010. DOI: 10.4271/2010-01-2115.

[107] A. Jess and P. Wasserscheid, *Chemical Technology: An Integral Textbook*. Weinheim, Germany: Wiley-VCH Verlag GmbH & Co. KGaA.

[108] D. J. Duvenhage and T. Shingles, "Synthol Reactor Technology Development", *Catalysis Today*, vol. 71, no. 3-4, pp. 301–305, 2002. DOI: 10.1016/S0920-5861(01)00456-4.

[109] A. P. Steynberg, R. L. Espinoza, B. Jager, and A. C. Vosloo, "High Temperature Fischer–Tropsch Synthesis in Commercial Practice", *Applied Catalysis A: General*, vol. 186, no. 1-2, pp. 41–54, 1999. DOI: 10.1016/S0926-860X(99)00163-5.

[110] B. I. Kamara and J. Coetzee, "Overview of High-Temperature Fischer-Tropsch Gasoline and Diesel Quality", *Energy & Fuels*, vol. 23, no. 4, pp. 2242–2247, 2009. DOI: 10.1021/ef800924z.

[111] M. E. Dry, "High Quality Diesel via the Fischer-Tropsch Process - A Review", *Journal of Chemical Technology & Biotechnology*, vol. 77, no. 1, pp. 43–50, 2002. DOI: 10.1002/jctb.527.

[112] A. Meurer and J. Kern, "Fischer–Tropsch Synthesis as the Key for Decentralized Sustainable Kerosene Production", *Energies*, vol. 14, no. 7, pp. 1–21, 2021. DOI: 10.3390/en14071836.

[113] H. Schulz, "Short History and Present Trends of Fischer–Tropsch Synthesis", *Applied Catalysis A: General*, vol. 186, no. 1-2, pp. 3–12, 1999. DOI: 10.1016/S0926-860X(99)00160-X.

[114] S. Teketel, U. Olsbye, K.-P. Lillerud, P. Beato, and S. Svelle, "Selectivity Control through Fundamental Mechanistic Insight in the Conversion of Methanol to Hydrocarbons over Zeolites", *Microporous and Mesoporous Materials*, vol. 136, no. 1-3, pp. 33–41, 2010. DOI: 10.1016/j.micromeso.2010.07.013.

[115] R. Ahmad, D. Schrempp, S. Behrens, J. Sauer, M. Döring, and U. Arnold, "Zeolite-Based Bifunctional Catalysts for the Single Step Synthesis of Dimethyl Ether from CO-Rich Synthesis Gas", *Fuel Processing Technology*, vol. 121, pp. 38–46, 2014. DOI: 10.1016/j.fuproc.2014.01.006.

[116] C. S. McEnally and L. D. Pfefferle, "Improved Sooting Tendency Measurements for Aromatic Hydrocarbons and their Implications for Naphthalene Formation Pathways", *Combustion and Flame*, vol. 148, no. 4, pp. 210–222, 2007. DOI: 10.1016/j.combustflame.2006.11.003.

[117] T. Mokrani and M. Scurrell, "Gas Conversion to Liquid Fuels and Chemicals: The Methanol Route–Catalysis and Processes Development", *Catalysis Reviews*, vol. 51, no. 1, pp. 1–145, 2009. DOI: 10.1080/01614940802477524.

[118] D. P. Serrano, J. A. Melero, G. Morales, J. Iglesias, and P. Pizarro, "Progress in the Design of Zeolite Catalysts for Biomass Conversion into Biofuels and Bio-Based Chemicals", *Catalysis Reviews*, vol. 60, no. 1, pp. 1–70, 2017. DOI: 10.1080/01614940.2017.1389109.

[119] V. F. Andersen, J. E. Anderson, T. J. Wallington, S. A. Mueller, and O. J. Nielsen, "Distillation Curves for Alcohol–Gasoline Blends", *Energy & Fuels*, vol. 24, no. 4, pp. 2683–2691, 2010. DOI: 10.1021/ef9014795.

[120] Y. Chen, Y. Yihao Zhang, and W. K. Cheng, "Effects of Ethanol Evaporative Cooling on Particulate Number Emissions in GDI Engines", *SAE Technical Papers*, no. 2018-01-0360, 2018. DOI: 10.4271/2018-01-0360.

[121] D.-P. Michalopoulou, M. Komiotou, Y. Zannikou, and D. Karonis, "Impact of Bio-Ethanol, Bio-ETBE Addition on the Volatility of Gasoline with Oxygen Content at the Level of E10", *Fuels*, vol. 2, no. 4, pp. 501–520, 2021. DOI: 10.3390/fuels2040029.

[122] G. Bozzano and F. Manenti, "Efficient Methanol Synthesis: Perspectives, Technologies and Optimization Strategies", *Progress in Energy and Combustion Science*, vol. 56, pp. 71–105, 2016. DOI: 10.1016/j.pecs.2016.06.001.

[123] H. C. Taljaard, C. Jordaan, and J. J. Botha, "The Effect of Oxygen Content in Different Oxygenate-Gasoline Blends on Performance and Emissions in a Single Cylinder, Spark-Ignition Engine", *SAE Technical Papers*, no. 910379, pp. 1–17, 1991. DOI: 10.4271/910379.

[124] M. A. Ratcliff et al., "Impact of Ethanol Blending into Gasoline on Aromatic Compound Evaporation and Particle Emissions from a Gasoline Direct Injection Engine", *Applied Energy*, vol. 250, pp. 1618–1631, 2019. DOI: 10.1016/j.apenergy.2019.05.030.

[125] R. A. Stein, C. J. House, and T. G. Leone, "Optimal Use of E85 in a Turbocharged Direct Injection Engine", *SAE International Journal of Fuels and Lubricants*, vol. 2, no. 1, pp. 670–682, 2009. DOI: 10.4271/2009-01-1490.

[126] X. He, M. A. Ratcliff, and B. T. Zigler, "Effects of Gasoline Direct Injection Engine Operating Parameters on Particle Number Emissions", *Energy & Fuels*, vol. 26, no. 4, pp. 2014–2027, 2012. DOI: 10.1021/ef201917p.

[127] J. E. Ketterer and W. K. Cheng, "On the Nature of Particulate Emissions from DISI Engines at Cold-Fast-Idle", *SAE International Journal of Engines*, vol. 7, no. 2, pp. 986–994, 2014. DOI: 10.4271/2014-01-1368.

[128] D. Karonis, G. Anastopoulos, E. Lois, and S. Stournas, "Impact of Simultaneous ETBE and Ethanol Addition on Motor Gasoline Properties", *SAE International Journal of Fuels and Lubricants*, vol. 1, no. 1, pp. 1584–1594, 2009. DOI: 10.4271/2008-01-2503.

[129] B. L. Smith and T. J. Bruno, "Improvements in the Measurement of Distillation Curves. 3. Application to Gasoline and Gasoline + Methanol Mixtures", *Industrial & Engineering Chemistry Research*, vol. 46, no. 1, pp. 297–309, 2007. DOI: 10.1021/ie060937u.

[130] M. N. Petre, P. Rosca, and R.-E. Dragomir, "The Effect of Bio-Ethers on the Volatility Properties of Oxygenated Gasoline", *Revista de Chimie*, vol. 62, no. 5, pp. 567–574, 2011.

[131] R. L. Furey and K. L. Perry, "Vapor Pressures of Mixtures of Gasolines and Gasoline-Alcohol Blends", *SAE International Journal of Fuels and Lubricants*, vol. 95, no. 6, pp. 779–789, 1986. DOI: 10.4271/861557.

[132] U. Domańska, Z. Żołek-Tryznowska, M. M. Tshibangu, D. Ramjugernath, and T. M. Letcher, "Separation of an Alcohol and a Tetrahydrofuran, Methyl Tert-Butyl Ether, or Ethyl Tert-Butyl Ether by Solvent Extraction with a Hyperbranched Polymer at T = 298.15 K", *Journal of Chemical & Engineering Data*, vol. 55, no. 8, pp. 2879–2885, 2010. DOI: 10.1021/je901038q.

[133] K. Dums et al., "Synthetic Fuels: From the Laboratory to the Road", 43rd International Vienna Motor Symposium, Vienna, Austria, 2022.

[134] D. Bisht and J. Petri, "Considerations for Upgrading Light Cycle Oil with Hydroprocessing Technologies", *Indian Chemical Engineer*, vol. 56, no. 4, pp. 321–335, 2014. DOI: 10.1080/00194506.2014.927179.

[135] S. van Dyk, J. Su, M. Ebadian, and J. Saddler, "Production of Lower Carbon-Intensity Fuels by Co-Processing Biogenic Feedstocks: Potential and Challenges For Refineries", *Fuel*, vol. 324, Part B, 2022. DOI: 10.1016/j.fuel.2022.124636.

[136] E. T. C. Vogt and B. M. Weckhuysen, "Fluid Catalytic Cracking: Recent Developments on the Grand Old Lady of Zeolite Catalysis", *Chemical Society Reviews*, vol. 44, no. 20, pp. 7342–7370, 2015. DOI: 10.1039/C5CS00376H.

[137] M. Al-Sabawi, J. Chen, and S. Ng, "Fluid Catalytic Cracking of Biomass-Derived Oils and Their Blends with Petroleum Feedstocks: A Review", *Energy & Fuels*, vol. 26, no. 9, pp. 5355–5372, 2012. DOI: 10.1021/ef3006417.

[138] A. Rezende Pinho, M. B. Almeida, F. L. Mendes, V. L. Ximenes, and L. C. Casavechia, "Co-Processing Raw Bio-Oil and Gasoil in an FCC Unit", *Fuel Processing Technology*, vol. 131, pp. 159–166, 2015. DOI: 10.1016/j.fuproc.2014.11.008.

[139] N. Thegarid et al., "Second-Generation Biofuels by Co-Processing Catalytic Pyrolysis Oil in FCC Units", *Applied Catalysis B: Environmental*, vol. 145, pp. 161–166, 2014. DOI: 10.1016/j.apcatb.2013.01.019.

[140] D. S. J. Jones and P. R. Pujadó, *Handbook of Petroleum Processing*. Dordrecht, The Netherlands: Springer, 2006. DOI: 10.1007/1-4020-2820-2.

[141] S. van Dyk, J. Su, J. D. McMillan, and J. N. Saddler, *'Drop-In' Biofuels: The Key Role that Co-Processing Will Play in its Production*, IEA Bioenergy: Task 39, Paris, France, 2019.

[142] A. H. Zacher, M. V. Olarte, D. M. Santosa, D. C. Elliott, and S. B. Jones, "A Review and Perspective of Recent Bio-Oil Hydrotreating Research", *Green Chemistry*, vol. 16, no. 2, pp. 491–515, 2014. DOI: 10.1039/C3GC41382A.

[143] E. Furimsky, "Selection of Catalysts and Reactors for Hydroprocessing", *Applied Catalysis A: General*, vol. 171, no. 2, pp. 177–206, 1998. DOI: 10.1016/S0926-860X(98)00086-6.

[144] J. Ancheyta-Juárez, E. Aguilar-Rodríguez, D. Salazar-Sotelo, G. Betancourt-Rivera, and M. Leiva-Nuncio, "Hydrotreating of Straight Run Gas Oil–Light Cycle Oil Blends", *Applied Catalysis A: General*, vol. 180, no. 1-2, pp. 195–205, 1999. DOI: 10.1016/S0926-860X(98)00351-2.

[145] D. Sági, P. Baladincz, Z. Varga, and J. Hancsók, "Co-Processing of FCC Light Cycle Oil and Waste Animal Fats with Straight Run Gas Oil Fraction", *Journal of Cleaner Production*, vol. 111, pp. 34–41, 2016. DOI: 10.1016/j.jclepro.2015.06.059.

[146] J. Ancheyta, S. Sánchez, and M. A. Rodríguez, "Kinetic Modeling of Hydrocracking of Heavy Oil Fractions: A Review", *Catalysis Today*, vol. 109, no. 1-4, pp. 76–92, 2005. DOI: 10.1016/j.cattod.2005.08.015.

[147] R. Palos et al., "Kinetic Modeling of Hydrotreating for Enhanced Upgrading of Light Cycle Oil", *Industrial & Engineering Chemistry Research*, vol. 58, no. 29, pp. 13 064–13 075, 2019. DOI: 10.1021/acs.iecr.9b02095.

[148] I. Hita et al., "Kinetic Modeling of the Hydrotreating and Hydrocracking Stages for Upgrading Scrap Tires Pyrolysis Oil (STPO) toward High-Quality Fuels", *Energy & Fuels*, vol. 29, no. 11, pp. 7542–7553, 2015. DOI: 10.1021/acs.energyfuels.5b01502.

[149] A. T. Jarullah, I. M. Mujtaba, and A. S. Wood, "Enhancement of Productivity of Distillate Fractions by Crude Oil Hydrotreatment: Development of Kinetic Model for the Hydrotreating Process", *Computer Aided Chemical Engineering*, vol. 29, pp. 261–265, 2011. DOI: 10.1016/B978-0-444-53711-9.50053-5.

[150] F. Alhumaidan, H. M. S. Lababidi, and H. A. Al-Adwani, "Hydrocracking of Atmospheric Residue Feedstock in Hydrotreating Processes", *Kuwait Journal of Science and Engineering*, vol. 37, no. 1B, pp. 129–159, 2010.

[151] S. Sánchez, M. A. Rodríguez, and J. Ancheyta, "Kinetic Model for Moderate Hydrocracking of Heavy Oils", *Industrial & Engineering Chemistry Research*, vol. 44, no. 25, pp. 9409–9413, 2005. DOI: 10.1021/ie050202.

[152] J. Martínez and J. Ancheyta, "Kinetic Model for Hydrocracking of Heavy Oil in a CSTR Involving Short Term Catalyst Deactivation", *Fuel*, vol. 100, pp. 193–199, 2012. DOI: 10.1016/j.fuel.2012.05.032.

[153] L. A. Soto-Azuara, R. Ramírez-López, M. del Carmen Monterrubio-Badillo, and I. Elizalde, "Mathematical Modeling of the Hydrocracking Kinetics of a Heavy Oil Fraction Using the Discrete Lumping Approach: The Effect of the Variation of the Lump Number", *Reaction Kinetics, Mechanisms and Catalysis*, vol. 135, pp. 655–667, 2022. DOI: 10.1007/s11144-022-02156-3.

[154] S. Sadighi, A. Ahmad, and M. Rashidzadeh, "4-Lump Kinetic Model for Vacuum Gas Oil Hydrocracker Involving Hydrogen Consumption", *Korean Journal of Chemical Engineering*, vol. 27, no. 4, pp. 1099–1108, 2010. DOI: 10.1007/s11814-010-0172-0.

[155] A. R. Ayasse, H. Nagaishi, E. W. Chan, and M. R. Gray, "Lumped Kinetics of Hydrocracking of Bitumen", *Fuel*, vol. 76, no. 11, pp. 1025–1033, 1997. DOI: 10.1016/S0016-2361(97)00104-X.

[156] S. Ramírez, J. Martínez, and J. Ancheyta, "Kinetics of Thermal Hydrocracking of Heavy Oils under Moderate Hydroprocessing Reaction Conditions", *Fuel*, vol. 110, pp. 83–88, 2013. DOI: 10.1016/j.fuel.2012.03.051.

[157] P. J. Becker, B. Celse, D. Guillaume, H. Dulot, and V. Costa, "Hydrotreatment Modeling for a Variety of VGO Feedstocks: A Continuous Lumping Approach", *Fuel*, vol. 139, pp. 133–143, 2015. DOI: 10.1016/j.fuel.2014.08.032.

[158] S. Texier, G. Berhault, G. Pérot, V. Harlé, and F. Diehl, "Activation of Alumina-Supported Hydrotreating Catalysts by Organosulfides: Comparison with H2S and Effect of Different Solvents", *Journal of Catalysis*, vol. 223, no. 2, pp. 404–418, 2004. DOI: 10.1016/j.jcat.2004.02.011.

[159] S. A. Qader and G. R. Hill, "Hydrocracking of Gas Oil", *Industrial & Engineering Chemistry Process Design and Development*, vol. 8, no. 1, pp. 98–105, 1969. DOI: 10.1021/i260029a017.

[160] L. A. Alcázar and J. Ancheyta, "Sensitivity Analysis Based Methodology to Estimate the Best Set of Parameters for Heterogeneous Kinetic Models", *Chemical Engineering Journal*, vol. 128, no. 2-3, pp. 85–93, 2007. DOI: 10.1016/j.cej.2006.10.012.

[161] M. Newville, T. Stensitzki, D. B. Allen, M. Rawlik, A. Ingargiola, and A. Nelson, *Lmfit: Non-Linear Least-Square Minimization and Curve-Fitting for Python*, available online: https://zenodo.org/record/11813 (accessed on 31 July 2023), 2014.

[162] P. Virtanen et al., "SciPy 1.0: Fundamental Algorithms for Scientific Computing in Python", *Nature Methods*, vol. 17, no. 3, pp. 261–272, 2020. DOI: 10.1038/s41592-019-0686-2.

[163] J. C. Vivas-Báez, A. Servia, G. D. Pirngruber, A.-C. Dubreuil, and D. J. Pérez-Martínez, "Insights in the Phenomena Involved in Deactivation of Industrial Hydrocracking Catalysts through an Accelerated Deactivation Protocol", *Fuel*, vol. 303, no. 120681, 2021. DOI: 10.1016/j.fuel.2021.120681.

[164] D. M. Hawkins, "The Problem of Overfitting", *Journal of Chemical Information and Computer Sciences*, vol. 44, no. 1, pp. 1–12, 2004. DOI: 10.1021/ci0342472.

Appendix A. Additional Information on Chapter 2

Table A.1: Composition of bioliq® heavy gasoline as used for Chapter 2 in wt.%.

C-Nr.	Naph.	i-Par.	n-Par.	Cy Ol.	Olef.	Arom.	Total
4	-	0.00	0.00	-	0.00	-	0.00
5	0.00	0.01	0.00	0.00	0.00	-	0.01
6	0.18	0.07	0.01	0.00	0.00	0.01	0.27
7	0.30	0.04	0.00	0.00	0.00	0.09	0.43
8	0.11	0.02	0.00	0.00	0.00	0.26	0.39
9	0.19	0.02	0.02	0.01	0.01	33.57	33.81
10	0.32	0.03	0.06	0.00	0.00	52.58	52.99
11	0.22	0.19	0.11	0.00	0.00	-	0.52
12+	0.91	0.00	0.00	0.00	0.00	10.44	11.35
Poly	0.22	-	-	0.00	0.00	-	0.22
Total	2.45	0.38	0.20	0.01	0.01	96.95	100.00

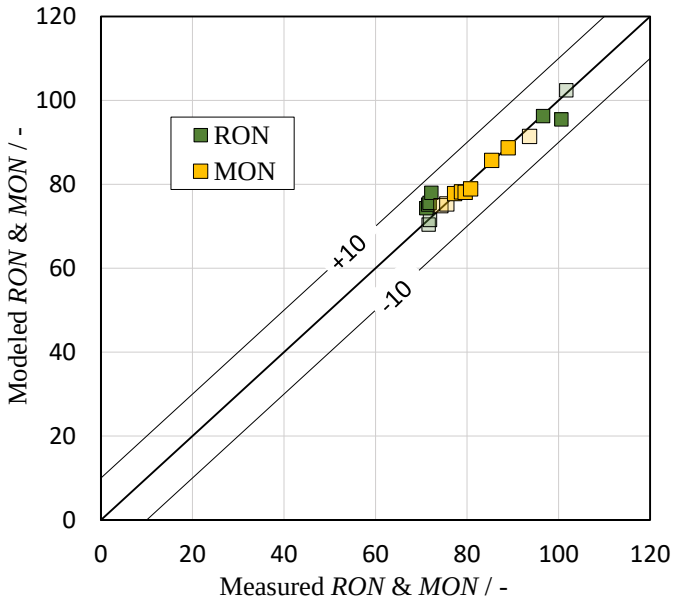


Figure A.1: Parity plot of RON (green) and MON (yellow) for modeled values and measurements taken with a CFR test engine. The measurements used to train the underlying model are marked transparently.

Table A.2: Petrochemical data obtained by hydroprocessing bioliq® heavy gasoline in a fixed bed reactor under variation of temperature.

Parameters	**Pt/Mor.**		**Pt/HZSM-5**						**Pt/SAPO-11**			
T_{Target} / °C	250	270	230	250	270	290	310	330	270	310	330	350
p / bar	90	90	50	50	50	50	50	60	90	90	90	90
$WHSV$ / h^{-1}	1.39	1.39	1.39	1.39	1.39	1.39	1.39	1.39	1.39	0.88	0.88	0.88
$\dot{V}_{H2,N}/\dot{V}_{Educt}$ / -	1667	1667	1667	1667	1667	1667	1667	1667	1058	1667	1667	1667
Measurments												
$T_{FB,min}$ / °C	249.1	268.1	228.6	248.4	269.8	290.2	310.1	329.9	270.1	309.0	328.9	348.7
$T_{FB,max}$ / °C	252.8	273.3	234.3	252.8	276.2	294.7	314.9	336.8	277.9	316.0	335.4	355.1
$Y_{Gasoline}$ / wt.%	96.88	91.19	98.98	98.95	97.39	94.51	88.67	78.18	98.01	97.22	97.15	N/A
RON / -	71.6[a]	71.9[a]	N/A	71.1[a]	N/A	71.5[a]	71.8[a]	72.2[a]	N/A	N/A	N/A	N/A
MON / -	74.3[a]	75.6[a]	77.7[b]	77.3[a]	78.1[b]	78.8[a]	79.6[a]	80.8[a]	76.8[b]	77.2[b]	77.3[b]	77.3[b]
ρ / kg m^{-3}	792.7	772.0	798.6	795.7	790.7	783.0	768.0	748.0	805.6	801.7	799.8	798.4
p_v / kPa	11.0	42.0	2.3	4.8	11.9	24.0	54.0	84.0	1.4	2.8	3.8	3.8
$E70$ / vol.%	0.0	1.2	0.0	0.0	0.2	0.7	2.5	14.0	0.0	0.0	0.0	0.0
$E100$ / vol.%	0.4	6.4	0.0	0.0	0.9	3.7	10.5	23.7	0.0	0.0	0.0	0.0
$E150$ / vol.%	17.0	44.8	2.7	5.8	17.6	29.8	40.0	48.7	0.91	2.0	3.0	4.4
$E180$ / vol.%	88.5	94.1	89.2	89.9	89.7	93.5	92.5	95.3	86.9	88.7	89.2	89.3
FBP / °C	245.0	215.0	242.0	240.0	240.0	223.3	219.7	208.3	243.0	239.0	241.0	238.0
$w_{Arom.}$ / wt.%	2.97	1.74	2.47	2.35	2.55	2.44	2.28	2.00	2.52	1.84	1.98	3.15
$w_{C10\text{-}Arom.}$ / wt.%	0.29	0.18	0.16	0.16	0.40	0.35	0.45	0.49	0.31	0.10	0.25	0.92
$w_{iso\text{-}Paraf.}$ / wt.%	1.66	6.64	0.77	1.26	2.79	3.60	6.69	12.06	0.61	0.66	0.80	0.86
$w_{n\text{-}Paraf.}$ / wt.%	0.17	0.62	0.35	0.56	2.44	2.26	3.82	6.67	0.35	0.42	0.48	0.78
$w_{Naphth.}$ / wt.%	95.17	90.96	96.39	95.84	92.19	91.64	87.16	79.22	96.51	97.08	96.70	95.16
$w_{Olef.}$ / wt.%	0.01	0.01	0.01	0.00	0.05	0.05	0.06	0.07	0.00	0.01	0.02	0.05

[a]Measured with CFR-test engine, [b]Measured with FTIR according to own method.

Table A.3: Petrochemical data obtained by hydroprocessing bioliq® heavy gasoline in a fixed bed reactor under variation of $WHSV$ and pressure for Pt/HZSM-5.

Parameters	**Pt/HZSM-5**									
T_{Target} / °C	330	330	330	330	330	330	330	330	330	330
p / bar	60	60	60	60	60	70	70	70	70	70
$WHSV$ / h^{-1}	0.84	1.39	1.81	2.23	2.66	0.84	1.39	1.81	2.23	2.66
$\dot{V}_{H2,N}/\dot{V}_{Educt}$ / -	2750	1667	1279	1038	873	2750	1667	1279	1038	873
Measurments										
$T_{FB,min}$ / °C	N/A	N/A	N/A	N/A	N/A	N/A	N/A	N/A	N/A	N/A
$T_{FB,max}$ / °C	N/A	N/A	N/A	N/A	N/A	N/A	N/A	N/A	N/A	N/A
$Y_{Gasoline}$ / wt.%	67.9	65.8	81.8	87.0	88.8	60.1	72.2	74.6	88.4	88.7
RON / -	N/A	N/A	N/A	N/A	N/A	N/A	N/A	N/A	N/A	N/A
MON / -	79.5[a]	80.0[a]	79.1[a]	79.0[a]	78.5[a]	80.0[a]	N/A	N/A	78.6[a]	78.7[b]
ρ / kg m^{-3}	N/A	N/A	N/A	N/A	N/A	N/A	N/A	N/A	N/A	N/A
p_v / kPa	N/A	N/A	N/A	N/A	N/A	N/A	N/A	N/A	N/A	N/A

Continued on next page ...

*E*70 / vol.%	28.4	18.0	11.8	12.9	2.0	23.7	N/A	N/A	7.5	9.8
*E*100 / vol.%	38.0	27.5	21.7	22.1	7.7	33.5	N/A	N/A	14.8	18.6
*E*150 / vol.%	60.3	54.4	47.0	46.4	28.0	56.1	N/A	N/A	40.0	41.7
*E*180 / vol.%	97.3	96.1	94.6	93.0	83.9	96.6	N/A	N/A	92.4	92.3
FBP / °C	191.7	201.8	210.8	214.5	219.4	199.6	N/A	N/A	220.8	217.7
$w_{\text{Arom.}}$ / wt.%	1.33	0.94	1.61	4.70	8.60	1.46	0.95	1.71	3.16	4.43
$w_{\text{C10-Arom.}}$ / wt.%	0.34	0.18	0.63	3.02	6.13	0.33	0.12	0.43	1.56	2.69
$w_{\text{iso-Paraf.}}$ / wt.%	20.62	14.93	11.04	9.07	7.38	19.42	13.57	11.45	8.38	7.77
$w_{\text{n-Paraf.}}$ / wt.%	13.63	10.75	8.72	7.44	6.15	12.58	10.05	8.66	6.68	6.28
$w_{\text{Naphth.}}$ / wt.%	64.39	73.34	78.60	78.73	77.82	66.50	75.41	78.14	81.74	81.47
$w_{\text{Olef.}}$ / wt.%	0.04	0.03	0.04	0.05	0.06	0.05	0.04	0.04	0.05	0.05

[a]Measured with FTIR according to own method.

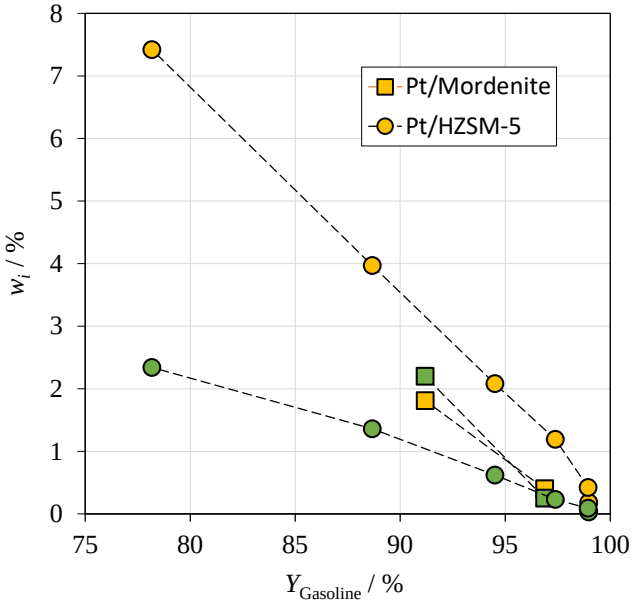


Figure A.2: C_5 iso-/n-paraffins (yellow) and C_4 iso-paraffins (green) as a function of Y_{Gasoline} for Pt/Mordenite and Pt/HZSM-5.

Table A.4: Composition of product fractions obtained by hydroprocessing bioliq® heavy gasoline in a fixed bed reactor under variation of temperature.

Parameters	**Pt/Mor.**		**Pt/HZSM-5**						**Pt/SAPO-11**			
T_{Target} / °C	250	270	230	250	270	290	310	330	270	310	330	350
p / bar	90	90	50	50	50	50	50	60	90	90	90	90
WHSV / h^{-1}	1.39	1.39	1.39	1.39	1.39	1.39	1.39	1.39	1.39	0.88	0.88	0.88
$\dot{V}_{\text{H2,N}}/\dot{V}_{\text{Educt}}$ /-	1667	1667	1667	1667	1667	1667	1667	1667	1058	1667	1667	1667
Y_{Gasoline} / wt.%	96.88	91.19	98.98	98.95	97.39	94.51	88.67	78.18	98.01	97.22	97.15	N/A
Naphthenes / wt.%												
C_5	0.03	0.11	0.00	0.00	0.02	0.03	0.07	0.11	0.00	0.00	0.00	0.01
C_6	0.99	3.09	0.06	0.18	0.53	1.07	1.52	1.39	0.03	0.05	0.08	0.13
C_7	1.26	3.38	0.49	0.78	1.16	1.65	1.97	1.49	0.59	0.62	0.65	0.48
C_8	2.33	4.67	1.32	1.42	1.52	2.01	2.38	1.54	1.19	1.21	1.23	1.26

Continued on next page ...

C_9	31.79	31.65	31.76	31.35	28.58	27.58	24.19	20.09	30.53	30.68	30.61	30.20
C_{10}	46.49	39.25	49.49	49.16	46.58	47.70	46.92	45.92	49.41	50.38	50.17	49.27
C_{11}	2.16	2.10	1.92	1.83	1.94	1.68	1.57	1.58	2.11	2.35	2.31	2.63
C_{+12}	6.83	4.52	7.79	7.88	9.12	7.52	6.65	5.61	10.07	9.51	9.40	9.13
C_{Poly}	3.29	2.19	3.56	3.24	2.74	2.40	1.89	1.49	2.58	2.28	2.25	2.05
iso-Paraffins / wt.%												
C_4	0.25	2.20	0.03	0.09	0.23	0.62	1.36	2.34	0.00	0.03	0.05	0.08
C_5	0.33	1.54	0.09	0.23	0.55	1.05	2.01	3.77	0.02	0.05	0.08	0.12
C_6	0.26	0.96	0.15	0.34	0.78	1.42	2.66	5.14	0.06	0.09	0.12	0.15
C_7	0.17	0.49	0.14	0.20	0.18	0.15	0.16	0.13	0.06	0.07	0.08	0.10
C_8	0.17	0.34	0.16	0.16	0.20	0.12	0.11	0.11	0.08	0.09	0.10	0.12
C_9	0.18	0.44	0.11	0.14	0.32	0.11	0.11	0.14	0.04	0.07	0.10	0.15
C_{10}	0.08	0.44	0.03	0.02	0.30	0.03	0.05	0.08	0.05	0.02	0.00	0.00
C_{11}	0.22	0.23	0.06	0.08	0.23	0.10	0.23	0.35	0.30	0.24	0.27	0.14
n-Paraffins / wt.%												
C_4	0.01	0.03	0.01	0.02	0.34	0.09	0.16	0.29	0.01	0.04	0.06	0.13
C_5	0.07	0.27	0.09	0.19	0.64	1.03	1.96	3.65	0.01	0.06	0.08	0.10
C_6	0.04	0.14	0.09	0.17	0.65	0.85	1.47	2.45	0.01	0.05	0.06	0.08
C_7	0.03	0.06	0.06	0.07	0.24	0.10	0.11	0.11	0.01	0.02	0.03	0.04
C_8	0.00	0.00	0.00	0.00	0.08	0.02	0.03	0.03	0.01	0.02	0.02	0.03
C_9	0.00	0.00	0.00	0.00	0.00	0.00	0.00	0.00	0.01	0.02	0.03	0.06
C_{10}	0.02	0.00	0.01	0.02	0.10	0.00	0.00	0.00	0.09	0.06	0.06	0.07
C_{11}	0.00	0.11	0.08	0.09	0.39	0.17	0.09	0.13	0.19	0.14	0.14	0.26
Aromatics / wt.%												
C_6	0.00	0.00	0.00	0.00	0.01	0.02	0.02	0.03	0.00	0.00	0.00	0.00
C_7	0.03	0.03	0.02	0.05	0.03	0.04	0.06	0.04	0.00	0.00	0.00	0.00
C_8	0.20	0.18	0.19	0.21	0.30	0.31	0.32	0.30	0.15	0.15	0.17	0.27
C_9	0.01	0.02	0.02	0.02	0.08	0.16	0.21	0.25	0.02	0.03	0.09	0.32
C_{10}	0.29	0.18	0.16	0.16	0.40	0.35	0.45	0.49	0.31	0.10	0.25	0.92
C_{11}	0.00	0.00	0.00	0.00	0.00	0.00	0.00	0.00	0.00	0.00	0.00	0.00
C_{+12}	2.44	1.32	2.09	1.92	1.73	1.56	1.23	0.89	2.05	1.55	1.47	1.64

Table A.5: Composition of product fractions obtained by hydroprocessing bioliq® heavy gasoline in a fixed bed reactor under variation of space velocity.

Parameters	**Pt/HZSM-5**									
T_{FB} / °C	330	330	330	330	330	330	330	330	330	330
p / bar	60	60	60	60	60	70	70	70	70	70
$WHSV$ / h^{-1}	0.84	1.39	1.81	2.23	2.66	0.84	1.39	1.81	2.23	2.66
$\dot{V}_{H2,N}/\dot{V}_{Educt}$ / -	2750	1667	1279	1038	873	2750	1667	1279	1038	873
$Y_{Gasoline}$ / wt.%	67.9	65.8	81.8	87.0	88.8	60.1	72.2	74.6	88.4	88.7
Naphthenes / wt.%										
C_5	0.13	0.12	0.12	0.13	0.12	0.11	0.10	0.12	0.11	0.11
C_6	1.45	1.50	1.44	1.48	1.52	1.21	1.20	1.20	1.17	1.26
C_7	1.55	1.66	1.70	1.85	2.00	1.34	1.34	1.40	1.45	1.61
C_8	0.99	1.54	1.96	2.26	2.49	0.82	1.31	1.59	1.78	2.02

Continued on next page ...

C_9	13.85	17.11	19.62	20.54	21.17	14.11	17.94	19.23	21.10	21.51
C_{10}	40.77	44.73	45.66	43.43	41.02	42.32	45.88	45.67	45.82	44.72
C_{11}	1.37	1.58	1.69	1.67	1.65	1.48	1.64	1.72	1.80	1.78
C_{+12}	3.58	4.49	5.66	6.20	6.59	4.32	5.31	6.16	7.25	7.18
C_{Poly}	0.70	0.61	0.75	1.17	1.26	0.79	0.69	1.05	1.26	1.28
iso-Paraffins / wt.%										
C_4	3.35	2.87	2.66	2.40	1.89	3.20	2.65	2.74	2.03	1.96
C_5	7.10	4.95	3.65	2.97	2.43	6.60	4.60	3.79	2.75	2.55
C_6	9.81	6.69	4.51	3.48	2.82	9.27	6.11	4.70	3.38	3.04
C_7	0.14	0.15	0.12	0.11	0.12	0.14	0.12	0.12	0.11	0.11
C_8	0.06	0.06	0.06	0.07	0.08	0.05	0.06	0.06	0.07	0.07
C_9	0.03	0.03	0.03	0.03	0.03	0.03	0.03	0.03	0.03	0.03
C_{10}	0.12	0.10	0.00	0.00	0.00	0.11	0.00	0.00	0.00	0.00
C_{11}	0.01	0.08	0.01	0.01	0.01	0.02	0.00	0.01	0.01	0.01
n-Paraffins / wt.%										
C_4	4.27	3.38	3.06	2.71	2.20	4.03	3.25	3.13	2.37	2.28
C_5	5.77	4.36	3.55	3.02	2.51	5.22	4.08	3.52	2.73	2.55
C_6	3.55	2.78	2.01	1.67	1.41	3.29	2.40	1.97	1.54	1.42
C_7	0.03	0.03	0.02	0.03	0.03	0.04	0.02	0.02	0.02	0.02
C_8	0.00	0.00	0.00	0.00	0.00	0.01	0.00	0.00	0.01	0.00
C_9	0.00	0.00	0.00	0.00	0.00	0.01	0.01	0.00	0.00	0.00
C_{10}	0.00	0.00	0.00	0.00	0.00	0.00	0.00	0.00	0.00	0.00
C_{11}	0.00	0.20	0.08	0.00	0.00	0.00	0.28	0.00	0.00	0.00
Aromatics / wt.%										
C_6	0.01	0.00	0.00	0.01	0.01	0.01	0.00	0.01	0.01	0.01
C_7	0.06	0.00	0.00	0.05	0.06	0.07	0.00	0.05	0.05	0.05
C_8	0.23	0.11	0.13	0.26	0.29	0.28	0.12	0.25	0.27	0.26
C_9	0.26	0.12	0.13	0.44	1.03	0.23	0.07	0.22	0.25	0.36
C_{10}	0.34	0.18	0.63	3.02	6.13	0.33	0.12	0.43	1.56	2.69
C_{11}	0.00	0.00	0.00	0.00	0.00	0.00	0.00	0.00	0.00	0.00
C_{+12}	0.44	0.52	0.72	0.92	1.09	0.52	0.64	0.75	1.03	1.06

Table A.6: Composition of the bioliq® blend in wt.%.

C-Nr.	Naph.	i-Par.	n-Par.	Cy. Ol.	Olef.	Arom.	Total
4	-	0.70	0.42	-	0.04	-	1.16
5	0.11	2.12	1.20	0.00	0.09	-	3.52
6	1.44	3.88	1.28	0.03	0.15	1.15	7.94
7	2.31	1.89	0.15	0.14	0.14	12.00	16.64
8	2.92	1.21	0.08	0.33	0.14	30.93	35.61
9	8.51	0.46	0.05	0.26	0.09	11.18	20.54
10	13.85	0.36	0.02	0.09	0.05	0.02	14.38
11	0.11	0.04	0.00	0.00	0.00	-	0.14
12+	0.06	0.00	0.00	0.00	0.00	-	0.06
Poly	0.00	-	-	0.00	0.00	-	0.00
Total	29.31	10.66	3.21	0.84	0.70	55.29	100.00

Table A.7: Petrochemical parameters of the bioliq® blend.

Parameter	*RON*	*MON*	ρ	p_v	*E*70	*E*100	*E*150	*FBP*	$\varphi_{\text{Aromatics}}$
Unit	-	-	$\mathrm{kg\,m^{-3}}$	kPa	vol.%	vol.%	vol.%	°C	vol.%
Value	92.4	86.2	806.22	29.7	2.5	10.4	84.4	163.2	51.4

Appendix B. Additional Information on Chapter 3

Table B.1: Composition of bioliq® light gasoline in vol.%.

C-Nr.	Naph.	Par.	Cy. Ol.	Olef.	Arom.	Oxyg.	Total
4	-	0.90	-	0.05	-	-	0.94
5	0.08	2.81	-	0.15	-	0.02	3.06
6	0.38	4.68	0.04	0.25	1.44	0.04	6.82
7	1.16	3.26	0.20	0.24	15.96	-	20.81
8	2.39	2.22	0.49	0.20	43.14	-	48.44
9	1.22	0.85	0.40	0.15	16.26	-	18.89
10	0.21	0.32	0.12	0.02	0.08	-	0.76
11+	-	0.25	-	-	-	-	0.25
Poly	0.02	-	-	-	-	-	0.02
Total	5.46	15.29	1.26	1.05	76.88	0.06	100.00

Table B.2: Composition of HG-HP@270 °C in vol.%.

C-Nr.	Naph.	i-Par.	n-Par.	Cy. Ol.	Olef.	Arom.	Total
4	-	0.16	0.14	-	-	-	0.30
5	0.01	0.46	0.47	-	-	-	0.94
6	0.48	0.71	0.47	-	-	0.01	1.67
7	1.38	0.23	0.09	-	-	0.05	1.76
8	2.14	0.16	0.03	-	-	0.37	2.70
9	38.66	0.13	-	0.02	-	0.06	38.87
10	51.99	0.01	0.10	0.03	-	0.01	52.14
11	0.08	0.04	-	-	-	-	0.12
12+	0.84	-	-	-	-	0.02	0.86
Poly	0.63	-	-	-	-	-	0.63
Total	96.21	1.90	1.29	0.05	-	0.53	100.00

Table B.3: Composition of HG-HP@310 °C in vol.%.

C-Nr.	Naph.	i-Par.	n-Par.	Cy. Ol.	Olef.	Arom.	Total
4	-	1.34	0.53	-	-	-	1.87
5	0.18	2.52	3.68	-	-	-	6.39
6	3.67	4.77	4.00	0.01	-	0.17	12.63
7	4.85	0.59	0.20	-	-	0.62	6.27
8	4.60	0.25	0.17	-	-	0.51	5.53
9	22.86	0.12	0.06	-	-	0.26	23.30
10	39.71	0.06	0.02	-	-	0.05	39.84
11	0.36	0.39	0.05	-	-	-	0.80
12+	2.32	-	-	-	-	0.01	2.34
Poly	1.04	-	-	-	-	-	1.04
Total	79.59	10.04	8.72	0.01	-	1.64	100.00

Table B.4: Composition of HG-HP@330 °C in vol.%.

C-Nr.	Naph.	i-Par.	n-Par.	Cy. Ol.	Olef.	Arom.	Total
4	-	1.45	1.09	-	-	-	2.55
5	0.25	3.84	8.30	-	-	-	12.39
6	4.09	8.22	8.68	-	-	0.01	21.00
7	4.57	0.39	0.15	-	-	0.02	5.14
8	3.25	0.18	0.01	-	-	0.19	3.63
9	27.59	0.08	-	0.02	-	0.07	27.75
10	26.19	0.08	-	0.03	-	0.07	26.36
11	0.41	0.02	0.04	-	-	-	0.46
12+	0.53	-	-	-	-	0.04	0.57
Poly	0.14	-	-	-	-	-	0.14
Total	67.02	14.26	18.27	0.05	-	0.39	100.00

Table B.5: Composition of FT-HP in vol.%.

C-Nr.	Naph.	i-Par.	n-Par.	Cy. Ol.	Olef.	Arom.	Total
4	-	0.98	1.82	-	-	-	2.80
5	0.07	8.94	10.40	-	-	-	19.41
6	0.70	15.50	11.78	-	0.02	-	27.99
7	1.42	13.56	6.60	-	0.01	0.04	21.63
8	1.34	10.59	3.34	-	0.01	0.03	15.31
9	0.62	6.28	1.14	-	-	0.01	8.05
10	0.14	2.68	0.29	-	-	0.03	3.14
11	-	0.72	0.30	-	-	-	1.02
12+	-	0.65	-	-	-	-	0.65
Poly	-	-	-	-	-	-	-
Total	4.29	59.89	35.67	-	0.05	0.10	100.00

Table B.6: Composition of bioliq® heavy gasoline as used for Chapter 3 in vol.%.

C-Nr.	Naph.	i-Par.	n-Par.	Cy. Ol.	Olef.	Arom.	Total
4	-	-	-	-	-	-	-
5	-	0.05	0.01	-	-	-	0.06
6	0.02	0.11	0.01	-	-	0.02	0.16
7	0.03	0.08	-	-	-	0.28	0.39
8	0.06	0.10	-	-	-	1.09	1.26
9	0.13	0.03	-	0.02	-	32.78	32.97
10	0.48	0.06	0.06	0.08	-	52.60	53.28
11	0.06	0.37	0.08	0.10	0.08	-	0.68
12+	-	0.95	-	-	-	10.20	11.14
Poly	0.06	-	-	-	-	-	0.06
Total	0.84	1.75	0.16	0.19	0.08	96.97	100.00

Table B.7: Composition of blend A in vol.%.

C-Nr.	Naph.	Par.	Cy. Ol.	Olef.	Arom.	Oxyg.	Total
1	-	-	-	-	-	3.10	3.10
2	-	-	-	-	-	5.81	5.81
3	-	-	-	-	-	-	-
4	-	2.17	-	0.02	-	-	2.19
5	0.09	9.08	-	0.07	-	0.01	9.25
6	0.99	13.48	0.02	0.11	0.62	0.02	15.24
7	1.64	8.25	0.09	0.11	6.85	-	16.94
8	1.90	5.69	0.22	0.10	18.52	-	26.43
9	4.72	2.89	0.19	0.07	6.99	-	14.86
10	3.97	1.16	0.06	0.01	0.04	-	5.24
11+	-	0.77	-	-	0.07	-	0.84
Poly	0.09	-	-	-	-	-	0.09
Total	13.39	43.50	0.58	0.49	33.09	8.95	100.00

Table B.8: Composition of blend B in vol.%.

C-Nr.	Naph.	Par.	Cy. Ol.	Olef.	Arom.	Oxyg.	Total
1	-	-	-	-	-	3.33	3.33
2	-	-	-	-	-	0.51	0.51
3	-	-	-	-	-	-	-
4	-	1.56	-	1.23	-	0.07	2.85
5	0.08	7.68	-	0.41	-	0.09	8.27
6	0.90	10.16	0.02	0.11	0.62	14.94	26.75
7	1.46	5.81	0.09	0.11	6.85	0.02	14.34
8	1.77	4.01	0.22	0.12	18.44	-	24.56
9	4.61	2.00	0.19	0.08	6.94	-	13.82
10	3.91	0.80	0.07	0.02	0.03	-	4.82
11+	-	0.65	-	-	0.05	-	0.70
Poly	0.04	-	-	-	-	-	0.04
Total	12.77	32.66	0.59	2.07	32.93	18.97	100.00

Appendix C. Additional Information on Chapter 4

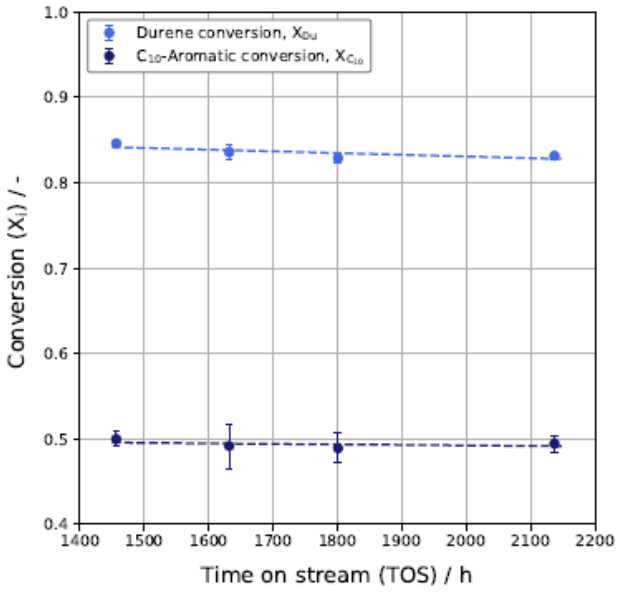


Figure C.1: Durene and C_{10} aromatics conversion at a reference point for the co-hydroprocessing of 15 wt.% durene and 85 wt.% middle distillate. Experimental conditions: T = 380 °C, $LHSV$ = 0.25 h^{-1}, p_{H2} = 59 bar, p_{Ar} = 3.9 bar and $\dot{V}_{H2}/\dot{V}_{Feed}$ = 1042 Nm^3 m^{-3}.

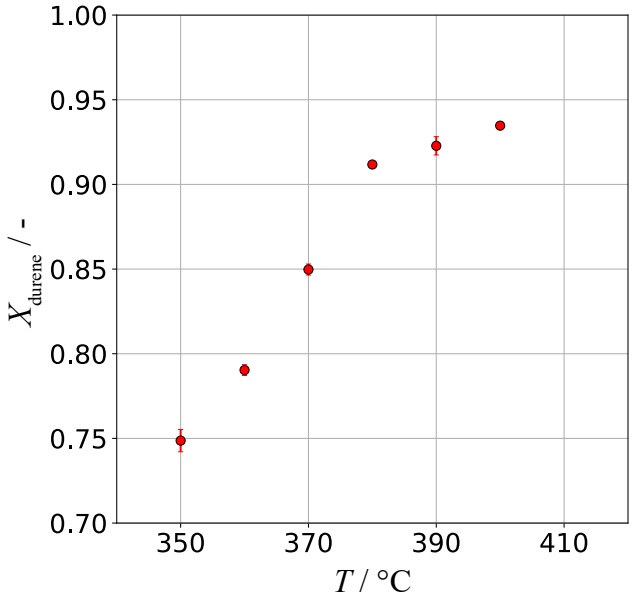


Figure C.2: Durene conversion under variation of temperature for the co-hydroprocessing of 15 wt.% durene and 85 wt.% middle distillate. Experimental conditions: $LHSV$ = 0.4 h^{-1}, p_{H2} = 59 bar, p_{Ar} = 3.9 bar and $\dot{V}_{H2}/\dot{V}_{Feed}$ = 1042 Nm^3 m^{-3}.

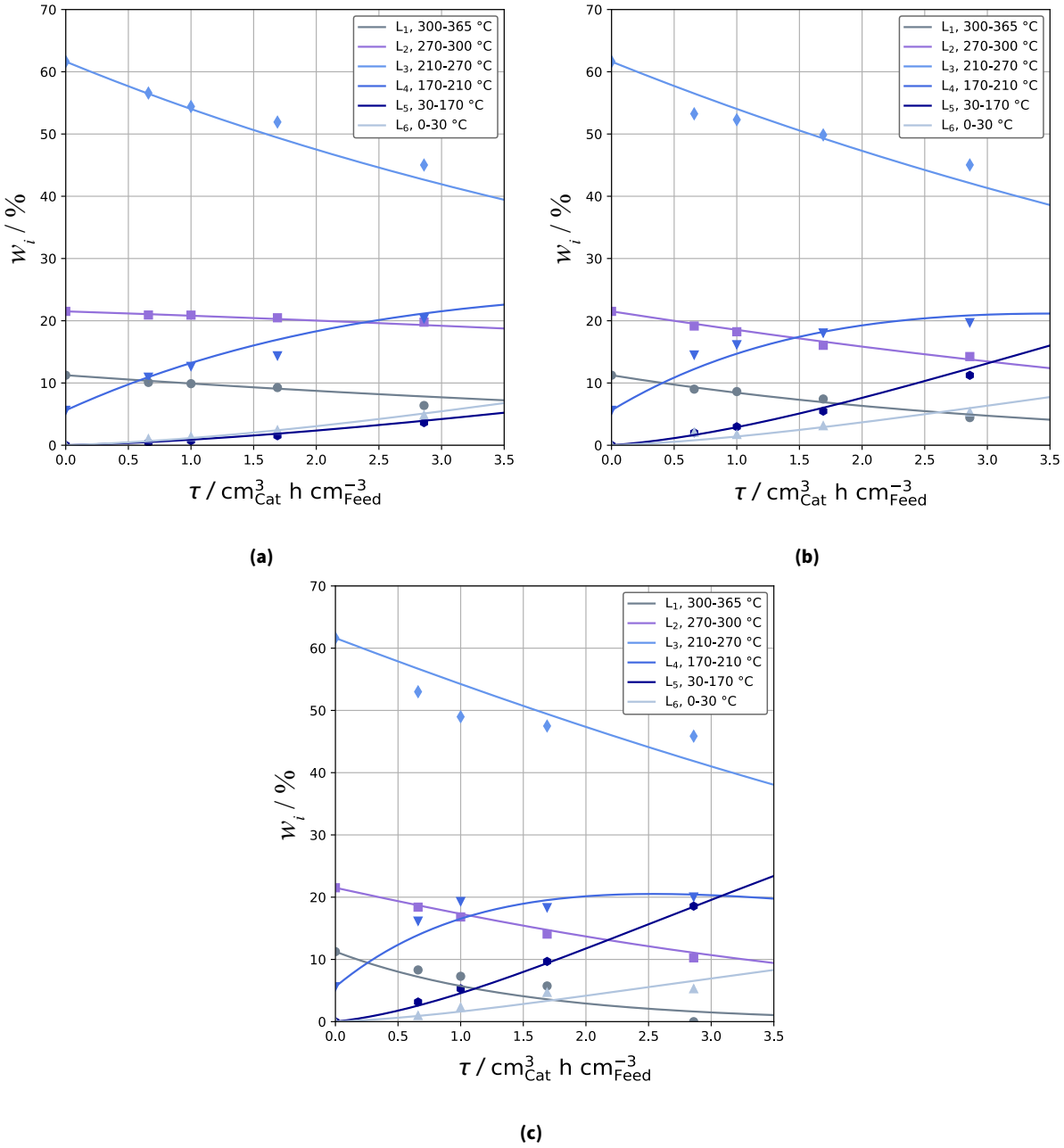


Figure C.3: Fitting results for the reduced model at **(a)** 350 °C, **(b)** 380 °C, and **(c)** 390 °C for the co-hydroprocessing of 15 wt.% durene and 85 wt.% middle distillate. Experimental conditions: p_{H2} = 59 bar, p_{Ar} = 3.9 bar and $\dot{V}_{H2}/\dot{V}_{Feed}$ = 1042 $Nm^3\ m^{-3}$. Note: Measuring point of Lump 1 in Figure C.3c for a space time of 2.86 h $cm^3_{Cat}\ cm^{-3}_{Feed}$ is probably too low due to measurement uncertainties in distillation.

Table C.1: Measured lump weight fractions at 340 °C, 350 °C, 370 °C, 380 °C and 390 °C for the co-hydroprocessing of 15 wt.% durene and 85 wt.% middle distillate. Experimental conditions: p_{H2} = 59 bar, p_{Ar} = 3.9 bar and $\dot{V}_{H2}/\dot{V}_{Feed}$ = 1042 $Nm^3\ m^{-3}$.

		Space time τ / $cm^3_{Cat}\ h\ cm^{-3}_{Feed}$				
T **/ °C**	**Lump**	**0.000**	**0.833**	**1.333**	**2.000**	**4.000**
340	6	0.00	1.01	2.39	3.12	4.00
	5	0.00	0.49	0.88	1.30	2.92
	4	5.61	11.46	12.33	19.70	21.31
	3	61.64	55.58	53.71	46.07	42.22
	2	21.51	21.12	20.23	21.44	20.59
	1	11.25	10.33	10.46	8.36	8.97
		Space time τ / $cm^3_{Cat}\ h\ cm^{-3}_{Feed}$				
T **/ °C**	**Lump**	**0.000**	**0.666**	**1.000**	**1.690**	**2.860**
350	6	0.00	1.04	1.39	2.44	4.84
	5	0.00	0.43	0.73	1.53	3.63
	4	5.61	10.94	12.67	14.37	20.35
	3	61.64	56.58	54.41	51.92	45.02
	2	21.51	20.92	20.90	20.48	19.77
	1	11.25	10.09	9.89	9.27	6.39
370	6	0.00	1.66	1.55	2.19	3.64
	5	0.00	1.13	1.91	3.29	7.92
	4	5.61	13.16	14.54	17.05	20.85
	3	61.64	54.27	52.84	50.81	43.54
	2	21.51	20.00	19.77	18.15	17.70
	1	11.25	9.78	9.39	8.50	6.36
380	6	0.00	2.08	1.73	3.14	5.35
	5	0.00	2.00	2.97	5.48	11.24
	4	5.61	14.50	16.15	18.04	19.70
	3	61.64	53.25	52.30	49.86	45.04
	2	21.51	19.15	18.23	16.06	14.25
	1	11.25	9.01	8.62	7.43	4.44
390	6	0.00	0.99	2.32	4.70	5.29
	5	0.00	3.16	5.29	9.67	18.56
	4	5.61	16.15	19.30	18.32	20.03
	3	61.64	53.00	48.98	47.50	45.87
	2	21.51	18.40	16.82	14.07	10.25
	1	11.25	8.31	7.29	5.74	0.00

Appendix D. Original Publications

This appendix presents the original published manuscripts and the supplementary materials for all three publications included in this doctoral thesis, in the order listed.

Energy Engineering

Tech Science Press

DOI: 10.32604/ee.2022.022759

ARTICLE

Hydroprocessing and Blending of a Biomass-Based DTG-Gasoline

David Graf, Philipp Neuner and Reinhard Rauch*

Department Fuel Technology (EBI-ceb), Karlsruhe Institute of Technology (KIT), Engler-Bunte-Institute, Karlsruhe, 76131, Germany

*Corresponding Author: Reinhard Rauch. Email: Reinhard.Rauch@kit.edu

Received: 24 March 2022 Accepted: 26 May 2022

ABSTRACT

The number of annually registered internal-combustion vehicles still exceeds electric-driven ones in most regions, e.g., Germany. Ambitious goals are disclosed with the European Green Deal, which calls for new technical approaches and greenhouse gas neutral transition technologies. Such bridging technologies are synthetic fuels for the transportation sector, e.g., using the bioliq® process for a CO_2-neutral gasoline supply. Fuels must meet the applicable national standards to be used in existing engines. Petrochemical parameters can be variably adapted to their requirements by hydroprocessing. In this work, we considered the upgrading of aromatic-rich DTG gasoline from the bioliq® process. The heavy gasoline was therefore separated from the light one by rectification. We investigated how to selectively modify the petrochemical parameters of the heavy gasoline, especially the boiling characteristics, to make the product suitable as a high-quality blending component. Three commercially available Pt/zeolite catalysts were tested over a wide range of temperature and space velocity. We achieved high gasoline yields, while the content of light end compounds up to a boiling temperature of 150°C could be increased significantly. In contrast to the high naphthenic content of the gasoline, the obtained octane numbers were satisfactory. Especially the Motor Octane Number turned out unexpectedly high and showed a dependency on the isomerization of the naphthenic rings. By blending the upgraded heavy gasoline with the previously separated light gasoline, we could finally show that hydroprocessing is suitable for adjusting petrochemical parameters. The aromatic concentration was 37.5% lower than that in the original raw gasoline, while the boiling characteristics improved significantly. Additionally, the final boiling point was 82°C lower, which is beneficial for the emission behavior.

KEYWORDS

Synthetic fuels; upgrading; durene; dimethyl ether to gasoline; refinery

Abbreviations

ASTM	American society for testing and materials
CFR	Cooperative fuel research
DIN	German industry standard
DMCP	Dimethylcyclopentane
DME	Dimethyl ether
DTG	Dimethyl ether to gasoline
ECP	Ethylcyclopentane
EN	European standard

This work is licensed under a Creative Commons Attribution 4.0 International License, which permits unrestricted use, distribution, and reproduction in any medium, provided the original work is properly cited.

FT	Fischer-Tropsch synthesis
FTIR	Fourier-transform infrared
GC	Gas chromatograph
GHG	Greenhouse gas
HP	Hydroprocessing
ISO	International organization for standardization
MCH	Methylcyclohexane
MFC	Mass flow controller
MTG	Methanol to gasoline
RC	Ring contraction
RO	Ring opening

Nomenclature

$E70$	Evaporated volume at 70°C
FBP	Final boiling point
H_{R}^{0}	Standard enthalpy of reaction
m	Mass
MON	Motor octane number
p_{v}	Vapor pressure
φ	Volume fraction
ρ	Density
RON	Research octane number
T	Reaction temperature
t_{R}	Reaction time
V	Volume
w	Mass fraction
$WHSV$	Weight hourly space velocity
x	Mole fraction
Y_{Gasoline}	Mass yield of gasoline

1 Introduction

As the greatest challenge of the present, the global climate crisis has underlined the urgency of a rapid expansion of renewable energies and the associated reduction of greenhouse gas (GHG) emissions. Many countries are starting to transform their energy sector towards greater sustainability, including the European Union with the Green Deal [1]. The transformation aims to comprehensively create a CO_2-neutral economy and society by 2050, which focuses on the sustainable use of available raw materials while preserving biodiversity [2]. This concept addresses all sectors of the energy system, of which the transport sector accounts for a significant share of total GHG emissions, e.g., 20% in Germany [3].

Automobiles based on electric drives are considered the most promising technology for decarbonizing the traffic sector in the medium to long term. According to official numbers of the German Federal Motor Transport Authority, the rate of new registered electric-driven cars increased in 2021 by 83.3% [4]. However, the share of car sales with internal-combustion engines still exceeds those of electric-driven ones. Newly registered vehicles counted 13.6% for fully electric drives and 12.4% for hybrid ones on German roads. Moreover, the average age of a car in Germany is approx. ten years, and

the number older than 30 years has increased by 15% (Jan 2022) [5]. Therefore, the ambitious climate targets can only be achieved if a GHG neutral alternative can be provided for the transition period of vehicles that still rely on an internal-combustion engine. A more distinct situation is emerging for the heavy transportation and aviation sectors, as they are strongly dependent on energy sources with high energy densities. These sectors are expected to depend on liquid hydrocarbon fuels in the long term. Due to these circumstances, it is important to continue investigating synthetic fuels as potential alternatives.

Feedstocks will become increasingly variable in the coming decades. Refineries will have to deal with biological feedstocks besides heavier fossil ones like tar sand [6]. Fischer-Tropsch (FT) and methanol to gasoline (MTG) or dimethyl ether to gasoline (DTG) are well known for decades. They can be considered part of the backbone for multifaceted hydrocarbon supply in the future. In contrast to process development and optimization, practical integration into refineries and the associated challenges have not been discussed in great detail. Processes such as FT and MTG or DTG place new demands on fuel upgrading. Due to the high concentration of aromatics, synthetic MTG and DTG gasolines differ considerably from fossil ones. Especially 1,2,4,5-Tetramethylbenzene (durene) can cause drivability problems. Crystallization resulting from the low melting temperature of 79°C can consequently clog fuel injection systems [7].

In refineries, several upgrading strategies are available or can be integrated, which are: a) transalkylation/disproportionation, b) extraction/crystallization, c) dilution and d) upgrading by hydroprocessing (HP). Processes for transalkylation and disproportionation have already been commercialized, for example with the Mobil TransPlus^{SM} process, which converts heavy aromatics into valuable BTX aromatics [8]. However, transalkylation is not available in every refinery. Due to increased process requirements resulting from the high reaction temperatures and thermodynamically limited conversion rates, significant investment costs must be considered. Crystallization or extraction of durene is promising as it opens synthesis routes with durene as a basic chemical, e.g., the production of polyimides [9]. However, this might only be a long-term solution, as new processes and infrastructures are required. Without major investment, the durene could be diluted into other hydrocarbon streams in the refinery by implementing a metering unit. Laboratory tests showed satisfactory engine performances with durene concentrations up to 5 wt.% [7,10,11]. However, heavy aromatics tend to form engine-out hydrocarbons [12] and soot [13,14]. Soot contributes to at least 10% of ambient particulate matter [15,16], which is one of the main reasons for reduced life expectancy worldwide [17]. A further strategy is the precise adjustment of chemical properties by HP. In 2018, Haldor Topsøe announced an isomerization process to upgrade synthetic gasoline [18]. To some extent, isomerization converts durene into other isomers. In this manner, crystallization can be avoided, however, without simultaneously addressing negative emission tendencies. Sooting behavior is expressed in the literature by parameters such as the Threshold Sooting Index [19] or the Novel Yield Sooting Index [14]. Generally, naphthenes and paraffins tend to form less soot [20]. Therefore, we decided to convert the heavy aromatics into saturated compounds using HP. An additional advantage is the possibility of co-processing with fossil feedstocks, as hydrotreating and hydrocracking units are available in modern oil refineries.

The object of this paper is a process approach in which the heavy aromatics are separated, converted by HP, and finally blended back into the original gasoline. We show how a deft catalyst choice can provide high-quality gasoline free of heavy aromatics like durene. For this purpose, we

varied the reaction temperature and space velocity over a wide range and investigated how the petrochemical parameters changed. In this regard, we also briefly discuss the catalytic processes involved.

2 Greenhouse Gas Neutral Gasoline Supply in a Refinery

2.1 Processes for the Production of Synthetic Gasoline

For the production of synthetic gasoline, there are various processes. In this study, MTG and DTG are considered, which are indirect catalytic processes using methanol and dimethyl ether (DME), respectively. Both processes are based on Mobil Oil's discovery in the 1970 s that methanol can be catalytically converted to hydrocarbons by a ZSM-5 zeolite [10]. The ZSM-5 zeolite has pores of medium size at relatively high acid strength, which determines its selectivity to products in the boiling range of gasoline [21]. Almost similar product spectra are observed for the MTG and DTG processes, consisting of paraffins, olefins, and especially methylated aromatics [22]. The bioliq® DTG raw gasoline is characterized by a high concentration of aromatics (approx. 75 wt.%), leading to a low proportion of light ends with boiling temperatures up to 150°C [23]. Such fuels are suitable for gasoline engines since the high aromatic concentration is accompanied by an increased octane number [10, 22]. The aromatic distribution ranges from C_6 to C_{10} and has a maximum at C_8. Depending on the synthesis conditions, the product contains 3 wt.%–6 wt.% of durene, while the concentration in fossil gasoline is only 0.2 wt.%–0.3 wt.% [10].

DTG offers an economic advantage over MTG due to lower investment costs. It is directly based on synthesis gas and does not need methanol as an intermediate product [24]. Furthermore, the increased economic efficiency results from the sequential reactions involved. Methanol formed in the equilibrium reaction (1) reacts directly to DME in reaction (2), which accelerates the conversion of synthesis gas due to the constant removal of the intermediate product methanol [25].

$$CO + 2H_2 \rightleftharpoons CH_3OH, \quad \Delta H^0_{R,298} = -182 \text{ kJ mol}^{-1} \tag{1}$$

$$2CH_3OH \rightleftharpoons CH_3OCH_3 + H_2O, \quad \Delta H^0_{R,298} = -23 \text{ kJ mol}^{-1} \tag{2}$$

In addition, the water formed in reaction (2) is converted with carbon monoxide by the water-gas shift reaction (3). This further increases the driving force, since the hydrogen formed is involved in the methanol synthesis of reaction (1) [26].

$$H_2O + CO \rightleftharpoons H_2 + CO_2, \quad \Delta H^0_{R,298} = -41 \text{ kJ mol}^{-1} \tag{3}$$

Consequently, the conversion is higher and the resulting recycle flow is lower, further reducing operating costs [27].

The feasibility of direct DME synthesis has already been demonstrated by companies such as JFE Holdings Inc., starting operation in 1999 in Hokkaido, Japan, and Haldor Topsøe A/S in Houston, USA [28]. On a pilot scale, the bioliq® process, developed at the Karlsruhe Institute of Technology (KIT) allows the conversion of low-grade lignocellulosic biomass into synthetic fuels [29,30]. As shown in Fig. 1, raw materials such as residual waste wood or straw are collected and liquified in regional fast-pyrolysis plants [31].

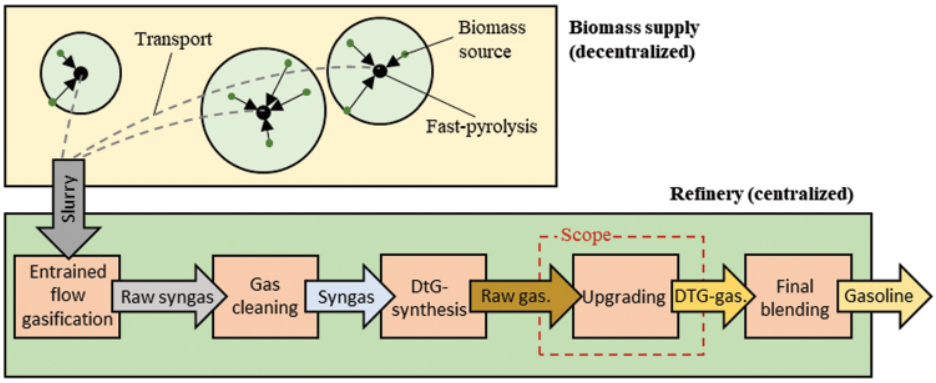


Figure 1: Production of synthetic gasoline using the bioliq® process. The biomass supply is decentralized and the DTG synthesis is centralized. Highlighted in red is the scope of this study, the upgrading of a DTG gasoline

The fast pyrolysis produces a slurry with ten times the energy density of the original biomass, resulting in lower transportation costs. In a central refinery, the slurry is converted into raw synthesis gas in an entrained flow gasifier [32]. Particulates and acid gas are subsequently removed in several gas purification stages to supply the refinery with high-quality, sulfur-free synthesis gas [30]. In the bioliq® process, the synthesis gas is fed to a DTG synthesis to produce raw gasoline [23]. Detailed considerations of efficiency and production cost estimates of the bioliq® process can be found in the work of Haro et al. [28] and Henrich et al. [33]. Regardless of their origin, synthetic DTG fuels do not necessarily meet motor gasoline standards. A further downstream upgrading is inevitably required. The upgraded DTG gasoline is piped into a blending unit, where it is mixed with additives such as ethanol or other hydrocarbon streams.

2.2 Upgrading Strategy for a Synthetic MTG/DTG Gasoline

In this study, we consider DTG gasoline from the bioliq® pilot plant at KIT in Karlsruhe, Germany. The standard DIN EN 228 must be met for gasoline in Germany [34]. Table 1 shows the petrochemical parameters of the raw gasoline as obtained directly from the bioliq® DTG synthesis. Compared with DIN EN 228, it can be seen that the boiling characteristics *E70*, *E100*, and *E150* are too low, which is equivalent to a shortage of light ends. These values indicate the volume fraction evaporated at a given temperature during distillation. For example, the measured value *E70* is the volume fraction evaporated at 70°C. The aromatic concentration significantly exceeds the permissible upper limit of 35 vol.%. Due to the high aromatic concentration, the density ρ is too high and the vapor pressure p_v is too low. It can be concluded that a stream containing an appropriate high proportion of saturated light ends is required to improve boiling characteristics while lowering the aromatic concentration.

We decided to upgrade the heavy gasoline in a downstream process by HP. As shown in Fig. 2, the total volume of raw gasoline is split into two-thirds light and one-third heavy gasoline by an atmospheric rectification.

Table 1: Petrochemical parameters of bioliq® raw gasoline, light gasoline, and heavy gasoline after rectification compared to DIN EN 228 standard [34]

Parameter	Unit	DIN EN 228	Raw gasoline bioliq®	Light gasoline bioliq®	Heavy gasoline bioliq®
RON	–	min. 95	N/A	101.7	N/A
MON	–	min. 85	N/A	93.7	N/A
ρ	kg m^{-3}	720.0–775.0	845.76	828.91	891.72
p_v (Class A)	kPa	45–60	45 ± 4	31 ± 5	0.15 ± 0.15
E70	vol.%	22.0–50.0	1.2 ± 0.7	1.1 ± 0.7	0.0
E100	vol.%	46.0–72.0	5.7 ± 0.7	6.4 ± 0.7	0.0
E150	vol.%	75.0	46.4 ± 0.7	85.4 ± 0.7	0.0
FBP	°C	210	245 ± 4	171 ± 4	290 ± 4
φ_{Benzene}	vol.%	max. 1.00	1.2 ± 0.7	1.6 ± 0.7	0.0
φ_{Olefins}	vol.%	max. 18.0	1.3 ± 0.1	1.1 ± 0.1	traces
$\varphi_{\text{Aromatics}}$	vol.%	max. 35	82.3 ± 0.7	76.3 ± 0.7	96.5 ± 0.7
$w_{\text{Oxygenates}}$	wt.%	max. 3.7	traces	traces	0.0

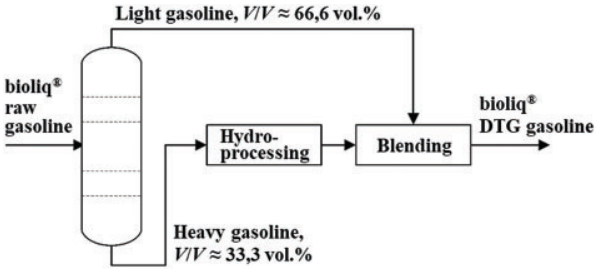


Figure 2: Schematic flow diagram for upgrading an MTG/DTG gasoline. The upgrading process consists of a rectification column, a hydroprocessing reactor, and a blending unit that yields the final DTG product by blending the light and the upgraded heavy gasoline

The petrochemical parameters for both fractions obtained by rectification are listed in Table 1. Due to its high concentration of aromatics (1.7 vol.% benzene, 17.2 vol.% toluene, 43.2 vol.% xylenes, 15.1 vol.% trimethylbenzens), bioliq® light gasoline is considered a valuable blending component. As shown in Fig. 2, we forward the heavy gasoline to a HP unit where the petrochemical parameters are adjusted accordingly. This fraction is then piped into a blending unit, where it is blended back into the light gasoline. In addition to adjusting the above parameters, the Research Octane Number (*RON*) and Motor Octane Number (*MON*) of the hydroprocessed heavy gasoline should remain as high as possible. Otherwise, there is a risk that the octane numbers of the blend will fall below the specifications required by DIN EN 228. Maintaining octane numbers can be challenging because saturated hydrocarbons usually have lower ones than aromatics [13]. If there is no volume loss during HP, the ratio of light to upgraded heavy gasoline must remain 2:1 as delivered during rectification. Table 1 shows that nearly 97 vol.% (96.95 wt.%) of the heavy gasoline is composed of aromatic hydrocarbons. At approx. 52.6 wt.%, the largest proportion consists of C_{10} (21.4 wt.% durene) and

approx. 10.4 wt.% of C_{12} aromatics. Accounting for 33.6 wt.%, the C_9 aromatics have the second largest share. The remaining 3 wt.% are mostly naphthenic. Measured data on the exact feed composition can be found in Table A1 in the Appendix A.

2.3 Hydroprocessing of Streams Rich in Heavy Aromatics

HP is a promising process for converting heavy aromatic hydrocarbons into light and saturated molecules. The term HP is used for different reactions with hydrogen. Depending on the process conditions and the chosen catalysts, this includes hydrogenation, hydrocracking, and hydroisomerization. Which reaction regime is most promising for a given feedstock depends on how the target petrochemical parameters are to be adjusted.

Depending on the used catalyst, hydrocracking can follow four reaction pathways, i.e., hydrocracking over bifunctional catalysts, hydrogenolysis on metal sites, catalytic hydrocracking on monofunctional catalysts (also referred to as Haag-Dessau mechanism), and thermal hydrocracking [35]. By using a bifunctional metal/zeolite catalyst, hydrocracking allows almost complete hydrogenation of aromatics in one reaction step. Simultaneously, a certain amount of highly branched naphthenes and paraffins are formed [36]. The saturated products have lower boiling temperatures than aromatics with the same number of carbon atoms. A further lowering of the boiling temperatures results from the formation of low-molecular cracking products.

Noble metals are particularly suitable as active sites for deep aromatic saturation. They can achieve high hydrogenation activities even at relatively low temperatures, where the thermodynamic equilibrium is on the side of the saturated products [37]. Therefore, the hydrogen pressure can be kept low. This maintains some flexibility in terms of operating temperature and pressure [38]. The latter is important because biomass-derived fuels are variable and contain a wide range of hydrocarbons that are not easily hydrogenated. With the operating temperature, the yield of light ends can be adjusted. The catalyst support must be chosen accordingly. Figueras et al. [39] described how the presence of an acidic support induced an electron deficit in palladium and thereby accelerated the benzene hydrogenation. Moreover, Tri et al. [40] explained the influence on the selectivity of co-hydrogenation of a benzene-toluene mixture by the electrophilic character of platinum resulting from the support's acidity. Due to their sufficient acidity, aluminosilicates are beneficial as catalytic supports. More precisely, the subgroup zeolites are in particular suitable for HP. An advantage over their forerunners in acid-catalyzed reactions, i.e., amorphous silica-alumina, is the superior acid strength of zeolites [41]. Further beneficial is the possible formation of selectively desired products by steric constraints within their structural environment [42]. Naphthenes, resulting from the hydrogenation of aromatics, can undergo sequential reactions. Mignard et al. [43] studied the reaction of methylcyclohexane (MCH) over a bifunctional Pt/USY catalyst. They observed that naphthenes undergo a ring contraction (RC) reaction, where C_6 rings shrink to C_5 rings while the molar mass remains constant. Figueras et al. [44], studying the RC reaction of MCH over platinum impregnated sulfated zirconias, showed that the distribution of acid strength has the greatest influence on selectivity and activity. Weitkamp et al. [45] also used MCH as probe molecule over Pt/HZSM-5, Pt/CaY, and Pd/LaY, among other naphthenes. Based on the isomer distribution, they demonstrated the shape selective influence of the zeolite structure, as some isomers were not found in the product mixture for HZSM-5. Using a Pt-Ir/ZrO_2-SO_4^{2-} and a pure ZrO_2-SO_4^{2-} catalyst, Belatel et al. [46] suggested that besides an acid site, a metal component also plays an active role in the isomerization process of MCH. The dehydrogenation at the metal site leads to a cycloalkene, which is protonated at a Brønsted acid site, yielding a (cyclic) carbenium ion [35]. RC leads to a variety of isomers that increase with the number of carbon atoms in the naphthene. The isomers differ considerably in their petrochemical parameters such as octane number [47], but the boiling temperatures also vary within a certain range.

For a better understanding, Fig. 3 shows the typical reaction pathways for the HP of aromatic hydrocarbons using the example of durene, since it is the substance with the highest concentration in the feed.

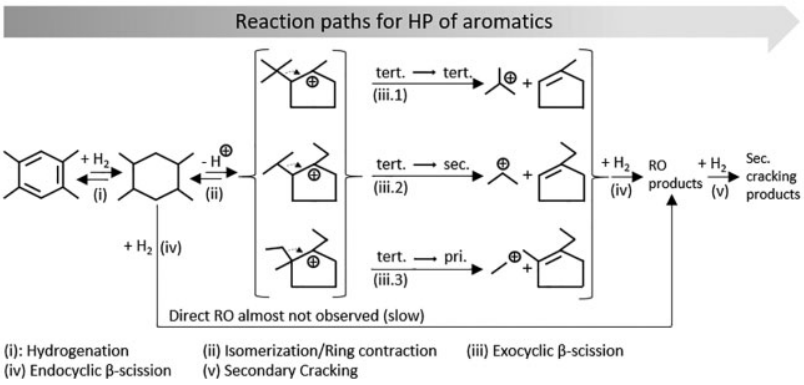


Figure 3: Reaction pathways for HP of durene, including (i) Hydrogenation, (ii) Isomerization/Ring contraction, (iii) Exocyclic β-scission, (iv) Endocyclic β-scission, and (v) Secondary cracking

Reaction (i) shows the hydrogenation of durene, followed by RC in reaction (ii). It should be noted that many other isomers can be formed, e.g., two methyl groups instead of one ethyl group attached to the ring at different positions. As explained above, the distribution is highly dependent on a) the acid strength distribution and b) the shape selective influence of the used catalyst. Besides hydrogenation and RC, β-scission of endo-and exocyclic carbon-carbon bonds are important reactions in bifunctional hydrocracking. Both reactions proceed via the formation of a carbenium ion. However, it can be stated that endocyclic carbon-carbon bonds are more difficult to break and the reaction is correspondingly slower [48]. Brouwer et al. [49] found the cause in the unfavorable orientation of the p-orbital of a positively charged carbon atom to the C-C bond to be broken. Endocyclic β-scission, also called ring opening (RO), yields paraffins. In general, RC products can subsequently be ring opened. Reaction (ii) shows the rearrangement of carbon atoms, which allows the formation of a stable tertiary cyclic carbenium ion in the ring structure. For naphthenes $\geq C_{10}$, the fast tertiary-tertiary β-scission is the predominant reaction, yielding an iso-butyl carbenium ion and methylcyclopentene (in case of durene) as products (reaction iii.1). Egan et al. [50] referred to this reaction as the paring reaction. Interestingly, the product spectrum of the paring reaction proved to be independent of the isomer configuration of the reactant [51]. It can be concluded that isomerization reactions (endo- and exocyclic alkyl shifts) are faster than exocyclic β-scission. Reactions (iii.2) and (iii.3) describe the tertiary-secondary and the tertiary-primary exocyclic β-scission of a C_{10} naphthene. The resulting secondary and primary carbenium ions lead to the formation of the products propane and ethane after a final hydrogen transfer. In an uninhibited reaction, the rates decrease in the order: tertiary-tertiary > tertiary-secondary > tertiary-primary, according to the stability of the respective carbenium ions. However, this might be influenced by shape selective constraints of the zeolites used on the bulky intermediates. As a result, a slower mechanism incorporating less spacious intermediates may be favored over the fast paring mechanism. Naphthenes $< C_9$ can only follow reaction pathways via the formation of secondary and primary carbenium ions, since tertiary-tertiary exocyclic β-scission is mechanistically hindered.

Bifunctional hydrocracking gained increased interest with the growing demand for fuels. Polynuclear aromatics are the least desirable products in diesel fuels. Besides too high densities, unfavorable cold-flow properties, and low cetane numbers [52], they also exhibit too high emission tendencies. Several approaches exist, one of which is the selective RO to yield products with high cetane numbers while maintaining high fuel yields [52–54]. The same considerations were made for heavy mononuclear aromatics in gasoline. Lower densities, higher octane numbers, and better combustion characteristics are possible when the rings are opened to form branched paraffins [47,55–57].

3 Material and Methods

In this study, a lab scale HP setup with a maximum throughput of approx. 7.2 L d^{-1} was used. As shown in Fig. 4, a fixed bed reactor with an inner diameter of 14.9 mm, was operated top-down in co-current mode. The reactor was electrically heated using three heat brackets.

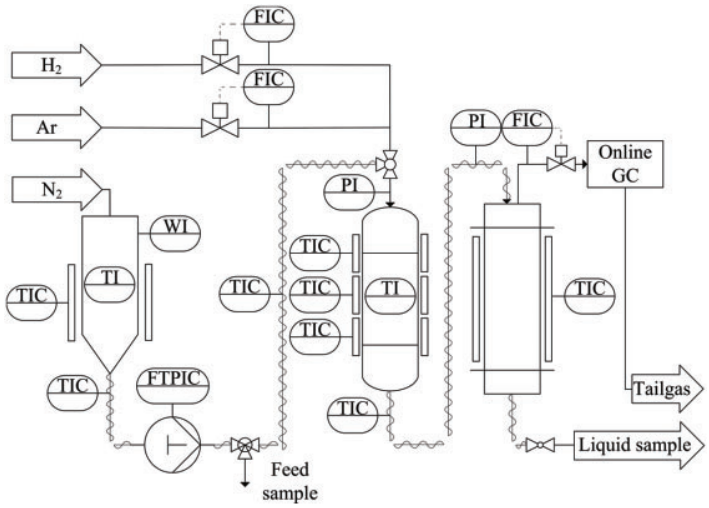


Figure 4: Flow diagram of the laboratory HP setup used in this study

A central probe tube with an outer diameter of 1/8″ was available to measure the catalyst bed temperature by axially moving a K-type thermocouple. Clariant AG loaded the three pelletized commercial catalysts with 0.3 wt.% platinum. The hand-grinded and sieved 100–200 µm fraction was diluted with silicon carbide of the same particle size distribution in a ratio of approx. 1:2 (V/V) and filled into the reactor between two further layers of pure silicon carbide. Table 2 lists the catalysts used in this work.

Table 2: Catalysts used for the experiments

Metal and Zeolite	Metal loading in wt.%	Catalyst mass in g	Bed height in mm
Pt/HZSM-5	0.3	12.694	405
Pt/Mordenite	0.3	12.689	466
Pt/SAPO-11	0.3	20.005	453

Catalyst bulk densities, and thus bed heights, varied due to the manual grinding process. Since the activity of Pt/SAPO-11 was the lowest observed, the catalyst mass was increased. This resulted from the need to produce large sample quantities for the analysis of the petrochemical parameters. The feed was placed in a storage tank tempered to 50°C to keep the durene dissolved. To build up the reaction pressure on the liquid side and to pipe the heavy gasoline at a flow rate of 0.01–5.00 mL min^{-1}, a Bischoff HPD pump–Multitherm 3351 heated to 50°C was used. In addition to the liquid feed, the gas was also fed to the top of the reactor. The H_2 with a purity of 99.999% was metered with a Bronkhorst EL-Flow® Select mass flow controller (MFC) and premixed with the liquid phase in the first 20 cm of the fixed bed, which consisted of pure silicon carbide and was tempered to reaction temperature. In a downstream separator with a volume of approx. 800 mL, the liquid-gas product mixture was separated at ambient temperature and reaction pressure. The liquid product was drawn off at the bottom of the separator via a cooling coil tempered to 0°C, in order that no noticeable pressure drop occurred in the reactor. The extracted liquid product was stored gas-tight at below 0°C and analyzed offline according to the parameters specified in DIN EN 228. A Reformulyzer M4 from the company PAC and an Agilent gas chromatograph (GC) 7890A calibrated according to ASTM D6730–01 [58] were used to measure the compositions of the liquid hydrocarbon samples. The Reformulyzer M4 provided a comprehensive insight into the sample by having the instrument distinguish between groups of substances and the number of carbon atoms. To measure individual components, e.g., the concentration of durene, the Agilent 7890A GC was used as a complementary method. *RON* and *MON* were determined following ISO 5164 [59] and ISO 5163 [60], respectively, by PetroLab in Speyer, Germany, using a frequently inspected Cooperative Fuel Research (CFR) test engine. In addition, octane numbers were measured using a PAC OptiFuel based on an infrared measurement followed by automatic spectrum analysis. Since the hydrocarbon mixtures studied were either rich in aromatics (feed) or naphthenes (products), the model underlying the OptiFuel was extended as part of the work. Octane numbers measured with a CFR test engine were used to train the new model, and a certain number of samples were retained for validation. An error of ±4 and ±2 could be determined for the *RON* and the *MON*, respectively. The calculation of the *E70*, *E100*, and *E150* values according to DIN EN 228 was based on the boiling curve measured with a PAC OptiDist calibrated according to ASTM D86 [61] for sample volumes > 100 mL or a PAC OptiPMD calibrated according to ASTM D7345 [62] for sample volumes < 100 mL. By interpolation between two measuring points recorded with a resolution of 1 vol.%, *E70*, *E100*, and *E150* were calculated. The vapor pressure was measured using a PAC Herzog HVP 972 according to ASTM D6378 [63] at 37.8°C. Finally, the density was measured at 15°C according to a self-developed method utilizing a Mettler&Toledo D5. The gas stream leaving the separator was directed to a Bronkhorst EL-Press® MFC, which was used to control the reaction pressure. Subsequently, it was depressurized to atmospheric pressure and fed into an Agilent 7890A GC. To calculate the mass balance, argon with a purity of 99.999% was fed as internal standard into the top of the reactor, using a Bronkhorst EL-Flow® Select MFC. Based on the change in argon concentration due to the reactions between the feedstock and hydrogen, the total outlet volume flow could be calculated.

Additional experiments were conducted in a self-designed batch reactor. The reactor was equipped with a hydrogen inlet by which the reaction pressure was adjusted. A heating jacket provided the necessary heat, while there was no cooling option. The hydrogen was dispersed into the liquid phase with a self-priming stirrer operated at 800 min^{-1}. Liquid samples were taken after specific time intervals and analyzed offline using the Agilent 7890A GC as described above. A model mixture of 27.1 wt.% toluene, 31.2 wt.% xylene isomers, 35.3 wt.% 1, 2, 4-trimethylbenzene and 6.3 wt.% 1,

2, 4, 5-tetramethlybenzene was used as feed. For each experiment, 0.3 g catalyst with a particle size distribution of 20–63 µm was added to 70 g of feed.

All measurements were repeated whenever possible and statistically evaluated according to the student's t-distribution, assuming a 95% confidence interval.

4 Results

4.1 Adjustment of Petrochemical Parameters

As shown in Fig. 5, several gasoline qualities were produced by HP bioliq® heavy gasoline with a fixed bed reactor to investigate how the petrochemical parameters can be adjusted. Fig. 5a shows the heavy gasoline stored at approx. 20°C (left) and 0°C (right). A representative product fraction after HP can be seen in Fig. 5b. Comparing Figs. 5a and 5b qualitatively shows the effect of HP the heavy gasoline. While the durene forms crystals in the heavy gasoline at 0°C there is nothing such observed after HP.

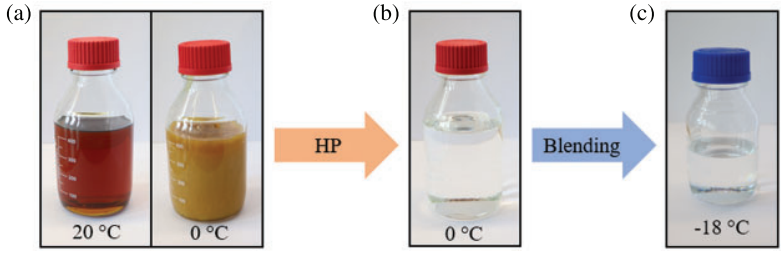


Figure 5: (a) bioliq® heavy gasoline, (b) product after HP with Pt/HZSM-5 ($p = 50$ bar, $T = 270$°C and $WHSV = 1.39\ h^{-1}$) and (c) bioliq® blend as discussed in the blending section, stored at temperatures as indicated in the respective image

For each experiment, a target temperature T_{target} for the catalyst bed was set. Due to the exothermic nature of the hydrogenation reaction, it was not possible to provide fully isothermal conditions. $T_{FB,min}$ and $T_{FB,max}$ are the minimum and maximum temperatures measured in the fixed bed and provided in the Appendix, if measured. As explained in the theoretical part on HP, cracking reactions lead to the formation of gaseous products, which reduces the yield of products in the boiling range of gasoline. The decision for a particular operating point is therefore not based solely on the maximum achievable quality of the product, but requires a comparison to the gasoline yield as defined by Eq. (4).

$$Y_{Gasoline} = \frac{\dot{m}_{Gasoline}}{\dot{m}_{Feed}} \tag{4}$$

Therefore, the petrochemical parameters to be optimized are discussed as a function of the gasoline yield. The pressures for the experiments were set to achieve an almost complete conversion of the aromatics. Table 3 shows the parameter ranges investigated for each catalyst. The Pt/HZSM-5 catalyst exhibited the highest hydrogenation activity, based on the applied pressures. An almost complete conversion of aromatics was achieved at a pressure of 50 bar.

Table 3: Parameter ranges investigated with the catalysts

	Pt/HZSM-5	Pt/Mordenite	Pt/SAPO-11
T in °C	230–330	250–270	270–350
p in bar	50–70	90	90
$WHSV$ in h^{-1}	0.84–2.66	1.39	1.39 and 0.88

For the other catalysts Pt/SAPO-11 and Pt/Mordenite, a pressure of up to 90 bar was required. Due to equilibrium limitations at temperatures of ≥310°C, the *WHSV* had to be additionally reduced from 1.39 h^{-1} to 0.88 h^{-1} for Pt/SAPO-11. Data obtained from the CFR motor experiments and FTIR measurements are used for evaluating the *MON* and *RON*. The standard deviation of ±4 for *RON*-FTIR measurements is considered too high. Therefore, these data are not used in this study, and no *RON* values can be reported for experiments with Pt/SAPO-11 since no CFR measurements were performed. The octane numbers measured in this study, as a function of various parameters, are displayed in Fig. 6. Fig. 6a shows the MON and RON as a function of the gasoline yield.

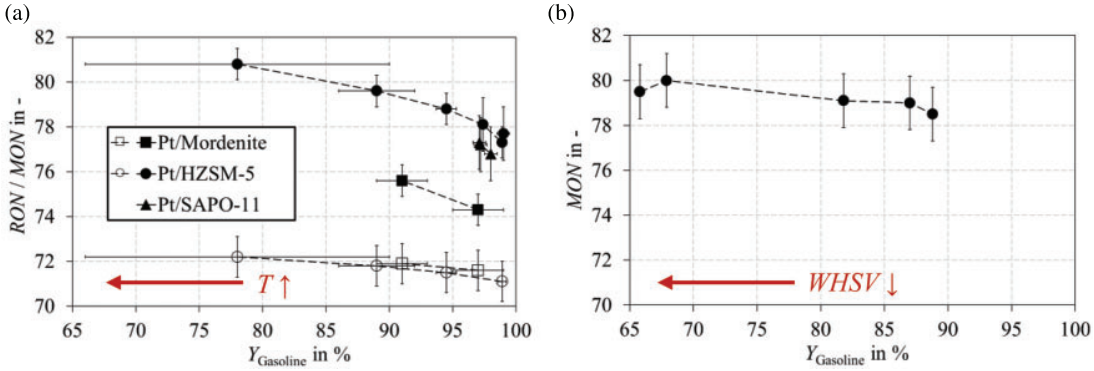


Figure 6: *RON* (white symbols) and *MON* (black symbols) as a function of gasoline yield, adjusted (a) by reaction temperature and (b) by space velocity. Experiments with Pt/Mordenite, Pt/HZSM-5, and Pt/SAPO-11 were performed in a fixed bed reactor according to the parameters listed in Table B1 (*T* variation) and Table B2 (*WHSV* variation) in Appendix B

Pressure and space velocity were kept constant during the experiments, while the gasoline yield was adjusted by varying the reaction temperature. The corresponding data can be found in Appendix B. Throughout the investigated parameter range, *MON* consistently exceeds *RON*, which is probably due to the samples' high C_9 and C_{10} naphthene content. For Pt/HZSM-5, the *MON* increases by 3.5 between a gasoline yield of 99 wt.% and 78 wt.%, while only by 1.1 for the *RON*. Compared to a *MON* of 85, as required by DIN EN 228, the measured values of up to 80 are promising. On the other hand, measured *RON* values of up to 72 do not meet 95 as demanded by the standard. However, it can be stated that the overall *RON* and *MON* values are favorable, as naphthenes larger C_9 are typically < 35 and < 30, respectively [64]. The *MON* varies depending on the catalyst used. It can be observed that the *MON* increases in the order: Pt/HZSM-5 > Pt/SAPO-11 > Pt/Mordenite. The selective isomerization of naphthenes explains these results since, especially at high gasoline yields of 97 wt.%–100 wt.%, hardly any paraffins are formed besides a negligible concentration of aromatics. McVicker et al. [65] found the same order as reported above for the RC of MCH expressed as the

1, 2-dimethylcyclopentane (DMCP)/1, 3-DMCP ratio. For Pt/HZSM-5, almost no 1, 2-DMCP was formed, whereas the isomer distribution was almost in equilibrium for Pt/Mordenite. In conclusion, the differences in *MON* values can clearly be attributed to the shape selective influence of the catalysts.

In contrast to the *MON*, no dependency on the catalyst selectivity is evident for the *RON* in the studied parameter range. The values obtained by the CFR engine are nearly congruent for Pt/Mordenite and Pt/HZSM-5. This is probably due to the less harsh test conditions for *RON* measurements, since the degree of isomerization and thus the thermal stability of the molecule does not play such a crucial role. In addition, the produced samples do not correspond to any standard fuel. The sample matrix and thus the high content of naphthenes must be considered. Considering the *MON* values for Pt/SAPO-11 lying between those of the other two investigated catalysts, it can be assumed that the *RON* values for Pt/SAPO-11 are comparable to those of Pt/Mordenite and Pt/HZSM-5.

Fig. 6b shows the *MON* for a constant reaction temperature of 330°C at a pressure of 60 bar for Pt/HZSM-5 under variation of the *WHSV*. In contrast to Fig. 6a, the *MON* does not increase as distinct. Fig. 7 shows the gasoline composition for both experiments carried out with Pt/HZSM-5 under variation of temperature (black symbols) and space velocity (white symbols).

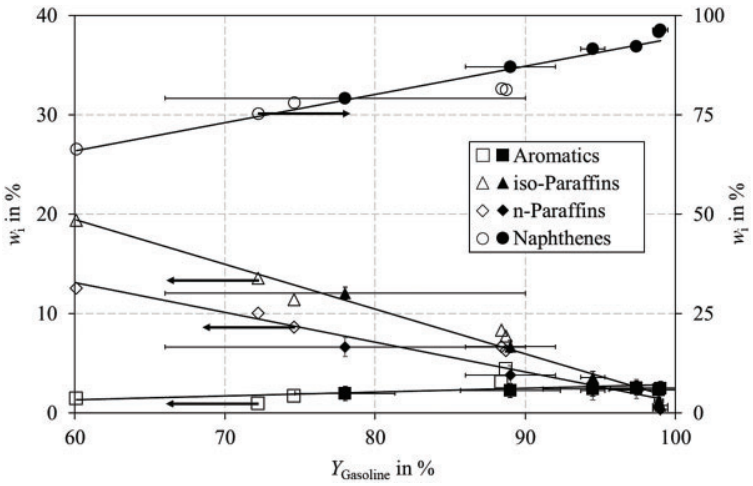


Figure 7: Gasoline composition plotted against gasoline yield for the experiments conducted under variation of the reaction temperature (black symbols) and *WHSV* (white symbols) for Pt/HZSM-5. Experiments with Pt/HZSM-5 were performed in a fixed bed reactor according to the parameters listed in Table B1 (*T* variation) and Table B2 (*WHSV* variation) in Appendix B

The fractions can be described with sufficient agreement by straight lines. In the experiments under variation of the *WHSV* (white symbols), the increasing yield of iso-paraffins does not drive the octane numbers as expected (Fig. 6b). We believe that the RC of naphthenes due to elevated reaction temperatures is responsible for the observed increase in the octane numbers, rather than the iso-paraffin yield. As described in materials and methods, we performed additional HP experiments in a batch reactor with a model mixture of aromatics and calculated the RC for the C_7 naphthenes according to Eq. (5) to prove this statement.

$$x_{RC,C7} = \frac{\sum x_{DMCP-isomers} + x_{ECP}}{\sum x_{C_7-Naphthenes}} \tag{5}$$

The RC of MCH is a well-known model reaction in the literature due to the accessible product spectrum [13,43,45,47,65]. During RC of MCH (hydrogenation product of toluene), DMCP isomers and ethylcyclopentane (ECP) are formed. Fig. 8 shows the RC as a function of time (Fig. 8a) and reaction temperature (Fig. 8b) for Pt/HZSM-5 and Pt/Mordenite. No RC was observed for Pt/SAPO-11 in the investigated temperature range.

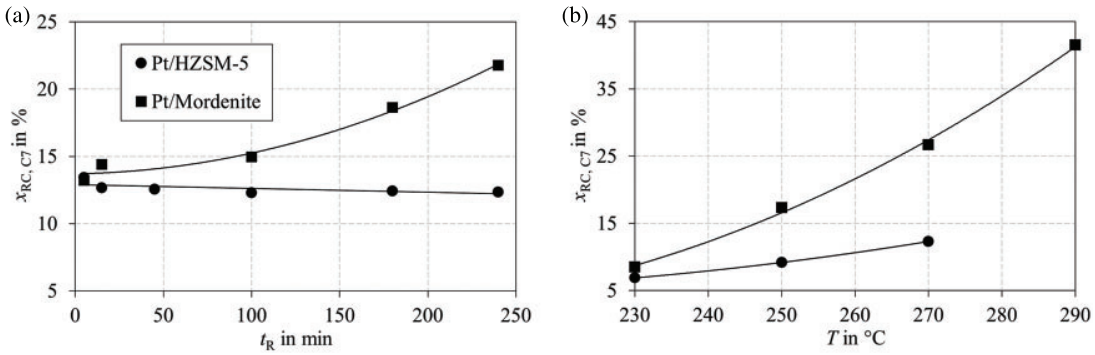


Figure 8: RC of MCH at a pressure of 50 bar for Pt/HZSM-5 and Pt/Mordenite measured in a batch reactor (a) as a function of reaction time at a temperature of 270°C and (b) as a function of temperature for a reaction time of 100 min

It is remarkable how fast the RC products in Fig. 8a for Pt/HZSM-5 reach a steady state, while the RC reaction for Pt/Mordenite still proceeds after four hours. This can be linked to the observations in Fig. 6b, where no clear dependence of *MON* on *WHSV* is seen for Pt/HZSM-5. In Fig. 8b, the temperature influence is shown on the RC. The RC products increase over the reaction temperature for both catalysts, which is especially pronounced for Pt/Mordenite. A dependence on reaction temperature was also described by Belatel et al. [46]. The degree of secondary isomerization of ECP to DMCP was strongly connected to the reaction temperature in their experiments. Overall, we conclude that the RC of naphthenes originating from the primary hydrogenation of aromatics and from exocyclic β-scission is responsible for increased octane numbers.

One main objective of this study is the production of light ends from heavy gasoline. The description of the HP reactions in Fig. 3 is recommended to better understand the following discussions of the cracking mechanisms. Fig. 9 illustrates the boiling characteristics *E70*, *E100*, and *E150* as defined according to DIN EN 228 and the additional value *E180*. The *E150* and *E100* benefit most clearly from cracking. At a gasoline yield of 90% using Pt/HZSM-5, the *E150* increases to almost 40 vol.%. A similarly sharp rise is observed for Pt/Mordenite. However, only two points were measured here. Pt/SAPO-11, on the other hand, shows only a slight cracking activity in the investigated temperature range. Most probably, the sharp increases in *E150* and *E100* are due to fast tertiary-tertiary exocyclic β-scission (paring reaction) of C_{10} naphthenes resulting in the production of C_6 naphthenes and iso-butane. The slightly higher *E100* for Pt/HZSM-5 than for Pt/Mordenite for all measured data points can be attributed to the shape selective influence of the zeolites. The narrower pores of HZSM-5 sterically hindered the paring reaction. This was verified by a high yield of C_5 paraffins in the product spectrum, which were almost not observed with Pt/Mordenite. C_5 paraffins are formed by the slow direct ring opening of C_9 and C_{10} naphthenes, followed by secondary cracking of the resulting paraffins. Direct RO results in a higher gasoline yield because less C_4 is formed. The same applies to the *E70*, which also benefits from an increased C_5 yield. The *E150* also benefits from the slower

tertiary-secondary and tertiary-primary exocyclic β-scission. This was verified by a high yield of C_6–C_8 naphthenes and corresponding ethane and propane in the product stream. The difference between the bioliq® raw gasoline and DIN EN 228 is particularly pronounced in the case of *E70* and is therefore the most crucial parameter. The proportion of light ends with a boiling temperature of up to 70°C is 1.2 vol.%, while the standard requires at least 22 vol.% (see Table 1). This parameter increases slowly for a decreasing gasoline yield and rises sharply at approx. 88 wt.%. The observed is probably due to the slow endocyclic β-scission (ring opening) of C_6 naphthenes previously formed by exocyclic β-scission, producing hexanes. From a process engineering point of view, the range below a mass yield of 90% is excluded because of the high carbon loss due to cracking.

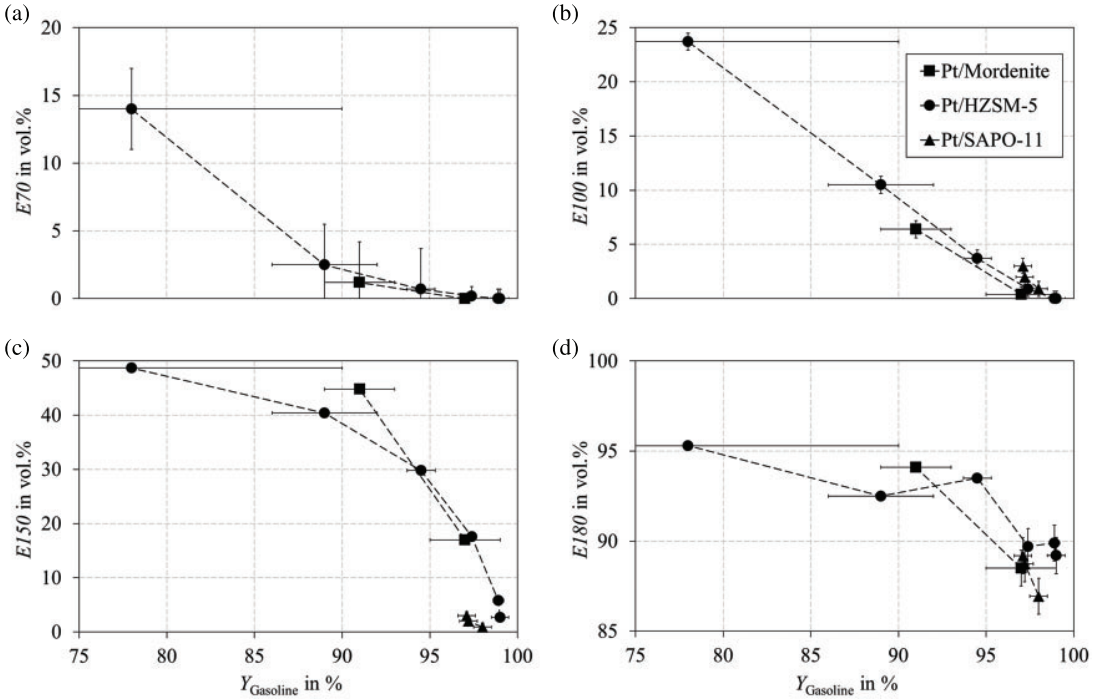


Figure 9: Boiling characteristics (a) *E70*, (b) *E100*, (c) *E150*, and (d) *E180* plotted against the gasoline yield. Experiments performed with Pt/Mordenite, Pt/HZSM-5, and Pt/SAPO-11 in a fixed bed reactor according to the parameters listed in Table B1 in Appendix B under variation of the reaction temperature

Table 1 shows further optimization potential for the density and vapor pressure of the bioliq® raw gasoline, which are too high and too low, respectively. Fig. 10 shows how the density and vapor pressure change with the gasoline yield. An almost linear relationship with gasoline yield can be observed for both parameters. The density decreases and the vapor pressure increases as a result of cracking reactions. Low molecular ring structures and paraffins lead to the observed trends in Fig. 10, which can also be seen in Fig. 7. There is little influence of the catalysts used on both parameters. The observed trends for the boiling characteristics in Fig. 9 can be applied to density and vapor pressure. For Pt/SAPO-11, a slightly higher density and lower vapor pressure result from lower cracking activity.

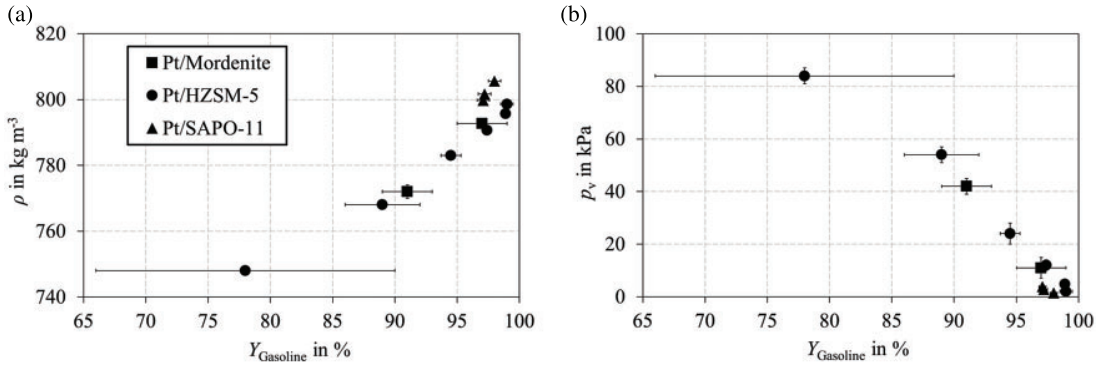


Figure 10: (a) Density and (b) vapor pressure plotted against the gasoline yield. Experiments with Pt/Mordenite, Pt/HZSM-5, and Pt/SAPO-11 were performed in a fixed bed reactor according to the parameters listed in Table B1 in Appendix B under variation of the reaction temperature

4.2 Blending

For a final discussion, we conducted blending experiments with the bioliq® light gasoline and the upgraded heavy gasoline. The heavy gasoline was upgraded in a fixed bed reactor with a capacity of 1 L h^{-1} filled with 0.3 wt.% Pt/HZSM-5 pellets. The product was comparable to the quality obtained in the lab scale experiments discussed above, except that it was rectified to a *FBP* of approx. 170°C. The bioliq® blend consisted of two-thirds light gasoline and one-third upgraded heavy gasoline, as this was the original volume ratio of light to heavy gasoline after separation following the bioliq® DTG synthesis. All relevant data, such as composition, can be found in Appendix C. An image of the final blend at −18°C is shown in Fig. 5c. No crystals formed as a result of durene removal, indicating the gasoline's operability under cold conditions. Fig. 11 shows the bioliq® raw gasoline in comparison with the blend. The most obvious change can be seen for the *FBP*, which results from the applied rectification. The aromatic concentration was relatively reduced by 37.5%, but remained too high compared to DIN EN 228. With the removal of most heavy aromatics and the lower *FBP* in general, a significant decrease in engine-out emissions is expected. The octane numbers of the blend decreased because the ones of the upgraded heavy gasoline were lower than those of the bioliq® light gasoline. However, both remained within the minimum values of the standard. A slight improvement can be seen in the density, which has dropped but still does not reach the limit values of DIN EN 228. The boiling characteristics *E70*, *E100*, and *E150* could be improved. In particular, the *E150* has increased significantly and meets the minimum value specified in the standard. The values for *E70* and *E100* improved slightly. If the density and vapor pressure are also considered, it becomes clear that further low-boiling components are required to meet the standard.

Up to 3.7 wt.% of O_2-equivalent oxygenates are allowed depending on the substance. Ethanol is the most popular species and is limited to 10 vol.%. In contrast, methyl tert-butyl ether and ethyl tert-butyl ether can be blended with gasoline at almost 22 vol.%, with boiling temperatures of 55.2°C and 73°C, respectively. With these considerations, *E70* could reach 22 vol.%, as specified by DIN EN 228. For adjusting the *E100*, an additional blending stream is necessary, since it is almost 36 vol.% below the minimum value of 46 vol.% defined in DIN EN 228. Methanol-to-olefin products or light ends from hydrocracked FT waxes are potentially renewable and available in a future refinery. The latter offers the possibility of co-HP with bioliq® heavy gasoline.

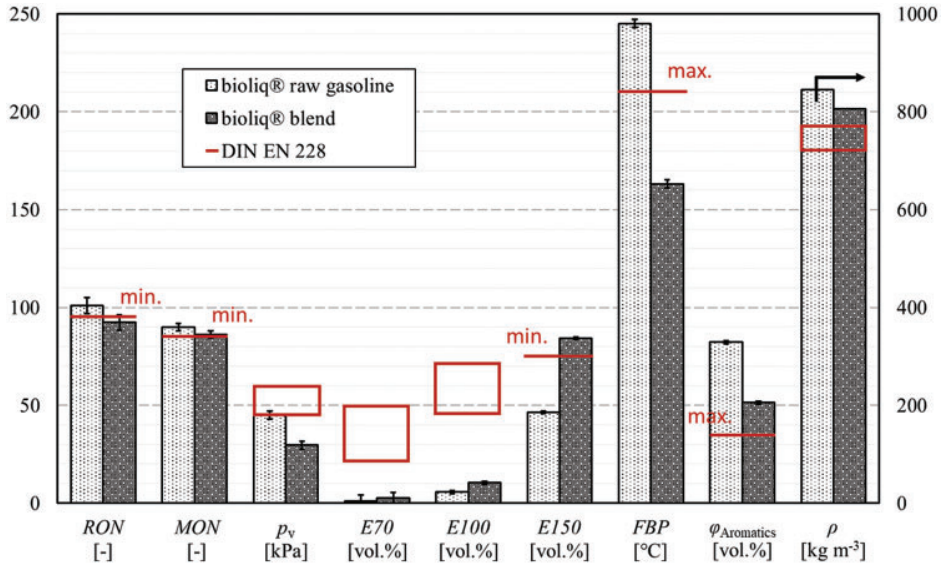


Figure 11: Petrochemical parameters of bioliq® raw gasoline and bioliq® blend in comparison with DIN EN 228

5 Conclusion

In this study, we investigated the single-stage upgrading of aromatic-rich heavy gasoline from the bioliq® process. The heavy gasoline was separated from the light gasoline and hydroprocessed using three different Pt/zeolites. Among the investigated catalysts, Pt/HZSM-5 performed the best for the purpose presented. The achieved octane numbers were the highest, which we concluded was most likely due to selective ring contraction at elevated temperatures. There was almost no difference in the yield of light ends between Pt/HZSM-5 and Pt/Mordenite. Pt/SAPO-11 showed only little cracking activity. In addition to the complete hydrogenation of the aromatic hydrocarbons, light ends with boiling temperatures up to 150°C (*E150*) and 100°C (*E100*) could be increased by approx. 40 vol.% and 10 vol.%, respectively, with a gasoline yield of 90 wt.%. Light ends were produced by fast tertiary-tertiary exocyclic β-scission, forming C_6 naphthenes and iso-butane. Moreover, the slower tertiary-secondary and tertiary-primary exocyclic β-scission, in which C_6–C_8 naphthenes and corresponding ethane and propane are formed, led to a sharp increase in *E150*. Further ring opening resulted in a slight increase in light ends with boiling temperatures up to 70°C (*E70*).

The petrochemical parameters of the bioliq® DTG gasoline were significantly improved by blending the upgraded heavy gasoline with the light gasoline. The *E150* and *FBP* of the bioliq® blend met the DIN EN 228 standard. The aromatic content was 37.5% lower than in bioliq® raw gasoline, which significantly improved the suitability as a drop-in in fossil fuels.

Acknowledgement: This publication is dedicated to the memory of Prof. Dr. rer. nat. Hans Schulz. We thank Dr. Thomas Otto and Doreen Neumann-Walter from the Institute of Catalysis Research and Technology (IKFT) as part of the Karlsruhe Institute of Technology for their strong support in characterizing the fuels. We would especially like to thank Clariant AG for providing the catalysts.

Availability of Data and Materials: All measurement data on which the diagrams presented in this study are based can be found in the Appendix.

Funding Statement: The authors acknowledge the financial support of the Federated State of Baden-Wuerttemberg for the Project reFuels–Rethinking Fuels.

Conflicts of Interest: The authors declare that they have no conflicts of interest to report regarding the present study.

References

1. European Commission (2019). Communication from the Commission of the European Parliament, the European Council, the Council, the European Economic and Social Committee and the Committee of the Regions: The European Green Deal. Brussels.
2. European Commission. Directorate General for Environment (2021). *EU biodiversity strategy for 2030: Bringing nature back into our lives.* Luxembourg: Publications Office of the European Union.
3. Petrowitsch, G., Pribil, A. (2021). Fridays for future demands climate neutral mobility and a complete mobility revolution. In: Liebl, J., Beidl, C., Maus, W. (Eds.), *Internationaler motorenkongress 2021, Proceedings*, pp. 589–595. Wiesbaden: Springer Vieweg.
4. Federal Motor Transport Authority Germany (2021). Annual report: New registrations 2021. https://www.kba.de/DE/Statistik/Fahrzeuge/Neuzulassungen/Jahresbilanz_Neuzulassungen/jahresbilanz_node.html;jsessionid=30A74ED01E115801E2E75BDF2ECAD7B2.live11292.
5. Federal Motor Transport Authority Germany (2022). Annual report: Inventory 2022. https://www.kba.de/DE/Statistik/Fahrzeuge/Bestand/Jahrebilanz_Bestand/fz_b_jahresbilanz_node.html.
6. Speight, J. G. (2020). *The refinery of the future.* Oxford: Gulf Professional Publishing.
7. Olsbye, U., Svelle, S., Bjørgen, M., Beato, P., Janssens, T. V. W. et al. (2012). Conversion of methanol to hydrocarbons: How zeolite cavity and pore size controls product selectivity. *Angewandte Chemie International Edition, 51(24),* 5810–5831. DOI 10.1002/anie.201103657.
8. Tsai, T. C., Liu, S. B., Wang, I. (1999). Disproportionation and transalkylation of alkylbenzenes over zeolite catalysts. *Applied Catalysis A: General, 181(2),* 355–398. DOI 10.1016/S0926-860X(98)00396-2.
9. Yegorov, A. S., Ivanov, V. S., Wozniak, A. I. (2014). International and Russian methods of synthesis and use of pyromellitic acid dianhydride and tendencies of their development (Review). *Biosciences Biotechnology Research Asia, 11(3),* 1765–1779. DOI 10.13005/bbra/1583.
10. Liederman, D., Yurchak, S., Kuo, J. C. W., Lee, W. (1982). Mobil methanol-to-gasoline process. *Journal of Energy, 6(5),* 340–341. DOI 10.2514/3.62614.
11. Chang, C. D. (1983). Hydrocarbons from methanol. *Catalysis Reviews Science and Engineering, 25(1),* 1–118. DOI 10.1080/01614948308078874.
12. Petit, A., Montagne, X. (1993). Effects of the gasoline composition on exhaust emissions of regulated and speciated pollutants. *SAE Technical Papers,* 932681. DOI 10.4271/932681.
13. Do, P. T. M., Crossley, S., Santikunaporn, M., Resasco, D. E. (2007). Catalytic strategies for improving specific fuel properties. *Catalysis, 20,* 33–64. DOI 10.1039/0140-0568.
14. McEnally, C. S., Pfefferle, L. D. (2007). Improved sooting tendency measurements for aromatic hydrocarbons and their implications for naphthalene formation pathways. *Combustion and Flame, 148(4),* 210–222. DOI 10.1016/j.combustflame.2006.11.003.
15. Fraser, M. P., Yue, Z. W., Tropp, R. J., Kohl, S. D., Chow, J. C. (2002). Molecular composition of organic fine particulate matter in Houston, TX. *Atmospheric Environment, 36(38),* 5751–5758. DOI 10.1016/S1352-2310(02)00725-2.

16. Zheng, M., Salmon, L. G., Schauer, J. J., Zeng, L., Kiang, C. S. et al. (2005). Seasonal trends in PM2.5 source contributions in Beijing, China. *Atmospheric Environment, 39(22),* 3967–3976. DOI 10.1016/j.atmosenv.2005.03.036.
17. Lim, S. S., Vos, T., Flaxman, A. D., Danaei, G., Shibuya, K. et al. (2012). A comparative risk assessment of burden of disease and injury attributable to 67 risk factors and risk factor clusters in 21 regions, 1990–2010: A systematic analysis for the global burden of disease study 2010. *The Lancet, 380(9859),* 2224–2260. DOI 10.1016/S0140-6736(12)61766-8.
18. Angelica Hidalgo Vivas, Finn Joensen (2018). *Process and catalyst for upgrading gasoline*. US10150714B2.
19. Calcote, H. F., Manos, D. M. (1983). Effect of molecular structure on incipient soot formation. *Combustion and Flame, 49(1–3),* 289–304. DOI 10.1016/0010-2180(83)90172-4.
20. Nakakita, K., Ban, H., Takasu, S., Hotta, Y., Inagaki, K. et al. (2003). Effect of hydrocarbon molecular structure in diesel fuel on in-cylinder soot formation and exhaust emissions. *SAE International Journal of Fuels and Lubricants, 112,* 1763–1775. DOI 10.4271/2003-01-1914.
21. Schmidt, F., Reichelt, L., Päctzold, C. (2014). Catalysis of Methanol Conversion to Hydrocarbons. In: Bertau, M., Offermanns, H., Plass, L., Schmidt, F., Wernicke, H. J. (Eds.), *Methanol: The basic chemical,* pp. 423–489. Berlin Heidelberg: Springer.
22. Cang, C. D., Silvestri, A. J. (1977). The conversion of methanol and other O-compounds to hydrocarbons over zeolite catalysts. *Journal of Catalysis, 47(2),* 249–259. DOI 10.1016/0021-9517(77)90172-5.
23. Michler, T., Wippermann, N., Toedter, O., Niethammer, B., Otto, T. et al. (2020). Gasoline from the bioliq® process: Production, characterization and performance. *Fuel Processing Technology, 206,* 106476. DOI 10.1016/j.fuproc.2020.106476.
24. Stiefel, M., Ahmad, R., Arnold, U., Döring, M. (2011). Direct synthesis of dimethyl ether from carbon-monoxide-rich synthesis gas: Influence of dehydration catalysts and operating conditions. *Fuel Processing Technology, 92(8),* 1466–1474. DOI 10.1016/j.fuproc.2011.03.007.
25. Ogawa, T., Inoue, N., Shikada, T., Ohno, Y. (2003). Direct dimethyl ether synthesis. *Journal of Natural Gas Chemistry, 12,* 219–227.
26. Mao, D., Xia, J., Chen, Q., Lu, G. (2009). Highly effective conversion of syngas to dimethyl ether over the hybrid catalysts containing high-silica HMCM-22 zeolites. *Catalysis Communications, 10(5),* 620–624. DOI 10.1016/j.catcom.2008.11.003.
27. Rostrup-Nielsen, T., Højlund Nielsen, P. E., Joensen, F., Madsen, J. (2007). Polygeneration–integration of gasoline synthesis and IGCC power production using topsøe's TIGAS process. *Risoe International Energy Conference*, 56–68. Roskilde, Denmark.
28. Haro, P., Trippe, F., Stahl, R., Henrich, E. (2013). Bio-syngas to gasoline and olefins via DME–A comprehensive techno-economic assessment. *Applied Energy, 108,* 54–65. DOI 10.1016/j.apenergy.2013.03.015.
29. Dahmen, N., Dinjus, E., Kolb, T., Arnold, U., Leibold, H. et al. (2012). State of the art of the bioliq® process for synthetic biofuels production. *Environmental Progress & Sustainable Energy, 31(2),* 176–181. DOI 10.1002/ep.10624.
30. Dahmen, N., Abeln, J., Eberhard, M., Kolb, T., Leibold, H. et al. (2017). The bioliq process for producing synthetic transportation fuels. *Wiley Interdisciplinary Reviews: Energy and Environment, 6(3),* e236. DOI 10.1002/wene.236.
31. Pfitzer, C., Dahmen, N., Tröger, N., Weirich, F., Sauer, J. et al. (2016). Fast pyrolysis of wheat straw in the bioliq pilot plant. *Energy & Fuels, 30(10),* 8047–8054. DOI 10.1021/acs.energyfuels.6b01412.
32. Dahmen, N., Henrich, E., Dinjus, E., Weirich, F. (2012). The bioliq® bioslurry gasification process for the production of biosynfuels, organic chemicals, and energy. *Energy, Sustainability and Society, 2(3),* 1–44.
33. Henrich, E., Dahmen, N., Dinjus, E. (2009). Cost estimate for biosynfuel production via biosyncrude gasification. *Biofuels, Bioproducts & Biorefining, 3(1),* 28–41. DOI 10.1002/bbb.126.

34. European Parliament and the Council (1998). Directive 98/70/EC of the european parliament and of the council of 13 October 1998 relating to the quality of petrol and diesel fuels and amending council directive 93/12/EEC.
35. Weitkamp, J. (2012). Catalytic hydrocracking—Mechanisms and versatility of the process. *ChemCatChem, 4(3),* 292–306. DOI 10.1002/cctc.201100315.
36. Valavarasu, G., Bhaskar, M., Balaraman, K. S. (2003). Mild hydrocracking—A review of the process, catalysts, reactions, kinetics, and advantages. *Petroleum Science and Technology, 21(7–8),* 1185–1205. DOI 10.1081/LFT-120017883.
37. Cooper, B. H., Donnis, B. B. L. (1996). Aromatic saturation of distillates: An overview. *Applied Catalysis A: General, 137(2),* 203–223. DOI 10.1016/0926-860X(95)00258-8.
38. van den Berg, J. P., Lucien, J. P., Germaine, G., Thielemans, G. L. B. (1993). Deep desulphurisation and aromatics saturation for automotive gasoil manufacturing. *Fuel Processing Technology, 35(1–2),* 119–136. DOI 10.1016/0378-3820(93)90088-L.
39. Figueras, F., Gomez, R., Primet, M. (1973). Adsorption and catalytic properties of palladium supported by silica, alumina, magnesia, and amorphous and crystalline silica-aluminas. In: Meier, W. M., Uytterhoeven, J. B. (Eds.), *Molecular sieves*, pp. 480–489. Washington: American Chemical Society.
40. Tri, T. M., Massardier, J., Gallezot, P., Imelik, B. (1982). Additives and support effects on Pt catalysts studied by the competitive hydrogenation of benzene and toluene. *Studies in Surface Science and Catalysis, 11,* 141–148. DOI 10.1016/S0167-2991(09)61385-9.
41. Weitkamp, J. (2000). Zeolites and catalysis. *Solid State Ionics, 131(1–2),* 175–188. DOI 10.1016/S0167-2738(00)00632-9.
42. Weisz, P. B. (1980). Molecular shape selective catalysis. *Pure and Applied Chemistry, 52(9),* 2091–2103. DOI 10.1351/pac198052092091.
43. Mignard, S., Caillette, P., Marchal, N. (1993). Hydroconversion of methyl-cyclohexane on a bifunctional catalyst. In: Oballa, M. C., Shih, S. S. (Eds.), *Catalytic hydroprocessing of petroleum and disillates*, pp. 447–458. New York: CRC Press.
44. Figueras, F., Coq, B., Walter, C., Carriat, J. Y. (1997). Hydroconversion of methylcyclohexane on bifunctional sulfated zirconia-supported platinum catalysts. *Journal of Catalysis, 169(1),* 103–113. DOI 10.1006/jcat.1997.1682.
45. Weitkamp, J., Jacobs, P. A., Ernst, S. (1984). Shape selective isomerization and hydrocracking of naphthenes over Pt/Hzsm-5 zeolite. *Studies in Surface Science and Catalysis, 18,* 279–290. DOI 10.1016/S0167-2991(09)61164-2.
46. Belatel, H., Al-Kandari, H., Al-Khorafi, F., Katrib, A., Garin, F. (2004). Catalytic reactions of methyl-cyclohexane (MCH) on partially reduced moO_3. *Applied Catalysis A: General, 275(1–2),* 141–147. DOI 10.1016/j.apcata.2004.07.029.
47. Santikunaporn, M., Alvarez, W. E., Resasco, D. E. (2007). Ring contraction and selective ring opening of naphthenic molecules for octane number improvement. *Applied Catalysis A: General, 325(1),* 175–187. DOI 10.1016/j.apcata.2007.03.029.
48. Martens, G. G., Thybaut, J. W., Marin, G. B. (2001). Single-event rate parameters for the hydrocracking of cycloalkanes on Pt/US-Y zeolites. *Industrial & Engineering Chemistry Research, 40(8),* 1832–1844. DOI 10.1021/ie000799n.
49. Brouwer, D. M., Hogeveen, H. (1970). The importance of orbital orientation as a rate-controlling factor in intramolecular reactions of carbonium ions. *Recueil des Travaux Chimiques des Pays-Bas, 89(2),* 211–224. DOI 10.1002/recl.19700890213.
50. Sullivan, R. F., Egan, C. J., Langlois, G. E., Sieg, R. P. (1961). A new reaction that occurs in the hydrocracking of certain aromatic hydrocarbons. *Journal of the American Chemical Society, 83,* 1156–1160. DOI 10.1021/ja01466a036.

51. Egan, C. J., Langlois, G. E., White, R. J. (1962). Selective hydrocracking of C_9- to C_{12}-alkylcyclohexanes on acidic catalysts. evidence for the paring reaction. *Journal of the American Chemical Society, 84,* 1204–1212. DOI 10.1021/ja00866a028.
52. Santana, R. C., Do, P. T., Santikunaporn, M., Alvarez, W. E., Taylor, J. D. et al. (2006). Evaluation of different reaction strategies for the improvement of cetane number in diesel fuels. *Fuel, 85(5–6),* 643–656. DOI 10.1016/j.fuel.2005.08.028.
53. Rabl, S., Santi, D., Haas, A., Ferrari, M., Calemma, V. et al. (2011). Catalytic ring opening of decalin on Ir- and Pt-containing zeolite Y–influence of the nature of the charge-compensating alkali cations. *Microporous and Mesoporous Materials, 146(1–3),* 190–200. DOI 10.1016/j.micromeso.2011.03.045.
54. Calemma, V., Giardino, R., Ferrari, M. (2010). Upgrading of LCO by partial hydrogenation of aromatics and ring opening of naphthenes over bi-functional catalysts. *Fuel Processing Technology, 91(7),* 770–776. DOI 10.1016/j.fuproc.2010.02.012.
55. McVicker, G., Daage, M., Touvelle, M. S., Hudson, C. W., Klein, D. P. et al. (2002). Selective ring opening of naphthenic molecules. *Journal of Catalysis, 210(1),* 137–148. DOI 10.1006/jcat.2002.3685.
56. Samoila, P., Boutzeloit, M., Especel, C., Epron, F., Marécot, P. (2009). Selective ring-opening of methylcyclopentane on platinum-based bimetallic catalysts. *Applied Catalysis A: General, 369(1–2),* 104–112. DOI 10.1016/j.apcata.2009.09.006.
57. Vicerich, M. A., Benitez, V. M., Especel, C., Epron, F., Pieck, C. L. (2013). Influence of iridium content on the behavior of Pt-ir/Al_2O_3 and Pt-ir/TiO_2 catalysts for selective ring opening of naphthenes. *Applied Catalysis A: General, 453,* 167–174. DOI 10.1016/j.apcata.2012.12.015.
58. ASTM D6730 – 01 (2001). *Standard test method for determination of individual components in spark ignition engine fuels by 100-metre capillary (with precolumn) high-resolution gas chromatography*. West Conshohocken, PA: ASTM International.
59. ISO 5164 (2014). *Petroleum products-determination of knock characteristics of motor fuels-research method*. Geneva: International Organization for Standardization.
60. ISO 5163 (2014). *Petroleum products-determination of knock characteristics of motor and aviation fuels-motor method*. Geneva: International Organization for Standardization.
61. ASTM D86 (2020). *Standard test method for distillation of petroleum products and liquid fuels at atmospheric pressure*. West Conshohocken, PA: ASTM International.
62. ASTM D7345 (2017). *Standard test method for distillation of petroleum products and liquid fuels at atmospheric pressure (micro distillation method)*. West Conshohocken, PA: ASTM International.
63. ASTM D6378 (2020). *Standard test method for determination of vapor pressure (VPX) of petroleum products, hydrocarbons, and hydrocarbon-oxygenate mixtures (triple expansion method)*. West Conshohocken, PA: ASTM International.
64. Ghosh, P., Hickey, K. J., Jaffe, S. B. (2006). Development of a detailed gasoline composition-based octane model. *Industrial & Engineering Chemistry Research, 45(1),* 337–345. DOI 10.1021/ie050811h.
65. McVicker, G. B., Feeley, O. C., Ziemiak, J. J., Vaughan, D. E. W., Strohmaier, K. C. et al. (2005). Methylcyclohexane ring-contraction: A sensitive solid acidity and shape selectivity probe reaction. *The Journal of Physical Chemistry B, 109(6),* 2222–2226. DOI 10.1021/jp040205k.

Appendix A. Feed Composition for the Experiments

Table A1: Composition of the bioliq® heavy gasoline (feed)

C-Nr.	Naph.	iso-Par.	n-Par.	Cycl Ol.	Olef.	Arom.	Total
4	-	0.00	0.00	-	0.00	-	0.00
5	0.00	0.01	0.00	0.00	0.00	-	0.01
6	0.21	0.10	0.02	0.00	0.00	0.01	0.33
7	0.35	0.05	0.00	0.00	0.00	0.09	0.49
8	0.12	0.03	0.00	0.00	0.00	0.26	0.41
9	0.21	0.02	0.02	0.01	0.01	33.76	34.03
10	0.35	0.03	0.08	0.00	0.00	52.00	52.46
11	0.24	0.23	0.13	0.00	0.00	-	0.59
12 +	1.05	0.00	0.00	0.00	0.00	10.41	11.46
Poly	0.22	-	-	0.00	0.00	-	0.22
Total	2.75	0.47	0.25	0.01	0.01	96.52	100.00

Appendix B. Petrochemical Parameters of Hydroprocessed bioliq® Heavy Gasoline with Pt/HZSM-5, Pt/SAPO-11 and Pt/Mordenite

Table B1: Experimental data obtained by hydroprocessing bioliq® heavy gasoline in a fixed bed reactor under variation of the temperature

Parameters	Pt/Mordenite		Pt/HZSM-5						Pt/SAPO-11			
$T_{FB,min}$ in °C	250	270	230	250	270	290	310	330	270	310	330	350
p in bar	90	90	50	50	50	50	50	60	90	90	90	90
$WHSV$ in h^{-1}	1.39	1.39	1.39	1.39	1.39	1.39	1.39	1.39	1.39	0.88	0.88	0.88
$\dot{V}_{H_2,N}/\dot{V}_{educt}$ in–	1667	1667	1667	1667	1667	1667	1667	1667	1058	1667	1667	1667
Measurements												
$T_{FB,min}$ in °C	249.1	268.1	228.6	248.4	269.8	290.2	310.1	329.9	270.1	309.0	328.9	348.7
$T_{FB,max}$ in °C	252.8	273.3	234.3	252.8	276.2	294.7	314.9	336.8	277.9	316.0	335.4	355.1
$Y_{Gasoline}$ in wt.%	96.88	91.19	98.98	98.95	97.39	94.51	88.67	78.18	98.01	97.22	97.15	N/A
RON in–	71.6[a]	71.9[a]	N/A	71.1[a]	N/A	71.5[a]	71.8[a]	72.2[a]	N/A	N/A	N/A	N/A
MON in–	74.3[a]	75.6[a]	77.7[b]	77.3[a]	78.1[b]	78.8[a]	79.6[a]	80.8[a]	76.8[b]	77.2[b]	77.3[b]	77.3[b]
ρ in kg m^{-3}	792.7	772.0	798.6	795.7	790.7	783.0	768.0	748.0	805.6	801.7	799.8	798.4
p_v in kPa	11.0	42.0	2.3	4.8	11.9	24.0	54.0	84.0	1.4	2.8	3.8	3.8
E70 in vol.%	0.0	1.2	0.0	0.0	0.2	0.7	2.5	14.0	0.0	0.0	0.0	0.0
E100 in vol.%	0.4	6.4	0.0	0.0	0.9	3.7	10.5	23.7	0.0	0.0	0.0	0.0
E150 in vol.%	17.0	44.8	2.7	5.8	17.6	29.8	40.0	48.7	0.91	2.0	3.0	4.4
E180 in vol.%	88.5	94.1	89.2	89.9	89.7	93.5	92.5	95.3	86.9	88.7	89.2	89.3
FBP in °C	245.0	215.0	242.0	240.0	240.0	223.3	219.7	208.3	243.0	239.0	241.0	238.0
$w_{Aromatics}$ in wt.%	2.97	1.74	2.47	2.35	2.55	2.44	2.28	2.00	2.52	1.84	1.98	3.15
$w_{C10-Aromatics}$ in wt.%	0.29	0.18	0.16	0.16	0.40	0.35	0.45	0.49	0.31	0.10	0.25	0.92
$w_{iso-Par.}$ in wt.%	1.66	6.64	0.77	1.26	2.79	3.60	6.69	12.06	0.61	0.66	0.80	0.86
$w_{n-Par.}$ in wt.%	0.17	0.62	0.35	0.56	2.44	2.26	3.82	6.67	0.35	0.42	0.48	0.78

(Continued)

Table B1 (continued)

Parameters	Pt/Mordenite			Pt/HZSM-5					Pt/SAPO-11		
$w_{Naphthenes}$ in wt.%	95.17	90.96	96.39	95.84	92.19	91.64	87.16	79.22	96.51	97.08	96.70	95.16
$w_{Olefines}$ in wt.%	0.01	0.01	0.01	0.00	0.05	0.05	0.06	0.07	0	0.01	0.02	0.05

Note: a) Measured with a CFR-test engine b) Measured with FTIR according to own method.

Table B2: Experimental data obtained by hydroprocessing bioliq® heavy gasoline in a fixed bed reactor under variation of WHSV and pressure for Pt/HZSM-5

Parameters	Pt/HZSM-5									
$T_{FB,min}$ in °C	330	330	330	330	330	330	330	330	330	330
p in bar	60	60	60	60	60	70	70	70	70	70
$WHSV$ in h^{-1}	0.84	1.39	1.81	2.23	2.66	0.84	1.39	1.81	2.23	2.66
$\dot{V}_{H_2,N}/\dot{V}_{educt}$ in–	2750	1667	1279	1038	873	2750	1667	1279	1038	873
Measurements										
$T_{FB,min}$ in °C	N/A	N/A	N/A	N/A	N/A	N/A	N/A	N/A	N/A	N/A
$T_{FB,max}$ in °C	N/A	N/A	N/A	N/A	N/A	N/A	N/A	N/A	N/A	N/A
$Y_{Gasoline}$ in wt.%	67.9	65.8	81.8	87.0	88.8	60.1	72.2	74.6	88.4	88.7
RON in–	N/A	N/A	N/A	N/A	N/A	N/A	N/A	N/A	N/A	N/A
MON in–	79.5[a]	80.0[a]	79.1[a]	79.0[a]	78.5[a]	80.0[a]	N/A	N/A	78.6[a]	78.7[a]
ρ in kg m^{-3}	N/A	N/A	N/A	N/A	N/A	N/A	N/A	N/A	N/A	N/A
p_v in kPa	N/A	N/A	N/A	N/A	N/A	N/A	N/A	N/A	N/A	N/A
$E70$ in vol.%	28.4	18.0	11.8	12.9	2.0	23.7	N/A	N/A	7.5	9.8
$E100$ in vol.%	38.0	27.5	21.7	22.1	7.7	33.5	N/A	N/A	14.8	18.6
$E150$ in vol.%	60.3	54.4	47.0	46.4	28.0	56.1	N/A	N/A	40.0	41.7
$E180$ in vol.%	97.3	96.1	94.6	93.0	83.9	96.6	N/A	N/A	92.4	92.3
FBP in °C	191.7	201.8	210.8	214.5	219.4	199.6	N/A	N/A	220.8	217.7
$w_{Aromatics}$ in wt.%	1.33	0.94	1.61	4.70	8.60	1.46	0.95	1.71	3.16	4.43
$w_{C10-Aromatics}$ in wt.%	0.34	0.18	0.63	3.02	6.13	0.33	0.12	0.43	1.56	2.69
$w_{iso-Par.}$ in wt.%	20.62	14.93	11.04	9.07	7.38	19.42	13.57	11.45	8.38	7.77
$w_{n-Par.}$ in wt.%	13.63	10.75	8.72	7.44	6.15	12.58	10.05	8.66	6.68	6.28
$w_{Naphthenes}$ in wt.%	64.39	73.34	78.60	78.73	77.82	66.50	75.41	78.14	81.74	81.47
$w_{Olefines}$ in wt.%	0.04	0.03	0.04	0.05	0.06	0.05	0.04	0.04	0.05	0.05

Note: a) Measured with FTIR according to own method.

Appendix C. Petrochemical Parameters and Composition of the bioliq® Blend

Table C1: Composition of the bioliq® blend

Carbon	Naph.	iso-Par.	n-Par.	Cycl Ol.	Olef.	Arom.	Total
4	-	0.70	0.42	-	0.04	-	1.16

(Continued)

Table C1 (continued)

Carbon	Naph.	iso-Par.	n-Par.	Cycl Ol.	Olef.	Arom.	Total
5	0.11	2.12	1.20	0.00	0.09	-	3.52
6	1.44	3.88	1.28	0.03	0.15	1.15	7.94
7	2.31	1.89	0.15	0.14	0.14	12.00	16.64
8	2.92	1.21	0.08	0.33	0.14	30.93	35.61
9	8.51	0.46	0.05	0.26	0.09	11.18	20.54
10	13.85	0.36	0.02	0.09	0.05	0.02	14.38
11	0.11	0.04	0.00	0.00	0.00	-	0.14
12+	0.06	0.00	0.00	0.00	0.00	-	0.06
Poly	0.00	-	-	0.00	0.00	-	0.00
Total	29.31	10.66	3.21	0.84	0.70	55.29	100.00

Table C2: Petrochemical parameters of the bioliq® blend

Parameter	*RON*	*MON*	ρ	p_v	*E70*	*E100*	*E150*	*FBP*	$\varphi_{\text{Aromatics}}$
Unit	-	-	kg m^{-3}	kPa	vol.%	vol.%	vol.%	°C	vol.%
Value	92.4	86.2	806.22	29.7	2.5	10.4	84.4	163.2	51.4

fuels

MDPI

Article

Standard-Compliant Gasoline by Upgrading a DTG-Based Fuel through Hydroprocessing the Heavy-Ends and Blending of Oxygenates

David Graf, Philipp Neuner and Reinhard Rauch *

Division of Fuel Technology (EBI-ceb), Engler-Bunte-Institute, Karlsruhe Institute of Technology (KIT), Engler-Bunte-Ring 1a, 76131 Karlsruhe, Germany
* Correspondence: reinhard.rauch@kit.edu

Abstract: Methanol-to-gasoline (MTG) and dimethyl ether-to-gasoline (DTG) fuels are rich in heavy aromatics such as 1,2,4,5-tetramethylbenzene, resulting in low volatilities due to a lack of light ends, increased emission tendencies and drivability problems due to crystallization. Approaches addressing these issues mainly focus on single aspects or are optimized for petroleum-based feedstocks. This research article introduces an upgrading strategy for MTG and DTG fuels through hydroprocessing (HP) heavy-ends and applying a sophisticated blending concept. Different product qualities were prepared by HP heavy gasoline (HG) and Fischer-Tropsch wax using commercially available Pt/HZSM-5 and Pt/SAPO-11 catalysts in a fixed-bed reactor. The products were used for blending experiments, focusing on gasoline volatility characteristics. Accordingly, methanol, ethanol, methyl tert-butyl ether (MTBE), and ethyl tert-butyl ether (ETBE) were evaluated in a second blending experiment. The results were finally considered for preparing blends meeting EN 228. HP of HG was found to improve the amount of light-ends and the vapor pressure of the DTG fuel with increasing reaction temperature without, however, satisfying EN 228. The front-end volatility was further improved by blending methanol due to the formation of near-azeotropic mixtures, while ethyl tert-butyl ether (ETBE) considerably supported the mid-range volatility. A final blend with an alcohol content of less than 3 vol.%, mostly meeting EN 228, could be provided, making it suitable even for older vehicles.

Keywords: bioliq; blending; green refinery; hydroprocessing; synthetic gasoline; upgrading

check for updates

Citation: Graf, D.; Neuner, P.; Rauch, R. Standard-Compliant Gasoline by Upgrading a DTG-Based Fuel through Hydroprocessing the Heavy-Ends and Blending of Oxygenates. *Fuels* **2023**, *4*, 156–173. https://doi.org/10.3390/fuels4020010

Academic Editor: Olivier Mathieu

Received: 27 January 2023
Revised: 5 March 2023
Accepted: 24 March 2023
Published: 12 April 2023

Copyright: © 2023 by the authors. Licensee MDPI, Basel, Switzerland. This article is an open access article distributed under the terms and conditions of the Creative Commons Attribution (CC BY) license (https://creativecommons.org/licenses/by/4.0/).

1. Introduction

The global climate crisis and its increasingly reported repercussions have caused a rethinking regarding the urgency of transforming the economy and society toward increasing sustainability. With the Green Deal, the European Union (EU) set the framework for complete greenhouse gas (GHG) neutrality by 2050 by focusing on the sustainable use of raw materials while preserving biodiversity [1]. In 2021, the European Commission presented the "Fit for 55" action plan to reduce the EU's GHG emissions by at least 55% until 2030 compared to 1990 [2]. This legislative overhaul recommends a broad package of measures for the traffic and transportation sectors. One major proposal is to cut the carbon emissions of newly registered cars by 100% until 2035 compared to 2021. In June 2022, the European member states' environmental ministers supported to ban the sale of CO_2-emitting cars and light-duty vehicles by 2035 [3], which was later approved by the EU [4]. A ban, however, is not tantamount to the sudden disappearance of vehicles relying on hydrocarbon fuels. The EU might work out rules for using vehicles powered with carbon-neutral fuels [3,5].

While the role of synthetic fuels compared with technologies such as electrification is controversial, their contribution as a bridging technology is essential to reach the ambitious climate targets set by the EU. Registration rates of new cars with alternative drive technologies are still modest nowadays. In 2021, Europe and China, as the fasted growing

markets for electromobility, counted 17% and 16%, respectively, for sales of electric and plug-in-hybrid vehicles [6]. Additionally, the medium age of a car is about twelve years on European roads [7]. Consequently, the number of vehicles relying on hydrocarbon fuels will gradually reduce over the coming decades. A more extended period can be expected internationally. Volkswagen, for instance, announced to stop selling internal combustion engines by 2035 in Europe, somewhat later, however, in countries such as the United States or China [8]. An even more distinct situation is emerging in sectors that are not easily electrified, i.e., aviation and maritime transport. Long-distance transport requires energy carriers with high energy densities, unrivaled provided by liquid hydrocarbons. Altogether, this leaves the necessity for developing supply concepts for renewable synthetic fuels that meet the applicable standards.

To date, the highest renewable share in the fuel market is covered by blending biogenic ethanol [9]. However, the share of bio-ethanol in gasoline can only be increased with limitations. Ethanol can lead to corrosion problems of engine parts [10,11], for example, the fuel injection delivery system [12]. Furthermore, blending rates of alcohol might result in the swelling or stiffening of polymeric materials, as used for O-rings and hoses [10,11]. Therefore, vehicles must be suitable for blends with high shares of ethanol or must be modified. The mentioned issues limit the potential impact of alcohol–gasoline blends, as a large share of the fleet is left out due to incompatibility. Besides blending single oxygenates, there is the approach to replace fossil gasoline with a renewable gasoline-like synthetic hydrocarbon mix. The clear advantage is that a vehicle's engine does not need to be modified, as synthetic fuels are chemically similar and meet the required standard. Therefore, such an approach provides a solution for all systems relying on fossil gasoline. Processes for the synthesis of hydrocarbons in the boiling range of gasoline are the Fischer–Tropsch (FT) synthesis, the methanol-to-gasoline (MTG) synthesis, and the further developed dimethyl ether (DME)-to-gasoline (DTG) synthesis. Porsche, Siemens Energy, and Exxon Mobil, for example, invested in an MTG plant in Punta Arenas, Chile commissioned in December 2022 [13]. During the pilot phase, the plant is expected to produce 130,000 liters per year, which shall be scaled up to 550 mil liters per year within the last years of this decade.

These processes, however, do not directly produce standard-compliant gasoline and consequently require an after-treatment and sophisticated blending concept. This paper presents an after-treatment and blending route based on a DTG process to provide gasoline with a high renewable share, which can replace fossil gasoline without constraints. We first discuss the requirements of EN 228 and highlight the challenges to meeting the standard. In this regard, we show that hydroprocessing (HP) can help to convert heavy-ends into low-boiling blending components. We further discuss ways in which a deliberated combination of oxygenates plays a major role in adjusting the boiling characteristics. Finally, we present and discuss a blend and its petrochemical parameters, which can be easily implemented based on an MTG or DTG synthesis and a regular blending infrastructure.

1.1. Requirements for Synthetic Gasoline to Meet EN 228

The use of fuels in internal combustion engines is linked to compliance with standards such as EN 228 for gasoline in Europe [14]. Fossil and renewable fuels are subject to the same regulations. In recent years, the government released directives to increase the renewable share of gasoline. An increase in renewables is, for example, notable by an increased oxygen content of up to 3.7 wt.% of O_2-equivalent in EN 228. Ethanol is the most common blended oxygenate in gasoline, as it is accessible via biological fermentation using sugar-containing feedstocks [15,16]. Further oxygenates such as ethers possessing five or more carbon atoms and higher alcohols are also permitted. Certain concentration limits apply to the various oxygenates, but these must not exceed the 3.7 wt.% O_2-equivalent already mentioned. Additional discussions on the pros and cons of oxygenates are offered in the following chapters. Besides an increased renewable share, oxygenates are blended due to their high octane numbers (ONs) [17]. The ON is essential because it is directly linked

to a gasoline's market price [18] and is crucial for the engine's performance and efficiency. With the ON, the propensity of the fuel to resist auto-ignition when the fuel/air mixture is compressed within a spark ignition engine is expressed [19]. A higher ON allows for an increased compression ratio, hence a higher thermal efficiency [20]. Several definitions for the ON exist, of which the research octane number (RON) and motor octane number (MON) are applied within EN 228. The RON represents a drive under mild conditions, whereby the MON is measured under severe conditions, as it is to expect, for example, on a climb with a high load and increased engine speed [21,22]. Besides oxygenates, aromatics are used to adjust the ON [9]. However, aromatics tend to increase engine-out hydrocarbons [23,24] and to form soot [25], wherefore their concentration is limited to 35 vol.% in EN 228. Besides RON and MON, the volatility of gasoline is of particular importance. In EN 228, the volatility is provided in terms of the boiling curve and vapor pressure. The boiling curve is defined by the evaporation characteristics E70, E100, and E150, representing the volume fractions evaporated at 70 °C, 100 °C, and 150 °C, respectively, and the final boiling point (FBP). As high ambient temperatures result in environmental issues due to the evaporation of highly volatile substances, which contribute to atmospheric pollution [26], the E70 has to stay within a certain range, which varies slightly depending on the time of the year. The front-end volatility is further important to ensure good cold-starting [18,27,28] and to assess the potential vapor lock under hot weather conditions [27]. The mid-range volatility (E100) is related to the cold weather performance and a hot engine's operational readiness and acceleration behavior under load [27]. The end-point volatility (E150 and FBP) is important to ensure a good fuel economy after engine warm-up, minimum engine deposits, fuel dilution of oil, and emissions of volatile organic hydrocarbons [27,28]. Automotive manufacturers usually demand fuels whose FBP is below the maximum value of 210 °C defined in EN 228, as large molecules tend to form soot [29]. The vapor pressure p_v is closely connected to the boiling curve and regulated in EN 228. As roughly proportional to the losses by evaporation, a high vapor pressure contributes to pollution [30], while a low one negatively influences cold start conditions [31]. It is also reasonable that low vapor pressures contribute to increased particle emissions due to diffusion combustion, as it bears an additional risk of condensation in the combustion chamber [32]. Consequently, the vapor pressure has to stay within a certain range depending on the time of the year. Finally, the gasoline density ρ must comply with EN 228, which is usually the case if the other parameters meet EN 228.

1.2. Synthesis Gas-Based Renewable Gasoline Supply and Associated Challenges

Well-investigated processes for the supply of synthetic gasoline are the FT, MTG, and DTG synthesis. These processes are based on syngas, which can be provided on a biomass basis by gasification or using renewable electric energy.

1.2.1. Fischer–Tropsch

FT was developed in the 1920s and is a synthesis route based on Co or Fe catalysts for producing linear paraffins, olefins, and oxygenates from syngas via a polymerization reaction [33]. The high-temperature FT is best suited for producing liquid hydrocarbons in the gasoline boiling range. It was successfully demonstrated in 1989 and commercialized under the Sasol Advanced Synthol (SAS) process [34,35]. With a carbon selectivity of 48%, the process produces gasoline and diesel in a ratio of 3:1, both rich in olefins [35]. However, further downstream processing is inevitable to increase the ON due to the low degree of olefin branching and low aromatic content [36].

FT in its low-temperature variant (LTFT) is applied to synthesize high-quality diesel [37]. LTFT is furthermore discussed for producing kerosene from syngas [38]. The German Federal Ministry for the Environment, Nature Conservation, Nuclear Safety and Consumer Protection (BMUV) aims with its power-to-liquid (PTL) roadmap for a ramp-up to at least 200,000 t a^{-1} of PTL kerosene by 2030 [39], underlining the perspective of processes like LTFT. Besides diesel and kerosene, LTFT yields a certain amount of waxes due to

the underlying chain growth mechanism [40]. Downstream hydrocracking of waxes is usually considered to increase kerosene yields and obtain valuable iso-paraffins that meet the freezing point requirements for Jet A-1 [38]. Hydrocracking of waxes also yields iso-paraffins in the gasoline boiling range, which show similar properties to fossil isomerate (see also Section 2).

This study discusses the ways in which gasoline from hydrocracking of waxes can be used as a valuable isomerate replacement.

1.2.2. Methanol and Dimethyl Ether to Gasoline

In the 1970s, Chang and Silvestri (MobilOil) discovered a synthesis route of high-octane gasoline from methanol using a zeolite catalyst [41]. A complex reaction network of aromatics methylation and subsequent cracking yields paraffins, naphthenes, olefins, and mono-ring aromatics [42]. The product spectrum strongly depends on the zeolite topology and aromatic species trapped therein [43]. MTG and DTG processes are usually catalyzed using an HZSM-5 zeolite as it produces hydrocarbons in the desired boiling range and possesses superior stability against coking [42]. The first commercial MTG plant was commissioned in New Zealand by Mobil in 1985, which supplied approx. 33% of the country's gasoline needs [44]. Other plants were brought into operation, e.g., in Shanxi, China in 2009 [42].

Haldor Topsøe was the first company to demonstrate the feasibility of direct DME synthesis as part of a 1 t d^{-1} plant for the production of synthetic gasoline [45]. DTG combines methanol synthesis and subsequent DME formation in one reactor. The integrated synthesis increases process efficiency and lowers investment costs, as no methanol isolation is required [42]. Since then, much effort has been made in further developing the DTG synthesis. The bioliq® demonstration plant was commissioned in 2014 [46,47]. A decentralized biomass fast pyrolysis is used to increase the energy density of the feedstock significantly [48,49]. The so-called biosyncrude® is then transported and fed to a centralized entrained flow gasifier where syngas free of tar is produced [50]. After several gas conditioning steps, the syngas is fed to a direct DME synthesis [51,52], followed by a DTG reactor [53].

This study shows that DTG synthesis such as the bioliq® process can be used to supply high-quality gasoline and highlights remaining challenges with potential solutions. It is important to note that MTG and DTG provide similar gasoline compositions [54]. Therefore, considerations made within this work apply to both process variants.

1.2.3. Suitability of MTG and DTG for Providing Drop-In and Stand-Alone Fuels

Recently, the suitability of synthetic DTG fuel as a drop-in was demonstrated. Michler et al. could successfully blend 10 vol.% of bioliq® gasoline into conventional E95 [55]. However, in their experiments, the aromatic concentration reached 33 vol.% with a relatively low drop-in rate. The high aromatic content resulted in limited direct applicability, as the blend must meet a maximum concentration of 35 vol.% according to EN 228 [14]. Additionally, the fuel had to be separated into light gasoline (LG) and heavy gasoline (HG) to get rid of 1,2,4,5-tetramethylbenzene (durene) as part of the HG. Durene is the largest aromatic hydrocarbon emerging in significant quantities due to the underlying mechanism in the methanol-to-hydrocarbon reaction [56]. Due to its symmetry, it has a high melting temperature of 79 °C and tends to crystallize, which can clog fuel injection systems or cause drivability problems [42]. Michler et al. only used the LG for their blending experiments. As a result, valuable bio-based hydrocarbons are left out, which directly affects the economics of the underlying process. In the conducted engine tests, the blend showed significantly increased particle emissions compared to the pure E95 since high molecular aromatics in general form soot [57,58]. Therefore, a sophisticated after-treatment is necessary, which allows the use of the entire product but also reduces the aromatic content. Mobil also recognized this problem originating from the heavy aromatics and decided to split the product into LG and HG for their fixed bed MTG process in New Zealand and the pilot-

scale fluidized bed version [59]. The HG was forwarded to a treatment reactor where the durene concentration could be lowered below 2 wt.% and was subsequently blended back into the LG. The HG treatment was developed to improve issues resulting from durene but neglected emission issues related to heavy aromatics. In an earlier study, we converted HG from the bioliq® process into highly isomerized paraffins and naphthenes by HP using a 0.3 wt.% Pt/HZSM-5 catalyst and conducted blending experiments [60]. The combination of noble metals with zeolites gained much attention for processing biomass(-derivatives) due to superior shape selectivity coupled with an increased hydrogenation activity [61]. As a result, the aromatic concentration could be significantly lowered while simultaneously improving petrochemical parameters. The suitability as drop-in fuel was greatly improved, but a stand-alone DTG fuel could not be achieved. Especially the E70 and E100 were significantly too low and needed to be addressed further.

In the present study, we highlight HP from a blending perspective, as the process was already discussed previously [60]. We produced three fuel qualities and investigated their influence on gasoline volatility in blending experiments.

1.3. The Potential of Oxygenates in Blending and Associated Challenges

Oxygenates are interesting blending components as they possess superior ONs and high renewable shares. Table 1 shows petrochemical parameters and properties of oxygenates permitted within EN 228 [20,62–65]. Methanol, ethanol, methyl tert-butyl ether (MTBE), and ethyl tert-butyl ether (ETBE) are considered in this study due to their low boiling temperatures of well below 100 °C.

Table 1. Properties of oxygenates in comparison to fossil oxygenate-free gasoline [20,62–65].

	Methanol	Ethanol	MTBE	ETBE	Gasoline
RON [-]	122	111	118	118	≥95
MON [-]	93	96	101	102	≥85
T_b [°C]	64.6	78.4	55.2	73.0	≤210
HoV [kJ kg^{-1}]	1170	921	338	290	≈335–350
O_2-content [wt.%]	49.9	34.7	18.2	15.7	none
Renewable share [wt.%]	100	100	35.21	44.10	0

Ethanol is mainly produced by fermentation and thus comes with a renewable share of 100% [15]. The methanol synthesis is a well-established syngas-based process, which can be sustainably operated by using biomass or renewable electrical energy [66]. MTBE and ETBE are produced based on methanol and ethanol, respectively. To the authors' best knowledge, there is no process commissioned for the renewable synthesis of iso-butene yet, which is also required for the synthesis. Therefore, MTBE and ETBE have a renewable share of 35.1 wt.% and 44.1 wt.%, respectively, the one of ETBE being higher as the molecular contribution of ethanol is higher compared to the one of methanol.

Oxygenates in general reduce emissions of incomplete combustion, i.e., CO and hydrocarbons, by the so-called "leaning effect", which means a replacement of high-sooting hydrocarbons by less-sooting oxygenates [67]. Oxygenates can further help to reduce soot formation, which is one main reason for reduced life expectancy worldwide [68]. However, the physical properties of oxygenates also bear a risk of increased soot formation. Table 1 shows the heat of vaporization (HoV) for the prior discussed oxygenates. Small alcohols such as methanol and ethanol possess high HoVs compared to MTBE and ETBE, which have HoVs in the gasoline range. When the fuel/air mixture is loaded into the combustion chamber and evaporates, a high HoV results in the charge-cooling effect [69]. Charge-cooling improves knocking resistance as the fuel/air mixture's temperature is reduced, which is, in general, positive [70]. However, charge-cooling might lead to disadvantages for existing engines, e.g., increased emissions for aromatic-rich fuels [63,71]. Oxygenates with high HoVs delay the evaporation of the fuel, which might result in the impingement of the spray with the cylinder walls or the piston top, resulting in fuel-rich combustion [69]

and, consequently, the formation of particulate matter [72]. Additionally, alcohols are associated with an increased vapor pressure and depression of the front end of the boiling curve due to the formation of positive azeotropic mixtures with hydrocarbons [65]. A high vapor pressure leads to increased evaporative emissions and a request after more expensive high-boiling blending fractions such as reformate in place of cheaper ones such as butane [18]. Due to their carbon-rich structure, ethers do not form azeotropic mixtures with hydrocarbons and therefore blend similarly to hydrocarbons [73]. MTBE and ETBE have boiling temperatures below 100 °C, hence are known to alter the mid-section of a gasoline's boiling curve [65]. As shown in Table 1, MTBE and ETBE can be blended in higher ratios than methanol, and ethanol until EN 228's limit of 3.7 wt.% is reached due to their lower oxygen content. While methanol and ethanol have a molecular oxygen content of 49.9 wt.% and 34.7 wt.%, MTBE and ETBE only come with 18.2 wt.% and 15.7 wt.%, respectively.

The present study examines the extent to which the mentioned oxygenates can improve the volatility of a DTG fuel to meet EN 228. Careful balancing must be observed in the case of alcohols, as a high blending rate carries the risk of emission issues and may limit applicability in older vehicles. However, a certain azeotropic effect might be beneficial as the considered DTG base fuel is of heavy nature and fossil butane as a volatility booster shall not be considered.

2. Materials and Methods

Table 2 lists the petrochemical parameters of bioliq® LG and hydrocarbon fractions originating from the HP of bioliq® HG (HG-HP) and FT wax (FT-HP), as used for the blending experiments in this study.

Table 2. Petrochemical parameters of hydrocarbon streams used for the blending experiments.

Parameter	EN 228 [14]	bioliq® LG	bioliq® HG-HP @ 270 °C	bioliq® HG-HP @ 310 °C	bioliq® HG-HP @ 330 °C	FT-HP
RON [-]	≥95	102.0 ± 2.7	76.9 ± 2.7	75.9 ± 2.7	77.0 ± 2.7	79.9 ± 2.7
MON [-]	≥85	91.2 ± 1.0	79.6 ± 1.0	77.4 ± 1.0	77.0 ± 1.0	73.9 ± 1.0
ρ [1] @ 15 °C [kg m^{-3}]	720–775	835.02 ± 0.05	n.A.	n.A.	n.A.	n.A.
ρ [1] @ 20 °C [kg m^{-3}]	-	829.30 ± 0.05	782.78 ± 0.05	753.86 ± 0.05	731.20 ± 0.05	673.03 ± 0.05
p_v [1] (Class A) [kPa]	45–60	23.0 ± 2.0	10.0 ± 2.0	36.0 ± 2.0	41.0 ± 2.0	n.A.
E70 [1] (Class A) [vol.%]	22–50	1.1 ± 0.9	0.0	5.5 ± 0.9	14.7 ± 0.9	35.1 ± 0.9
E100 [1] (Class A) [vol.%]	46–72	8.0 ± 0.8	1.2 ± 0.8	20.1 ± 0.8	37.6 ± 0.8	67.9 ± 0.8
E150 [1] (Class A) [vol.%]	75	90.7 ± 0.6	39.5 ± 0.6	66.0 ± 0.6	81.7 ± 0.6	96.4 ± 0.6
FBP [1] [°C]	≤210	163.0 ± 2.0	163.0 ± 2.0	163.0 ± 2.0	163.0 ± 2.0	168.0 ± 2.0
$\varphi_{Benzene}$ [1] [vol.%]	≤1	1.4 ± 0.7	0.0	0.2 ± 0.7	0.0	0.0
$\varphi_{Olefins}$ [1] [vol.%]	≤18	2.3 ± 0.1	0.1 ± 0.1	0.0	0.0	0.0
$\varphi_{Naphthenes}$ [1] [vol.%]	-	5.5 ± 0.1	96.2 ± 0.1	79.6 ± 0.1	67.0 ± 0.1	4.5 ± 0.1
$\varphi_{Paraffins}$ [1] [vol.%]	-	15.3 ± 0.6	3.2 ± 0.6	18.8 ± 0.6	32.5 ± 0.6	95.5 ± 0.6
$\varphi_{Aromatics}$ [1] [vol.%]	≤35	76.9 ± 0.7	0.5 ± 0.7	1.6 ± 0.7	0.4 ± 0.7	0.1 ± 0.7

[1] Measurement errors estimated using a representative sample.

The compositions of all samples were measured with a Reformulyzer M4 from AC PAC (Houston, TX, USA) and can be found in the Supplementary Materials in Tables S1–S5. Figure 1 shows the boiling curves, measured according to ASTM D7345 [74] using an OptiPMD from PAC. Each boiling curve is measured with a resolution of 1 vol.% and depicted as a solid line for clearness reasons. The boiling curve is further used to calculate the boiling characteristics E70, E100, and E150.

For the reasons discussed in the Introduction, bioliq® raw gasoline was rectified, yielding LG and HG (for composition, see Tables S1 and S6 in the Supplementary Materials) in a ratio of 2:1. The LG, with an FBP of 163.0 °C, is free of C_{10} aromatics such as durene. Due to its high C_7 and C_8 aromatic content (16.0 vol.% toluene, 43.1 vol.% C_8 aromatics, 16.3 vol.% C_9 aromatics) resulting in a high ON, the LG is considered a valuable blending component. It has to be mentioned that the gasoline slightly differs from the one used for our last publication [60] due to variations in the bioliq® synthesis and rectification. However, the challenges remain the same. Significant derivations of 20.9 vol.% and 38.0 vol.% compared to EN 228 can be seen for E70 and E100, respectively. Thus, bioliq® LG lacks a significant amount of light boiling components with temperatures up to 100 °C. The

heavy nature of the bioliq® LG is also reflected in the relatively flat boiling curve shown in Figure 1. Following the procedure described in our earlier study [60], the bioliq® HG was hydroprocessed at 270 °C, 310 °C and 330 °C using a 0.3 wt.% Pt/HZSM-5 catalyst in a fixed bed reactor. The final blending components were obtained by rectification to an FBP slightly above 160 °C. Depending on the reaction temperature, the HP experiments were either conducted under hydrogenation or hydrocracking conditions yielding streams rich in naphthenes and paraffins. In Table 2, it can be seen that E70, E100, and E150 increase significantly from 0 vol.% to 14.7 vol.%, 1.2 vol.% to 37.6 vol.% and 39.5 vol.% to 81.7 vol.%, respectively, for the process temperature increased from 270 °C to 330 °C. In Figure 1, the improvement of the boiling characteristics also can be seen as the front end of the boiling curve is further depressed as the reaction temperature increases.

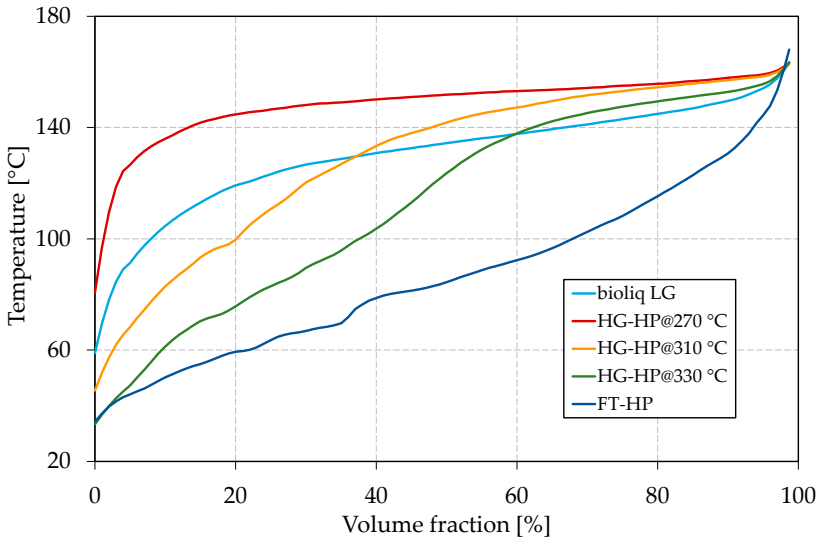


Figure 1. Boiling curves of bioliq® light gasoline (LG), hydroprocessed (HP) heavy gasoline (HG) for different processing temperatures and hydroprocessed Fischer–Tropsch (FT) wax.

For an HP temperature of 270 °C, the boiling curve lies above the one of bioliq® LG because the reaction was carried out in the hydrogenation regime where cracking reactions were strongly suppressed. Therefore, the product is rich in heavy C_9 and C_{10} naphthenes, having boiling temperatures of approx. 140–155 °C.

RON and MON were determined using an OptiFuel from PAC. The device's method was extended by training the underlying model with a data set obtained from a frequently inspected Cooperative Fuel Research (CFR) test engine at PetroLab in Speyer, Germany. RON and MON could be predicted using a held-back validation data set with an accuracy of ±2.7 and ±1.0, respectively. Interestingly, the MONs are higher than the RONs for HG hydroprocessed at 270 °C and 310 °C, and both are equal for an HP temperature of 330 °C. Comparably high MONs are detected due to the high content of naphthenes, which was already reported in our previous work [60]. The difference between MON and RON decreases for higher reaction temperatures as the paraffin content increases due to intensified cracking reactions. The comparably high MONs are of interest as blending could result in gasoline having a lower octane sensitivity (difference of RON and MON), which provides higher reliability under different driving conditions [73].

The FT gasoline was produced by HP of wax, as described in our early publication [75]. Neuner et al. studied the production of high-quality pharmaceutical oils from low-valuable FT wax using a 0.3 wt.% Pt/SAPO-11 catalyst. Besides the desired oil, 10–20 wt.% of highly isomerized paraffinic gasoline was produced. As no laboratory FT synthesis in the required scale was available, wax from SASOL (Sandton, South Africa) was used for simulating a potentially GHG-neutral FT wax. The FT gasoline was rectified to an FBP of approx. 168 °C. Due to its high paraffinic content and high content of light-ends, it can be most

likely compared to fossil isomerate [65,73]. The main difference is a comparably lower ON and a higher FBP of the FT gasoline.

In addition to the mentioned hydrocarbon streams, methanol (≥99.5%, VWR chemicals, Radnor, PA, USA), ethanol (99.95%, VWR chemicals), MTBE (≥99.0%, Merck, Darmstadt, Germany), and ETBE (77.7 vol.%, Mineralölraffinerie Oberrhein, Karlsruhe, Germany) were used for the blending experiments. ETBE was provided by Mineralölraffinerie Oberrhein, Germany from an industrial scale plant in operation, therefore having approx. 22 vol.% by-products, mainly iso-butene (10.5 vol.%) and pentane (6.5 vol.%).

An HVP 972 from Herzog PAC (Houston, TX, USA) was used for measuring the vapor pressure at 37.8 °C according to ASTM D6378 [76]. The density was measured with a density meter Excellent D5 from Mettler Toledo (Columbus, OH, USA) using a self-developed method.

For the blending experiments, the share of each compound or fraction was calculated on a volume basis, as most of the petrochemical parameters listed in EN 228 are given as volume fractions. However, due to the higher precision of weighting, we measured the density of each fraction or substance at 20 °C and calculated the mass required for a given volume.

All measurements were repeated whenever possible and were statistically evaluated according to the student's t-distribution, assuming a 95% confidential interval.

3. Results and Discussion

As mentioned, we distilled the bioliq® raw gasoline and hydroprocessed the HG according to our previous study [60] at different reaction temperatures. In the following, we discuss the ways in which HP can help to improve the blending volatility characteristics, especially E70 and E100. We also investigate the ways in which oxygenates might help to further improve the boiling characteristics. Finally, we examine if a blend with a high renewable share while meeting the petrochemical parameters of EN 228 can be provided.

3.1. Influence of Hydroprocessing on Boiling Characteristics and Vapor Pressure

The hydroprocessed HG's petrochemical parameters are greatly dependent on the reaction temperature; thus, three qualities were produced in this study. Figure 2 shows the obtained results for the E70, E100, and vapor pressure for the blending experiments by continuously increasing the blending rate of HG-HP into bioliq® LG.

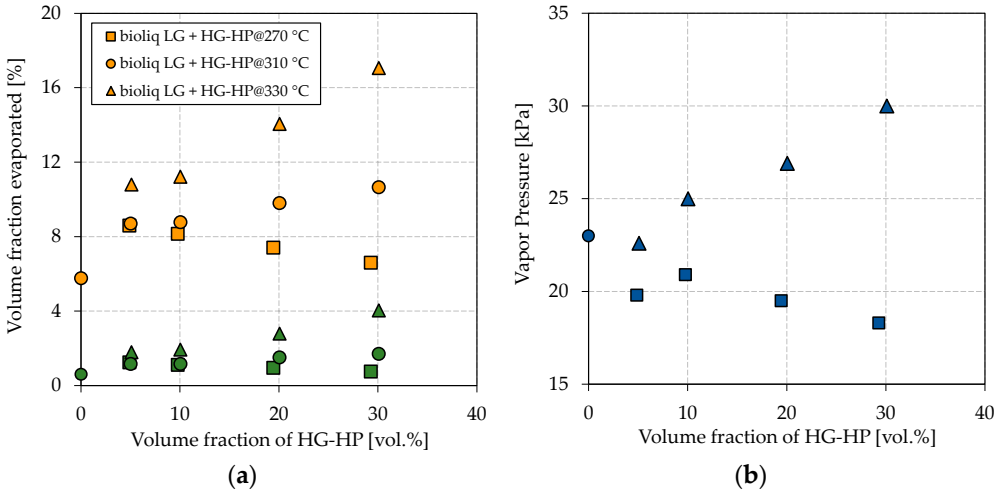


Figure 2. Influence of blending HG-HP@270 °C (squares), HG-HP@310 °C (circles) and HG-HP@330 °C (triangles) into bioliq® LG on (**a**) the volatility characteristics E70 (green), E100 (orange) and (**b**) the vapor pressure.

Figure 2a shows a directly proportional dependency of the E70 and E100 on the blending rate of the respective HG-HP fractions. This dependency can be attributed to

the similar nature of bioliq® LG and HG-HP, consisting exclusively of hydrocarbons. A more substantial increase in E70 and E100 can be seen for HG-HP@330 °C than for HG-HP@310 °C as that fraction contains more light-ends in the respective boiling ranges. The same applies to HG-HP@270 °C, for which E70 and E100 decrease with the blending rate. For an HP temperature of 330 °C and a blending rate of 30 vol.%, E70 and E100 reach 4.0 vol.% and 17.1 vol.%, respectively. However, E70 and E100 have to meet 22 vol.% and 46 vol.%, respectively, according to EN 228. Therefore, HP can help to increase the light-ends, but further measures must be taken. A higher blending ratio of LG:HG-HP of 2:1 cannot be realized in our specific case, as this was roughly the split right after the rectification, as explained in Materials and Methods. A higher HP temperature has not been investigated, as we expected the cracking losses would no longer be justified.

Similar tendencies as for the boiling characteristics can be observed for the vapor pressure, as shown in Figure 2b. A higher overall vapor pressure is observed for blends with HG-HP@330 °C than those with HG-HP@270 °C. While the vapor pressure increases for a higher blending ratio of HG-HP@330 °C, it decreases for HG-HP@270 °C. The direct proportional dependency can again be attributed to the similar nature of the hydrocarbon fractions. As outlined in the Introduction, the vapor pressure is crucial for a correct engine functioning but is also connected to evaporative emissions. For 330 °C, the highest reaction temperature investigated, and a blending rate of 30 vol.%, the vapor pressure is far from violating the upper boundary of 60 kPa of EN 228 for summertime gasoline (Class A). HP seems to be an effective tool for adjusting the vapor pressure in a particular range.

As outlined above, comparing E70, E100, and vapor pressure to EN 228, the necessity of further blending components becomes apparent, even for an HP temperature of 330 °C. In the Introduction, we discussed that oxygenates can help to lower the boiling curve due to low boiling temperatures and by forming an azeotropic mixture with gasoline hydrocarbons. Therefore, the influence of the common oxygenates methanol, ethanol, MTBE, and ETBE on the boiling curve of the bioliq® gasoline is discussed in the following.

3.2. Influence of Oxygenates on Boiling Characteristics and Vapor Pressure

Figure 3 shows the boiling characteristics E70, E100, and E150 together with the vapor pressure in dependence on the oxygen mass fraction. The oxygen mass fraction is limited in EN 228 to 3.7 wt.% and thus chosen over the blended volume fraction. The maximum share of each oxygenate is chosen accordingly to the maximum permitted in EN 228, such that Figure 3 represents the potential effect of each oxygenate. As base gasoline, a blend of two-thirds bioliq® LG and one-third HG-HP@270 °C was chosen, with an E70, E100, and E150 of 0.6 vol.%, 5.8 vol.%, and 85.0 vol.%, respectively, and a vapor pressure of 13.7 kPa. Therefore, it represents the heavy nature of a typical DTG or MTG fuel.

As shown in Figure 3a, all blended oxygenates increase the E70 as their boiling points are below or in the region of 70 °C (see Table 1 for boiling temperatures). While MTBE and ETBE increase the E70 up to approx. 4 vol.%, blending of methanol and ethanol results in a maximum E70 of 7.8 vol.% and 8.0 vol.%, respectively. It has to be noted that ETBE contains approx. 22 vol.% by-products. Such a strong increase for methanol and ethanol can be attributed to the formation of azeotropic mixtures, as explained in the Introduction. Methanol shows the strongest effect with the blended oxygen equivalent, while a maximum of 3 vol.% could be blended to meet the restriction of EN 228. The overall greatest increase can be seen for ethanol at about 2 wt.% oxygen (5.9 vol.% ethanol) blended. A further addition leads to no further increase of the E70. The strong azeotropic effect of methanol and ethanol can also be seen in Figure 4, where the oxygenates' boiling curves for their highest blending rates are shown. Both alcohols strongly depress the front end of the boiling curve, which is in accordance with other studies [65,73]. Especially for the blend with ethanol, a distinct step shape can be observed, which indicates the formation of an azeotropic mixture [77]. The boiling curve again reaches the base gasoline's one after the alcohol is distilled completely [77]. No azeotrope seems to be formed for methanol due to the lower volume blended and as smaller alcohols in general tend to form an azeotropic

mixture at higher blending rates [62]. An azeotropic mixture is unfavorable as it results in an unsteady evaporating behavior of the fuel, as explained in the Introduction. Thus, methanol seems more promising than ethanol for adjusting the front-end volatility of the considered bioliq® fuel. As indicated above, MTBE and ETBE only slightly increase E70. However, considering Figure 4, both ethers show a significant flattening, especially of the mid-part of the curve, which is also confirmed by other researchers [65,73,78].

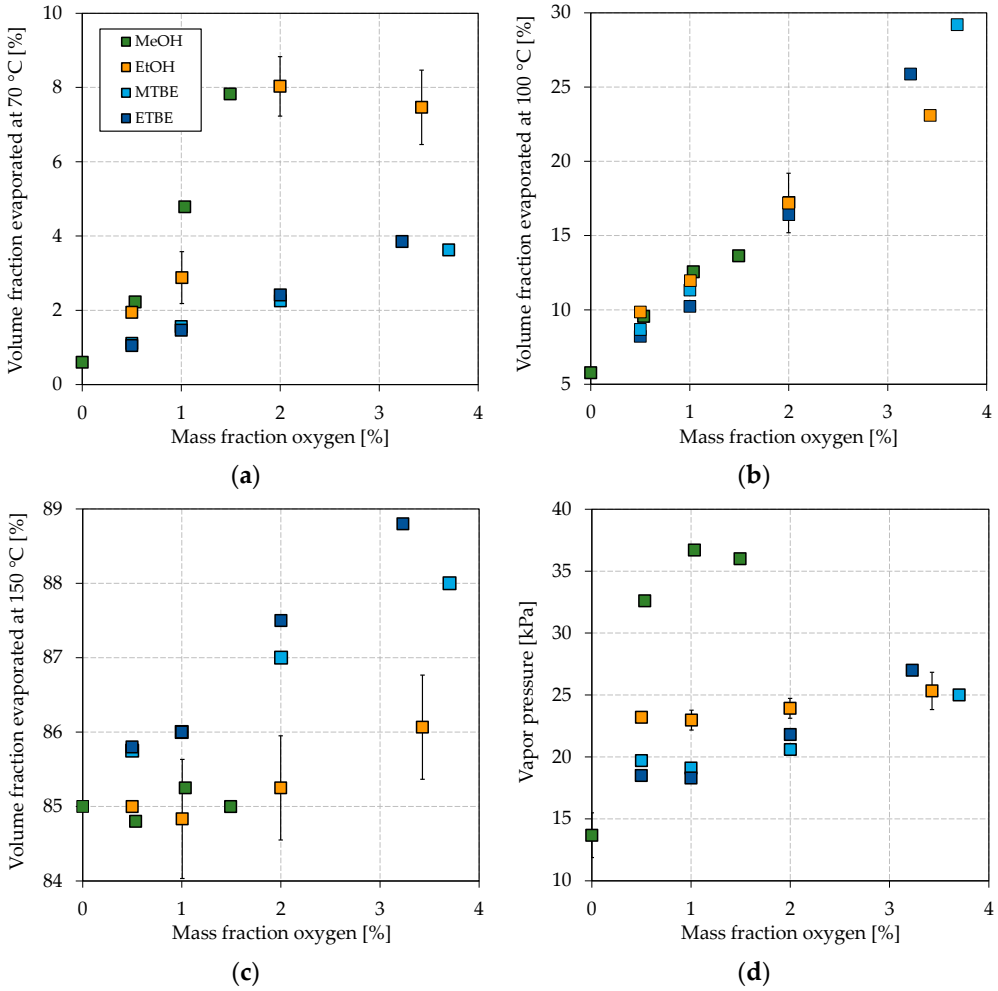


Figure 3. Influence of different oxygenates on the volatility characteristics. (**a**) E70, (**b**) E100, (**c**) E150, and (**d**) vapor pressure.

The influence on the mid-section can also be seen for the E100 in Figure 3b, which increases the most for ETBE and MTBE. Blending MTBE leads to the most substantial increase in the E100, as also determined by Petre et al. [78]. In general, however, no significant differences between the investigated oxygenates regarding their influence on the E100 with oxygen equivalent blended can be emphasized. Karonis et al. also detected no apparent difference in the E100 whether they blended ethanol or ETBE [73]. The overall substantial increase in the E100 for MTBE and ETBE can be attributed to the high volume blended, resulting from a low molecular oxygen content and a high permitted blending rate by EN 228.

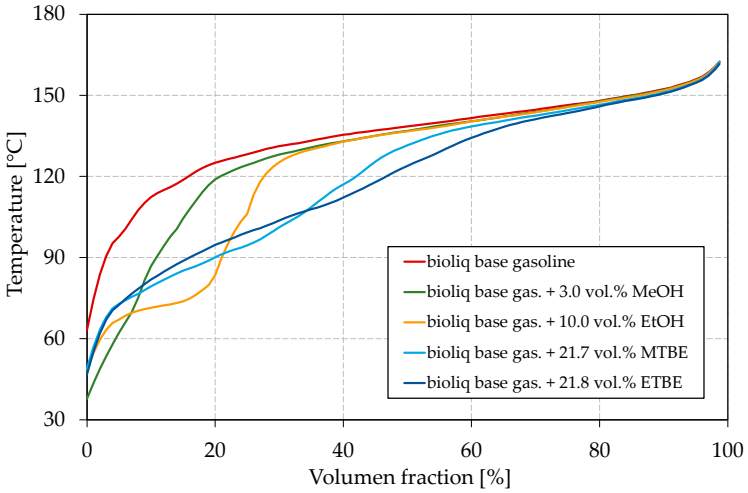


Figure 4. Influence of different oxygenates on the boiling curve.

As shown in Figure 3c, the E150 increases most by blending ETBE, followed by MTBE, and less significantly by ethanol and methanol. The considered alcohols show a less distinct effect on the back end of the boiling curve, as the (near-)azeotropic mixtures do not influence this part of the boiling curve.

Besides a smooth boiling curve, the vapor pressure is important for a well-working engine, emitting fewer emissions, as explained in the Introduction. The influence of the different oxygenates on the vapor pressure can be seen in Figure 3d. Remarkable is the substantial increase in the base fuel's vapor pressure if methanol is blended, while the ones of the ethanol blends are in the region of the MTBE and ETBE blends. In other studies, ethanol increased the vapor pressure more significantly [21,73]. The weak influence of ethanol on the vapor pressure in this study might be due to the heavy nature of the bioliq® gasoline, as the effect of an oxygenate on the volatility is always connected to the base fuel [21,73]. bioliq® gasoline considered in this study is rich in aromatics, which exhibit a lower increase in the vapor pressure when blended with alcohols [21]. As shown in Figure 4, the ethanol/gasoline azeotrope does not significantly influence the initial part of the boiling curve compared to MTBE and ETBE. In contrast, a significant lowering can be observed for methanol, probably because it can form a near-azeotropic mixture with light-ends, available in low concentrations. This becomes more obvious by comparing the different blends' initial boiling points (IBPs). For the blends reported in Figure 4 with methanol, ethanol, MTBE, and ETBE, the IBPs are 37.8 °C, 48.7 °C, 48.9 °C, and 46.7 °C, respectively. For each oxygenate considered, the vapor pressure increases with a growing blending rate of oxygen equivalent, except for a blending rate of 1 wt.% oxygen equivalent of methanol, after which the vapor pressure seems to drop. This observation is not significant, as not enough data were collected. However, sources report behavior in which the vapor pressure increased for low blending rates and decreased for higher ones or stayed almost the same [73,79]. For blending rates of up to 2 wt.% oxygen equivalent, the vapor pressure is slightly higher for ethanol than both ethers. The differences disappear for blending rates higher than 3 wt.% oxygen equivalent.

It can be concluded that methanol is promising to improve the boiling characteristics and vapor pressure. Interestingly, the results were obtained with a maximum blending rate of 3 vol.%, which makes it likely that such a fuel would be compatible with older engines, since standard gasoline in Europe contains up to 5 vol.% ethanol. It further seems ETBE is promising as it has a remarkable flattening effect on the boiling curve. MTBE increased the E100 the most, which makes it the favorite oxygenate for adjusting the mid-section of the bioliq® fuel.

In the following, we blended 3 vol.% methanol into the bioliq® base gasoline (two-thirds LG and one-third HG-HP@270 °C) and investigated the effect of a second oxygenate

blended, i.e., ethanol, MTBE, and ETBE until an oxygen content of 3.7 wt.% was reached. Methanol was chosen as it increases the E70 most considerably with the blended oxygen equivalent, as shown in Figure 3. There is also no drawback regarding the E100 compared to the other oxygenates. Both parameters are critical if the bioliq® DTG gasoline is considered [60]. Methanol also seems a good choice as it is available as a process intermediate in the case of MTG. Figure 5 shows the dual-oxygenate blends' boiling characteristics, vapor pressures, and boiling curves.

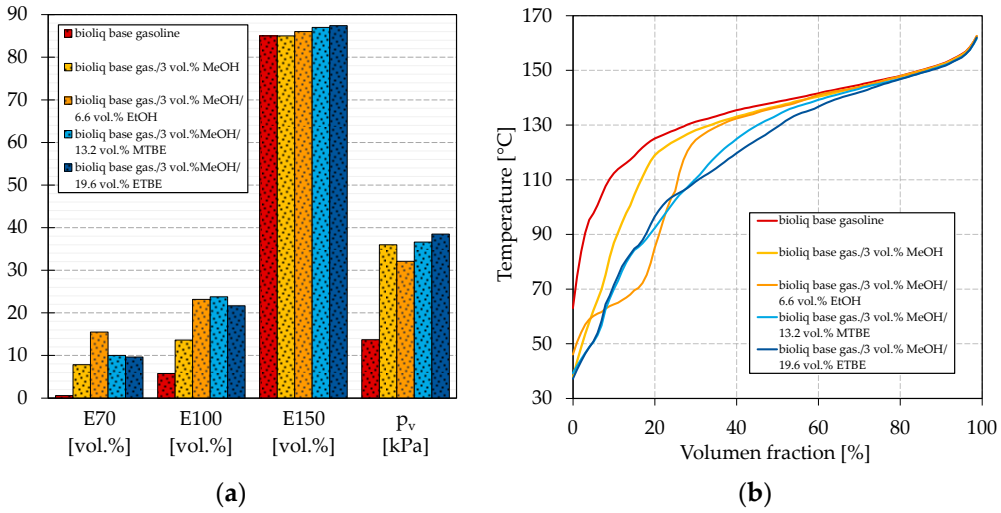


Figure 5. Influence on (**a**) the boiling characteristics and vapor pressure and (**b**) the boiling curve for blends of bioliq® base gasoline and methanol with ethanol, MTBE, and ETBE.

As shown in Figure 5a, the E70, E100, and vapor pressure are greatly improved for all oxygenates blended into the methanol-containing base gasoline. A significant increase in the E70 can be observed for ethanol and a lower one for MTBE and ETBE, which are at similar levels. The differences also become visible in Figure 3a, where the same tendencies are observable for the single oxygenate blends. E150 increases for the added oxygenates in the order ETBE > MTBE > ethanol, which is once more what was detected for the single-oxygenate blends in Figure 3c. E100 also improves significantly for the dual-oxygenate blends, whereby all values are of the same magnitude. The same was discovered in Figure 3b, where all oxygenates improved the E100 similarly.

Figure 5a shows the vapor pressure for the dual-oxygenate blends. The vapor pressure decreases in the order ETBE > MTBE > ethanol, which is turned around when Figure 3d is considered. For the blend containing methanol/ethanol, the vapor pressure lies between the vapor pressures measured for the blends with the single oxygenates (Figure 3d). The vapor pressure of the blends containing methanol/MTBE and methanol/ETBE are clearly above the values obtained for the blends containing only MTBE and ETBE (Figure 3d) and slightly above the one just containing methanol. The observed can be explained in two ways. First, methanol/ethanol may not increase the vapor pressure as significantly as methanol/MTBE and methanol/ETBE since an increased blending rate of alcohol leads to a decrease in vapor pressure after a certain point. Second, alcohols can form azeotropic mixtures with ethers, as reported, for example, by Domańska et al. [80], which could also explain the disproportionate increase in vapor pressures for these mixtures. A higher vapor pressure for blending methanol/ETBE than methanol/MTBE can be explained by the formation of an (near-)azeotropic mixture of the low-boiling by-products contained in ETBE with methanol. The aforementioned can also be seen in Figure 5b, where the IBPs are significantly lower for the blends with methanol/MTBE and methanol/ETBE than for those with methanol/ethanol. For all blends, the vapor pressures are within EN 228. Regarding the boiling curve, the observations from Figure 4 can be approved for the dual-oxygenate blends. The blend with methanol/ethanol shows a strong step

shape, indicating an azeotropic mixture. Both methanol/MTBE and methanol/ETBE help to flatten the boiling curve, whereby the effect is the strongest for methanol/ETBE, as can be seen around a distilled volume of 40%, where the methanol/MTBE curve shows a slight bump.

The boiling characteristics could be improved by simultaneously blending two different of oxygenates into the bioliq® base gasoline. A combination of methanol and ethanol achieved the highest E70 of 15.5 vol.%, while for methanol/MTBE and methanol/ETBE, E70 reached 10.0 vol.% and 9.6 vol.%, respectively. Regarding E100 and E150, the values were within a range of 21.6–23.8 vol.% and 86.0–87.4 vol.%, respectively, for all investigated dual-oxygenate blends. E70 and E100 thus do not meet EN 228, for which at least 22 vol.% and 46 vol.% are required, respectively. Therefore, further light boiling components free of oxygen must be considered. As discussed, the HP of HG at higher temperatures can increase the E70 and E100 to some extent. In the Introduction, we also discussed the possibility of using an FT gasoline fraction as an isomerate replacement. In the following, we combine all these measures. We used a combination of methanol/ethanol and methanol/ETBE in our experiments, as they were superior in terms of the boiling characteristics and the shape of the boiling curve, respectively. To prove its suitability as a possible fossil gasoline replacement, we measured the remaining petrochemical parameters covered by EN 228.

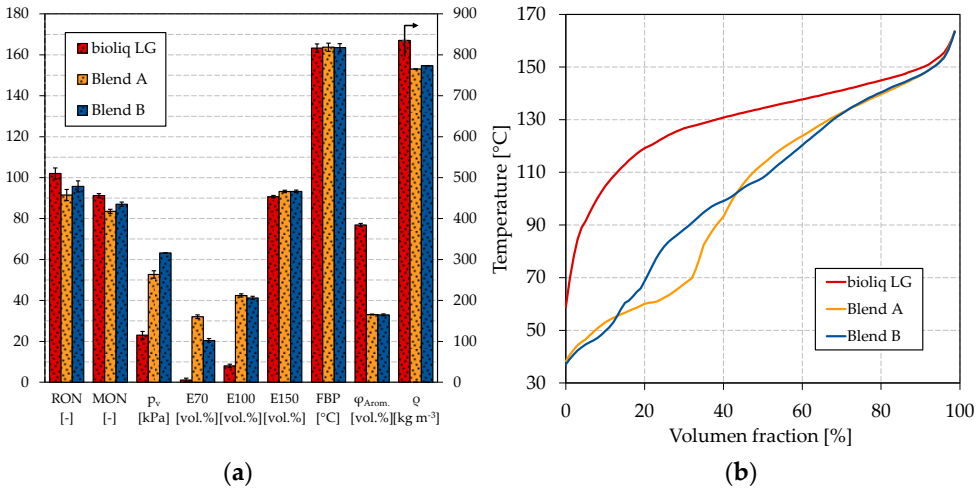
3.3. Expanded Blending Concept

Table 3 shows the fractions used to prepare the final blends A and B.

Table 3. Fractions used for the blends A and B.

Volume Fraction [%]	bioliq® LG	HG-HP@330 °C	FT-HP	Methanol	Ethanol	ETBE
Blend A	42.8	14.6	33.7	3.0	5.9	0.0
Blend B	42.7	14.5	21.2	3.1	0.0	18.5

For blends A and B, we chose a blend of bioliq® LG and HG-HP@330 °C as base gasoline, as outlined before. The ratio of LG:HG-HP was lowered due to two reasons. First, a higher HP temperature means increased cracking losses. Second, the ON of the HG-HP is comparably low; thus, we decided to blend more of the high-octane bioliq® LG. Figure 6 shows the petrochemical parameters of the blends compared to bioliq® LG and the respective boiling curves. The exact composition of the blends A and B can be found in Tables S7 and S8 in the Supplementary Materials.



(**a**) (**b**)

Figure 6. (**a**) Petrochemical parameters and (**b**) boiling curves of blend A and B and bioliq® LG.

As can be seen in Figure 6a, the boiling characteristics of blend A and B are significantly improved compared to bioliq® LG. The E70 counts 32.1 vol.% and 20.4 vol.% for blends

A and B, respectively. As already shown in Figure 5a, the combination of methanol and ethanol highly improves the E70 due to forming of an azeotropic mixture. This can also be seen in Figure 6b, where blend A shows a strong depression up to a distilled volume of 30 vol.%. Blend B scarce does not meet the 22 vol.% of EN 228 for the E70. Regarding the E100, blend A counts 42.4 vol.% and blend B 41.2 vol.%; thus, both do not meet EN 228's minimum value of 46 vol.%. For E150, both blends meet EN 228. In general, the boiling characteristics show similar results to the dual-oxygenate blends shown in Figure 5a. Regarding the vapor pressure, only blend A was measured, as the quantity of blend B was too low; however, we made an estimate based on the similarity to the dual-oxygenate blends. The vapor pressure of blend A and blend B is 52.7 kPa and 63.2 kPa, respectively. Blend A is within 45–60 kPa for Class A gasoline according to EN 228, while blend B is slightly too high. One might already conclude that MTBE is probably the better choice over ETBE. In Figure 5a, E70 and E100 are slightly higher for the dual-oxygenate blend with MTBE, while the vapor pressure is lower.

For blend A, the RON and MON are 91.5 and 83.5, respectively, which is too low to satisfy EN 228. The low ONs are explainable by the comparably low ON of HG-HP@330 °C and FT-HP (see Table 2), which cannot be compensated by ethanol as its blending rate is relatively low due to its high molecular oxygen content. Counting 95.7 and 87.0 for the RON and MON, respectively, significantly higher ONs, meeting EN 228, are detected for blend B. ETBE compensates better for the ON loss because its lower molecular oxygen content allows it to be blended at a higher ratio until the 3.7 wt.% oxygen equivalent is reached. Additionally, ETBE was determined to increase the RON and MON more distinct than ethanol [73]. The higher ON of blend A offers the possibility to increase the quantity of light-ends, for example, by increasing the share of HG-HP@330 °C or FT-HP. Additionally, with MTBE instead of ETBE, this could help to finally meet EN 228. MTBE and ETBE have similar RONs and MONs (see Table 1); therefore, the ON should not be a limiting factor.

The remaining parameters, density, and aromatics content lie within EN 228 for both blends. Regarding the boiling curves, a significant improvement can be seen for both blends compared to bioliq® LG. The stepped shape for blend A with methanol and ethanol is still observable. However, compared to Figure 5b, it is shifted towards higher volume fractions. The shift is not surprising, as a higher share of light boiling components was contained in the blends considered in Figure 6, as FT-HP and HG-HP@330 °C were blended here. A smoother boiling curve can be seen for blend B with methanol and ETBE, where no distinct disturbances are visible besides a flat bump between 20 vol.% and 40 vol.%. Therefore, a similar smooth boiling curve would be expected for MTBE, as only a slight difference was detected in Figure 5b. Further blending experiments are thus encouraging.

4. Conclusions

The bioliq® LG's critical volatility parameters E70 and E100 could be improved from 0.6 vol.% to 4.0 vol.% and 5.8 vol.% to 17.1 vol.%, respectively, through HP the HG, using a Pt-HZSM-5 catalyst. A more substantial improvement of the E70 from 0.6 vol.% to 7.8 vol.% and 0.6 vol.% to 8.0 vol.% was achieved by blending methanol and ethanol, respectively, within their permitted blending volumes by EN 228. ETBE and MTBE significantly improved the E100 from 5.8 vol.% to 25.9 vol.% and from 5.8 vol.% to 29.2 vol.%, respectively. The blending of ETBE additionally led to a considerable flattening of the boiling curve, while ethanol caused deformations due to formation of an azeotropic mixture. All vapor pressures were within EN 228, while blending of methanol led to the most substantial increase in the bioliq® gasoline's low vapor pressure from 13.7 kPa to 36.7 kPa. A blending of methanol and ethanol with bioliq® gasoline further improved the E70 to 15.5 vol.%, while it reached approx. 10 vol.% when methanol was blended with MTBE or ETBE. The E100 increased for all dual-oxygen blends to a similar level of 21.6 vol.% to 23.8 vol.%. Due to the high alcohol content, the boiling curve showed strong deformations for the blend with methanol and ethanol, while it was smooth for blending methanol and ETBE. Two final blends were prepared using bioliq® LG, HP-HG@330 °C, FT-HP, and a combination of

methanol and ethanol or methanol and ETBE. With 91.5 and 83.5 for the RON and MON, respectively, the blend with methanol and ethanol did not meet EN 228 in this regard. The blend with methanol and ETBE met the standard, with a RON and MON of 95.7 and 87, respectively. With the exceptions of E70 and E100 having slightly too low values of 20.4 vol.% and 41.2 vol.%, respectively, all petrochemical parameters could be met for the latter blend. The blend comes additionally with a low alcohol content of 3 vol.% and should thus be compatible even with older vehicles. A clear advantage over established upgrading processes such as Mobil's [59] is the complete conversion of heavy aromatics to saturated compounds, resulting in lower emission tendencies as reported for such fuels [55].

E70 and E100 could be further increased by server cracking of whether the FT wax or the HG. Since blending methanol and MTBE into the bioliq® gasoline increased the E70 and E100 slightly more than a blend with methanol and ETBE, it should be investigated whether replacing ETBE with MTBE could contribute to meet EN 228. A blend with methanol and MTBE would be additionally beneficial, as these oxygenates would be based entirely on methanol (and iso-butene). It should also be examined to lower the separation temperature of LG and HG in the rectification right after the gasoline synthesis. This would lower the boiling curve and is additionally promising as the gasoline supply might be based solely on MTG/DTG with additional oxygenates, allowing the omission of FT wax cracking. Finally, further research should include engine tests, especially under high loads, to investigate whether any evaporation issues exist.

Supplementary Materials: The following are available online at https://www.mdpi.com/article/10.3390/fuels4020010/s1, Table S1: Composition of bioliq® LG in vol.%., Table S2: Composition of HG-HP@270 °C in vol.%., Table S3: Composition of HG-HP@310 °C in vol.%., Table S4: Composition of HG-HP@330 °C in vol.%., Table S5: Composition of FT-HP in vol.%., Table S6: Composition of bioliq® HG in vol.%., Table S7: Composition of blend A in vol.%., Table S8: Composition of blend B in vol.%.

Author Contributions: Conceptualization, D.G.; Data curation, D.G.; Formal analysis, D.G.; Funding acquisition, R.R.; Investigation, D.G. and P.N.; Methodology, D.G.; Project administration, R.R.; Resources, R.R.; Software, D.G.; Supervision, R.R.; Validation, D.G., P.N. and R.R.; Visualization, D.G.; Writing—Original draft, D.G.; Writing—Review and editing, D.G., P.N. and R.R. All authors have read and agreed to the published version of the manuscript.

Funding: This work was supported by the Strategic Dialogue Automotive Industry SDA and the Ministry of Transport Baden Wuerttemberg as part of the project "refuels–rethinking fuels".

Data Availability Statement: The data presented in this study, if not included in the Supplementary Materials, are available on request from the corresponding author.

Acknowledgments: We thank Thomas Otto and Doreen Neumann-Walter from the Institute of Catalysis Research and Technology (IKFT) as part of Karlsruhe Institute of Technology for their strong support in characterizing the fuels.

Conflicts of Interest: The authors declare no conflict of interest. The funders had no role in the design of the study; in the collection, analyses, or interpretation of data; in the writing of the manuscript, or in the decision to publish the results.

References

1. European Commission. *Communication from the Commission of the European Parliament, the European Council, the Council, the European Economic and Social Committee and the Committee of the Regions*; The European Green Deal: Brussels, Belgium, 2019.
2. European Commission. *Communication from the Commission to the European Parliament, the Council, the European Economic and Social Committee and the Committee of the Regions: 'Fit for 55': Delivering the EU's 2030 Climat Target on the way to climate neutrality*; European Commission: Brussels, Belgium, 2021.
3. Sean Goulding Carroll. EU Deal on Car CO2 Standards Leaves Door Ajar for e-Fuels. Available online: https://www.euractiv.com/section/alternative-renewable-fuels/news/eu-deal-on-car-co2-standards-leaves-door-ajar-for-e-fuels/ (accessed on 7 July 2022).
4. Abnett, K. EU Approves Effective Ban on New Fossil Fuel Cars from 2035. Available online: https://www.reuters.com/markets/europe/eu-approves-effective-ban-new-fossil-fuel-cars-2035-2022-10-27/ (accessed on 25 November 2022).

5. Jonathan, M.G. No New Combustion-Engine Cars From 2035, Says European Union. Available online: https://arstechnica.com/cars/2022/10/eu-agrees-to-ban-new-combustion-engine-cars-from-2035/ (accessed on 25 November 2022).
6. International Energy Agency (IEA). *Global EV Outlook 2022: Securing Supplies for an Electric Future*; IEA: Paris, France, 2022.
7. European Automobile Manufacturers' Association (ACEA). *Vehicles in Use Europe 2023*; ACEA: Brussels, Belgium, 2023.
8. Randall, C. VW to Phase Out Combustion Vehicles by 2035. Available online: https://www.electrive.com/2021/06/27/vw-to-phase-out-combustion-vehicles-by-2035/ (accessed on 27 January 2023).
9. Surisetty, V.R.; Dalai, A.K.; Kozinski, J. Alcohols as alternative fuels: An overview. *Appl. Catal. A* **2011**, *404*, 1–11. [CrossRef]
10. Jeuland, N.; Montagne, X.; Gautrot, X. Potentiality of Ethanol as a Fuel for Dedicated Engine. *Oil Gas Sci. Technol.* **2004**, *59*, 559–570. [CrossRef]
11. Munsin, R.; Laoonual, Y.; Jugjai, S.; Imai, Y. An experimental study on performance and emissions of a small SI engine generator set fuelled by hydrous ethanol with high water contents up to 40%. *Fuel* **2013**, *106*, 586–592. [CrossRef]
12. Jafari, H.; Idris, M.H.; Ourdjini, A.; Rahimi, H.; Ghobadian, B. EIS study of corrosion behavior of metallic materials in ethanol blended gasoline containing water as a contaminant. *Fuel* **2011**, *90*, 1181–1187. [CrossRef]
13. Stappen, H.-J.; Gräve, P. eFuels Pilot Plant in Chile Officially Opened. Available online: https://newsroom.porsche.com/en/2022/company/porsche-highly-innovative-fuels-hif-opening-efuels-pilot-plant-haru-oni-chile-synthetic-fuels-30732.html (accessed on 27 January 2023).
14. DIN Deutsches Institut für Normung e. V. *Automotive Fuels–Unleaded Petrol–Requirements and Test Methods; German Version EN 228:2012+A1:2017*; Beuth Verlag GmbH: Berlin, Germany, 2017.
15. Federal Office for Agriculture and Food. *Evaluation and Progress Report 2020*; Federal Office for Agriculture and Food: Bonn, Germany, 2021.
16. Turdera, M.V. Energy balance, forecasting of bioelectricity generation and greenhouse gas emission balance in the ethanol production at sugarcane mills in the state of Mato Grosso do Sul. *Renew. Sustain. Energy Rev.* **2013**, *19*, 582–588. [CrossRef]
17. Ghosh, P.; Hickey, K.J.; Jaffe, S.B. Development of a Detailed Gasoline Composition-Based Octane Model. *Ind. Eng. Chem. Res.* **2006**, *45*, 337–345. [CrossRef]
18. Jiang, Y.; Phillips, S.D.; Singh, A.; Jones, S.B.; Gaspar, D.J. Potential economic values of low-vapor-pressure gasoline-range bio-blendstocks: Property estimation and blending optimization. *Fuel* **2021**, *297*, 120759. [CrossRef]
19. Heywood, J.B. *Internal Combustion Engine Fundamentals*, 2nd ed.; McGraw-Hill: New York, NY, USA, 1988; ISBN 0071004998.
20. Milpied, J.; Jeuland, N.; Plassat, G.; Guichaous, S.; Dioc, N.; Marchal, A.; Schmelzle, P. Impact of Fuel Properties on the Performances and Knock Behaviour of a Downsized Turbocharged DI SI Engine: Focus on Octane Numbers and Latent Heat of Vaporization. *SAE Int. J. Fuels Lubr.* **2009**, *2*, 118–126. [CrossRef]
21. da Silva, R.; Cataluña, R.; de Menezes, E.W.; Samios, D.; Piatnicki, C.M.S. Effect of additives on the antiknock properties and Reid vapor pressure of gasoline. *Fuel* **2005**, *84*, 951–959. [CrossRef]
22. Santikunaporn, M.; Alvarez, W.E.; Resasco, D.E. Ring contraction and selective ring opening of naphthenic molecules for octane number improvement. *Appl. Catal. A* **2007**, *325*, 175–187. [CrossRef]
23. Morgan, T.D.B.; den Otter, G.J.; Lange, W.W.; Doyon, J.; Barnes, J.R.; Yamashita, T. An Integrated Study of the Effects of Gasoline Composition on Exhaust Emissions Part I: Programme Outline and Results on Regulated Emissions. *SAE Tech. Pap.* **1993**, *932678*, 1–18. [CrossRef]
24. Petit, A.; Montagne, X. Effects of the Gasoline Composition on Exhaust Emissions of Regulated and Speciated Pollutants. *SAE Tech. Pap.* **1993**, *932681*, 1–11. [CrossRef]
25. Nakakita, K.; Ban, H.; Takasu, S.; Hotta, Y.; Inagaki, K.; Weissman, W.; Farrell, J.T. Effect of Hydrocarbon Molecular Structure in Diesel Fuel on In-Cylinder Soot Formation and Exhaust Emissions. *SAE Int. J. Fuels Lubr.* **2003**, *112*, 1763–1775. [CrossRef]
26. Meyers, R.A. *Handbook of Petroleum Refining Processes*, 3rd ed.; McGraw-Hill: New York, NY, USA, 2003; ISBN 978-0-07-139109-2.
27. Bruno, T.J.; Wolk, A.; Naydich, A. Composition-Explicit Distillation Curves for Mixtures of Gasoline with Four-Carbon Alcohols (Butanols). *Energy Fuels* **2009**, *23*, 2295–2306. [CrossRef]
28. Tan, E.C.D.; Talmadge, M.; Dutta, A.; Hensley, J.; Snowden-Swan, L.J.; Humbird, D.; Schaidle, J.; Biddy, M. Conceptual process design and economics for the production of high-octane gasoline blendstock via indirect liquefaction of biomass through methanol/dimethyl ether intermediates. *Biofuels Bioprod. Bioref.* **2016**, *10*, 17–35. [CrossRef]
29. Calcote, H.F.; Manos, D.M. Effect of Molecular Structure on Incipient Soot Formation. *Combust. Flame* **1983**, *49*, 289–304. [CrossRef]
30. Furey, R.L.; King, J.B. Emissions, Fuel Economy, and Driveability Effects of Methanol/Butanol/Gasoline Fuel Blends. *SAE Tech. Pap.* **1982**, *821188*, 47–59. [CrossRef]
31. Yanowitz, J.; Christensen, E.; McCormick, R.L. *Utilization of Renewable Oxygenates as Gasoline Blending Components, Technical Report NREL/TP-5400-50791*; National Renewable Energy Laboratory: Colorado, CO, USA, 2011.
32. Aikawa, K.; Sakurai, T.; Jetter, J.J. Development of a Predictive Model for Gasoline Vehicle Particulate Matter Emissions. *SAE Int. J. Fuels Lubr.* **2010**, *3*, 610–622. [CrossRef]
33. Jess, A.; Wasserscheid, P. *Chemical Technology: An Integral Textbook*; Wiley-VCH Verlag GmbH & Co. KGaA: Weinheim, Germany, 2013; ISBN 978-3-527-30446-2.
34. Duvenhage, D.J.; Shingles, T. Synthol reactor technology development. *Catal. Today* **2002**, *71*, 301–305. [CrossRef]
35. Steynberg, A.P.; Espinoza, R.L.; Jager, B.; Vosloo, A.C. High temperature Fischer–Tropsch synthesis in commercial practice. *Appl. Catal. A* **1999**, *186*, 41–54. [CrossRef]

36. Kamara, B.I.; Coetzee, J. Overview of High-Temperature Fischer−Tropsch Gasoline and Diesel Quality. *Energy Fuels* **2009**, *23*, 2242–2247. [CrossRef]
37. Dry, M.E. High quality diesel via the Fischer-Tropsch process–a review. *J. Chem. Technol. Biotechnol.* **2002**, *77*, 43–50. [CrossRef]
38. Meurer, A.; Kern, J. Fischer–Tropsch Synthesis as the Key for Decentralized Sustainable Kerosene Production. *Energies* **2021**, *14*, 1836. [CrossRef]
39. Federal Ministry for the Environment, Nature Conservation, Nuclear Safety and Consumer Protection. *PtL Roadmap: Sustainable Aviation Fuel from Renewable Energy Sources for Aviation in Germany*; Federal Ministry for the Environment, Nature Conservation, Nuclear Safety and Consumer Protection: Bonn, Germany, 2021.
40. Schulz, H. Short history and present trends of Fischer–Tropsch synthesis. *Appl. Catal. A* **1999**, *186*, 3–12. [CrossRef]
41. Chang, C.D.; Silvestri, A.J. The Conversion of Methanol and Other O-Compounds to Hydrocarbons over Zeolite Catalysts. *J. Catal.* **1977**, *47*, 249–259. [CrossRef]
42. Olsbye, U.; Svelle, S.; Bjørgen, M.; Beato, P.; Janssens, T.V.W.; Joensen, F.; Bordiga, S.; Lillerud, K.P. Conversion of Methanol to Hydrocarbons: How Zeolite Cavity and Pore Size Controls Product Selectivity. *Angew. Chem. Int. Ed.* **2012**, *51*, 5810–5831. [CrossRef]
43. Teketel, S.; Olsbye, U.; Lillerud, K.-P.; Beato, P.; Svelle, S. Selectivity control through fundamental mechanistic insight in the conversion of methanol to hydrocarbons over zeolites. *Microporous Mesoporous Mater.* **2010**, *136*, 33–41. [CrossRef]
44. Chang, C.D. The New Zealand Gas-to-Gasoline plant: An engineering tour de force. *Catal. Today* **1992**, *13*, 103–111. [CrossRef]
45. Topp-Jørgensen, J. Topsøe Integrated Gasoline Synthesis–The Tigas Process. *Stud. Surf. Sci. Catal.* **1988**, *36*, 293–305. [CrossRef]
46. Dahmen, N.; Abeln, J.; Eberhard, M.; Kolb, T.; Leibold, H.; Sauer, J.; Stapf, D.; Zimmerlin, B. The bioliq process for producing synthetic transportation fuels. *Wiley Interdiscip. Rev. Energy Environ.* **2017**, *6*, e236. [CrossRef]
47. Dahmen, N.; Dinjus, E.; Kolb, T.; Arnold, U.; Leibold, H.; Stahl, R. State of the Art of the Bioliq®Process for Synthetic Biofuels Production. *Environ. Prog. Sustain. Energy* **2012**, *31*, 176–181. [CrossRef]
48. Pfitzer, C.; Dahmen, N.; Tröger, N.; Weirich, F.; Sauer, J.; Günther, A.; Müller-Hagedorn, M. Fast Pyrolysis of Wheat Straw in the Bioliq®Pilot Plant. *Energy Fuels* **2016**, *30*, 8047–8054. [CrossRef]
49. Trippe, F.; Fröhling, M.; Schultmann, F.; Stahl, R.; Henrich, E. Techno-Economic Analysis of Fast Pyrolysis as a Process Step Within Biomass-to-Liquid Fuel Production. *Waste Biomass Valorization* **2010**, *1*, 415–430. [CrossRef]
50. Dahmen, N.; Henrich, E.; Dinjus, E.; Weirich, F. The bioliq®bioslurry gasification process for the production of biosynfuels, organic chemicals, and energy. *Energy Sustain. Soc.* **2012**, *2*, 3. [CrossRef]
51. Ahmad, R.; Schrempp, D.; Behrens, S.; Sauer, J.; Döring, M.; Arnold, U. Zeolite-based bifunctional catalysts for the single step synthesis of dimethyl ether from CO-rich synthesis gas. *Fuel Process. Technol.* **2014**, *121*, 38–46. [CrossRef]
52. Stiefel, M.; Ahmad, R.; Arnold, U.; Döring, M. Direct synthesis of dimethyl ether from carbon-monoxide-rich synthesis gas: Influence of dehydration catalysts and operating conditions. *Fuel Process. Technol.* **2011**, *92*, 1466–1474. [CrossRef]
53. Zimmermann, M.C.; Otto, T.N.; Wodarz, S.; Zevaco, T.A.; Pitter, S. Mesoporous H-ZSM-5 for the Conversion of Dimethyl Ether to Hydrocarbons. *Chem. Ing. Tech.* **2019**, *91*, 1302–1313. [CrossRef]
54. Fujimoto, K.; Asami, K.; Saima, H.; Shikada, T.; Tominaga, H.-O. Two-Stage Reaction System for Synthesis Gas Conversion to Gasoline. *Ind. Eng. Chem. Prod. Res. Dev.* **1986**, *25*, 262–267. [CrossRef]
55. Michler, T.; Wippermann, N.; Toedter, O.; Niethammer, B.; Otto, T.; Arnold, U.; Pitter, S.; Koch, T.; Sauer, J. Gasoline from the bioliq®process: Production, characterization and performance. *Fuel Process. Technol.* **2020**, *206*, 106476. [CrossRef]
56. Liederman, D.; Yurchak, S.; Kuo, J.C.W.; Lee, W. Mobil Methanol-to-Gasoline Process. *J. Energy* **1982**, *6*, 340–341. [CrossRef]
57. Do, P.T.M.; Crossley, S.; Santikunaporn, M.; Resasco, D.E. Catalytic strategies for improving specific fuel properties. *Catalysis* **2007**, *20*, 33–64. [CrossRef]
58. McEnally, C.S.; Pfefferle, L.D. Improved sooting tendency measurements for aromatic hydrocarbons and their implications for naphthalene formation pathways. *Combust. Flame* **2007**, *148*, 210–222. [CrossRef]
59. Mokrani, T.; Scurrell, M. Gas Conversion to Liquid Fuels and Chemicals: The Methanol Route-Catalysis and Processes Development. *Catal. Rev.* **2009**, *51*, 1–145. [CrossRef]
60. Graf, D.; Neuner, P.; Rauch, R. Hydroprocessing and Blending of a Biomass-Based DTG-Gasoline. *Energy Eng.* **2022**, *119*, 2169–2192. [CrossRef]
61. Serrano, D.P.; Melero, J.A.; Morales, G.; Iglesias, J.; Pizarro, P. Progress in the design of zeolite catalysts for biomass conversion into biofuels and bio-based chemicals. *Catal. Rev.* **2017**, *60*, 1–70. [CrossRef]
62. Andersen, V.F.; Anderson, J.E.; Wallington, T.J.; Mueller, S.A.; Nielsen, O.J. Distillation Curves for Alcohol−Gasoline Blends. *Energy Fuels* **2010**, *24*, 2683–2691. [CrossRef]
63. Chen, Y.; Yihao Zhang, Y.; Cheng, W.K. Effects of Ethanol Evaporative Cooling on Particulate Number Emissions in GDI Engines. *SAE Tech. Pap.* **2018**, *2018*, 1–9. [CrossRef]
64. Kubic, W.L. *A Group Contribution Method for Estimating Cetane and Octane Numbers LA-UR-16-25529*; Los Alamos National Lab. (LANL): Los Alamos, NM, USA, 2016.
65. Michalopoulou, D.-P.; Komiotou, M.; Zannikou, Y.; Karonis, D. Impact of Bio-Ethanol, Bio-ETBE Addition on the Volatility of Gasoline with Oxygen Content at the Level of E10. *Fuels* **2021**, *2*, 501–520. [CrossRef]
66. Bozzano, G.; Manenti, F. Efficient methanol synthesis: Perspectives, technologies and optimization strategies. *Prog. Energy Combust. Sci.* **2016**, *56*, 71–105. [CrossRef]

67. Taljaard, H.C.; Jordaan, C.F.P.; Botha, J.J. The Effect of Oxygen Content in Different Oxygenate-Gasoline Blends on Performance and Emissions in a Single Cylinder, Spark-Ignition Engine. *SAE Tech. Pap.* **1991**, *910379*, 1–17. [CrossRef]
68. Lim, S.S.; Vos, T.; Flaxman, A.D.; Danaei, G.; Shibuya, K.; Adair-Rohani, H.; AlMazroa, M.A.; Amann, M.; Anderson, H.R.; Andrews, K.G.; et al. A comparative risk assessment of burden of disease and injury attributable to 67 risk factors and risk factor clusters in 21 regions, 1990–2010: A systematic analysis for the Global Burden of Disease Study 2010. *Lancet* **2012**, *380*, 2224–2260. [CrossRef] [PubMed]
69. Ratcliff, M.A.; Windom, B.; Fioroni, G.M.; St. John, P.; Burke, S.; Burton, J.; Christensen, E.D.; Sindler, P.; McCormick, R.L. Impact of ethanol blending into gasoline on aromatic compound evaporation and particle emissions from a gasoline direct injection engine. *Appl. Energy* **2019**, *250*, 1618–1631. [CrossRef]
70. Stein, R.A.; House, C.J.; Leone, T.G. Optimal Use of E85 in a Turbocharged Direct Injection Engine. *SAE Int. J. Fuels Lubr.* **2009**, *2*, 670–682. [CrossRef]
71. He, X.; Ratcliff, M.A.; Zigler, B.T. Effects of Gasoline Direct Injection Engine Operating Parameters on Particle Number Emissions. *Energy Fuels* **2012**, *26*, 2014–2027. [CrossRef]
72. Ketterer, J.E.; Cheng, W.K. On the Nature of Particulate Emissions from DISI Engines at Cold-Fast-Idle. *SAE Int. J. Engines* **2014**, *7*, 986–994. [CrossRef]
73. Karonis, D.; Anastopoulos, G.; Lois, E.; Stournas, S. Impact of Simultaneous ETBE and Ethanol Addition on Motor Gasoline Properties. *SAE Int. J. Fuels Lubr.* **2009**, *1*, 1584–1594. [CrossRef]
74. *ASTM D7345*; Standard Test Method for Distillation of Petroleum Products and Liquid Fuels at Atmospheric Pressure (Micro Distillation Method). ASTM International: West Conshohocken, PA, USA, 2017.
75. Neuner, P.; Graf, D.; Mild, H.; Rauch, R. Catalytic Hydroisomerisation of Fischer–Tropsch Waxes to Lubricating Oil and Investigation of the Correlation between Its Physical Properties and the Chemical Composition of the Corresponding Fuel Fractions. *Energies* **2021**, *14*, 4202. [CrossRef]
76. *ASTM D6378*; Standard Test Method for Determination of Vapor Pressure (VPX) of Petroleum Products, Hydrocarbons, and Hydrocarbon-Oxygenate Mixtures (Triple Expansion Method). ASTM International: West Conshohocken, PA, USA, 2020.
77. Smith, B.L.; Bruno, T.J. Improvements in the Measurement of Distillation Curves. 3. Application to Gasoline and Gasoline + Methanol Mixtures. *Ind. Eng. Chem. Res.* **2007**, *46*, 297–309. [CrossRef]
78. Petre, M.N.; Rosca, P.; Dragomir, R.-E. The Effect of Bio-ethers on the Volatility Properties of Oxygenated Gasoline. *Rev. Chim.* **2011**, *62*, 567–574.
79. Furey, R.L.; Perry, K.L. Vapor Pressures of Mixtures of Gasolines and Gasoline-Alcohol Blends. *SAE Int. J. Fuels Lubr.* **1986**, *95*, 779–789. [CrossRef]
80. Domańska, U.; Żołek-Tryznowska, Z.; Tshibangu, M.M.; Ramjugernath, D.; Letcher, T.M. Separation of an Alcohol and a Tetrahydrofuran, Methyl tert -Butyl Ether, or Ethyl tert -Butyl Ether by Solvent Extraction with a Hyperbranched Polymer at T = 298.15 K. *J. Chem. Eng. Data* **2010**, *55*, 2879–2885. [CrossRef]

Disclaimer/Publisher's Note: The statements, opinions and data contained in all publications are solely those of the individual author(s) and contributor(s) and not of MDPI and/or the editor(s). MDPI and/or the editor(s) disclaim responsibility for any injury to people or property resulting from any ideas, methods, instructions or products referred to in the content.

Standard-Compliant Gasoline by Upgrading a DTG-Based Fuel through Hydroprocessing the Heavy-Ends and Blending of Oxygenates

David Graf, Philipp Neuner and Reinhard Rauch

Karlsruhe Institute of Technology (KIT), Engler-Bunte-Institute, Division of Fuel Technology (EBI-ceb), Engler-Bunte-Ring 1a, 76131 Karlsruhe, Germany

Supplementary Materials

Table S1. Composition of bioliq® LG in vol.%.

C-Nr.	Naph.	Paraf.	Cycl Ol.	Olef.	Arom.	Oxyg.	Total
4	-	0.90	-	0.05	-	-	**0.94**
5	0.08	2.81	-	0.15	-	0.02	**3.06**
6	0.38	4.68	0.04	0.25	1.44	0.04	**6.82**
7	1.16	3.26	0.20	0.24	15.96	-	**20.81**
8	2.39	2.22	0.49	0.20	43.14	-	**48.44**
9	1.22	0.85	0.40	0.15	16.26	-	**18.89**
10	0.21	0.32	0.12	0.02	0.08	-	**0.76**
11+	-	0.25	-	-	-	-	**0.25**
Poly	0.02	-	-	-	-	-	**0.02**
Total	**5.46**	**15.29**	**1.26**	**1.05**	**76.88**	**0.06**	**100.00**

Table S2. Composition of HG-HP@270 °C in vol.%.

C-Nr.	Naph.	i-Par.	n-Par.	Cycl Ol.	Olef.	Arom.	Total
4	-	0.16	0.14	-	-	-	**0.30**
5	0.01	0.46	0.47	-	-	-	**0.94**
6	0.48	0.71	0.47	-	-	0.01	**1.67**
7	1.38	0.23	0.09	-	-	0.05	**1.76**
8	2.14	0.16	0.03	-	-	0.37	**2.70**
9	38.66	0.13	-	0.02	-	0.06	**38.87**
10	51.99	0.01	0.10	0.03	-	0.01	**52.14**
11	0.08	0.04	-	-	-	-	**0.12**
12+	0.84	-	-	-	-	0.02	**0.86**
Poly	0.63	-	-	-	-	-	**0.63**
Total	**96,21**	**1.90**	**1.29**	**0.05**	-	**0.53**	**100.00**

Table S3. Composition of HG-HP@310 °C in vol.%.

C-Nr.	Naph.	i-Par.	n-Par.	Cycl Ol.	Olef.	Arom.	Total
4	-	1.34	0.53	-	-	-	**1.87**
5	0.18	2.52	3.68	-	-	-	**6.39**
6	3.67	4.77	4.00	0.01	-	0.17	**12.63**
7	4.85	0.59	0.20	-	-	0.62	**6.27**
8	4.60	0.25	0.17	-	-	0.51	**5.53**
9	22.86	0.12	0.06	-	-	0.26	**23.30**
10	39.71	0.06	0.02	-	-	0.05	**39.84**
11	0.36	0.39	0.05	-	-	-	**0.80**
12+	2.32	-	-	-	-	0.01	**2.34**
Poly	1.04	-	-	-	-	-	**1.04**
Total	**79.59**	**10.04**	**8.72**	**0.01**	-	**1.64**	**100.00**

Table S4. Composition of HG-HP@330 °C in vol.%.

C-Nr.	Naph.	i-Par.	n-Par.	Cycl Ol.	Olef.	Arom.	Total
4	-	1.45	1.09	-	-	-	**2.55**
5	0.25	3.84	8.30	-	-	-	**12.39**
6	4.09	8.22	8.68	-	-	0.01	**21.00**
7	4.57	0.39	0.15	-	-	0.02	**5.14**
8	3.25	0.18	0.01	-	-	0.19	**3.63**
9	27.59	0.08	-	0.02	-	0.07	**27.75**
10	26.19	0.08	-	0.03	-	0.07	**26.36**
11	0.41	0.02	0.04	-	-	-	**0.46**
12+	0.53	-	-	-	-	0.04	**0.57**
Poly	0.14	-	-	-	-	-	**0.14**
Total	**67.02**	**14.26**	**18.27**	**0.05**	-	**0.39**	**100.00**

Table S5. Composition of FT-HP in vol.%.

C-Nr.	Naph.	i-Par.	n-Par.	Cycl Ol.	Olef.	Arom.	Total
4	-	0.98	1.82	-	-	-	**2.80**
5	0.07	8.94	10.40	-	-	-	**19.41**
6	0.70	15.50	11.78	-	0.02	-	**27.99**
7	1.42	13.56	6.60	-	0.01	0.04	**21.63**
8	1.34	10.59	3.34	-	0.01	0.03	**15.31**
9	0.62	6.28	1.14	-	-	0.01	**8.05**
10	0.14	2.68	0.29	-	-	0.03	**3.14**
11	-	0.72	0.30	-	-	-	**1.02**
12+	-	0.65	-	-	-	-	**0.65**
Poly	-	-	-	-	-	-	-
Total	**4.29**	**59.89**	**35.67**	**-**	**0.05**	**0.10**	**100**

Table S6. Composition of bioliq® HG in vol.%.

C-Nr.	Naph.	i-Par.	n-Par.	Cycl Ol.	Olef.	Arom.	Total
4	-	-	-	-	-	-	-
5	-	0.05	0.01	-	-	-	**0.06**
6	0.02	0.11	0.01	-	-	0.02	**0.16**
7	0.03	0.08	-	-	-	0.28	**0.39**
8	0.06	0.10	-	-	-	1.09	**1.26**
9	0.13	0.03	-	0.02	-	32.78	**32.97**
10	0.48	0.06	0.06	0.08	-	52.60	**53.28**
11	0.06	0.37	0.08	0.10	0.08	-	**0.68**
12+	-	0.95	-	-	-	10.20	**11.14**
Poly	0.06	-	-	-	-	-	**0.06**
Total	**0.84**	**1.75**	**0.16**	**0.19**	**0.08**	**96.97**	**100.00**

Table S7. Composition of blend A in vol.%.

C-Nr.	Naph.	Paraf.	Cycl Ol.	Olef.	Arom.	Oxyg.	Total
1	-	-	-	-	-	3.10	**3.10**
2	-	-	-	-	-	5.81	**5.81**
3	-	-	-	-	-	-	-
4	-	2.17	-	0.02	-	-	**2.19**
5	0.09	9.08	-	0.07	-	0.01	**9.25**
6	0.99	13.48	0.02	0.11	0.62	0.02	**15.24**
7	1.64	8.25	0.09	0.11	6.85	-	**16.94**
8	1.90	5.69	0.22	0.10	18.52	-	**26.43**
9	4.72	2.89	0.19	0.07	6.99	-	**14.86**
10	3.97	1.16	0.06	0.01	0.04	-	**5.24**
11+	-	0.77	-	-	0.07	-	**0.84**
Poly	0.09	-	-	-	-	-	**0.09**
Total	**13.39**	**43.50**	**0.58**	**0.49**	**33.09**	**8.95**	**100.00**

Table S8. Composition of blend B in vol.%.

C-Nr.	Naph.	Paraf.	Cycl Ol.	Olef.	Arom.	Oxyg.	Total
1	-	-	-	-	-	3.33	**3.33**
2	-	-	-	-	-	0.51	**0.51**
3	-	-	-	-	-	-	-
4	-	1.56	-	1.23	-	0.07	**2.85**
5	0.08	7.68	-	0.41	-	0.09	**8.27**
6	0.90	10.16	0.02	0.11	0.62	14.94	**26.75**
7	1.46	5.81	0.09	0.11	6.85	0.02	**14.34**
8	1.77	4.01	0.22	0.12	18.44	-	**24.56**
9	4.61	2.00	0.19	0.08	6.94	-	**13.82**
10	3.91	0.80	0.07	0.02	0.03	-	**4.82**
11+	-	0.65	-	-	0.05	-	**0.70**
Poly	0.04	-	-	-	-	-	**0.04**
Total	**12.77**	**32.66**	**0.59**	**2.07**	**32.93**	**18.97**	**100.00**

reactions

MDPI

Article

Co-Hydroprocessing of Fossil Middle Distillate and Bio-Derived Durene-Rich Heavy Ends under Hydrotreating Conditions

David Graf, Johannes Waßmuth and Reinhard Rauch *

Engler-Bunte-Institute–Division of Fuel Technology, Karlsruhe Institute of Technology, Engler-Bunte-Ring 1a, 76131 Karlsruhe, Germany; david.graf@kit.edu (D.G.); wassmuth.johannes@gmail.com (W.B.)
* Correspondence: reinhard.rauch@kit.edu

Abstract: Methanol-to-gasoline (MTG) and dimethyl ether-to-gasoline (DTG), as industrially approved processes for producing greenhouse gas-neutral gasoline, yield byproducts rich in heavy mono-ring aromatics such as 1,2,4,5-tetramethylbenzene (durene). Due to its tendency to crystallize and the overall poor fuel performance, the heavy fuel fraction is usually further processed using after-treatment units designed for this purpose. This research article discusses the co-hydroprocessing (HP) of bio-derived heavy gasoline (HG) with fossil middle distillate (MD), drawing on available refinery hydrotreaters. Co-HP experiments were conducted in a laboratory-scale fixed bed reactor using an industrial CoMo/γ-Al_2O_3 catalyst, varying the space-time between 0.7 and 4.0 cm^3_{Cat} h cm^{-3}_{Feed} and the reaction temperature between 340 and 390 °C. In addition to the durene conversion, special attention was paid to the octane and cetane numbers (CN) of gasoline and MD, respectively. A six-lump model with ten parameters was developed to predict relevant fuel yields dependent on the process conditions. Under stable catalyst conditions, C_{10} aromatic conversions of more than 60% were obtained, while the CN remained close to that of pure MD. Harsh process conditions increased the gasoline yield up to 20% at the cost of MD, while the kerosene yield remained almost constant. With an optimized lumping model, fuel yields could be predicted with an R^2 of 0.998. In this study, co-HP heavy aromatic-rich MTG/DTG fuels with fossil MD were proven to be a promising process strategy compared to a stand-alone after-treatment.

Keywords: co-hydroprocessing; durene; refinery; sustainable fuels; upgrading

check for updates

Citation: Graf, D.; Waßmuth, J.; Rauch, R. Co-Hydroprocessing of Fossil Middle Distillate and Bio-Derived Durene-Rich Heavy Ends under Hydrotreating Conditions*Reactions* **2023**, *4*, 531–551. https://doi.org/10.3390/reactions4030032

Academic Editors: Sibudjing Kawi, Valérie Meille and Francesco Frusteri

Received: 31 July 2023
Revised: 7 September 2023
Accepted: 18 September 2023
Published: 21 September 2023

Copyright: © 2023 by the authors. Licensee MDPI, Basel, Switzerland. This article is an open access article distributed under the terms and conditions of the Creative Commons Attribution (CC BY) license (https://creativecommons.org/licenses/by/4.0/).

1. Introduction

Primary energy consumption has risen steadily over the last few centuries, showing an exponential increase since 1940 [1]. While most of the 20th century's demand was met with fossil energy carriers, global warming and its evermore noticeable repercussions urgently call for a greenhouse gas (GHG)-neutral, cross-sector energy supply. The European Union (EU) committed its willingness toward GHG neutrality with the European Green Deal [2]. In June 2021, the European Parliament and Council enforced a binding regulation to all member states to lower the EU's GHG emissions by 55% until 2030 compared to 1990 [3]. With the "Fit for 55" action plan, the European Commission has published proposals for adapting laws to the climate targets mentioned above [4] and to pave the way to full GHG neutrality by 2050.

Transportation is one of the most intensively debated sectors and was recently involved in an incisive decision: the EU-wide ban of cars relying on internal combustion engines by 2035 [5]. However, a ban does not tantamount to the sudden disappearance of liquid hydrocarbon-fueled vehicles. Especially, aviation and maritime transport will further rely on energy carriers with high energy densities. The EU has recognized this and supports the implementation of synthetic fuels in these sectors [4]. Germany, for example, aims to produce at least 200,000 t a^{-1} of Power-to-Liquid kerosene by 2030 [6]. Synthetic fuels will

further play an important role during the transition toward technologies such as electrification. Registration rates of electric vehicles were still modest in 2022, e.g., 21% and 29% for Europe and China, respectively, as the fastest-growing markets [7]. Moreover, automobiles on European roads are on average twelve years old [8]. Consequently, vehicles relying on liquid hydrocarbon fuels will only gradually disappear, and it is therefore inevitable to supply GHG-neutral synthetic fuels in order to reach the EU's ambitious targets.

Over the last decades, bioethanol and fatty acid methyl esters (FAME) were blended into gasoline and diesel, respectively, to meet the mandatory renewable shares [9]. The blending rate of bioethanol and FAME is limited by the applicable standards to 10 vol.% and 7 vol.%, respectively [10,11]. Higher shares are possible but may require the adjustment of engine components, as both bioethanol [12,13] and FAME [14] can cause problems with plastics and metals. Another approach is the blending of GHG-neutral synthetic hydrocarbons. Owing to their similarity to fossil hydrocarbons, the advantage of such synthetic fuels is their unfettered applicability, even in older vehicles, without the necessity for constructional adjustments.

Methanol to gasoline (MTG) and dimethyl ether to gasoline (DTG) are processes based on Mobil's discovery for synthesizing high-octane gasoline using a zeolite catalyst [15]. The high octane number (ON) is due to the composition of the fuels, consisting of paraffins, naphthenes, olefins, and, for the most part, methylated aromatics [16]. Both process variants were already commercialized by Mobil and Haldor Topsøe, respectively [17,18], producing similar hydrocarbon product ranges [19]. Research is still underway, for example, with the bioliq® pilot plant at the Karlsruhe Institute of Technology, which produces synthetic gasoline from straw. A decentralized fast pyrolysis is used for biomass liquefaction [20,21], followed by a centralized entrained flow gasification process [22] and a DTG synthesis [23,24]. Synthetic hydrocarbons are a great measure to gradually defossilize the refinery sector in its product variety. For example, mineral oil refinery Oberrhein (MiRO) in Karlsruhe, Germany, recently announced plans to integrate such GHG-neutral hydrocarbon streams into its portfolio [25].

Raw products of an MTG or DTG synthesis are usually separated into light gasoline (LG) and heavy gasoline (HG) to get rid of 1,2,4,5-tetramethylbenzene (durene), which is the largest compound accruing in significant amounts of 3–6 wt.% as a consequence of the underlying methanol-to-hydrocarbon mechanism [26]. While the aromatic-rich LG can be easily incorporated into a refinery due to its similarity to fossil reformate, HG consists almost entirely of C_9–C_{11} aromatics and is especially rich in durene (see Section 2.1 for detailed information). Durene tends to crystallize due to its high melting temperature of 79 °C, which bears the danger of clogging the fuel injection system, causing driveability problems [16]. A further reason for cutting off the heavy aromatics is their strong correlation with increased engine-out hydrocarbon [27] and soot emissions [28], one of the main factors for reduced life expectancy worldwide [29].

Besides its drawbacks, HG originating from a sustainably operated MTG or DTG plant has a GHG reduction potential and thus is of high economic value. Consequently, refineries must search for solutions to process streams rich in heavy aromatics and overcome the negative properties. In Section 1.1, we discuss the most promising processing options and outline the experimental scope of this study. A brief overview of modeling approaches on co-processing is presented in Section 1.2, including the questions that this study aims to answer.

1.1. Processing of Feedstocks Rich in Heavy Mono-Ring Aromatics

Refineries have several options to incorporate an aromatic-rich stream. With little effort, the durene containing HG could be blended into reformate or middle distillate (MD) to dilute durene below a particular concentration at which it no longer crystallizes. Chang [30] found a concentration below 3% sufficient, whereas Olsbye et al. [16] emphasized that there might be climate conditions at which crystallization could still occur. Therefore, such a measure would only be feasible for small volumes of HG. Addi-

tionally, even if crystallization issues are solved, emission tendencies and petrochemical parameters such as the cetane number (CN) remain negatively affected by aromatics [31]. Therefore, an after-treatment is usually applied, e.g., isomerization [32,33] or HP [32,34]. As such processes are capital intensive [35] but are also available in most refineries, the co-processing of bio-derived feedstocks with fossil intermediates is frequently discussed. Besides defossilizing the refinery sector, co-processing bio-derived feedstocks comes with self-evident advantages. It makes biofuels more competitive by saving capital investment, as a highly integrated processing infrastructure [36–38] and a reliable blending and fuel distribution system can be drawn on [39]. Therefore, co-processing is an attractive way to lower production costs while decreasing the GHG impact of synthetic fuels.

Processes regularly found in refineries are (a) transalkylation/disproportionation, (b) fluid catalytic cracking (FCC), and (c) hydrotreating or generally HP. Even if transalkylation and disproportionation are already commercialized, for example, with the Mobil TransPlus^{SM} process [40], these options are not available in every refinery. Additionally, low molecular aromatic streams such as toluene are required for the transalkylation of C_9–C_{11} aromatics, present in HG, toward lighter aromatics. FCC is frequently discussed for co-processing various bio-derived and fossil feedstocks as it is readily found in the refinery environment [41]. Typical FCC feedstocks are vacuum gas oil (VGO) and heavy atmospheric gas oil with boiling temperatures between 280 and 580 °C [42]. Therefore, high boiling feedstocks, such as vegetable oils, animal fats [43], and bio-oils obtained, for example, by flash pyrolysis of biomass [37,44,45], are usually co-processed in FCC units. HG from MTG and DTG processes comes with a boiling range of approx. 177–290 °C (see Section 2.1 for detailed petrochemical parameters) and, therefore, lies below the boiling temperature of typical FCC feedstocks. As HG consists almost entirely of aromatics, it is to expect that almost no reaction takes place besides some dealkylation of ring-attached side chains [46]. Like FCC, HP is virtually found in any refinery [42]. Typically, HP is used to remove heteroatoms such as sulfur, nitrogen, and oxygen from MD [42,47,48]. One of the most commonly applied catalysts is a cobalt-molybdenum (CoMo)-based catalyst for hydrodesulfurization (HDS) [36,49]. HP also became increasingly important for the partial hydrogenation of aromatics [42,50]. For example, the data of Bisht et al. show that hydrogenation of aromatic compounds to naphthenes helps to improve the CN [31]. Simultaneously, the expected emissions are reduced because naphthenes have lower sooting tendencies [51]. HP is reportedly suitable for co-processing aromatic-rich feedstocks such as light cycle oil (LCO), which is comparable to the HG considered in this study in terms of high aromatic content [50,52]. Ancheyta-Juárez proved a product quality improvement for the co-HP of MD and LCO, using a CoMo/γ-Al_2O_3 catalyst [50]. Sági et al. investigated the co-HP of LCO with animal fats and straight run gas oil using a nickel-molybdenum (NiMo)/Al_2O_3 catalyst [52]. Depending on the process conditions, the aromatics were significantly reduced, which resulted in a primarily standard-compliant diesel.

The aim of the experimental part of our study was to investigate the suitability of a common hydrotreater for the co-HP of fossil MD and durene-rich bioliq® HG. We conducted experiments with a feedstock of 15 wt.% durene and 85 wt.% MD according to a local refinery's reaction parameters using a commercially available CoMo/γ-Al_2O_3 catalyst. An important aim was to find stable operating conditions, as high deactivation rates would affect the product quality and the lifespan of the catalyst before regeneration [35]. The results were further used to calculate the hydrogenation and isomerization selectivity of the durene conversion in order to evaluate the catalyst's suitability to improve important fuel parameters linked to the aromatic content. We conducted additional experiments with the aim of evaluating the resulting fuel yields and qualities using a feedstock of 15 wt.% bioliq® HG and 85 wt.% MD. The fuel yields of gasoline, kerosene, and diesel and the economically important parameters ON and CN [53] were of particular interest.

1.2. Modeling of Hydroprocessing

HP involves various reactions, e.g., hydrogenation and dehydrogenation, isomerization, C–C bond scission, hydrogen transfer, and disproportionation [54]. C–C bond scission represents all types of cracking reactions, including exo- and endo-cyclic β-scission of cyclic compounds. Exo-cyclic β-scission means the dealkylation of side chains attached to naphthenes and aromatics, while endo-cyclic β-scission is the ring opening that forms olefins and paraffins [55]. An especially fast mechanism is the so-called paring reaction, becoming relevant for cyclic molecules $\geq C_{10}$, yielding iso-Butane and the respective remaining cyclic carbenium ion by fast tertiary–tertiary β-scission [56]. Which reaction predominates strongly depends on the catalyst used and the reaction conditions [57]. While mostly hydrogenation, i.e., hydrotreating reactions, are favored at medium temperatures, isomerization and cracking reactions become more predominant as the temperature increases [55,58].

Due to the numerous reactions involved and the complex compositions of fossil and biomass-derived feedstocks, HP is regularly modeled with simplified approaches such as discrete lumping models, e.g., [57–67], and substance group lumping models, e.g., [58,59]. In discrete and substance group lumping models, the sample is subdivided into lumps of specific boiling ranges or substance groups [59]. Lumps can be typical refinery products, for example, gasoline, kerosene, and diesel, if boiling ranges are considered, or paraffins, naphthenes, and aromatics in the case of substance groups [54,60]. Lumping by boiling ranges has the advantage of practical accessibility, as boiling curves are convenient to measure [60], while detailed hydrocarbon analysis requires sophisticated techniques such as GC*GC to gain integral information on a sample's composition. Such are available but not as regularly found as boiling range analyzers. As shown in Figure 1, lumps are treated as chemical compounds, and a reaction network is constructed in between [61], where all the individual reactions are lumped together [54,68].

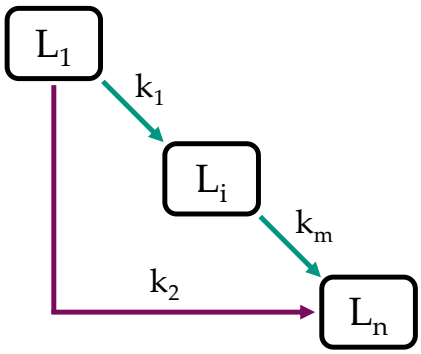


Figure 1. Lumping model with n lumps and m reactions.

In general, a model's predictive power improves as the number of lumps increases, which, however, is also accompanied by an over-proportional increase in kinetic parameters to be determined [54,69]. Further modeling techniques, relying on more detailed knowledge, are continuous lumping models, where a feedstock's reactivity is described as a continuous function, e.g., [54,68], and single event models, where a more in-detail mechanistic knowledge is required, e.g., [69]. Depending on the task, lumping models are as precise as the more complex ones while, however, being restricted to the prediction of prior defined lumps, which must therefore be chosen deftly [57]. Nevertheless, complex reaction systems are relatively straightforward to implement with lumping models, for example, into process simulation software [58,63].

The aim of our study's theoretical part was to develop an application-oriented lumping model for predictions during daily refinery operations about the co-HP of bioliq® HG and fossil MD. By this modeling approach, we strived to precisely predict the fuel yields of gasoline, kerosene, and diesel. The results of the parameter estimation were further evaluated to gain information on the main reactions involved.

2. Materials and Methods

2.1. Experimental Setup and Procedure

Besides the relevant information presented here, a more detailed description of the experimental setup can be found in our prior study [34]. The co-HP experiments were conducted in an electrically heated fixed bed reactor with an inner diameter of 14.9 mm, operated top-down in co-current mode. A total of 67.689 g of a commercially available CoMo/γ-Al_2O_3 catalyst with a particle size distribution of 100–200 µm was filled into the reactor. The first 15 cm of the reactive zone consisted of catalyst diluted with SiC (weight-ratio 70:30) of the same particle size distribution. Further, 30 cm of pure catalyst completed the reactive zone. By this measure, the axial reactor temperature profile could be maintained within ±0.9 °C of the set reaction temperature for all experiments performed. The inlet and outlet of the reactor were additionally filled with SiC (210 µm) over a length of 15 cm and 20 cm, respectively, to keep the catalyst in position and ensure an ideal mixing of the feed components. A central probe tube with an outer diameter of 1/8″ was available for measuring the reactor's temperature profile by axially moving a K-Typ thermocouple.

Table 1 lists the petrochemical parameters of the hydrocarbon fractions used for the experiments in this study.

Table 1. Hydrocarbon fractions used for the experiments in this study.

	Middle Distillate (MD)	**bioliq® Heavy Gasoline (HG)**	**Feedstock**
CN [-]	60.3	N/A	N/A
ρ_{20} [kg m^{-3}]	823.0	890.0	827.6
$w_{sul.}$ [mg kg^{-1}]	<5	0	0
$CFPP$ [°C]	−14	N/A	N/A
$w_{Aromatics}$ [wt.%]	5.7	97.0	approx. 19.4
IBP [°C]	179.7	176.7	175.0
T25 [°C]	247.7	185.7	230.6
T50 [°C]	263.2	190.0	257.5
T75 [°C]	277.6	198.2	275.1
FBP [°C]	365.2	289.8	365.2

MD was provided by ASG Analytik-Service, Neusaess, Germany. It consists mainly of paraffins, about 5.7 wt.% polycyclic aromatic hydrocarbons, and has a sulfur content of below 5 wppm. HG was obtained by rectification of the bioliq® raw gasoline to a top temperature of approx. 176 °C and consists of 33.6 wt.% C_9 and 52.6 wt.% C_{10} aromatics, of which 21.4 wt.% is durene. Another large proportion are C_{12} aromatics at 10.4 wt.%, with the remainder consisting mainly of paraffins and naphthenes. Additionally, dimethyl disulfide (DMDS) (≥99%, Alfa Aesar, Heysham, United Kingdom) and durene (97%, Fisher Scientific GmbH, Schwerte, Germany) were used. The feedstock for the experiments consisted of 15 wt.% HG and 85 wt.% MD (see right column of Table 1), which had a boiling range of 175.0–365.2 °C and an aromatics content of approx. 19.4 wt.%. Additionally, a mixture of 15 wt.% pure durene and 85 wt.% MD with a total aromatic content of approx. 19.8 wt.% was used as feed for several experiments. The boiling range could not be provided as the condenser of the boiling range analyzer got clogged by the crystallization of durene due to its high concentration. Which feed was used for the respective experiments will be indicated in the discussion.

Before the experiments, the CoMo/γ-Al_2O_3 catalyst was activated using a sulfur-enriched stream of MD. Sulfur was added as DMDS, which comes with a sulfur content of 68 wt.% and is frequently used to activate traditional hydrotreating catalysts [65,70]. The amount of DMDS added to the MD was calculated based on the catalyst mass and expected sulfur uptake according to the manufacturer. To ensure complete catalyst activation, the theoretical mass of sulfur was multiplied with a security factor of 1.25. In total, 15.305 g DMDS dissolved in 716 g MD was used as feed to carry out the activation procedure

of 67.689 g catalyst. For the sulfiding process, the following procedure, related to the findings of Texier et al. [70], was applied. Before the sulfidation, the catalyst was dried at 150 °C for 60 h in a pure argon atmosphere. The pump was then set to a feed flow rate of 0.29 mL min^{-1}. Simultaneously, the gas supply was adjusted to a hydrogen and argon flow of 300 mL min^{-1} and 20 mL min^{-1}, respectively. All flow rates were kept constant over the whole sulfidation process. Right after the flows were adjusted, the temperature was increased from 150 °C to 225 °C with a rate of approx. 18.8 °C h^{-1} and held constant at 225 °C for 8 h. After this period, a second temperature ramp of approx. 14.7 °C h^{-1} was applied for 8.5 h, increasing the temperature from 225 °C to 350 °C. The temperature was again kept constant for 8 h at 350 °C, after which the activation procedure was completed. For all following experiments, the feed was enriched with 1000 wppm of sulfur equivalent in the form of DMDS to preserve the active state of the catalyst.

The first set of experiments focused on the conversion, the selectivity, i.e., differentiation between hydrogenation and isomerization of durene, and the catalyst deactivation. For these experiments, MD was enriched with 15 wt.% of durene. For approx. 860 h on stream, experiments were conducted at 320 °C, 350 °C, and 380 °C for a constant LHSV of 0.4 h^{-1}, a constant total pressure of 62.9 bar (59 bar H_2, 3.9 bar Ar), and a ratio $\dot{V}_{H_2}/\dot{V}_{Feed}$ of 1042 Nm^3 m^{-3}. Argon was added as an internal standard for calculating the volume flow rates of the gaseous products. Related product concentrations were measured with an Agilent 7890A online gas chromatograph (GC). All liquid samples' compositions were measured using an Agilent 7890B according to ASTM 6730-01 [71].

As shown in Figure 2, a reference point at T = 380 °C and LHSV = 0.25 h^{-1} was set every weekend to keep track of possible catalyst deactivation. After approx. 1000 h on stream, the catalyst deactivation was negligibly low and further experiments were conducted under nearly steady-state conditions (see Figure S1 in Supplementary Materials).

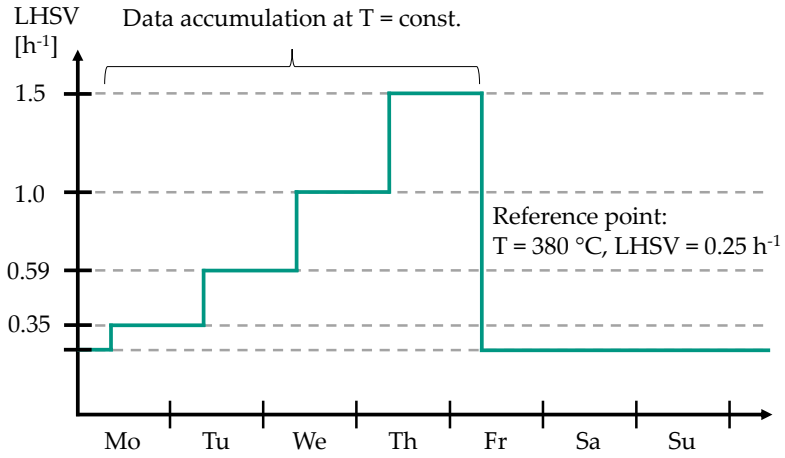


Figure 2. Weekly experimental procedure for the parameter study with a feedstock of 85 wt.% MD and 15 wt.% bioliq® HG.

For these experiments, 85 wt.% MD was enriched with 15 wt.% bioliq® HG (see Table 1 for petrochemical parameters). A parameter study was conducted to investigate durene and C_{10} aromatics conversions in dependence on temperature and LHSV. Additionally, the fuel yields, i.e., gasoline, kerosene, and diesel, were measured for the conducted experiments. Typical HP temperatures of 340–390 °C were set at weekly intervals. As can be seen in Figure 2, for 350 °C, 370 °C, 380 °C, and 390 °C, the LHSV was set to 0.35 h^{-1}, 0.59 h^{-1}, 1.0 h^{-1}, and 1.5 h^{-1} on a daily basis. At 340 °C, LHSVs of 0.25 h^{-1}, 0.5 h^{-1}, 0.75 h^{-1}, and 1.20 h^{-1} were investigated. The ratio $\dot{V}_{H_2}/\dot{V}_{Feed}$ was kept constant at 1042 Nm^3 m^{-3} for all conducted experiments. All samples obtained from the feedstock consisting of 15 wt.% bioliq® HG and 85 wt.% MD were additionally separated into LG (30–170 °C) and diesel (170–365 °C) using a water-cooled laboratory-scale rectification column with a capacity of 250 mL. ONs and CNs of the obtained gasoline and diesel fractions were measured using

an OptiFuel from PAC (Houston, TX, USA). Additionally, the compositions of the gasoline samples were measured using a Reformulyzer M4 from AC PAC (Houston, TX, USA). The data obtained from the parameter study were subsequently used to develop three lumping models, the methodology of which is explained in the following.

2.2. Model Structure and Procedure

Three lumping models are presented in this study, two of which are based on different assumptions regarding the reaction network. Based on the findings, a third optimized model is developed. As mentioned in Section 2.1, all models are based on the data obtained from the experiments with a feedstock of 15 wt.% bioliq® HG and 85 wt.% MD (see Table 1 for petrochemical parameters). Four datasets at reaction temperatures of 340 °C, 350 °C, 380 °C, and 390 °C were used for the parameter estimation, with one dataset at 370 °C left out for independent validation of each model. The experimental data for the parameter estimation can be found in Table S1 in the Supplementary Materials.

Boiling curves of feed and products were measured according to ASTM D7345 [72] and subdivided into lumps. The number of lumps was chosen based on the results of other researchers. Alhumaidan et al. [63] investigated three models for the same dataset having four, five, and ten lumps, respectively. They found no significant increase in the models' performances if the number of lumps was increased from five to ten and highlighted the tendency of over-fitting. Similar results were reported by Ayasse et al. [61], who compared three models with five, six, and seven lumps for modeling the hydrocracking of bitumen. They achieved similar accuracies for all three models and stated an over-determination for the seven-lump model. It can be concluded that the number of lumps should be chosen only as high as necessary to describe the product composition at hand with the required accuracy. In this study, five liquid lumps were found sufficient to describe the fuels of interest, i.e., gasoline, kerosene, and diesel. A sixth lump represents the gaseous losses, calculated based on a mass balance. Table 2 lists the six lumps considered in this study. Besides their boiling ranges, information on their rough compositions and initial mass fractions (feedstock) is also given.

Table 2. Boiling ranges, compositions, and inital mass fractions of the lumps used for modeling (Naph. ≙ Naphtenes, Par. ≙ Paraffins, Aro. ≙ Aromatics).

Lump	Boiling Range [°C]	Approx. Composition	L_i @ τ = 0 [wt.%]
1	300–365	Mainly Par.	11.25
2	270–300	Aro., Par.	21.51
3	210–270	Aro., Par.	61.64
4	170–210	Aro., Par. and Naph.	5.61
5	30–170	Aro., Par. and Naph.	0
6	0–30	Par.	0

Gaseous losses (0–30 °C) are represented by lump 6, LG (30–170 °C) by lump 5, HG by lump 4, kerosene (170–270 °C) by the summation of lumps 3 and 4, and diesel (170–365 °C) by the summation of lumps 1–4. Lumps 1–4 consist primarily of paraffins as they strongly overlap with the MD-rich feedstock. Lumps 2–5 are additionally enriched with aromatics originating from bioliq® HG, of which lump 4 has the highest share of aromatics according to the HG boiling range. Gas lump 6 is, with good approximation, entirely paraffinic, resulting from cracking and dealkylation reactions. Cracking and hydrogenation reactions will further result in an enrichment of the lighter lumps with paraffins and naphthenes. Discussions on the mass distribution due to HP reactions will be presented in Sections 3.2 and 3.3.

The modeling of the experimental data was based on assumptions, which are highlighted in the following. After approx. 1000 h on stream, the catalyst activity could be considered constant, so the experiments for data acquisition were conducted under near steady-state conditions. For constant monitoring, a reference point was adjusted every 6th

and 7th day on stream (see Figure 2). Deactivation was quantified as a relative conversion loss of 1.1–2.2% between 1450 h and 2150 h on stream, which is within measurement uncertainty (see Figure S1 in the Supporting Materials). Furthermore, the experiments were considered to be conducted under isothermal conditions, which was ensured by catalyst dilution, as explained in Section 2.1. As proven experimentally [73], HP reactions, e.g., HDS, HDN, and hydrocracking, are frequently considered independent of the hydrogen concentration and thus of first order with respect to the feed [58,61,63,66]. Due to a high excess of hydrogen in the experiments of this study, the rate expressions are considered first order. For all three models, the reactions are further considered irreversible. This seems difficult since up to 19.4 wt.% aromatics are present in the feed, whose hydrogenation is a thermodynamically limited equilibrium reaction [74]. However, with such simplification, good results were obtained in the literature [59,66]. To review the validity of this assumption, we conducted an additional temperature variation from 350 °C to 400 °C in 10 °C steps at a relatively low LHSV of 0.4 h^{-1} (see Figure S2 in the Supplementary Materials). It was found that the durene conversion increases rapidly from 350 °C to 380 °C and slower between 380 °C and 390 °C, which indicates the equilibrium getting noticeable. Therefore, it can be assumed that the reverse reactions can be neglected for the parameter range and the catalyst investigated in this study. Considering the above-stated and by assuming ideal plug flow reactor conditions, the component mass balances of each lump,

$$\frac{dw_i}{d\tau} = -w_i \sum_{z=1}^{N} k_{i,z} + \sum_{z=1}^{N} w_z \cdot k_{z,i}, \tag{1}$$

are developed, where w_i and w_z are the mass fractions of lump i and z , respectively, and $k_{i,z}$ and $k_{z,i}$ are the rate constants for reactions from lump i to z and lump z to i, respectively. The space-time τ,

$$\tau = \frac{1}{LHSV}, \tag{2}$$

is directly linked to the $LHSV$, which was calculated based on the actual catalyst volume. For the CoMo/γ-Al_2O_3 catalyst used in this study, a particle density of 2.69 $\pm$ 0.14 g cm^{-3} was measured using an Ultrapyc 1200e from Quantachrome (Boynton Beach, FL, USA). The temperature dependencies of the reaction rates in Equation (1) were modeled using the reparameterized Arrhenius equation,

$$k_j = k_{0,j} \cdot e^{-\frac{E_{A,j}}{R}\left(\frac{1}{T}-\frac{1}{T_{Ref}}\right)}, \tag{3}$$

where k_j is the rate constant of reaction j, $k_{0,j}$ is the pre-exponential factor for a given reference temperature T_{ref}, $E_{A,j}$ is the activation energy and T the reaction temperature. T_{ref} was set to 365 °C, which lies in the middle of the investigated temperature range in this study. The reparameterized equation avoids strong correlations between activation energies and rate constants during fitting [58].

The model equations are constructed from Equations (1)–(3) and solved considering each lump's initial conditions (τ = 0) listed in Table 2. Depending on the number of lumps and reactions, the pre-exponential factors and activation energies in the resulting model equations must be determined. The best set of kinetic parameters was obtained by minimization of the objective function,

$$SSE = \sum_{j=1}^{n_e} \sum_{i=1}^{n_l} (w_{exp,i} - w_{calc,i})^2, \tag{4}$$

based on the sum of square errors between the measured product weight fractions $w_{exp,i}$ and the calculated product weight fractions $w_{calc,i}$, for all lumps n_l and conducted experiments n_e [75]. For the least-squares minimization, the lmfit package in Python was used [76]. A first estimation of the parameter set was either performed by the Levenberg–Marquardt

or the Nelder–Mead algorithm. In most cases, the slower but more robust Nelder–Mead algorithm provided a more promising first guess. In contrast, the final parameter estimation was mainly performed with the Levenberg–Marquardt algorithm, as it is strong in finding an optimum if the set of parameters is already close to the global solution [76]. The system of ODEs was solved using scipy.integrate, a sub-package of scipy [77] based on the Runga–Kutta algorithm. However, in some cases, Runga–Kutta was found to fail. If so, the algorithm was switched automatically using the LSODA algorithm. LSODA is a method with automatic stiffness detection and subsequent switching of the solver, e.g., Adams (non-stiff) to BDF (stiff) [77].

As mentioned, three models are developed and compared based on the same data in this study. If the data are described more precisely by model B than by model A, and model B does so with different degrees of freedom, it is helpful to evaluate whether this improvement is statistically valid, for example, using Fisher's exact test. A lower error with model B than model A is significant if the condition,

$$F_{A-B} = \frac{\frac{SSE_A - SSE_B}{SSE_B}}{\frac{\nu_A - \nu_B}{\nu_B}} > F_{1-\alpha}(\nu_A - \nu_B, \nu_B), \tag{5}$$

is fulfilled, where $F_{1-\alpha}(\nu_A - \nu_B, \nu_B)$ is the critical value of the F-distribution, $SSE_{A/B}$ are the sums of square errors (SSE) and $\nu_{A/B}$ the degrees of freedom [58]. The degrees of freedom of model i,

$$\nu_i = n_{l,i} \cdot n_{e,i} - n_{p,i}, \tag{6}$$

are calculated based on the number of lumps n_l, number of parameters n_p, and number of experiments n_e. $F_{1-\alpha}(\nu_A - \nu_B, \nu_B)$ depends on the level of significance, which was chosen with 95 % (α = 0.05) [58]. If the condition of Equation (5) is not fulfilled, the improvement of model B over model A is insignificant, meaning the model with fewer parameters is preferred. The critical values of the F-distribution $F_{1-\alpha}(\nu_A - \nu_B, \nu_B)$ were calculated with Excel®'s finv function. Input parameters are the degrees of freedom, ν_A and ν_B, and the probability α.

3. Results and Discussion

3.1. Co-Hydroprocessing of Middle Distillate and Heavy Mono-Ring Aromatics

Data discussed in the following were collected over 860 h on stream at three reaction temperatures of 320 °C, 350 °C, and 380 °C for a constant LHSV of 0.4 h^{-1}, a constant total pressure of 62.9 bar (59 bar H_2, 3.9 bar Ar), and a ratio $\dot{V}_{H_2}/\dot{V}_{Feed}$ of 1042 $Nm^3\ m^{-3}$ using a feedstock consisting of 15 wt.% pure durene and 85 wt.% MD. Additionally, data originating from a temperature variation between 350 °C and 400 °C at pseudo-steady state conditions is discussed in this section.

Figure 3a shows the durene conversion,

$$X_{durene} = \frac{w_{durene,in} - w_{durene,out}}{w_{durene,in}}, \tag{7}$$

where $w_{durene,in}$ and $w_{durene,out}$ are the respective mass fractions of durene in the feedstock and product, respectively, over a time on stream (TOS) of approx. 860 h, in dependence on temperature. Dashed curves are drawn to clarify the trend and are not based on any mathematical model. At all temperatures studied, especially 320 °C and 350 °C, the durene conversion decreases rapidly in the first hours on stream. The substantial decrease can be explained by catalyst coking, occurring disproportionately in the first hours on stream [65,78]. After a certain decline, the deactivation seems to continue to decrease linearly at all three temperatures, with a pseudo-steady-state presumed at 380 °C. Similar findings were reported by Vivas-Báez et al. [78], who investigated the HP of VGO using a sulfided NiMo/USY catalyst. In their experiments, the catalyst activity decreased significantly in the first 170 h on stream. After this period, deactivation decelerated, and

the conversion developed toward a steady-state after approx. 1700 h on stream. In our experiments, it is also noticeable that the hydrogenation conversion increases strongly with increasing reaction temperature, which was also found by other authors [50,58,66]. More precisely, in the present study, durene conversion increased up to the highest reaction temperature investigated, 400 °C (see Figure S2 in the Supplementary Materials), while no conversion maximum was observed as a consequence of equilibrium influence, as found by other authors [52]. This is due to the additional influence of other process parameters on the hydrogenation equilibrium, e.g., an increased hydrogen pressure, which shifts the hydrogenation maximum toward higher reaction temperatures [50,74]. As explained in Section 1.1, aromatics negatively influence a fuel's petrochemical parameters and emission tendencies. Therefore, we additionally considered the durene isomerization selectivity,

$$S_{iso-C10} = \frac{w_{iso-C10,out} - w_{iso-C10,in}}{w_{durene,in} - w_{durene,out}}, \quad (8)$$

where $w_{iso-C10,in}$ and $w_{iso-C10,out}$ are the mass fractions of all C_{10} aromatics besides durene in the feedstock and product, respectively.

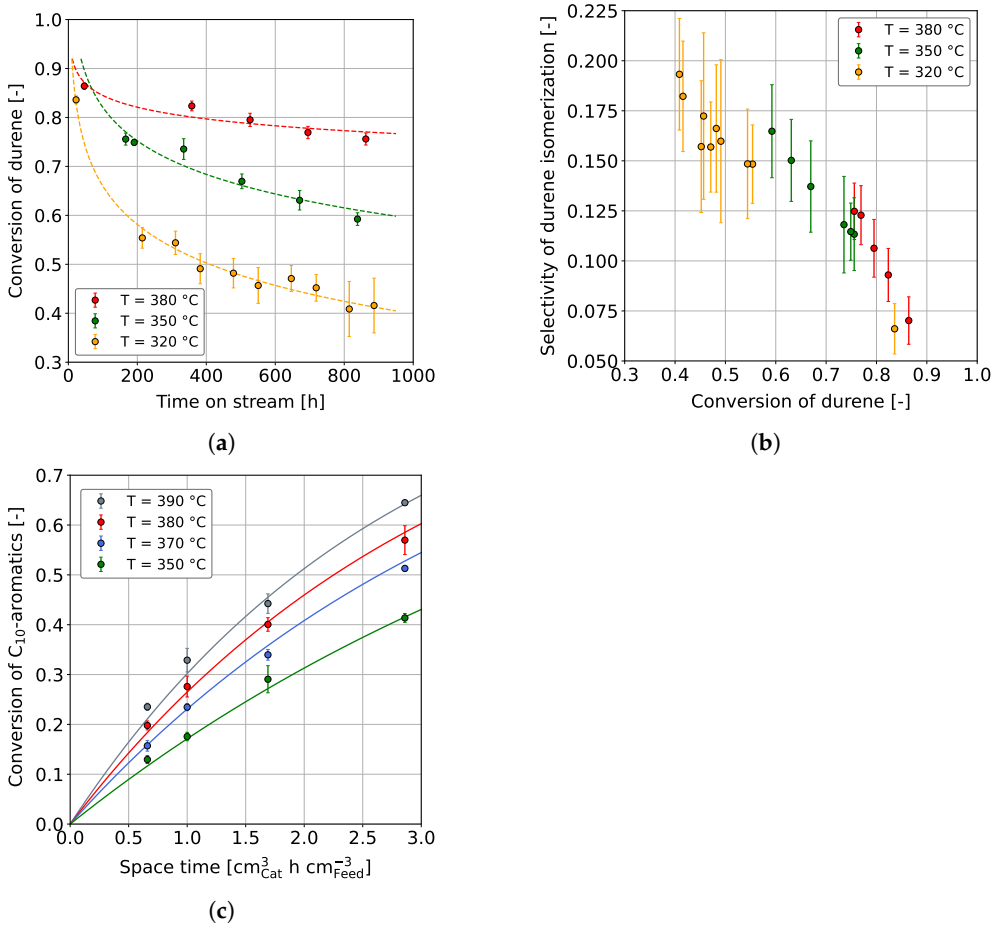


Figure 3. (**a**) Durene conversion and (**b**) durene isomerization selectivity for the co-HP of durene (15 wt. %) and MD (85 wt. %) at constant $LHSV$ = 0.40 h^{-1}, and (**c**) C_{10} aromatic conversion for the co-HP of HG (15 wt. %) and MD (85 wt. %); $\dot{V}_{H_2}/\dot{V}_{Feed}$ = 1042 Nm^3 m^{-3}, $\bar{p}_{H_2}$ = 59 bar, and $\bar{p}_{Ar}$ = 3.9 bar.

From the prior mentioned, the selectivity must be low to favor hydrogenation. In Figure 3b, the durene isomerization selectivity is plotted over durene conversion for the temperatures 320 °C, 350 °C, and 380 °C. In general, the isomerization selectivity decreases with conversion, on the first view independent of the reaction temperature. However, slight differences can be observed, although these are not highly significant due to measurement

error. The selectivity curve slightly shifts upward at higher reaction temperatures, favoring isomerization. This change in selectivity is most likely due to the influence of the chemical equilibrium on the hydrogenation of aromatics at increased reaction temperatures [74]. An influence of the deactivation is unlikely since the data points were measured over 860 h on stream and no trend could be perceived between points measured early compared to points measured later in the campaign.

We finally investigated the co-HP at nearly steady-state catalyst conditions (1.1–2.2% of relative activity loss), using a blend of 15 wt.% bioliq® HG and 85 wt.% MD as feedstock. Additionally, the data obtained from these experiments were used for modeling purposes, as discussed in Section 3.3. The experiments' scope can be comprehended in Table S1 in the Supplementary Materials.

Figure 3c shows the C_{10} aromatics conversion over space-time in dependence on temperature. The C_{10} aromatics conversion increases with higher temperature, similar to Figure 3a for a feedstock containing pure durene. As expected, a higher space-time also increases the conversion of C_{10} aromatics, which is also confirmed by other studies [50,58,63,64]. Figure 3c also shows the modeled conversions, applying the reparameterized Arrhenius equation at T_{ref} = 365 °C. For the hydrogenation of C_{10} aromatics, a pre-exponential factor k_0 of 0.26 cm^3_{Feed} h^{-1} cm^{-3}_{Cat} and an activation energy E_A of 55.8 kJ mol^{-1} were found, which lies in the range of activation energies found by other authors for various catalysts and aromatics [74].

It can be concluded that a high reaction temperature is beneficial for the co-HP of heavy aromatics such as durene and MD. The overall aromatic conversion is higher, reducing the isomerization selectivity in favor of hydrogenation. An increased reaction temperature of ≥380 °C is further beneficial as the catalyst reaches pseudo-steady-state conditions faster. A higher C_{10} aromatics conversion was additionally reached by increasing the space-time (lower LHSV). Controlling the aromatic hydrogenation over temperature is preferred due to the mentioned benefits but also for process reasons, as the throughput remains unchanged. At the same time, the reaction temperature cannot be increased without constraints. This is partly for constructional reasons, and partly because the reaction temperature is regularly increased to counteract ongoing deactivation. Therefore, the options need to be weighed individually.

3.2. Fuel Yields and Qualities

In addition to removing aromatics, fuel yields, i.e., gasoline, kerosene, and diesel, and the corresponding petrochemical parameters are also of interest to a refinery. The economically most important parameters for gasoline and diesel are the ON, i.e., research octane number (RON) and motor octane number (MON), and the CN, respectively. In the case of kerosene, no further parameters were investigated besides the yield. As the feed mainly consists of linear paraffins and no strong isomerization activity of the catalyst was found in the durene experiments, further downstream processing, such as hydroisomerization, is likely required to meet the low temperature requirements of Jet-A1 [79]. The discussions in this section are based on the samples collected from the experiments presented in Section 3.1 with a feedstock of 15 wt.% bioliq® HG and 85 wt.% MD.

Figure 4a shows the mass fractions of LG, kerosene, and diesel as a function of space-time in dependence on reaction temperature. The gas fraction is not shown, as it does not represent a valuable product fraction. However, further information can be found in Section 3.3 and in the Supporting Materials in Figure S3. It has to be noted that the boiling ranges of kerosene and diesel overlap each other. Consequently, adding up all three fractions would result in a mass fraction above 100%. The mass fraction of diesel decreases while LG increases with rising space-time. This is further enhanced by a higher reaction temperature, which is especially visible for a temperature increase from 380 °C to 390 °C. The observed is due to temperature-sensitive reactions involved in hydrocracking [67]. Similar dependencies on the process conditions are reported in the literature [62,63,66]. For example, Alhumaidan et al. found the same strong influence of the temperature on

the hydrocracking of atmospheric residues [63]. In the present study, the hydrogenation of C_9 and C_{10} aromatics in the HG forms naphthenes with the same carbon number; however, at a lower boiling range of approx. 140–155 °C. Additionally, the dealkylation of cyclic molecules leads to the formation of smaller aromatics and naphthenes in the gasoline boiling range. This can be comprehended in Figure 5, which shows the weight fractions of aromatic and naphthene lumps in LG for a reaction temperature of 370 °C in dependence on space-time. The C_9 and C_{10} aromatics decrease with space-time due to enhanced hydrogenation, as previously shown in Figure 3c, while C_9 and C_{10} naphthenes, the direct hydrogenation products, increase. The weight fraction of $\leq C_8$ aromatics follows that of the lumped C_9 and C_{10} aromatics, indicating that the dealkylation of aromatics is responsible for their occurrence. Naphthenes $\leq C_8$ are formed by hydrogenation of the respective aromatics and by dealkylation of large naphthenes. Simultaneously, this fraction reacts to paraffins (not shown), thus being an intermediate that shows a maximum at a space-time of 1 cm^3_{Cat} h cm^{-3}_{Feed} in the investigated parameter range.

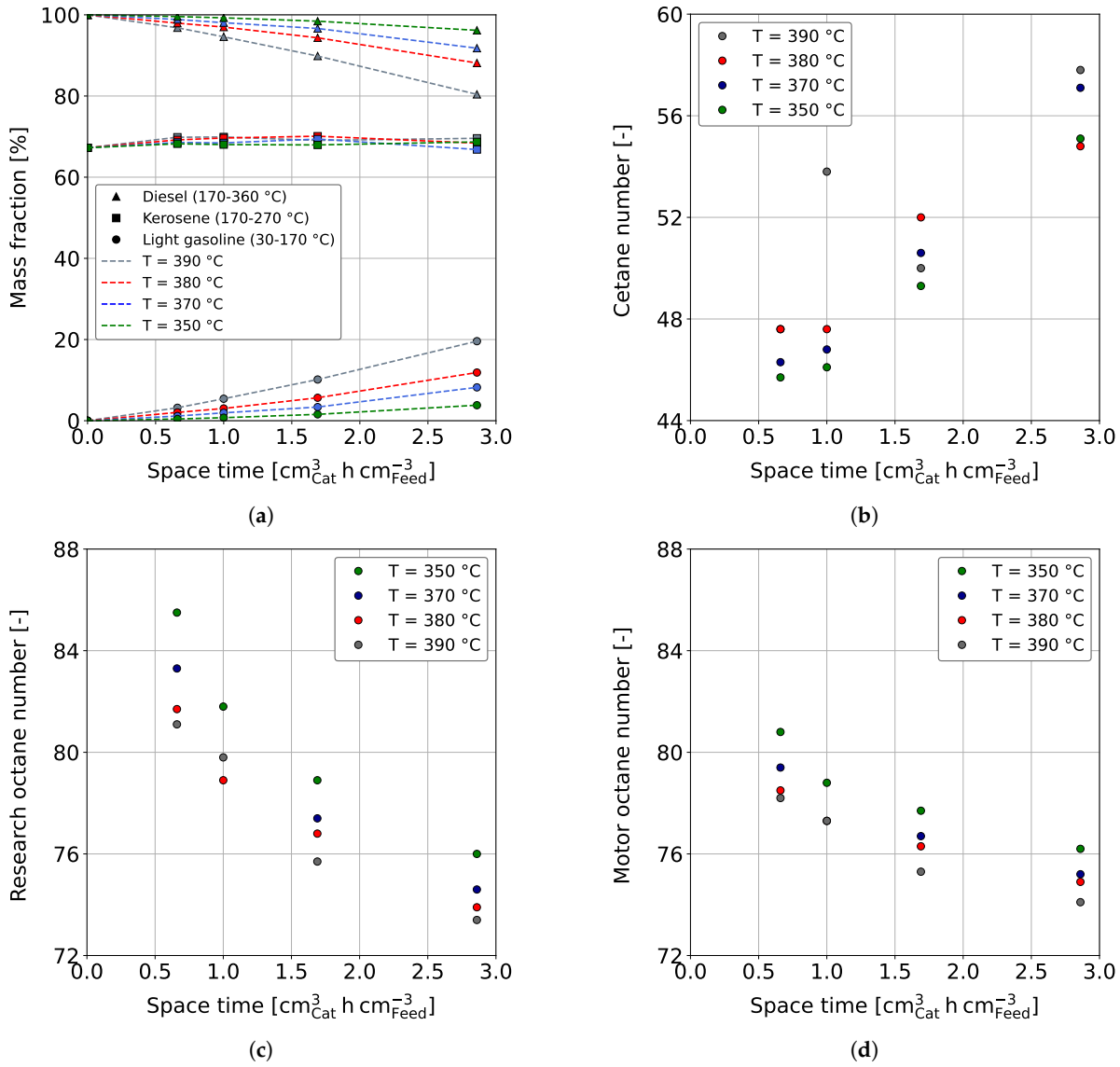


Figure 4. (**a**) Yield of diesel (triangles), kerosene (squares), and LG (circles), (**b**) CN of diesel, (**c**) RON of LG, and (**d**) MON of LG for the co-HP of HG (15 wt.%) and MD (85 wt.%) at $LHSV$ = 0.40 h^{-1}, $\dot{V}_{H_2}/\dot{V}_{Feed}$ = 1042 Nm^3 m^{-3}, $\bar{p}_{H_2}$ = 59 bar and $\bar{p}_{Ar}$ = 3.9 bar.

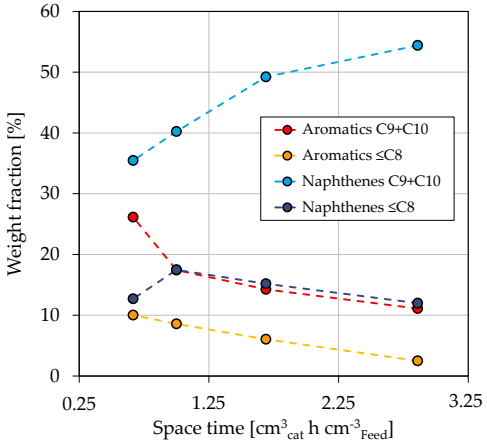


Figure 5. Concentration of aromatics and naphthenes in LG in dependence on space-time at T = 370 °C, $\dot{V}_{H_2}/\dot{V}_{Feed}$ = 1042 Nm^3 m^{-3}, $\bar{p}_{H_2}$ = 59 bar and $\bar{p}_{Ar}$ = 3.9 bar.

Following this argumentation, one would also expect a decreasing yield for kerosene, as the boiling range of HG strongly overlaps with the one of kerosene (see Table 1). However, the kerosene yield stays almost constant over the parameter range investigated. This is probably explained by a pseudo-equilibrium of kerosene-producing and reducing reactions. In fact, there are reactions that exclusively increase kerosene yield, such as the partial hydrogenation of poly-aromatic hydrocarbons (PAHs) already contained in MD. Decalin, the hydrogenation product of the smallest existing PAH naphthalene, has a boiling temperature of approx. 189 °C. Thus, it can be assumed that hydrogenation products of PAHs increase the kerosene yield (170–270 °C) while being of minor influence on the LG yield (30–170 °C). Additionally, it is reported by several authors that catalysts, as used in the present study, are highly cracking selective toward MD fractions [63,65,66] while of a comparably low selectivity toward light boiling hydrocarbons such as gasoline and gases. Consistent with the mentioned, gases were reported to be produced mainly from heavy hydrocarbons [61,62,64,65] and, in fact, stayed within 5.4 wt.% in the present study. Authors stated that increasing cracking activation energies [65] and lower overall reaction rates [63] from heavy to lighter feedstocks are responsible for the observed. Interestingly, such selectivity is typical for catalysts such as CoMo/γ-Al_2O_3, as used in this study, whereby HP catalysts based on zeolites are reported to produce significantly more gasoline [66].

As outlined in Section 2.1, we separated each sample into gasoline and diesel and measured the ONs (RON and MON) and CN, respectively. Figure 4b shows the CN in dependence on space-time and temperature. It can be observed that the CN increases with space-time and reaction temperature. This is due to a decrease in the concentration of aromatics, as shown in Figure 3c, which generally have poor CNs [31]. The required space-time to provide a respective CN is thus higher if a lower reaction temperature is considered. An increasing diesel quality with higher reaction temperature and space-time was also reported by Ancheyta et al. for the co-processing of MD and LCO [50]. Figure 4b shows some outliers, which are due to measurement uncertainties and, in particular, uncertainties in sample distillation. The CN reaches over a wide range of approx. 46–58 for the investigated process conditions. Therefore, diesel that meets the minimum CN of 51 of EN 590 can be provided for every reaction temperature investigated, even if a loss is observable for all samples taken compared to the pure MD (CN = 60.3).

Figure 4c,d shows the RON and MON, respectively, in dependence on space-time and reaction temperature. It can be seen that RON and MON decrease with space-time and temperature due to increased hydrogenation of aromatics (see Figure 3c), having high ONs [80]. In general, CN and ONs are oppositely dependent on the reaction conditions. The more significant decrease in RON compared to MON can be explained by the change in

the chemistry of the samples with increasing degrees of hydrogenation and cracking. While aromatics have high RONs, naphthenes and paraffins have comparably high MONs [80].

It can be concluded that high reaction temperatures and space-times reduce diesel yield and increase gasoline yield, while kerosene yield remains constant over the range of parameters studied. Additionally, high reaction temperatures and space-times are favorable for the CN but negatively influence RON and MON due to enhanced hydrogenation of aromatics. Even if beneficial for ONs, a high aromatic content is not to strive for in the case of this study. As outlined in Section 1, heavy aromatics, especially durene, have clear downsides. Therefore, we emphasize that a further evaluation of the fuels' petrochemical parameters should be carried out. In particular, the cold filter plugging point (CFPP) should be considered, as durene could have negative effects due to crystallization issues.

3.3. Parameter Estimation and Model Validation

To make process decisions in daily operations, refineries must have models that can predict important product yields. Due to the high complexity of the reactions involved in HP, lumping models are frequently applied. Discrete lumping models can differ in the number of lumps and reaction paths, making it interesting to investigate how different model frameworks fit the same set of experimental data. Figure 6 shows the three lumping models we investigate in this work, all based on six lumps but on different assumptions regarding the reaction network. Five liquid lumps and one gaseous one were chosen as it was identified as the sweet spot between predictive power and the number of parameters to be estimated (see Section 2.2).

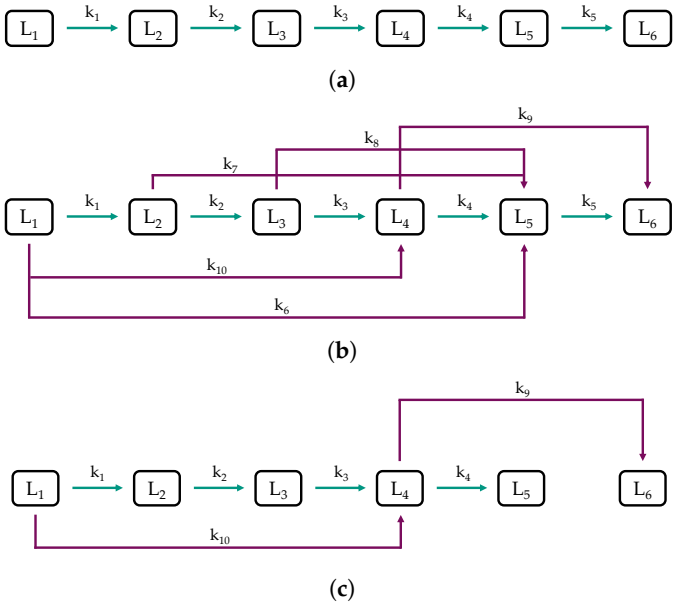


Figure 6. Structures of the (**a**) sequential model, (**b**) combined model, and (**c**) reduced model.

Figure 6a shows the sequential model, consisting of a cascade of reactions toward lower boiling lumps. It was considered because such simplified models obtained good results in the literature [58,63,65]. As shown in Figure 6b, the combined model is a detailed discrete lumping model based on the sequential model with additional assumptions, which are also frequently found in the literature [57,58,60–62,64–66]. As the feedstock used in this study consists almost exclusively of paraffins and mono-ring aromatics (see Section 2.1), important reactions are the hydrogenation of aromatics and cracking reactions, i.e., dealkylation of naphthenes and aromatics, and cracking of paraffins. We assumed an ideal hydrocracking of paraffins, which was, for example, reported by Becker et al. for the HP of VGO using a common hydrotreating catalyst [68]. Ideal hydrocracking is tantamount to predominant cracking in the middle of the hydrocarbon chain, resulting in a bell-shaped

molar distribution curve [55]. For example, lump 1, rich in C_{19} paraffins, would react mainly to C_{10} and C_9 paraffins, which end up as a large share in lump 5 (reaction k_{10}) due to their boiling range. The reactions k_6, k_7, k_8, and k_{10} are constructed following the same assumptions. Additionally, as the feed is rich in C_9 and C_{10} aromatics, which are primarily concentrated in lump 4, due to their boiling temperatures, dealkylation was considered with reaction k_9. Dealkylation forms of lighter naphthenes and aromatics besides gaseous compounds $\leq C_4$, as outlined in Section 1.2. Finally, a reduced model was developed based on the findings obtained from the sequential and combined model to minimize the number of parameters and thus the risk of over-fitting [81]. The experimental datasets used to develop the models can be found in Table S1 in the Supplementary Materials.

Figure 7a,b show the parity plots of the sequential and the combined model, respectively, for the validation dataset at 370 °C.

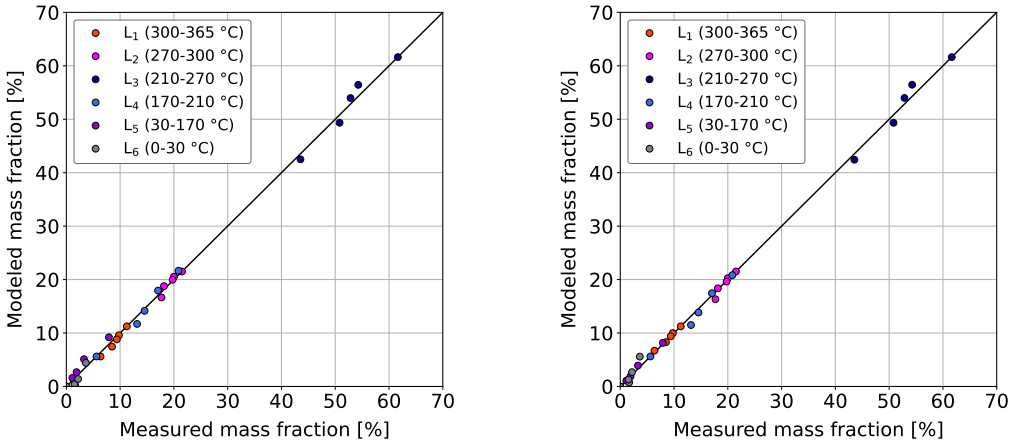


Figure 7. Parity plots of the (**a**) sequential model and (**b**) combined model for the experimental validation dataset at T = 370 °C, $\dot{V}_{H_2}/\dot{V}_{Feed}$ = 1042 $Nm^3\ m^{-3}$, $\bar{p}_{H_2}$ = 59 bar and $\bar{p}_{Ar}$ = 3.9 bar.

It can be seen that both models provide similar qualitative agreements between the measurements and respective model predictions, whereby the combined model returns a slightly better coefficient of determination (0.9978 > 0.9971). Therefore, it can already be concluded that the additional cracking reactions do not bring major benefits. This could be because ideal hydrocracking is insignificant because of the comparatively low acidity of the CoMo/γ-Al_2O_3 catalyst used. As a result, a non-carbenium ion-based reaction pathway, such as thermal cracking, could become more important [55]. This gets additional meaning since ideal hydrocracking is usually observed at lower reaction temperatures of about 250 °C [55]. Similar good performances of sequential lumping models for the hydrocracking of heavy hydrocarbons were also reported by other authors [58,63,65]. The same can be comprehended in Table 3, where the reactions k_6, k_7, and k_8 have pre-exponential factors clearly below those of the remaining ones.

The low but still significant pre-exponential factor of reaction k_{10} and the insignificance of reaction k_5 can be interpreted as high cracking selectivity of heavy lumps toward gases, as observed for similar sulfided catalysts [61,62,64,65]. Reaction k_9, with its high pre-exponential factor, in the first view, is not in line with the prior statement as gas is formed from the low boiling LG. The observed can be explained with dealkylation reactions (see Figure 5), producing low boiling aromatics, naphthenes, and gases.

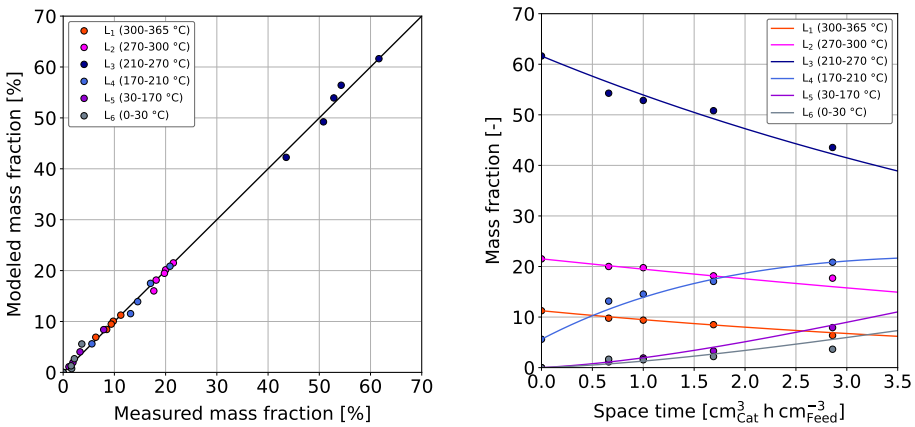
For most of the reactions, the calculated activation energies lie in the magnitude found by other authors [57,64,65], even though it must be stated that kinetic parameters of lumping models are highly dependent on the system, e.g., feed and model structure, and should therefore be compared with care [61]. The $E_{A,7}$ of the combined model is comparatively high, which, together with the small pre-exponential factor, emphasizes the overall insignificance of reaction k_7. $E_{A,10}$ also appears comparably high, which might be due to two

reasons. The investigated temperature range could be too low for a pronounced cracking, and the high activation energy indicates its importance for increased temperatures. More likely is that the reaction is misplaced or another is missing, better representing the actual reaction mechanism. As discussed above, other studies have identified heavy fractions as major sources for the production of low molecular hydrocarbons, which correspond to a reaction of heavy lump 1 (maybe also lump 2) to lump 6.

Table 3. Reaction constants $k_{0,i}$ and activation energies $E_{A,i}$ of the different models.

	$k_{0,j}$ $\left[\mathrm{cm}^3_{Feed}\ \mathrm{h}^{-1}\ \mathrm{cm}^{-3}_{Cat}\right]$				$E_{A,i}$ $\left[\mathrm{kJ\ mol}^{-1}\right]$		
	Sequential	**Combined**	**Reduced**		**Sequential**	**Combined**	**Reduced**
$k_{0,1}$	0.206	0.119	0.123	$E_{A,1}$	116.3	0	0
$k_{0,2}$	0.156	0.135	0.142	$E_{A,2}$	142.4	79.9	89.8
$k_{0,3}$	0.186	0.181	0.185	$E_{A,3}$	54.1	19.1	22.9
$k_{0,4}$	0.264	0.160	0.161	$E_{A,4}$	97.0	109.9	122.4
$k_{0,5}$	0.360	6.09×10^{-7}	-	$E_{A,5}$	0	24.9	-
$k_{0,6}$	-	3.20×10^{-7}	-	$E_{A,6}$	-	0	-
$k_{0,7}$	-	9.25×10^{-8}	-	$E_{A,7}$	-	1845.5	-
$k_{0,8}$	-	9.65×10^{-7}	-	$E_{A,8}$	-	15.8	-
$k_{0,9}$	-	0.126	0.126	$E_{A,9}$	-	12.1	11.0
$k_{0,10}$	-	0.036	0.025	$E_{A,10}$	-	382.6	435.4

The results from the sequential and combined models were further used to develop a reduced model in which insignificant reactions were omitted. In general, the obtained kinetic parameters (see Table 3) agree with those found for the combined model, and the prior interpretation can be drawn on. Figure 8 shows the results obtained for the reduced model.



(**a**) (**b**)

Figure 8. (**a**) Parity plot and (**b**) curve fitting results of the reduced model for the experimental validation dataset at T = 370 °C, $\dot{V}_{H_2}/\dot{V}_{Feed}$ = 1042 $\mathrm{Nm^3\ m^{-3}}$, $\bar{p}_{H_2}$ = 59 bar and $\bar{p}_{Ar}$ = 3.9 bar.

The parity plot shown in Figure 8a confirms a qualitatively good fit. As expected, with 0.9976, the coefficient of determination lies between the ones for the sequential and combined model ($R^2_C > R^2_R > R^2_S$).

Fisher's exact test was applied to the model predictions for the validation dataset at 370 °C to verify that a parameter reduction justifies a loss of accuracy. Calculations were made according to Equations (5) and (6) as described in Section 2.2. The parameters and results are shown in Table 4. By comparing the sequential and reduced model, it was obtained that $F_{S-R} > F_{1-\alpha}$, which means that the condition is fulfilled. Therefore, the improvement from the sequential to the reduced model is statistically significant, and one should prefer the reduced model. If the reduced and the combined model are compared by

Fisher's exact test, it is obtained that $F_{R-C} < F_{1-\alpha}$. The statistical difference between the reduced and combined model is insignificant, so the reduced model should be preferred. Consequently, the combined model is more accurate but insignificant in terms of the higher number of parameters involved.

Figure 8b additionally shows measured and computed mass fractions of the different lumps for the experimental validation dataset at 370 °C. As can be seen, all measurements of the different lumps are described very well, and no significant over or under-determination can be recognized.

It can be concluded that the reduced model is very well suited for modeling the co-HP of bioliq® HG and fossil MD in the investigated parameter range.

Table 4. Statistical comparison of the reduced model with the sequential and combined model according to Fisher's exact test for the experimental validation dataset at T = 370 °C.

Parameters	Sequential Model	Reduced Model	Combined Model
n_p	10	12	20
n_l	6	6	6
n_e	16	16	16
v_i	86	84	76
R_i^2 [-]	0.9971	0.9976	0.9978
SSE [kg kg^{-1}]	27.16	22.24	20.51
F	-	9.29 (F_{S-R})	0.8 (F_{R-C})
$F_{1-\alpha}$	-	3.11	2.06

4. Conclusions

In this study, the co-HP of HG originating from the bioliq® process and fossil MD was investigated over a broad parameter range using a commercial CoMo/γ-Al_2O_3 catalyst under realistic hydrotreating process conditions. Attention was especially paid to 1,2,4,5-tetramethylbenzene (durene), the most critical component originating from MTG and DTG processes because of its crystallization and high emission tendencies.

High reaction temperatures and space-times significantly improved the durene conversion and simultaneously decreased the isomerization selectivity in favor of hydrogenation. Additionally, cracking of aromatics and naphthenes was greatly enhanced, which decreased the diesel yield in favor of the gasoline yield. In contrast, the kerosene yield stayed almost constant over the investigated parameter range. At high reaction temperatures, the catalyst reached pseudo-steady-state conditions faster, for example, after approx. 1000 h on stream at 380 °C.

The hydrogenation of aromatics led to a considerable improvement of the CN in the diesel fraction, while MON and, more significantly, RON of the gasoline samples decreased. Depending on the parameters applied, a loss of CN between approx. 2.3 and 14.3 was found compared to the original MD (60.3). Hence, diesel meeting a CN of 51 (EN590) could be provided for the co-HP of 15 wt.% bioliq® HG and 85 wt.% MD.

In this work, three models were developed that can accurately predict the data in the experimentally investigated parameter range. As found by other authors, sequential reactions from heavier to lighter lumps were the most important for modeling the HP reactions [58,63,65]. In contrast, adding ideal hydrocracking reactions resulted in only a little more predictive accuracy. Highly significant were incorporated dealkylation reactions, producing gaseous compounds, as well as aromatics and naphthenes in the gasoline boiling range.

Further experiments should be conducted under variation of the feed compositions, i.e., bioliq® HG and heteroatoms, as aromatics were reported to compete in hydrotreating reactions [50]. Co-HP of feedstocks rich in aromatics is highly exothermic and thus challenging [35]. Therefore, the studies performed at a laboratory scale should be repeated at a larger scale where exothermic reactions become a critical factor. In addition, it may be interesting to investigate other catalysts, such as those based on nickel-molybdenum,

which have been reported to have high aromatics hydrogenation activity [74]. Finally, it should be clarified under which legal regulations and process conditions co-HP can be run economically profitably, as petrochemical parameters such as the CN decline to some extent.

Supplementary Materials: The following are available online at https://www.mdpi.com/article/10.3390/reactions4030032/s1, Figure S1: Durene and C_{10} aromatics conversion at a reference point for the co-HP of 15 *wt*.% durene and 85 *wt*.% MD.; Figure S2: Duren conversion under variation of temperature for the co-HP of 15 *wt*.% durene and 85 *wt*.% MD.; Figure S3: Fitting results for the reduced model at (a) 350 °C, (b) 380 °C, and (c) 390 °C for the co-HP of 15 wt.% durene and 85 wt.% MD.; Table S1: Experimental data (weight fractions) at 340 °C, 350 °C, 370 °C, 380 °C, and 390 °C for the co-HP of 15 wt.% durene and 85 wt.% MD.

Author Contributions: Conceptualization, D.G. and J.W.; methodology, D.G. and J.W.; software, J.W.; validation, D.G., J.W. and R.R.; formal analysis, D.G. and J.W.; investigation, D.G. and J.W.; resources, R.R.; data curation, D.G. and J.W.; writing—original draft preparation, D.G. and J.W.; writing—review and editing, D.G., J.W. and R.R.; visualization, D.G. and J.W.; supervision, R.R.; project administration, R.R.; funding acquisition, R.R. All authors have read and agreed to the published version of the manuscript.

Funding: This work was supported by the Strategic Dialogue Automotive Industry SDA and the Ministry of Transport Baden-Wuerttemberg as part of the project "refuels–rethinking fuels".

Data Availability Statement: The data presented in this study, if not included in the Supplementary Materials, are available upon request from the corresponding author.

Acknowledgments: We thank Thomas Otto and Doreen Neumann-Walter from the Institute of Catalysis Research and Technology (IKFT) as part of Karlsruhe Institute of Technology, Germany, for their strong support in characterizing the fuels. We would particularly like to thank our partners from Mineralölraffinerie Obberrhein (MiRO), Karlsruhe, Germany, for constructive discussions during the conduction of this study.

Conflicts of Interest: The authors declare no conflict of interest. The funders had no role in the design of the study; in the collection, analyses, or interpretation of data; in the writing of the manuscript; or in the decision to publish the results.

References

1. Our World in Data. Global Direct Primary Energy Consumption. Available online: https://ourworldindata.org/grapher/global-primary-energy (accessed on 6 February 2023).
2. European Commission. *Communication from the Commission of the European Parliament, the European Council, the Council, the European Economic and Social Committee and the Committee of the Regions: The European Green Deal*; European Commission: Brussels, Belgium, 2019.
3. The European Parliament and the Council of the European Union. *Regulation (EU) 2021/1119 of the European Parliament and of the Council of 30 June 2021 Establishing the Framework for Achieving Climate Neutrality and Amending Regulations (EC) No 401/2009 and (EU) 2018/1999 ('European Climate Law'): Regulation 2021/1119*; The European Parliament and the Council of the European Union: Strasbourg, France, 2021.
4. European Commission. *Communication from the Commission to the European Parliament, the Council, the European Economic and Social Committee and the Committee of the Regions: 'Fit for 55': Delivering the EU's 2030 Climat Target on the Way to Climate Neutrality*; European Commission: Brussels, Belgium, 2021.
5. Abnett, K. EU Approves Effective Ban on New Fossil Fuel Cars from 2035. Available online: https://www.reuters.com/markets/europe/eu-approves-effective-ban-new-fossil-fuel-cars-2035-2022-10-27/ (accessed on 25 November 2022).
6. Federal Ministry for the Environment, Nature Conservation, Nuclear Safety and Consumer Protection. *PtL Roadmap: Sustainable Aviation Fuel from Renewable Energy Sources for Aviation in Germany*; Federal Ministry for the Environment, Nature Conservation, Nuclear Safety and Consumer Protection: Berlin, Germany, 2021.
7. International Energy Agency. *Global EV Outlook 2023: Catching up with Climate Ambitions*; International Energy Agency (IEA): Paris, France, 2023.
8. European Automobile Manufacturers' Association. *Vehicles in Use Europe*; European Automobile Manufacturers' Association (ACEA): Brussels, Belgium, 2023.
9. Alvarez-Majmutov, A.; Badoga, S.; Chen, J.; Monnier, J.; Zhang, Y. Co-Processing of Deoxygenated Pyrolysis Bio-Oil with Vacuum Gas Oil through Hydrocracking. *Energy Fuels* **2021**, *35*, 9983–9993. [CrossRef]

10. DIN Deutsches Institut für Normung e.V. *Automotive Fuels–Unleaded Petrol–Requirements and Test Methods*; German version EN 228:2012+A1:2017; Beuthe Verlag GmbH: Berlin, Germany, 2017.
11. DIN Deutsches Institut für Normung e.V. *Automotive fuels—Diesel—Requirements and Test Methods*; German version EN 590:2022; Beuthe Verlag GmbH: Berlin, Germany, 2022.
12. Jeuland, N.; Montagne, X.; Gautrot, X. Potentiality of Ethanol as a Fuel for Dedicated Engine. *Oil Gas Sci. Technol.-Rev. l'IFP* **2004**, *59*, 559–570, 2004040. [CrossRef]
13. Munsin, R.; Laoonual, Y.; Jugjai, S.; Imai, Y. An experimental study on performance and emissions of a small SI engine generator set fuelled by hydrous ethanol with high water contents up to 40%. *Fuel* **2013**, *106*, 586–592. [CrossRef]
14. Haseeb, A.; Fazal, M.A.; Jahirul, M.I.; Masjuki, H.H. Compatibility of automotive materials in biodiesel: A review. *Fuel* **2011**, *90*, 922–931. [CrossRef]
15. Chang, C.D.; Silvestri, A.J. The Conversion of Methanol and Other O-Compounds to Hydrocarbons over Zeolite Catalysts. *J. Catal.* **1977**, *47*, 249–259. [CrossRef]
16. Olsbye, U.; Svelle, S.; Bjørgen, M.; Beato, P.; Janssens, T.V.W.; Joensen, F.; Bordiga, S.; Lillerud, K.P. Conversion of Methanol to Hydrocarbons: How Zeolite Cavity and Pore Size Controls Product Selectivity. *Angew. Chem. Int. Ed.* **2012**, *51*, 5810–5831. [CrossRef]
17. Chang, C.D. The New Zealand Gas-to-Gasoline plant: An engineering tour de force. *Catal. Today* **1992**, *13*, 103–111. [CrossRef]
18. Topp-Jørgensen, J. Topsøe Integrated Gasoline Synthesis—The Tigas Process. *Stud. Surf. Sci. Catal.* **1988**, *36*, 293–305. [CrossRef]
19. Fujimoto, K.; Asami, K.; Saima, H.; Shikada, T.; Tominaga, H.o. Two-Stage Reaction System for Synthesis Gas Conversion to Gasoline. *Ind. Eng. Chem. Prod. Res. Dev.* **1986**, *25*, 262–267. [CrossRef]
20. Trippe, F.; Fröhling, M.; Schultmann, F.; Stahl, R.; Henrich, E. Techno-Economic Analysis of Fast Pyrolysis as a Process Step Within Biomass-to-Liquid Fuel Production. *Waste Biomass Valorization* **2010**, *1*, 415–430. [CrossRef]
21. Pfitzer, C.; Dahmen, N.; Tröger, N.; Weirich, F.; Sauer, J.; Günther, A.; Müller-Hagedorn, M. Fast Pyrolysis of Wheat Straw in the Bioliq® Pilot Plant. *Energy Fuels* **2016**, *30*, 8047–8054. [CrossRef]
22. Dahmen, N.; Henrich, E.; Dinjus, E.; Weirich, F. The bioliq® bioslurry gasification process for the production of biosynfuels, organic chemicals, and energy. *Energy Sustain. Soc.* **2012**, *2*, 3. [CrossRef]
23. Stiefel, M.; Ahmad, R.; Arnold, U.; Döring, M. Direct synthesis of dimethyl ether from carbon-monoxide-rich synthesis gas: Influence of dehydration catalysts and operating conditions. *Fuel Process. Technol.* **2011**, *92*, 1466–1474. [CrossRef]
24. Zimmermann, M.C.; Otto, T.N.; Wodarz, S.; Zevaco, T.A.; Pitter, S. Mesoporous H–ZSM–5 for the Conversion of Dimethyl Ether to Hydrocarbons. *Chem. Ing. Tech.* **2019**, *91*, 1302–1313. [CrossRef]
25. Amelang, S. Pilot Project in Germany's Largest Refinery to Produce Synthetic Fuels. 2021. Available online: https://www.cleanenergywire.org/news/pilot-project-germanys-largest-refinery-produce-synthetic-fuels (accessed on 8 March 2023).
26. Liederman, D.; Yurchak, S.; Kuo, J.C.W.; Lee, W. Mobil Methanol-to-Gasoline Process. *J. Energy* **1982**, *6*, 340–341. [CrossRef]
27. Petit, A.; Montagne, X. Effects of the Gasoline Composition on Exhaust Emissions of Regulated and Speciated Pollutants. *SAE Tech. Pap.* **1993**, *932681*, 1–11. [CrossRef]
28. Calcote, H.F.; Manos, D.M. Effect of Molecular Structure on Incipient Soot Formation. *Combust. Flame* **1983**, *49*, 289–304. [CrossRef]
29. Lim, S.S.; Vos, T.; Flaxman, A.D.; Danaei, G.; Shibuya, K.; Adair-Rohani, H.; AlMazroa, M.A.; Amann, M.; Anderson, H.R.; Andrews, K.G.; et al. A comparative risk assessment of burden of disease and injury attributable to 67 risk factors and risk factor clusters in 21 regions, 1990–2010: A systematic analysis for the Global Burden of Disease Study 2010. *Lancet* **2012**, *380*, 2224–2260. [CrossRef]
30. Chang, C.D. Hydrocarbons from Methanol. *Catal. Rev. Sci. Eng.* **1983**, *25*, 1–118. [CrossRef]
31. Bisht, D.; Petri, J. Considerations for Upgrading Light Cycle Oil with Hydroprocessing Technologies. *Indian Chem. Eng.* **2014**, *56*, 321–335. [CrossRef]
32. Mokrani, T.; Scurrell, M. Gas Conversion to Liquid Fuels and Chemicals: The Methanol Route–Catalysis and Processes Development. *Catal. Rev.* **2009**, *51*, 1–145. [CrossRef]
33. Vivas, A.H.; Joensen, F. Process and Catalyst for Upgrading Gasoline. U.S. Patent US10150714B2, 11 December 2018.
34. Graf, D.; Neuner, P.; Rauch, R. Hydroprocessing and Blending of a Biomass-Based DTG-Gasoline. *Energy Eng.* **2022**, *119*, 2169–2192. [CrossRef]
35. van Dyk, S.; Su, J.; Ebadian, M.; Saddler, J. Production of lower carbon-intensity fuels by co-processing biogenic feedstocks: Potential and challenges for refineries. *Fuel* **2022**, *324*, 124636. [CrossRef]
36. van Dyk, S.; Su, J.; Mcmillan, J.D.; Saddler, J. Potential synergies of drop–in biofuel production with further co–processing at oil refineries. *Biofuels Bioprod. Biorefin.* **2018**, *13*, 760–775. [CrossRef]
37. Lappas, A.A.; Bezergianni, S.; Vasalos, I.A. Production of biofuels via co-processing in conventional refining processes. *Catal. Today* **2009**, *145*, 55–62. [CrossRef]
38. Marker, T.L. *Opportunities for Biorenewables in Oil Refineries*; U.S. Department of Energy: Washington, DC, USA, 2005. [CrossRef]
39. Le Wu.; Wang, Y.; Zheng, L.; Shi, M.; Li, J. Design and optimization of bio-oil co-processing with vacuum gas oil in a refinery. *Energy Convers. Manag.* **2019**, *195*, 620–629. [CrossRef]
40. Tsai, T.C.; Liu, S.B.; Wang, I. Disproportionation and transalkylation of alkylbenzenes over zeolite catalysts. *Appl. Catal. A Gen.* **1999**, *181*, 355–398. [CrossRef]

41. Vogt, E.T.C.; Weckhuysen, B.M. Fluid catalytic cracking: Recent developments on the grand old lady of zeolite catalysis. *Chem. Soc. Rev.* **2015**, *44*, 7342–7370. [CrossRef]
42. Bezergianni, S.; Dimitriadis, A.; Kikhtyanin, O.; Kubička, D. Refinery co-processing of renewable feeds. *Prog. Energy Combust. Sci.* **2018**, *68*, 29–64. [CrossRef]
43. Al-Sabawi, M.; Chen, J.; Ng, S. Fluid Catalytic Cracking of Biomass-Derived Oils and Their Blends with Petroleum Feedstocks: A Review. *Energy Fuels* **2012**, *26*, 5355–5372. [CrossRef]
44. Pinho, A.d.R.; de Almeida, M.B.; Mendes, F.L.; Ximenes, V.L.; Casavechia, L.C. Co-processing raw bio-oil and gasoil in an FCC Unit. *Fuel Process. Technol.* **2015**, *131*, 159–166. [CrossRef]
45. Thegarid, N.; Fogassy, G.; Schuurman, Y.; Mirodatos, C.; Stefanidis, S.; Iliopoulou, E.F.; Kalogiannis, K.; Lappas, A.A. Second-generation biofuels by co-processing catalytic pyrolysis oil in FCC units. *Appl. Catal. B Environ.* **2014**, *145*, 161–166. [CrossRef]
46. Jones, D.S.J.S.; Pujadó, P.R. *Handbook of Petroleum Processing*; Springer: Dordrecht, The Netherlands, 2006. [CrossRef]
47. van Dyk, S.; Su, J.; Mcmillan, J.D.; Saddler, J. *'Drop-In' Biofuels: The Key Role That Co-Processing Will Play in Its Production*; IEA Bioenergy: Paris, France, 2019.
48. Zacher, A.H.; Olarte, M.V.; Santosa, D.M.; Elliott, D.C.; Jones, S.B. A review and perspective of recent bio-oil hydrotreating research. *Green Chem.* **2014**, *16*, 491–515. [CrossRef]
49. Furimsky, E. Selection of catalysts and reactors for hydroprocessing. *Appl. Catal. A Gen.* **1998**, *171*, 177–206. [CrossRef]
50. Ancheyta-Juárez, J.; Aguilar-Rodríguez, E.; Salazar-Sotelo, D.; Betancourt-Rivera, G.; Leiva-Nuncio, M. Hydrotreating of straight run gas oil–light cycle oil blends. *Appl. Catal. A Gen.* **1999**, *180*, 195–205. [CrossRef]
51. Nakakita, K.; Ban, H.; Takasu, S.; Hotta, Y.; Inagaki, K.; Weissman, W.; Farrell, J.T. Effect of Hydrocarbon Molecular Structure in Diesel Fuel on In-Cylinder Soot Formation and Exhaust Emissions. *SAE Int. J. Fuels Lubr.* **2003**, *112*, 1763–1775. [CrossRef]
52. Sági, D.; Baladincz, P.; Varga, Z.; Hancsók, J. Co-processing of FCC light cycle oil and waste animal fats with straight run gas oil fraction. *J. Clean. Prod.* **2016**, *111*, 34–41. [CrossRef]
53. Jiang, Y.; Phillips, S.D.; Singh, A.; Jones, S.B.; Gaspar, D.J. Potential economic values of low-vapor-pressure gasoline-range bio-blendstocks: Property estimation and blending optimization. *Fuel* **2021**, *297*, 120759. [CrossRef]
54. Laxminarasimhan, C.S.; Verma, R.P.; Ramachandran, P.A. Continuous lumping model for simulation of hydrocracking. *AIChE J.* **1996**, *42*, 2645–2653. [CrossRef]
55. Weitkamp, J. Catalytic Hydrocracking—Mechanisms and Versatility of the Process. *ChemCatChem* **2012**, *4*, 292–306. [CrossRef]
56. Sullivan, R.F.; Egan, C.J.; Langlois, G.E.; Sieg, R.P. A New Reaction That Occurs in the Hydrocracking of Certain Aromatic Hydrocarbons. *J. Am. Chem. Soc.* **1961**, *83*, 1156–1160. [CrossRef]
57. Ancheyta, J.; Sánchez, S.; Rodríguez, M.A. Kinetic modeling of hydrocracking of heavy oil fractions: A review. *Catal. Today* **2005**, *109*, 76–92. [CrossRef]
58. Palos, R.; Gutiérrez, A.; Hita, I.; Castaño, P.; Thybaut, J.W.; Arandes, J.M.; Bilbao, J. Kinetic Modeling of Hydrotreating for Enhanced Upgrading of Light Cycle Oil. *Ind. Eng. Chem. Res.* **2019**, *58*, 13064–13075. [CrossRef]
59. Hita, I.; Aguayo, A.T.; Olazar, M.; Azkoiti, M.J.; Bilbao, J.; Arandes, J.M.; Castaño, P. Kinetic Modeling of the Hydrotreating and Hydrocracking Stages for Upgrading Scrap Tires Pyrolysis Oil (STPO) toward High-Quality Fuels. *Energy Fuels* **2015**, *29*, 7542–7553. [CrossRef]
60. Soto-Azuara, L.A.; Ramírez-López, R.; del Carmen Monterrubio-Badillo, M.; Elizalde, I. Mathematical modeling of the hydrocracking kinetics of a heavy oil fraction using the discrete lumping approach: The effect of the variation of the lump number. *React. Kinet. Mech. Catal.* **2022**, *135*, 655–667. [CrossRef]
61. Ayasse, A.R.; Nagaishi, H.; Chan, E.W.; Gray, M.R. Lumped kinetics of hydrocracking of bitumen. *Fuel* **1997**, *76*, 1025–1033. [CrossRef]
62. Jarullah, A.T.; Mujtaba, I.M.; Wood, A.S. Enhancement of Productivity of Distillate Fractions by Crude Oil Hydrotreatment: Development of Kinetic Model for the Hydrotreating Process. *Comput. Aided Chem. Eng.* **2011**, *29*, 261–265. [CrossRef]
63. Alhumaidan, F.; Lababidi, H.M.S.; Al-Adwani, H. Hydrocracking of atmospheric residue feedstock in hydrotreating processes. *Kuwait J. Sci. Eng.* **2010**, *37*, 129–159.
64. Sánchez, S.; Rodríguez, M.A.; Ancheyta, J. Kinetic Model for Moderate Hydrocracking of Heavy Oils. *Ind. Eng. Chem. Res.* **2005**, *44*, 9409–9413. [CrossRef]
65. Martínez, J.; Ancheyta, J. Kinetic model for hydrocracking of heavy oil in a CSTR involving short term catalyst deactivation. *Fuel* **2012**, *100*, 193–199. [CrossRef]
66. Sadighi, S.; Ahmad, A.; Rashidzadeh, M. 4-Lump kinetic model for vacuum gas oil hydrocracker involving hydrogen consumption. *Korean J. Chem. Eng.* **2010**, *27*, 1099–1108. [CrossRef]
67. Ramírez, S.; Martínez, J.; Ancheyta, J. Kinetics of thermal hydrocracking of heavy oils under moderate hydroprocessing reaction conditions. *Fuel* **2013**, *110*, 83–88. [CrossRef]
68. Becker, P.J.; Celse, B.; Guillaume, D.; Dulot, H.; Costa, V. Hydrotreatment modeling for a variety of VGO feedstocks: A continuous lumping approach. *Fuel* **2015**, *139*, 133–143. [CrossRef]
69. Martens, G.G.; Thybaut, J.W.; Marin, G.B. Single-Event Rate Parameters for the Hydrocracking of Cycloalkanes on Pt/US-Y Zeolites. *Ind. Eng. Chem. Res.* **2001**, *40*, 1832–1844. [CrossRef]
70. Texier, S. Activation of alumina-supported hydrotreating catalysts by organosulfides: Comparison with H2S and effect of different solvents. *J. Catal.* **2004**, *223*, 404–418. [CrossRef]

71. *ASTM D6730-01*; Standard Test Method for Determination of Individual Components in Spark Ignition Engine Fuels by 100-Metre Capillary (with Precolumn) High-Resolution Gas Chromatography. ASTM International: West Conshohocken, PA, USA, 2001. [CrossRef]
72. *ASTM D7345*; Standard Test Method for Distillation of Petroleum Products and Liquid Fuels at Atmospheric Pressure (Micro Distillation Method). ASTM International: West Conshohocken, PA, USA, 2017. [CrossRef]
73. Qader, S.A.; Hill, G.R. Hydrocracking of Gas Oil. *Ind. Eng. Chem. Process. Des. Dev.* **1969**, *8*, 98–105. [CrossRef]
74. Cooper, B.H.; Donnis, B.B. Aromatic saturation of distillates: An overview. *Appl. Catal. A Gen.* **1996**, *137*, 203–223. [CrossRef]
75. Alcázar, L.A.; Ancheyta, J. Sensitivity analysis based methodology to estimate the best set of parameters for heterogeneous kinetic models. *Chem. Eng. J.* **2007**, *128*, 85–93. [CrossRef]
76. Newville, M.; Stensitzki, T.; Allen, D.B.; Antonino, I. LMFIT: Non-Linear Least-Square Minimization and Curve-Fitting for Python 2014. Available online: https://zenodo.org/record/11813 (accessed on 31 July 2023).
77. Virtanen, P.; Gommers, R.; Oliphant, T.E.; Haberland, M.; Reddy, T.; Cournapeau, D.; Burovski, E.; Peterson, P.; Weckesser, W.; Bright, J.; et al. SciPy 1.0: Fundamental algorithms for scientific computing in Python. *Nat. Methods* **2020**, *17*, 261–272. [CrossRef]
78. Vivas-Báez, J.C.; Servia, A.; Pirngruber, G.D.; Dubreuil, A.C.; Pérez-Martínez, D.J. Insights in the phenomena involved in deactivation of industrial hydrocracking catalysts through an accelerated deactivation protocol. *Fuel* **2021**, *303*, 120681. [CrossRef]
79. Meurer, A.; Kern, J. Fischer–Tropsch Synthesis as the Key for Decentralized Sustainable Kerosene Production. *Energies* **2021**, *14*, 1836. [CrossRef]
80. Kubic, W.L. *A Group Contribution Method for Estimating Cetane and Octane Numbers*; Los Alamos National Laboratory: Los Alamos, NM, USA, 2016. https://www.osti.gov/biblio/1291241/.
81. Hawkins, D.M. The Problem of Overfitting. *J. Chem. Inf. Comput. Sci.* **2004**, *44*, 1–12. [CrossRef]

Disclaimer/Publisher's Note: The statements, opinions and data contained in all publications are solely those of the individual author(s) and contributor(s) and not of MDPI and/or the editor(s). MDPI and/or the editor(s) disclaim responsibility for any injury to people or property resulting from any ideas, methods, instructions or products referred to in the content.

Co-Hydroprocessing of Fossil Middle Distillate and Bio-Derived Durene-Rich Heavy Ends under Hydrotreating Conditions

David Graf[1], Johannes Waßmuth[1] and Reinhard Rauch[1]

1 Karlsruhe Institute of Technology (KIT), Engler-Bunte-Institute, Division of Fuel Technology (EBI-ceb), Engler-Bunte-Ring 1a, 76131 Karlsruhe, Germany

Supplementary Materials

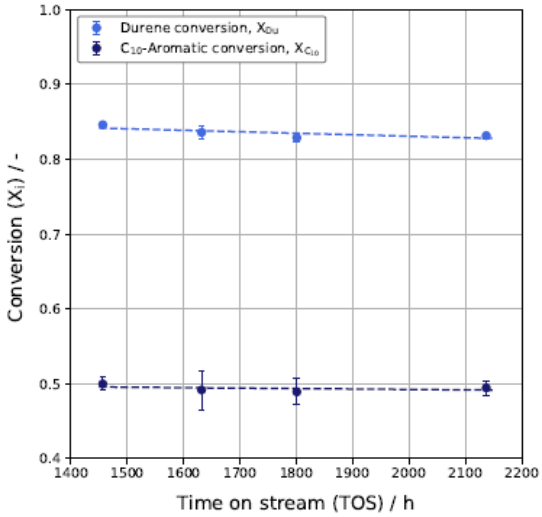


Figure S1. Durene and C_{10} aromatics conversion at a reference point for the co-HP of 15 wt.% durene and 85 wt.% MD. Experimental conditions: T = 380 °C, LHSV = 0.25 h^{-1}, p_{H2} = 59 bar, p_{Ar} = 3.9 bar and V_{H2}/V_{Feed} = 1042 $Nm^3\ m^{-3}$.

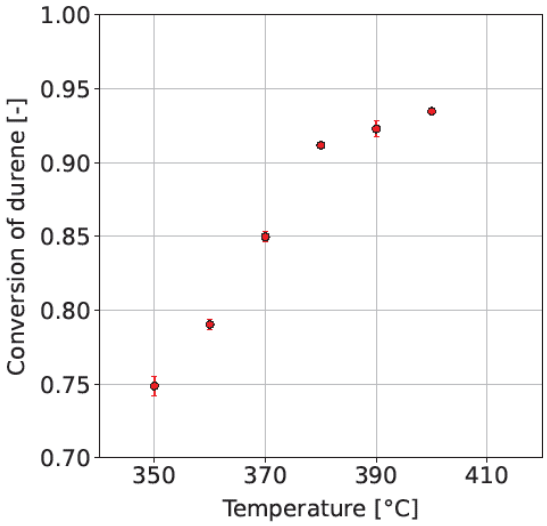


Figure S2. Duren conversion under variation of temperature for the co-HP of 15 wt.% durene and 85 wt.% MD. Experimental conditions: LHSV = 0.4 h^{-1}, p_{H2} = 59 bar, p_{Ar} = 3.9 bar and V_{H2}/V_{Feed} = 1042 $Nm^3\ m^{-3}$.

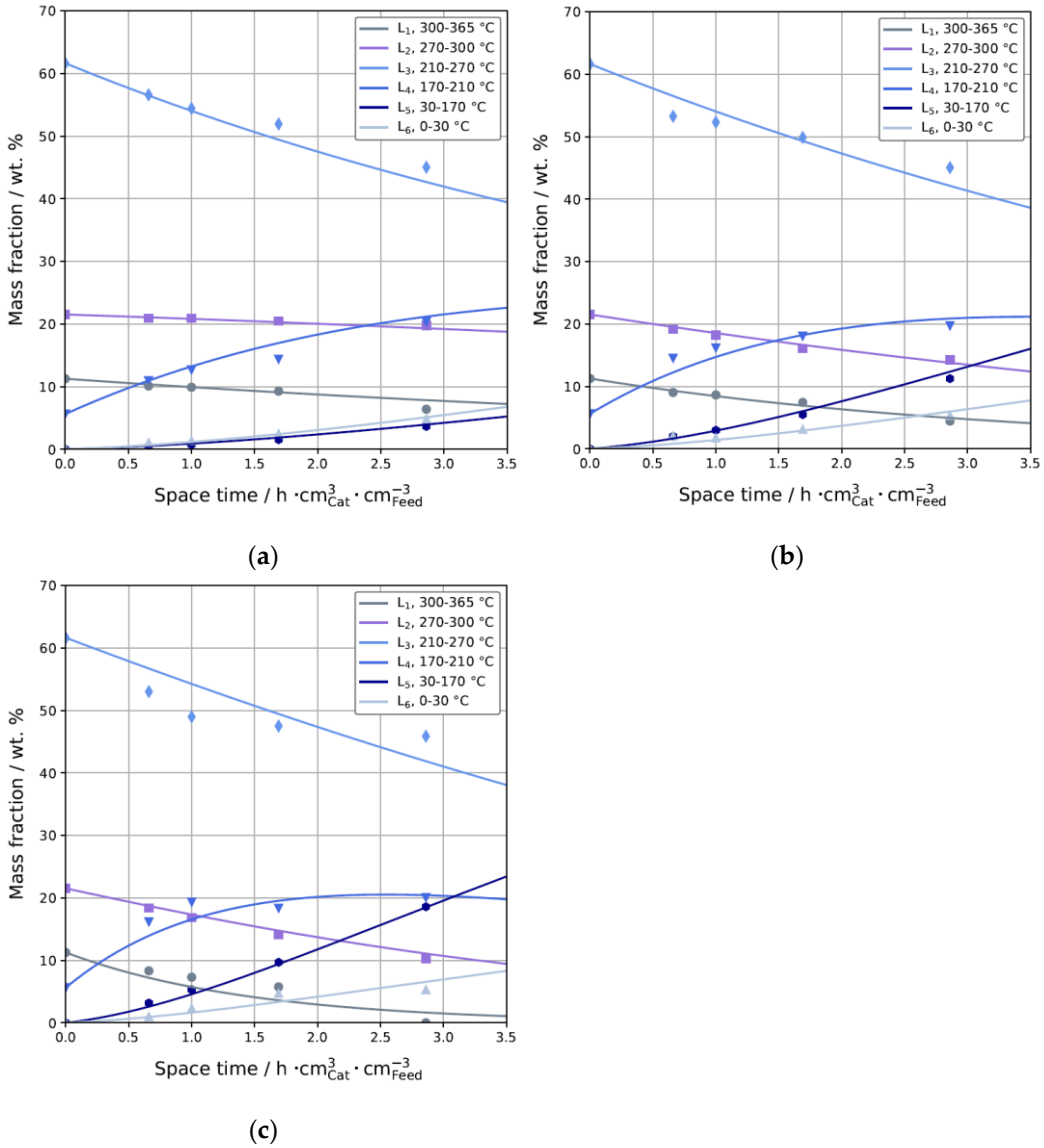


Figure S3. Fitting results for the reduced model at **(a)** 350 °C, **(b)** 380 °C, and **(c)** 390 °C for the co-HP of 15 wt.% durene and 85 wt.% MD. Experimental conditions: $\bar{p}_{H2}$= 59 bar, $\bar{p}_{Ar}$= 3.9 bar and $\dot{V}_{H2}/\dot{V}_{Feed}$=1042 Nm³ m⁻³.
Note: Measuring point of Lump 1 in Figure S3c for a space time of 2.86 h cm^3_{Cat} cm^{-3}_{Feed} is probably too low due to measurement uncertainties in distillation.

Table S1. Experimental data (weight fractions) at 340 °C, 350 °C, 370 °C, 380 °C and 390 °C for the co-HP of 15 wt.% durene and 85 wt.% MD. Experimental conditions: $\bar{p}_{H2}$= 59 bar, $\bar{p}_{Ar}$= 3.9 bar and $\dot{V}_{H2}/\dot{V}_{Feed}$=1042 $Nm^3\ m^{-3}$.

		Space time / h^{-1}				
T / °C	**Lump**	**0**	**0.833**	**1.333**	**2.000**	**4.000**
340	**6**	0.00	1.01	2.39	3.12	4.00
	5	0.00	0.49	0.88	1.30	2.92
	4	5.61	11.46	12.33	19.70	21.31
	3	61.64	55.58	53.71	46.07	42.22
	2	21.51	21.12	20.23	21.44	20.59
	1	11.25	10.33	10.46	8.36	8.97
		Space time / h^{-1}				
T / °C	**Lump**	**0.000**	**0.666**	**1.000**	**1.690**	**2.860**
350	**6**	0.00	1.04	1.39	2.44	4.84
	5	0.00	0.43	0.73	1.53	3.63
	4	5.61	10.94	12.67	14.37	20.35
	3	61.64	56.58	54.41	51.92	45.02
	2	21.51	20.92	20.90	20.48	19.77
	1	11.25	10.09	9.89	9.27	6.39
370	**6**	0.00	1.66	1.55	2.19	3.64
	5	0.00	1.13	1.91	3.29	7.92
	4	5.61	13.16	14.54	17.05	20.85
	3	61.64	54.27	52.84	50.81	43.54
	2	21.51	20.00	19.77	18.15	17.70
	1	11.25	9.78	9.39	8.50	6.36
380	**6**	0.00	2.08	1.73	3.14	5.35
	5	0.00	2.00	2.97	5.48	11.24
	4	5.61	14.50	16.15	18.04	19.70
	3	61.64	53.25	52.30	49.86	45.04
	2	21.51	19.15	18.23	16.06	14.25
	1	11.25	9.01	8.62	7.43	4.44
390	**6**	0.00	0.99	2.32	4.70	5.29
	5	0.00	3.16	5.29	9.67	18.56
	4	5.61	16.15	19.30	18.32	20.03
	3	61.64	53.00	48.98	47.50	45.87
	2	21.51	18.40	16.82	14.07	10.25
	1	11.25	8.31	7.29	5.74	0.00

Appendix E. Author Contributions

This appendix presents the author contributions for all three publications included in this doctoral thesis, in the order listed.

Verification of the contribution from the co-authors

Title: Hydroprocessing and Blending of a Biomass-Based DTG-Gasoline

Journal: Energy Engineering 119(6), 2169–2192, 2022.
DOI: 10.32604/ee.2022.022759
Authors: David Graf, Philipp Neuner, Reinhard Rauch

Position in the dissertation: The content of this paper has been included in Chapter 2 and Chapter 1.

Declaration of contributions

David Graf conceptualized the work and methodology, designed and conducted the hydroprocessing experiments, analyzed the hydroprocessing samples, analyzed and discussed the results, and conceptualized and wrote the manuscript.

Philipp Neuner supported in conducting the hydroprocessing experiments and reviewed the manuscript.

Reinhard Rauch was in charge of the scientific lead and reviewed the manuscript.

Verification of the contribution from the co-authors

Title: Standard-Compliant Gasoline by Upgrading a DTG-Based Fuel through Hydroprocessing the Heavy-Ends and Blending of Oxygenates

Journal: Fuels 4(2), 156–173, 2023.

DOI: 10.3390/fuels4020010

Authors: David Graf, Philipp Neuner, Reinhard Rauch

Position in the dissertation: The content of this paper has been included in Chapter 3 and Chapter 1.

Declaration of contributions

David Graf conceptualized the work and methodology, designed and conducted the hydroprocessing experiments, designed and conducted the blending experiments, analyzed the samples of the hydroprocessing and blending experiments, analyzed and discussed the results, and conceptualized and wrote the manuscript.

Philipp Neuner supported in conducting the hydroprocessing experiments and reviewed the manuscript.

Reinhard Rauch was in charge of the scientific lead and reviewed the manuscript.

Verification of the contribution from the co-authors

Title: Co-Hydroprocessing of Fossil Middle Distillate and Bio-Derived Durene-Rich Heavy Ends under Hydrotreating Conditions

Journal: Reactions 4(3), 531–551, 2023.

DOI: 10.3390/reactions4030032

Authors: David Graf, Johannes Waßmuth, Reinhard Rauch

Position in the dissertation: The content of this paper has been included in Chapter 4 and Chapter 1.

Declaration of contributions

David Graf conceptualized the work and methodology, designed and significantly supported in conducting the co-hydroprocessing experiments, designed and provided support in conducting the distillation experiments, significantly supported in analyzing the co-hydroprocessing and distillation samples, supported in modeling the experimental data, analyzed and discussed the results, and conceptualized and wrote the manuscript.

Johannes Waßmuth conducted the co-hydroprocessing and distillation experiments, analyzed the co-hydroprocessing and distillation samples, modeled the experimental data, analyzed and discussed the results, supported in writing the manuscript, and reviewed the manuscript.

Reinhard Rauch was in charge of the scientific lead and reviewed the manuscript.